The assessment and manipulation of brown adipose tissue in early life and during adulthood

by Hannah Scotney B.Sc (Hons)., M.Sc.

Thesis submitted to the University of Nottingham for the degree of Doctor of Philosophy

September 2018

Abstract

The re-discovery of functional brown adipose tissue (BAT) in adult humans, has renewed interest in exploring the metabolic capabilities of this tissue as a potential target for novel obesity and metabolic disease treatments. Glucocorticoids (GCs), the end-product of the hypothalamic-pituitary-adrenal (HPA) axis in the brain, acutely increase BAT thermogenesis in humans. To better understand the role of BAT in early life, and later metabolic risks, we need to develop new methods of assessment, suitable for infants, and experimental models of stress. This thesis aimed to 1) explore the role of GCs and stress on BAT, 2) explore the potential of emerging technologies to assess BAT activation with particular adaptation to the newborn period. A series of studies were conducted during adulthood in humans, and in the early postnatal period in newborn infants and in a rodent model, to help address the aforementioned aims.

Infrared thermography imaging (IRT) of the supraclavicular (SCR) region, was used to examine BAT function during the pharmacological induction of hypercortisolaemia. A 15-hour infusion of hydrocortisone (HC), resulted in a 0.5℃ increase in SCR temperature in 8 healthy adult males, compared to saline infusion. This study also investigated the effect of diet and a non-specific β-adrenoreceptor (β-AR) agonist, Isoprenaline, on BAT function, demonstrating similar rises in SCR temperature to that achieved by HC.

The next aim explored the feasibility of whether BAT function could be assessed by the complementary use of non-invasive near infrared spectroscopy (NIRS) with IRT in healthy adults, during cold stress. Forearm blanket cooling increased SCR BAT temperature by 0.3℃, as assessed by IRT and was associated with increases in venous oxygenation over the SCR region assessed by NIRS, suggesting a change in the metabolic requirement of oxygen for thermogenesis.

Given the demonstration of IRT as a promising assessment tool for BAT function in adults and children, a pilot study was conducted to develop an

imaging protocol to assess the practicability of detecting changes in skin temperature overlying known BAT regions, in newborn infants. Skin temperatures overlying the interscapular BAT region were demonstrated to be greater than that of a reference region located on the lower back. However, further protocol development remains, given that numerous challenges were faced when acquiring thermograms in this population.

Cortisol plays a vital stimulatory role in the onset of thermogenesis at birth, with subsequent maturation of BAT in the first weeks of life, essential for independent thermoregulation. This thesis utilised a rodent model to assess the effects of a single episode of vibrational stress on selected BAT genes involved in its transcription and function, during critical developmental time points. This study demonstrated that whilst early-life stress at postnatal day (PND) 21 induced a state of enhanced corticosterone response at this age, and its activating enzyme, 11-Beta-dehydrocorticosterone (11β-HSD1), stress induced at this critical age did not significantly change gene expression of BAT specific genes including the uncoupling protein (UCP)1 and β3-adrenoreceptor (β3-AR).

In conclusion, this thesis demonstrates that excess GCs increase BAT thermogenesis in adults and, in a rodent model, was associated with elevated corticosterone concentrations and no change in essential BAT thermoregulatory genes, namely UCP1 and β3-AR. In adults, cold–stress increased BAT activation can be detected by NIRS in association with IRT. With additional development, these measurement techniques could be optimised for the real-time assessment of BAT activity in healthy adults and, in newborn infants, potentially allowing exploration of the impact of stressful early-life events on the developing metabolic system.

Acknowledgements

I would firstly like to thank my funding organisation, the Medical Research Council, whose financial support enabled me to present my work at both national and international scientific conferences, as well as allowing me to complete my studies.

I sincerely thank my project supervisors, Professor Mike Symonds and Dr. Don Sharkey, for their continued guidance, mentorship and support throughout my study period. Many thanks go to Dr Konstantinos Manopolous and the clinical research nursing team at the Biomedical Research Unit at the University of Birmingham, for their tremendous support through one of my studies. Many thanks also go to all staff and students within the Academic Division of Child Health, Obstetrics and Gynaecology Department at the Queen's Medical Centre, Nottingham, who have helped me feel at ease both when first beginning my PhD and through the most difficult of times.

Special thanks to Dr Ian Bloor and Dr Lara Shipley who performed the rodent experimentation work including the collection of tissue and plasma samples for subsequent laboratory analysis. I would also like to thank Dr James Law, Mark Pope and Victoria Wilson for their excellent technical support and expertise, which allowed me to conduct my experimental analysis with self-confidence.

Finally, I would like to thank my parents and friends for their continual support, patience, encouragement and inspiration through my academic journey.

To my Grandad, Kenneth, whom I'll always be thankful for beginning this journey with me.

Table of Contents

Abstract iii
Acknowledgements v
Table of Contents vi
Declaration xiii
Abbreviations xiv
List of figures xvii
List of tables xxxi

Chapter 1- Introduction 1
1.1 Obesity 1
1.1.1 Definition 1
1.1.2 Global estimate of obesity prevalence 2
1.1.3 Complications of excess adiposity 4
1.2 Brown Adipose Tissue (BAT) 4
1.2.1 Biological relevance of BAT 4
1.2.2 The metabolic significance of BAT in humans 5
1.2.3 Characteristics of BAT 6
1.2.3.1 Tissue Characteristics 6
1.2.3.2 BAT's specific Uncoupling Protein (UCP)1 10
1.2.3.3 UCP1 is the catalyst of 'Uncoupling' respiration 10
1.2.4 Ontogeny of BAT 12
1.2.4.1 Developmental origins of adipose tissue 12
1.2.4.2 Ontogeny of BAT in Precocial Species 13
1.2.4.2.1 A proliferative stage in mid-gestation 14
1.2.4.2.2 Preparatory phase for thermogenesis in late gestation 15
1.2.4.2.3 Birth and Non-shivering thermogenesis 15
1.2.4.2.4. Loss of UCP1 and accumulation of lipid 16
1.2.4.3 Ontogeny of BAT in Altricial Species 16
1.2.4.3.1 Immature phase 17
1.2.4.3.2 Mature Phase 17
1.2.4.3.3 Endocrine regulation of BAT thermogenesis at birth 17

1.2.5 The stress response system and cortisol **18**
1.2.5.1 Neuronal circuits controlling cortisol release in response to stress in immature and adult brains **18**
1.2.5.2 Effects of glucocorticoids on the programming of HPA functionality, BAT and disease risk in later life **21**
1.2.5.2.1 Prenatal glucocorticoid exposure **21**
1.2.5.2.2 Early life postnatal glucocorticoid exposure **22**
1.2.5.2.3 Effects of glucocorticoid exposure on BAT **24**
1.2.5.3 Acute stimulation of BAT thermogenesis by catecholamine release from the hypothalamus **26**
1.2.6 The Identification and assessment of BAT **30**
1.2.6.1 Original histological identification of BAT deposits in humans and rodents **30**
1.2.6.2 Imaging modalities to measure BAT **32**
1.2.6.2.1 PET-CT **32**
1.2.6.2.2 The development of non-invasive techniques for the detection and monitoring of BAT function **34**
1.2.6.2.2.1 Infrared Thermography **35**
1.2.6.2.2.2 Near Infrared Spectrophotometry (NIRS) **36**
1.2.7 Utilisation of protocols for acute BAT stimulation **38**
1.2.7.1 Cold exposure **38**
1.2.7.2 Pharmacological stimulation of the β-adrenergic system **40**
1.2.7.3 Diet-induced thermogenesis and BAT **42**
1.3 Experimentation outlined in this thesis **45**
1.3.1 Endocrine stimulation of BAT thermogenesis **45**
1.3.1.1 Human studies **45**
1.3.1.2 Rodent study **46**
1.3.2 Non-invasive BAT quantification and monitoring **47**
1.4 Main hypothesis and aims **49**

Chapter 2 – Materials and Methods **51**
2.1 Procedural and legislative declaration and ethical approvals **51**
2.1.1 Approvals for human studies **51**
2.1.2 Approval for rodent study **52**

2.2 Human studies 52
2.2.1 Infrared thermography imaging in adults 52
2.2.1.1 Image acquisition 53
2.2.1.2 Image analysis 55
2.2.1.3 IRT imaging in newborn infants 56
2.2.1.4 Near Infrared Thermography in adults 57
2.2.1.4.1 Study set up 61
2.2.1.5 Laser Doppler Flowmetry in adults 62
2.2.1.5.1 Instrumentation set up 63
2.3. Rodent study 64
2.3.1 Collection of serum samples 64
2.3.2 Collection of Tissue Samples 65
2.3.3 Analysis of Tissue Samples 65
2.3.4 Ribonucleic acid extraction from rodent tissue samples 66
2.3.4.1 RNA extraction procedure 66
2.3.4.2 Determination of RNA concentration purity and integrity 68
2.3.4.3 Reverse Transcription Polymerase Chain Reaction (RT-PCR) 69
2.3.4.4. Procedure for Reverse Transcription Polymerase Chain Reaction 71
2.3.4.5 Polymerase Chain Reaction 72
2.3.4.6 Quantitative Polymerase Chain Reaction 74
2.3.4.7 The standard curve 75
2.3.4.8 Identifying non-specific PCR products 76
2.3.4.9 Quantification of gene expression 78
2.3.5 Selection of a reference gene 78
2.3.6 Development of oligonucleotide primers for Q-PCR 79
2.3.7 Procedure for Polymerase Chain Reaction 81
2.2.7.1 Hot Start PCR 81
2.3.8 Agarose Gel Electrophoresis 83
2.3.9 QPCR procedure 85
2.3.9.1 Standard curve 85
2.3.9.2 Q-PCR of unknown samples 85

2.3.9.3 Taqman Probes **86**
2.3.9.3.1 Preparation of PCR reaction mix **86**
2.3.10 Analysis of Serum Samples **87**
2.3.10.1 Corticosterone **87**
2.3.10.2 Corticosterone Assay Procedure **88**
2.3.11 Statistical Analysis **89**

Chapter 3 - The effects of acute hypercortisolaemia on the thermogenic function of human brown adipose tissue 90
3.1 Introduction **90**
3.1.1 Main Aim **92**
3.3 Materials and Methods **92**
3.4 Results **98**
3.4.1 Anthropometric and Metabolic Characteristics **98**
3.4.2 Effects of acute hypercortisolaemia on systemic metabolites **101**
3.4.3 Metabolic responses to acute β-AR stimulation **104**
3.4.4 Acute hypercortisolaemia increases basal thermogenic activity of brown adipose tissue **106**
3.4.5 Acute β-AR stimulation increases the thermogenic activity of brown adipose tissue during both control and hypercortisolaemia conditions **108**
3.4.6 The thermogenic effect of meal ingestion **116**
3.5 Discussion **117**
3.5.1 Effect of acute hypercortisolaemia on basal thermogenic and metabolic responses **117**
3.5.2 Pharmacological activation of BAT thermogenesis in humans **118**
3.5.3 Acute hypercortisolaemia induces peripheral insulin resistance **119**
3.5.4 Infrared thermography can assess thermogenic changes in brown adipose tissue **120**
3.5.5 BAT and Diet Induced Thermogenesis **122**
3.5.6 Study Limitations and Strengths **123**
3.6 Conclusion **124**

Chapter 4 - A multimodal approach for the non-invasive detection of brown adipose tissue activation in healthy adults 125

4.1 Introduction **125**

4.1.1 Main Aims **126**

4.2 Materials and Methods **127**

4.3 Results **137**

4.3.1 Subjects **137**

4.3.2 Study A **139**

4.3.3 Study B **146**

4.3.4 Differences between subjects in study A and study B **153**

4.4 Discussion **158**

4.4.1 Acute cold exposure stimulates SCR BAT Thermogenesis **159**

4.4.2 Detection of cold-induced increases in BAT oxygenation by NIRS **161**

4.4.3 The use of $NIRS_{CW}$ to complement IRT in the assessment of BAT activity in healthy, lean adults **166**

4.5 Conclusions and summary **168**

Chapter 5 - Infrared Thermography Imaging for the identification and quantification of newborn brown adipose tissue 171

5.1 Introduction **171**

5.1.1 Main Aim **174**

5.2 Materials and Methods **174**

5.3 Results **185**

5.3.1 Subjects **185**

5.3.2 Phase 1 ..... **188**

5.3.2.1 Excluded thermograms **188**

5.3.2.2 Assessment of skin temperature by IRT imaging **189**

5.3.2.3 Skin temperature change over time **190**

5.3.2.4 Skin temperatures **191**

5.3.2.5 Core temperature **192**

5.3.3 Phase 2 ..... **193**

5.3.3.1 Excluded thermograms **193**

5.3.3.2 Assessment of skin temperature by IRT imaging **193**

5.3.3.3 Skin temperature change over time **195**
5.3.3.4 Skin temperature **201**
5.3.3.5 Core temperature **202**
5.4 Discussion **203**
5.4.1 Methodological challenges faced in phase 1 ..... **204**
5.4.2 Phase 2 ..... **206**
5.4.3 Advantages and disadvantages of the study protocol **208**
5.4.4 Future considerations **210**

Chapter 6 - A pilot study to assess how acute early postnatal stress will impact on selected BAT genes and markers of brain damage in the subsequent 24 hours **214**
6.1 Introduction **214**
6.1.1 Aims **218**
6.2 Materials and Methods **218**
6.3 Results **222**
6.3.1 Expression stability of Reference Genes **222**
6.3.2 Body weight and BAT weights **224**
6.3.3 Early life stress induced alterations in the stress response and biomarkers of brain injury **226**
6.3.4 The effects whole body vibration on the mRNA expression of selected BAT genes at 7 and 21 days of life **227**
6.4 Discussion **229**
6.4.1 Early postnatal changes in mRNA expression of genes regulating BAT transcriptional control and development **229**
6.4.2 Effects of early life stress on alterations in the mRNA expression of BAT genes regulation transcriptional control and development **22931**
6.4.3 Early life stress induces dysregulation of the HPA axis; broader implications for the development of brain injury and metabolic disturbance **238**
6.4.4 Study limitations **240**
6.5 Conclusion **244**

Chapter 7 - Conclusion **246**

References **2577**
Appendices **312**
Appendix A - Paper ..... Error! Bookmark not defined.**2**
Appendix B - Conference abstracts **32019**
Appendix B Details of suppliers **32322**

Declaration

The work in this thesis was performed within the Academic Child Health Division, School of Clinical Sciences, University of Nottingham and Institute of Metabolism and Systems Research, University of Birmingham between October 2014 and September 2018.

This thesis illustrates my own work, completed under the supervision of Professor Michael Symonds and Dr Don Sharkey. This report is an accurate representation of the work performed and no other study reproducing this work, to my knowledge, has been carried out within the University of Nottingham or the University of Birmingham.

Hannah Scotney

September 2018

Abbreviations

11β-HSD	11 beta hydroxysteroid dehydrogenase
$^{[18F]}$F-FDG	18F-Fluorodeoxyglucose
β3-AR	Beta-3 (β3)-adrenoreceptor
β-ox	Beta-oxidation
AC	Adenylyl cyclase
ACTH	Adrenocorticotropic hormone
ADP	Adenosine diphosphate
ANOVA	Analysis of variance
ATP	Adenosine triphosphate
AUC	Area under the curve
B2m	Beta-2-Microglobulin
BAT	Brown adipose tissue
BBB	Blood brain barrier
BMI	Body mass index
BMP	Bone morphogenic protein
BPM	Beats per minute
C/EBPβ	CCAAT-enhancer-binding protein β
cAMP	Cyclic AMP
Cap	Capillary
cDNA	Complimentary deoxyribonucleic acid
CIT	Cold-induced thermogenesis
C-jun	C-Jun N-terminal kinase
CMO	Chief medical officer
CNS	Central nervous system
COSHH	Control of substances hazardous to health
CRH	Corticotropin releasing hormone
CT	Computed tomography
CVD	Cardiovascular disease
Cyt c	Cytochrome C
DIT	Diet-induced thermogenesis
DNA	Deoxyribonucleic acid
dNTP	Deoxyribonucleotide
EE	Energy expenditure
ERK	Extracellular signal regulated kinase
ETC	Electron transport chain
ELISA	Enzyme linked immunosorbent assay
FA	Fatty acid
FAD	Flavin adenine dinucleotide
FADH	Flavin adenine dinucleotide dehydrogenase
FFA	Free fatty acid

FGF21	Fibroblast growth factor 21
GC	Glucocorticoid
GR	Glucocorticoid receptor
H_2O	Water
H^+	Hydrogen ion
H&E	Haematoxylin and eosin
HCl	Hydrochloric acid
HOMA-IR	Homeostatic model assessment for insulin resistance
HOX	Homeobox
HPA	Hypothalamic pituitary adrenal axis
HRP	Hyporesponsive period
HSL	Hormone sensitive lipase
IGF	Insulin growth factor
IHC	Immunohistochemistry
IL	Interleukin
Interscap	Interscapular
IRT	Infrared thermography
ISO	Isoprenaline
IUGR	intrauterine growth restriction
JPEG	Joint photographic experts group
LBW	Low birth weight
MC	Mineralocorticoid receptor
MR	Mineralocorticoid receptor
mRNA	Messenger ribonucleic acid
Myf5	Myogenic factor 5
Myf5+	Myogenic factor 5 positive
Myf5-	Myogenic factor 5 negative
NAD	Nicotinamide adenine dinucleotide
NADH	Nicotinamide adenine dinucleotide dehydrogenase
NCBI	National centre for biotechnology information
NE	Norepinephrine
NEFA	Non-esterified fatty acid
NIRS	Near infrared spectroscopy
NST	Non shivering thermogenesis
O_2	Oxygen
PCR	Polymerase chain reaction
PET	Positive emitting topography
PGC1α	Proliferator-activated receptor c coactivator
PKA	Protein kinase A
PND	Postnatal day
POA	Preoptic area
PPARα	Peroxisome proliferator activated receptor alpha
PPARγ	Peroxisome proliferator activated receptor gamma

PRLR	Prolactin receptor
PVN	Paraventricular nucleus
Q	Cofactor Q
QPCR	Quantitative polymerase chain reaction
r18s	Ribosomal 18s
RC	Respiratory chain
RIP140	Corepressor receptor-interacting protein 140
RNA	Ribonucleic acid
ROI	Region of interest
RPLPO	Ribosomal Protein, Large, P0
PRDM16	PR domain containing 16
rSO_2	Regional tissue oxygen saturation
RT-PCR	Reverse transcription polymerase chain reaction
SCR	Supraclavicular
SNS	Sympathetic nervous system
Sub-scap	Sub-scapular
TNFα	Tumour necrosis factor alpha
TEE	Total energy expenditure
TG	Triglycerides
TWIST1	Twist Family BHLH Transcription Factor 1
UCP1	Uncoupling protein 1
VMN	Ventromedial nucleus
WAT	White adipose tissue
WBV	Whole body vibration
WHO	World health organisation
YWHAZ	Tyrosine 3-monooxygenase/tryptophan 5-monooxygenase activation protein

List of figures

Figure 1.1. The growing prevalence of childhood obesity (%) in Britain. Children were classified as obese based on a BMI ≥95th centile of the British 1990 (UK90) growth reference. Adapted from Chief Medical Officer's Report 2012 (data source Public Health England; PHE) (CMO, 2012)……..**3**

Figure 1.2. Specimens of brown and white adipose tissue from the supraclavicular region in a 46-year-old female. Top panel; Specimens stained with haematoxylin and eosin show characteristic features; BAT, granular cytoplasm containing mitochondria and multiple fat vacuoles, and WAT, a single large lipid vacuole in each white fat cell. Lower panel; Specimens stained for UCP1 using immunofluorescence assay, together with the nuclei-staining dye 4',6-diamidino-2-phenylindole, shows positive immunostaining for UCP1 (green) in BAT, but not WAT specimens. Figure from (Wouter D. van Marken Lichtenbelt et al., 2009)……..**7**

Figure 1.3. Histological representation of brown and white adipose tissue. A section of paraffin-embedded interscapular BAT was treated with haematoxylin to stain nuclei in blue. UCP1 was immunodetected and is indicated by a brownish colour. Typical multilocular brown adipocytes positive for UCP1 can be seen in the left half of the picture, while unilocular white adipocytes devoid of UCP1 dominate the right half. Figure from (Klingenspor & Fromme, 2014)……..**8**

Figure 1.4. Transmission electron microscopic appearance of BAT. Of relevance is the cytoplasm filled with numerous large mitochondria packed with cristae (m), the small lipid droplets (L), part of the nucleus (N) and a parenchymal nerve amongst the adipocytes. Cap, capillary. Figure from (Frontini & Cinti, 2010)……..**9**

Figure 1.5. The uncoupling of respiration in the mitochondria of BAT, catalysed by the actions of UCP1. Electron transport chain (ETC) complex I: ETC complex II, ETC complex III, ETC complex IV; NAD: nicotinamide adenine dinucleotide; NADH: nicotinamide adenine dinucleotide dehydrogenase; FAD: Flavin adenine dinucleotide; FADH: Flavin adenine dinucleotide dehydrogenase; H^+: hydrogen ion; Q: cofactor Q; ADP: adenosine diphosphate; ATP: adenosine triphosphate; syn: ATP synthase; H_2O: water; Cyt c: cytochrome c. Figure from Ojha, Budge and Symonds (2014)……..**11**

Figure 1.6. Origins of adipose tissue development. WAT adipocyte precursors can derive from both MYF5+ and MYF5– lineages, whereas BAT adipocyte precursors derive exclusively from a MYF5+ lineage. Figure from (Peirce, Carobbio, & Vidal-Puig, 2014)……..**13**

Figure 1.7. The hypothalamic-pituitary-adrenal (HPA) axis mediates the stress response. The perception of real of presumed physical and social threats causes the activation of the hypothalamic-pituitary-adrenal

(HPA) axis. The paraventricular nucleus (PVN) in the hypothalamus releases hypothalamic neuropeptides; corticotrophin releasing hormone (CRH) and arginine vasopressin (AVP) which promote the synthesis and secretion of adrenocorticotrophin (ACTH) from the pituitary. ACTH promotes the secretion of glucocorticoids from the adrenal glands. These hormones circulate the brain and throughout the body to bind to intracellular nuclear steroid receptors. Hippocampal mineralocorticoid (MR) receptors act to the onset of stress response, whereas glucocorticoid receptors (GR) in the hippocampus, PVN and anterior pituitary, act to terminate the stress response. GCs also mediate effects in adipose tissue. Modified figure from (Raabe & Spengler, 2013)……**20**

Figure 1.8. Sympathetically stimulated BAT thermogenesis. The requirement to produce heat for the defence against regulated body temperature (thermoregulatory thermogenesis) or to combust excess energy intake (metaboregulatory thermogenesis) is coordinated in an area of the brain named the ventromedial hypothalamic nucleus (VMN). From thereon, a signal is transmitted by the sympathetic nerve fibres which innervate the individual brown adipocytes. They release the transmitter, norepinephrine (NE) which signals through ß-adrenoreceptors placed on the plasma membrane. The intracellular signal is transmitted via cAMP and protein kinase A, leading to the release from triglycerides (TG) of fatty acids (FA) that are both the acute substrate for thermogenesis and (in some form) the regulators of the activity of uncoupling protein-1 (UCP1). Combustion of the fatty acids in the respiratory chain (RC) leads to extrusion of H^+ and UCP1 thus allows for mitochondrial combustion of substrates, uncoupled from the production of ATP. The outcome is that an increased fraction of the food and the oxygen available in the blood is taken up by the tissue and combusted therein, leading to an increased heat production. Figure from (Nedergaard & Cannon, 2010)……**27**

Figure 1.9. The pathway for β-adrenergic stimulation of thermogenesis. Figure from (B Cannon & Nedergaard, 2004)……**28**

Figure 1.10. Norepinephrine-induced stimulation of thermogenesis in brown adipocytes: events downstream of the protein kinase A (PKA) activation illustrated in Figure 1.9. HSL, hormone-sensitive lipase; TG, triglyceride droplet; AcCoA, acetyl CoA. Free fatty acids (FFA) activated to acyl CoAs by acyl-CoA synthetase are first transferred to acylcarnitine by the highly expressed muscle form of carnitine palmitoyl transferase I (M-CPT I), which is the CPT I form found in both brown and white adipose tissue (205) and which is very sensitive to inhibition by malonyl CoA. The acyl-carnitine enters the mitochondria through the carnitine transporter and is reconverted to acyl CoA by CPT II. The ensuing ß-oxidation (ß-ox) of the fatty acids (acyl CoAs) as well as the activity of the citric acid cycle (CAC) lead to the formation of the reduced electron carriers FADH and NADH, which are then oxidized by the electron transport chain (respiratory chain; here indicated by the series of 3 grey boxes), ultimately

through oxygen consumption. This results in a pumping out of protons from the mitochondria and the formation of a proton-motive force that drives the protons back into the mitochondrial matrix through the uncoupling protein UCP1. The energy stored in the proton-motive force is then released as heat. Figure from Cannon and Nedergaard (2004)……**29**

Figure 1.11. The main locations of human BAT. A) thyroid/tracheal, (B), mediastinal, (C) supraclavicular, (D) parathoracical, (E) perirenal. In the infant, a kite shaped thin layer of BAT has been described (in light brown). Figure from (Enerbäck, 2010)……**31**

Figure 1.12. The adipose organ of an adult mouse kept at 28°C. Figure from (Giordano, Frontini, & Cinti, 2016)……**32**

Figure 1.13. PET-FDG scans performed in the same subject after cold exposure to 16°C and under thermoneutral conditions (21-22°C) (van Marken Lichtenbelt et al., 2009)……**39**

Figure 2.1. Schematic diagram demonstrating the setup of thermal imaging of BAT in adult humans. The suggested distance of the camera to the participant is 1m and 1m from the ground. A screen is placed behind the camera so the participant can look straight ahead to expose the supraclavicular region and to maintain a stable head and shoulder position……**54**

Figure 2.2. Thermogram output in Matlab software program. For each thermogram (displayed on the left), black and white '.png' images displaying the left and right 'region of interest' (ROI) are produced. The figure represents one participant. The pixels within each ROI comprise of the radiometric temperature data in the 10% of values and are highlighted by the red colouring in right image……**56**

Figure 2.3. Near-infrared system set up, supplied by Nonin Medical Inc. (Plymouth, Mn, USA). NIRS system comprises of a monitor, hub, signal processors and NIRS sensors to assess tissue oxygenation.

Figure 2.4. The smallest (neonatal) dual-emitter and dual-receiver probe used in the Nonin Medical Inc. Near-infrared system……**58**

Figure 2.5. Differences in regional tissue oxygen saturation (rSO_2) sensors between Nonin Medical Inc. and other companies ([Covidien (Dublin, Ireland]). Nonin rSO_2 sensors use two emitters and two detectors that are minimally affected by intervening tissue. Whereas, other sensors use one emitter and two detectors, which have a greater signal contamination from shallow tissue. Figure taken from http://www.nonin.com/equanoxtechnology……**60**

Figure 2.6. Mechanistic properties of laser doppler flow. An illustration of a laser light being directed to the tissue surface by an optic fibre and the resultant Doppler shift causes scattered light to be reflected from the tissue and transmitted by an optical fibre to a photo detector where an estimate of the blood flow can be achieved. Figure taken from http://www.moor.co.uk/ckfinder/userfiles/files/Moor_Laser_doppler_theory_Issue_1.pdf.....**62**

Figure 2.7. Determination of RNA concentration purity and integrity. The typical nucleic acid sample holds a characteristic profile. Pure nucleic acids typically yield a 260/280 ratio of ~1.8 and a 260/280 ratio of ~2.0 for DNA and RNA, respectively. Information from https://mlz-garching.de/files/nanodrop_2000_user_manual.pdf.....**68**

Figure 2.8. The process of Reverse Transcription Polymerase Chain Reaction. A primer binds to the single stranded messenger RNA (mRNA) and the sequence is elongated by the addition of complementary nucleotides by the enzyme reverse transcriptase to synthesize a complementary DNA (cDNA) strand. The double stranded cDNA is then amplified by polymerase chain reaction.....**70**

Figure 2.9. Polymerase chain reaction with Taq DNA polymerase. DNA amplification is achieved by three steps; Denaturation, in which doubled stranded DNA templates heated to 95°C denature into two separate strands; Subsequent cooling to 54°C allows for annealing, in which primers hybridise to the complementary DNA strands; Reheating the sample mixture to 72□C allows for extension, in which Taq DNA polymerase extends the 3′ end of each primer along the template strands. The cycle is repeated 'n' number of times to produce 2^n number of cDNA strands.....**73**

Figure 2.10. The sigmoidal curves in Q-PCR. Fluorescent signal crosses threshold and increases exponentially until plateau from expenditure of reagents or cycle number. Red lines represent external standards, green are unknown samples and blue represent negative controls.....**75**

Figure 2.11. The standard curve. A standard curve produced from Q-PCR. A linear graph of exponential polymerase chain reaction is produced by plotting the cycle number at a cycle threshold against the logarithm of the known dilution series. Standard dilutions are created by using duplicated ten-fold serial dilutions of purified template of the target cDNA. The assays have a six log linear dynamic range from 10^{-2} to 10^{-7} copies of the template cDNA.....**76**

Figure 2.12. A typical melt curve produced as a result of Q-PCR. The single peak indicates specificity of product amplified.....**77**

Figure 2.13. Agarose gel from UCP1 and PRDM16 genes.....**84**

Figure 3.1. An illustrated overview of the experimental study design for Chapter 3 (n=8)……**95**

Figure 3.2. Plasma cortisol concentrations following saline infusion or hydrocortisone infusion at baseline and during an isoprenaline infusion (ISO, dotted lines indicate infusion period) in healthy male subjects (n=8). Data are shown as mean ± standard error of mean. *p < 0.05 vs. control……**102**

Figure 3.3. Non-esterified fatty acid concentrations (NEFA) following saline infusion or hydrocortisone infusion at baseline and during an isoprenaline infusion (ISO, dotted lines indicate infusion period) in healthy male subjects (n=8). Values are mean ± standard error of mean. *p < 0.05 vs. control, †p < 0.05 vs. baseline……**102**

Figure 3.4. Glucose (A) and insulin (B) concentrations following saline infusion or hydrocortisone infusion at baseline and during an isoprenaline infusion (ISO, dotted lines indicate infusion period) in healthy male subjects (n=8). Values are mean ± standard error of mean. *p < 0.05 vs. control, †p < 0.05 vs. baseline……**103**

Figure 3.5. Delta change in systemic metabolites; insulin (A) and C-peptide (B) during basal and isoprenaline stimulated conditions, after an overnight infusion of saline or hydrocortisone (n=8). Values are mean ± standard error of mean. *p<0.05 vs. saline……**105**

Figure 3.6. Whole body energy expenditure under saline conditions and following an overnight infusion of hydrocortisone, at baseline and after isoprenaline infusion (maximal) in 8 adult male subjects. Data are shown as mean ± standard deviation**.** *$p \leq 0.05$ compared to basal control. ##$p \leq 0.05$ compared to basal hydrocortisone. Energy expenditure calculated based on heart rate, age and weight using the equation as previously described by Keytel et al, 2005: EE = gender x (-55.0969 + 0.6309 x heart rate + 0.1988 x weight + 0.2017 x age) + (1 - gender) x (-20.4022 + 0.4472 x heartrate - 0.1263 x weight + 0.074 x age)……**106**

Figure 3.7. Supraclavicular BAT temperature responses at baseline following saline or hydrocortisone infusion in healthy males (n=8). All responses were greater upon hypercortisolaemia. Values are mean ± standard error of mean. *p < 0.05 vs. control……**107**

Figure 3.8. Core temperature responses at baseline following saline or hydrocortisone infusion in 8 healthy adult males. Values are mean ± standard error of mean. *p < 0.05 vs. control……**107**

Figure 3.9. Basal cardiovascular responses following saline or hydrocortisone infusion in 8 male subjects. Values are means ± standard error of mean. sys, systolic; dia, diastolic blood pressure (BP); HR, Heart Rate……**108**

Figure 3.10. The thermogenic responses of brown adipose tissue. Supraclavicular temperature (T_{SCR}) and a non-adipose tissue reference point (T_{REF}) following saline infusion (A) or hydrocortisone infusion (B) during and post isoprenaline stimulation (ISO, dotted lines indicate infusion period) in 8 healthy adult males. Supraclavicular temperature (T_{SCR}; open circles), Reference temperature (T_{REF}; green squares). Values are mean ± standard error of mean. *p < 0.05 vs. Control, †p < 0.05 vs. baseline……**110**

Figure 3.11. Individual basal and maximal T_{SCR} responses during isoprenaline infusion following an overnight infusion of saline (A) or hydrocortisone (B) in eight healthy male subjects. *p < 0.05 vs. baseline……**111**

Figure 3.12. Individual maximal supraclavicular skin temperatures during isoprenaline infusion following an overnight infusion of saline or hydrocortisone in eight healthy adult male subjects. Values are mean ± standard error of mean. *p < 0.05 vs. control……**112**

Figure 3.13. Delta change in supraclavicular temperature during isoprenaline infusion after an overnight infusion of saline or hydrocortisone in 8 healthy adult male subjects. Values are mean ± standard deviation. *p < 0.05 vs. supraclavicular temperature, #p < 0.05 vs. Saline T_{REF}……**113**

Figure 3.14. Mean basal and maximal skin temperature responses to isoprenaline during saline and hydrocortisone infusions, using skin contact temperature sensors placed over the supraclavicular BAT region (n=8). Values are mean ± standard deviation. *p <0.05 vs. baseline……**113**

Figure 3.15. Individual maximal core temperature responses during isoprenaline infusion following an overnight infusion of saline or hydrocortisone (n=8). Data are shown as mean ± standard error of mean ……**114**

Figure 3.16. Basal and maximal heart rate (A) and blood pressure (B) responses during isoprenaline infusion in control and hydrocortisone conditions (n=8). Values are mean ± standard error of mean. *p <0.05 compared to baseline……**115**

Figure 3.17. Thermogenic (A) and core temperature (B) responses of ingesting a single calorie controlled meal in healthy adult males (n=8). Meal was ingested at time point '0'. Pre, pre-ingestion; Post, post-prandial; Supraclavicular temperature (T_{SCR}); Reference temperature (T_{REF}). Values are mean ± standard deviation. *p <0.05 compared to pre-ingestion. #p <0.05 compared to T_{SCR}……**116**

Figure 4.1. Study assessment protocols for the assessment of brown adipose tissue activation in healthy adults Chapter 4. Protocols of the

assessments conducted prior to and after cooling in study A and the refinements added to study B. During the single study visit, BAT heat production was measured based on IR thermography imaging (IRT) of the SCR region, alongside the continuous assessment of blood flow (NIRS and LD) in this region, prior to, during and post- a 15-minute cold-exposure intervention. IRT Imaging was captured at 2 images per minute during resting pre-stimulatory and post-stimulatory periods and at 4 images per minute during cold-stimulation. Vascular assessments were continuously recorded throughout the study visit……**130**

Figure 4.2a. Experimental set up for study A, Chapter 4. Each subject received the same placement of sensors. NIRS sensors measured oxygenation of BAT and of a non-adipose tissue site; deltoid muscle (Ref). A single LD sensor which measured dermal blood flow was placed next to the BAT NIRS sensor in the SCR region. Cold-stimulated (16°C) heat production in the SCR region was assessed by IRT prior to, during and post the cooling challenge……**131**

Figure 4.2b. Experimental set up for study B, Chapter 4. In study B, the addition of the following sensors (highlighted in the red boxes) included; skin temperature sensors which were placed on the on the forearm being cooled and in the SCR region and; a NIRS sensor, placed on the forearm receiving cold-stimulation in order to assess oxygenation during presumed vasoconstriction. Cold-stimulated (16°C) heat production in the SCR region was assessed by IRT prior to, during and post the cooling challenge……**132**

Figure 4.3. Cold-induced thermogenic responses, assessed by IRT Mean ± standard deviation BAT thermogenic responses to cold-exposure (white circles) compared to a non-adipose tissue reference region (T_{REF}) (A) and mean values of T_{SCR} at resting (grey circles) vs. maximal thermogenic responses (black circles) during cold-stimulation (B). Asterisk (*) denotes a significant difference compared to resting T_{SCR} ($P < 0.05$). Hashtag (*#*) denotes a significant difference compared to a non-adipose tissue reference region at that time-point ($P < 0.05$)……**141**

Figure 4.4. Cold-stimulated SNS responses to cold-stimulation Acute sympathetic nervous system responses to 15 minutes of cold-exposure in 15 subjects in study A; (A) Heart rate (B) Blood pressure and (C) Core temperature. Asterisk (*) denotes a significant difference compared to resting ($P < 0.05$). SBP, systolic blood pressure; DBP, diastolic blood pressure. Data are shown as mean ± standard deviation. *$p < 0.05$ vs. resting……**142**

Figure 4.5. Anterior thermal images of the neck and upper thorax. Representative example of thermograms of the skin overlying the ROI located at the SCR (black triangle) and sternal (blue circular reference region) in the same individual at resting (A) and during cold-stimulation at 16°C for 15-minutes (B)……**143**

Figure 4.6. Localised tissue oxygen saturations upon cold-stimulation
Cold-induced stimulation of mean (± standard deviation) BAT SCR oxygenation values, over the SCR region (white circles) compared to over a non-adipose tissue reference site (Ref; black squares) (A) and mean values of SCR temperature at resting (grey circles) vs. maximal tissue oxygenation responses over the SCR region (black circles) during cold-stimulation (B). Asterisk (*) denotes a significant difference compared to resting SCR oxygenation ($P < 0.05$)..... **144**

Figure 4.7. Cold-stimulated blood flow over SCR region
Mean (± standard deviation) change in blood perfusion over the SCR region in response to 15 minutes of cold-insult to the forearm in 15 subjects in study A. Asterisk (*) denotes a significant difference compared to resting SCR oxygenation ($P < 0.05$).....**145**

Figure 4.8. Cold-stimulated responses during cold-stimulation
Mean (± standard deviation) changes from resting (time point '0') every minute during cold-stimulation of the forearm only, in 15 participants; BAT thermogenic responses (T_{SCR}; orange triangles; right axis); SCR tissue oxygenation (StO_2; blue circles; left axis); and SCR blood flow (BF; grey squares; left axis) (n=15). **145**

Figure 4.9. Maximal tissue oxygenation responses relative to peak BAT heat production during forearm cold-stimulation
Individual maximal tissue oxygenation (StO_2) responses and SCR skin temperature responses (T_{SCR}) to cold stimulation. The greatest increments StO_2 occur precede maximal BAT thermogenesis in all subjects (n=15) **146**

Figure 4.10. Cold- stimulated thermogenic responses, assessed by IRT
Mean (± standard deviation) BAT thermogenic responses to cold-exposure (white circles) compared to a non-adipose tissue reference region (T_{REF}) (A) and mean values of T_{SCR} at resting (grey circles) vs. maximal thermogenic responses (black circles) during cold-stimulation (B). Asterisk (*) denotes a significant difference compared to resting T_{SCR} ($P < 0.05$). Hashtag (#) denotes a significant difference compared to a non-adipose tissue reference region at that time-point ($P < 0.05$).....**148**

Figure 4.11. Cold-stimulated SNS responses to cold-stimulation
Mean (± standard deviation) sympathetic nervous system responses to 15 minutes of cold-exposure in 9 subjects in study B; (A) Heart rate ($P = 0.003$) (B) Blood pressure ($P = 0.001$) and (C) Core temperature ($P = 0.001$). Asterisk (*) denotes a significant difference compared to resting ($P < 0.05$). SBP, systolic blood pressure; DBP, diastolic blood pressure.....**149**

Figure 4.12. Cold-stimulated skin temperatures over SCR and peripheral regions
Gradient of skin temperature change between the skin temperature sensor placed over the SCR BAT region (BAT_{SK}) and the peripheral skin temperature sensor placed over the cooled forearm prior to, during and post-cold stimulation in the 9 subjects participating in study B. Asterisk (*) denotes a significant difference between BAT_{SK} and $Peripheral_{SK}$ temperatures ($P < 0.05$). Data are shown as mean ± standard error of mean.....**150**

Figure 4.13. Oxygen saturation of the cooled site during cold-stimulation
Mean (± standard deviation) change in peripheral oxygenation over the forearm receiving the cooling stimulus in the 9 subjects in study B. Asterisk (*) denotes a significant difference compared to resting SCR oxygenation ($P = 0.001$).....**150**

Figure 4.14. Oxygen saturations of the SCR region upon cold-stimulation
Cold-induced stimulation of mean BAT SCR oxygenation values, over the SCR region (white circles) compared to over a non-adipose tissue reference site (REF; black squares) (A) and mean values of SCR temperature at resting (grey circles) vs. maximal tissue oxygenation responses over the SCR region (black circles) during cold-stimulation (B). Values are shown as mean ± standard deviation. Asterisk (*) denotes a significant difference compared to resting SCR oxygenation ($P<0.05$) **151**

Figure 4.15. Cold-stimulated oxygen saturation over the forearm
Mean (± standard deviation) change in oxygenation in response to 15 minutes of cold-insult to the forearm in 9 subjects in study B. Asterisk (*) denotes a significant difference compared to resting SCR oxygenation ($P < 0.05$).....**152**

Figure 4.16. Cold-stimulated responses during cold-stimulation
Mean (± standard deviation) changes from resting (time point '0') every minute during cold-stimulation of the forearm only, in 9 subjects in study B; BAT thermogenic responses (T_{SCR}; orange triangles; right axis); SCR tissue oxygenation (StO_2; blue circles; left axis); and SCR blood flow (BF; grey squares; left axis) (n=9).....**152**

Figure 4.17. Maximal tissue oxygenation responses relative to peak BAT heat production in 9 healthy adult subjects during cold-stimulation
Individual maximal tissue oxygenation (StO_2) responses and SCR skin temperature responses (T_{SCR}) to cold stimulation. The greatest increments StO_2 occur precede maximal BAT thermogenesis in 7 of 9 subjects.....**153**

Figure 4.18. SCR skin temperature responses between study A and study B. Intra-subject differences demonstrated no significant difference

in mean resting TSCR (A) and maximal change from resting between studies (B)…… ……..**154**

Figure 4.19. SCR tissue oxygenation responses to forearm cold stimulation between study A and study B
Intra-subject differences demonstrated no significant difference in mean resting StO_2 (A) and maximal change from resting between ……**156**

Figure 4.20. SCR blood flow responses to forearm cold-stimulation between study A and study B
Intra-subject differences demonstrated no significant difference in the magnitude of change in blood flow from resting between studies ……**157**

Figure 4.21. Summary diagram of cold-induced sympathetic stimulation of BAT thermogenesis in healthy, lean adults, as assessed by IRT/NIRS and LD. NE – Norepinephrine; POA - preoptic area. Blue circle is reference region for IRT analysis. Left, black triangle is ROI for IRT imaging analysis of participant's right supraclavicular (SCR) region. Right black circle provides a mechanistic view of beneath SCR region, once stimulated……..**170**

Figure 5.1. Identification of BAT deposits in the newborn using MRI. A single water-fat separated MRI scan of the neonatal back, demonstrates bilateral BAT deposits in the subscapular and spinal regions. Image taken from (Rasmussen et al., 2013). Fat- and water-based images of 22 neonates were acquired during natural sleep and the ratios of fat to the combined signal from fat and water (fat signal fraction) were calculated to quantify BAT……..**172**

Figure 5.2. The initial thermal imaging platform used for the detection of heatspots over brown fat deposits, in clinically stable infants. Infants in phase 1 (n=9), were laid down onto an open resuscitaire (Drager Medical, Telford, PA) (A) with an overhead radiant heater rotated to a 45° angle (B)……**177**

Figure 5.3. A developed imaging protocol used in phase 2 for the detection of heatspots over brown fat deposits, in clinically stable infants. Infants in phase 2 (n=6), were imaged at a height of 40cm above the infant, whilst laid in a babytherm cot, with an attachable heat retaining lid……..**178**

Figure 5.4. An 'overhead shot' of the infant back whilst laid in a prone position. IRT imaging from above the infant, laid on a mattress of a resuscitaire or cot……..**181**

Figure 5.5. Initial analysis method of IRT thermograms taken of the interscapular BAT region in healthy newborns
An example neonatal image (A) captured in the prone position, with the corresponding thermogram (B) demonstrating the grid analysis created in

phase 1. Spot measurements labelled El2 and El5 correspond to regions of the skin that overlay the interscapular BAT depot. The red and blue triangles represent areas of the hottest and coolest data points in each ROI (n=6)……**183**

Figure 5.6. Improvement in the grid analysis method for phase 2. A neonatal JPEG image (A) captured in the prone position, with the corresponding thermogram (B) demonstrating a squared grid analysis method for phase 2, which enabled a greater amount of the back to be analysed. Spot measurements labelled Bx2 and Bx5 correspond to regions of the skin that overlay the interscapular BAT depot. The red and blue triangles represent areas of the hottest and coolest data points in each ROI (n=6)……**184**

Figure 5.7. Recruitment statistics into phase 1 and phase 2 of the study. Enrolment into phase 1 resulted in an original cohort of 9 subjects, of which 3 subjects were excluded, leaving 6 subjects (3 males: 3 females) as the final study cohort for phase 1. Six subjects (4 males: 2 females) enrolled into phase 2 and retained a core temperature of above 36.5°C, all completing the study……**186**

Figure 5.8. Representative examples of excluded thermograms from phase. Distorted thermograms from two infants, which could not be analysed due to reflective heat on the surface of the skin from the overhead radiant heater (A) and a neonate laid in a curled fetal position (B)……**189**

Figure 5.9. The visual observation of hotter areas of the back corresponding to the interscapular and spinal regions (white heat) in a single thermogram captured in phase 1……**190**

Figure 5.10. Interscapular skin temperatures of thermograms analysed in phase 1, immediately upon the removal of clothing (T0, n=18) and after an hour of exposure to room temperature (25.5°C) (n=17)
Data are shown as mean ± standard deviation. Asterisk denotes a significant difference over time ($P \leq 0.001$). ……**191**

Figure 5.11. Neonatal skin temperature of the lower back as assessed by a single skin temperature probe
Skin temperature was assessed using a thermal probe after a 10-minute acclimation period at time point '0' and at 60 minutes after an hour of exposure to room temperature (25.5°C) (n=6). Data are shown as mean ± standard deviation. * denotes a significant difference over time ($P < 0.05$)……**192**

Figure 5.12. Neonatal core temperatures immediately upon the removal of clothing (time point '0') and after an hour of exposure to room temperature (25.5°C) (n=6)
No significant change was observed over the study period of an hour. Data are shown as mean ± standard deviation ($P \leq 0.05$)……**192**

Figure 5.13. Application of the grid analysis method to the thermogram initially captured as a JPEG image. An example image of a newborn laying in the prone position (A) and the corresponding neonatal thermogram (B). Interscapular temperature (C) (Box Bx2), was greater than the temperature over a reference region (small circle located on the lower right side), with no brown adipose tissue deposits (P = 0.004)……..**194**

Figure 5.14. Mean skin temperatures of the scapular region at time point '0' in the 17 analysed thermograms
At T0 skin temperatures of the left subscapular (A), interscapular (B) and right subscapular (C) regions were significantly greater than the reference region in the lower right side of the infant back. * $P \leq 0.05$. Left Subscap, left subscapular; Interscap, interscapular; Right Subscap, right subscapular……**196**

Figure 5.15. Maximal temperatures at T60 over the scapular region of the infant back
After an hour of exposure to room temperature (25°C), 11 of the 23 thermograms, demonstrated the hottest area of the back overlaid the interscapular region. * $P \leq 0.05$. Left Subscap, left subscapular; Interscap, interscapular; Right Subscap, right subscapular. Data are shown as mean ± standard deviation……**197**

Figure 5.16. Reference temperatures of the neonatal back upon initial removal of clothing (T0) and after an hour of exposure to room temperature (25°C)
No observed difference in reference temperatures overlying a region where there are no known brown adipose deposits between T0 (17 thermograms) and T60 (23 thermograms). Data are shown as mean ± standard error of mean. ($P \leq 0.05$)……**198**

Figure 5.17. Mean skin temperatures of the scapular region throughout the duration of study, from time point '0' (T0) in (17 thermograms), to T60 (23 thermograms)
Skin temperatures of the left subscapular (A), interscapular (B) and right subscapular (C) regions did not significantly differ upon an hour exposure to room temperature (25°C). Left subscap, left subscapular; Interscap, interscapular; Right subscap, right subscapular. Data are shown as mean ± standard error of mean……**199**

Figure 5.18. Representative example of scattered heatspots. An example thermogram demonstrating scattered heat spots observed over the subscapular and interscapular regions……**200**

Figure 5.19. Neonatal skin temperatures of the lower back assessed by a skin temperature probe during two periods separated by 60 minutes, whereby the infant was laid on their abdomen (n=6)

Significant increases in skin temperatures were observed after 40 minutes of exposure to room temperature (25°C). Data are shown as mean ± standard deviation. *p < 0.05 vs. baseline.....**201**

Figure 5.20. Neonatal core temperatures at baseline (time point '0') and after an hour of exposure to room temperature (25°C) (n=6)
The exposure to room temperature (25°C) for 60 minutes, had no effect on core temperature in the six clinically stable infants. Data are shown as mean ± standard deviation.....**202**

Figure 5.21. Summary of the assessment of skin temperatures performed over the back region of full-term infants in phase 1 (n=6) (A) and phase 2 (n=6) (B).....**213**

Figure 6.1. Experimental design of Chapter 6. Forty-eight female pups were born to 6 dams. Upon randomisation in to cohorts (7 or 21 PND), one pup per dam per treatment was taken and entered into the study. PND, postnatal day.....**219**

Figure 6.2. Vibration platform used to induce acute stress. A personalised vibration box was developed and comprised of four individual compartments, each could hold a single rat pup. All compartments contained a small amount of nesting material taken from the varying dams cages....**221**

Figure 6.3. Expression stability of reference genes. The cycle threshold (C_t) values of TBP and B2m remained stable across samples.....**223**

Figure 6.4. Influence of WBV on body weight (BW) and Interscapular BAT weight (Interscap BAT) at PND 7 and 21
Age increased body weight (A) and BAT weight (B). There was a strong correlation between interscap BAT weight and BW (C). Values are mean ± SD, *P <0.05. Ctrl, control; WBV, whole body vibration. PND 7; ctrl n=4, wbv n=4; PND 21; ctrl n=5, wbv n=4. Data are shown as mean ± standard deviation. *p < 0.05 vs. control.....**225**

Figure 6.5. Corticosterone plasma levels in control and WBV groups at PND 7 and PND 21
Trunk blood was collected after decapitation between 9:00 and 11:00 am. Data are mean ± 95% confidence interval. (4–5 pups per group). (*) denotes a significant difference with age (P <0.05). (#) denotes a significant difference compared to control group (P <0.05). Ctrl, Control; WBV, whole-body vibration.....**226**

Figure 6.6. Effect of whole body vibration (WBV, black squares) on the mRNA expression of selected BAT adipogenic and molecular genes at postnatal days 7 and 21, compared to control (Ctrl, white circles)
Values are mean ± standard deviation. Significance set at P < 0.05. (#) denotes a significant difference with age; (*) denotes a significant difference

in response to WBV. postnatal day; UCP1, uncoupling protein 1; PRDM16, PR domain containing 16; ADRB3**,** beta-3 (β3)-adrenoreceptor; FGF21, fibroblast growth factor 21; PPARγ, peroxisome proliferator-activated receptor gamma**;** 11β-HSD1, 11-Beta-dehydrocorticosterone 1……..**228**

Figure 6.7. Early life stress-induced effects on HPA axis regulation and BAT characteristics in rodents. Early life stress induced by WBV at PND 7 was not shown to increase the stress-hormone corticosterone, or mediate alterations in BAT genes, due to the protective effects of the stress-hyporesponsive period in the first two weeks of life. At PND 21, WBV increased corticosterone concentrations, which was associated with elevations in mRNA expression of its activating enzyme; 11β-HSD1, in BAT. WBV induced at this age, also demonstrated to reduce mRNA expression of transcription factors PRDM16 and PPARγ, with no effects on UCP1 or the β3-AR through with its acts. Mechanisms driving the reductions in BAT genes have been directed towards dysfunction of the HPA axis resulting in the elevation of the 11β-HSD1 enzyme. Although further studies are required to investigate the effects of WBV stress in early life on HPA axis functionality; concentrations of CRH and ATCH, as well as the subsequent downstream effects on 11β-HSD1 and BAT genes. Observations demonstrated from the current study are in yellow boxes. Observations from published studies of early life stress effects in adult rodents, are in green boxes. Figure modified from (Yau & Seckl, 2012)……..**245**

List of tables

Table 2.1. Major differences in the acquisition of thermograms between adults and healthy newborns 57

Table 2.2. General parameter guidelines for optimal polymerase chain reaction primer design (Dieffenbach et al, 1993)....74

Table 2.3. PCR primer sequences and TaqMan probe identification numbers for rodent investigation....80

Table 2.4. Classical PCR reaction mix....81

Table 2.5. Hot Start PCR programme conditions. Second phase of the program repeats for 35 cycles....**82**

Table 2.6. Q-PCR reaction mixture....85

Table 2.7. Q-PCR programme conditions....86

Table 2.8. PCR reaction mix....87

Table 2.9. Concentrations of corticosterone for standards....89

Table 3.1. Inclusion and exclusion criteria to the study (n=8)....93

Table 3.2. Anthropometric and metabolic characteristics of male adult participants entered into the study (n=8)....99

Table 3.3. Indoor and outdoor environmental temperatures between participants throughout the study, prior to and after saline (A) and hydrocortisone (B) infusions. Environmental outdoor temperature; data obtained from the Meteorological office based on temperatures in Birmingham, UK for each study day (metoffice.gov.uk, 2015). Date of study represents the evening of which participants began study....**100**

Table 3.4. Anthropometric and metabolic characteristics of adult male participants entered into the study (n=8)....104

Table 4.1. The time of year in relation to the outside environmental temperature for each individual participating in study A (*n* = 15) and study B (*n* = 9)....138

Table 4.2. Characteristics of study subjects....138

Table 4.3. Intra-subject comparisons of resting T_{SCR} and its magnitude of change (n=9) 155

Table 5.1. Anthropometric and demographic characteristics of infants enrolled into phase 1 and phase 2 of the study in Chapter 5...187

Table 5.2. Environmental room temperatures for phase 1 and phase 2 of the study in Chapter 5……**188**

Table 5.3. Exclusion criteria for thermograms which could not be analysed……**189**

Table 6.1. Expression stability of reference gene pairings. The most stable pairing of reference genes was TBP:B2m (M = 0.25)……**225**

Chapter 1

Introduction

My thesis investigates how acute conditions of elevated cortisol concentrations regulate BAT in adults and rodents. My thesis also addresses the potential of radiation-free technologies to assess BAT function in early postnatal life and during adulthood. This chapter will review and discuss experimental literature surrounding the effects of cortisol on metabolism and adipose tissue and the ontogeny and characteristics of BAT, highlighting disparities across studies and the current limits preceding the potential to assessing BAT function in humans.

1.1 Obesity

1.1.1 Definition

Obesity is a multifactorial disorder of energy balance, defined by a greater energy intake than expenditure, resulting in excess body fat accumulation (Jebb, 1996). Although there is no universal definition of "healthy weight", the World Health Organisation (WHO) expert committee has proposed a classification of overweight and obese using body mass index (BMI) (WHO (2016).

BMI is calculated using the following equation:

$$\frac{mass\ (kg)}{height\ (m)^2}$$

According to this widely accepted classification system, an individual with a BMI between the range of 25 kg/m^2 to 29.9 kg/m^2 is defined as overweight, whilst a BMI equal to or more than 30 kg/m^2 is classified as obese. Although BMI is the internationally recognised index of obesity (WHO, 1997), the measure is regarded an assessment tool for disease risk (Stevens et al, 1998) and fails to assess the distribution of body fat (Wei et al, 1997). Alternative body composition measures such as waist-to-hip ratio (WHR) or waist circumference (WC) have been demonstrated to be better predictors of metabolic health compared to that of BMI (Pi-Sunyer, 2000; Wei et al, 1997). The importance of these measures cannot be overstated, given that individuals with a high proportion of abdominal fat have greater risks for developing diabetes (Seidell et al, 1997) and cardiovascular disease (Dipietro et al, 1999). Waist circumference measures have been recommended as better indicators of abdominal obesity compared to BMI and a better predictor for cardiovascular disease than either BMI or waist-to-hip ratio (Stevens et al, 1998; WHO, 2017).

1.1.2 Global estimate of obesity prevalence

The overwhelming increase in the prevalence of overweight and obese individuals in recent years represents one of the greatest threats to public health in the developing world (Ebbeling, 2002). With the adoption of a "western lifestyle", involving decreased physical activity and the overconsumption of energy-dense food, the WHO estimated that in 2014 more than 1.9 billion adults worldwide, aged 18 years and older, were overweight. Of these, 600 million were classed as clinically obese, more than double that since 1980 (WHO, 2016). In England alone, just over a quarter of adults (26%) are classified as clinically obese, an increase of 13% since 1993 (Health and Social Care Information Centre, 2015). Similar trends are seen in other western countries with the prevalence of obesity in Europe having risen three-fold in the last two decades (WHO, 2016). Alarmingly, the WHO have projected that by the year 2030, levels of obesity could be as high as 50-80% in the USA, between 30-40% in England and

over 20% in some developing countries (Ahmad, Ahmad & Ahmad, 2010; WHO, 2016).

Similar to the trend in adults, of concern, is the current rising epidemic of obesity amongst children (WHO, 2016). In 2011, an estimated 170 million children (aged 18 years and younger), worldwide, were classified as overweight or obese. This estimate has increased from 4.2% in 1980 to 6.7% in 2010 and includes more than 25% of all children in some countries, more than double the proportions from the start of the epidemic (De Onis, Blössner & Borghi, 2010; Swinburn et al, 2011).

Current UK data from The National Child Measurement Programme (NCMP), which measures the height and weight of around one million school children in England per year, estimates that 31% of girls and 32% of boys were classed as clinically overweight or obese in 2014 (Public Health England, 2016). Statistics from the NCMP in 2016, indicate that compared to the school year 2006-2007, children are entering reception class weighing less but are leaving primary school weighing more (Figure 1.1). In 2015, at the end of the school year, 9.6% of boys and 9.0% of girls in Reception (aged 4-5 years) and 21.7% of boys and 17.9% of girls in Year 6 (aged 10-11 years), were classified as obese (BMI ≥ 95th centile of the British 1990 (UK90) growth reference) (Public Health England, 2016).

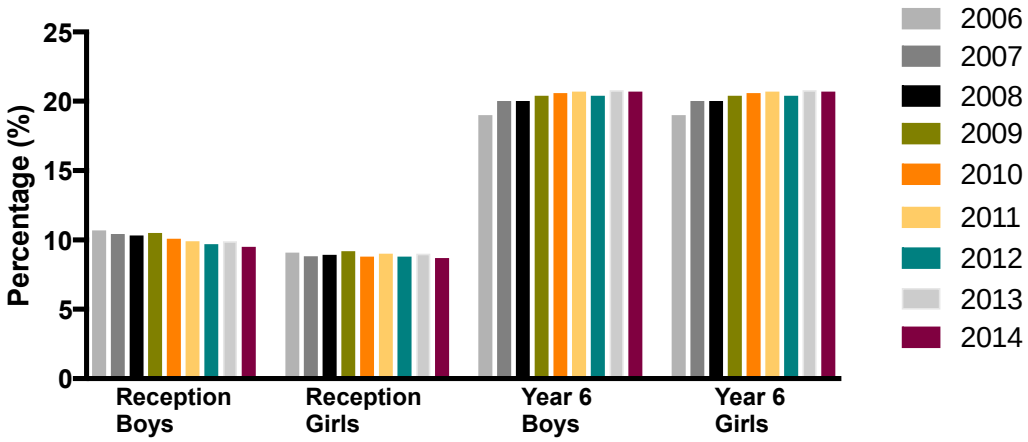

Figure 1.1. The growing prevalence of childhood obesity (%) in Britain. Children were classified as obese based on a BMI ≥95th centile of the British 1990 (UK90) growth reference. Adapted from Chief Medical Officer's Report 2012 (data source Public Health England; PHE) (CMO, 2012).

1.1.3 Complications of excess adiposity

Fatal consequences may arise from the development of excess adiposity. In both adults and children, obesity can result in chronic inflammation, hypertension, hyperinsulinemia, endothelial dysfunction and dyslipidemia (Srinivasan, 2002; Tounian, 2001). In 2001, this clustering of cardiovascular disease (CVD) risk factors became known as the metabolic syndrome (Young-Hyman, 2001); defined as the co-existence of 3 or more of the following 5 abnormalities; a blood pressure of >130/85mmHg; blood serum triglyceride level of >1.5g/L; serum cholesterol (LDL) of >0.4g/L [male], or >0.5g/L [female]; abdominal circumference of >102cm [male] or >88cm [female]; and an impaired fasting blood glucose of >1.1g/L or >6.1mmol/L) (Reaven, 1988) and has been identified in children as young as 5 years of age (Young-Hyman, 2001). Overweight and obese individuals with the metabolic syndrome, have an elevated risk of premature mortality and obesity related morbidities during adulthood, such as type 2 diabetes, coronary heart disease, stroke and myocardial infarction (Poirier et al, 2006). During a 20-year follow-up study, Hoffmans and colleagues observed that the risk of death in adolescents (>18 years of age) with a BMI of >25 kg/m^2, was doubled compared to adolescents with a BMI of <25 kg/m^2 (Hoffmans, Kromhout & de Lezenne Coulander, 1988). Thus, even modest weight reduction may significantly help to reduce the risk of these serious health conditions.

1.2 Brown Adipose Tissue (BAT)

1.2.1 Biological relevance of BAT

Over the past decade, through its promising role in the regulation of body weight, brown adipose tissue (BAT) has emerged as a potential therapeutic target to combat childhood and adult obesity.

The original discovery and identification of BAT was by a Swiss naturalist, Conrad Gessner, some 400 years ago in an alpine marmot (Gessner, 1551).

However, it wasn't until the twentieth century that BAT was regarded as a distinct tissue and its thermogenic capacity realised (Smith, 1961). Since this observation, the finding of a distinct marker, uncoupling protein-1 (UCP1), as the mitochondrial protein responsible for BAT's unique function of heat dissipation has been made (Nicholls, Bernson, & Heaton, 1978). Subsequently, BAT has been found to play a plausible role in the regulation of body weight in rodents through cold- and possibly diet-induced thermogenesis (Lowell et al, 1993). Until recently, it was thought that BAT was lost during the newborn period, however, its rediscovery in 2009 due to cold exposure studies using Positron Emission Tomography-Computed Tomography (PET-CT) imaging, revealed functional BAT in humans, and confirmed the presence of increased levels of UCP1 in this tissue (Cypess et al, 2009; Saito et al, 2009; van Marken Lichtenbelt et al, 2009; Virtanen et al, 2009). Since the process of 'uncoupling' dissipates metabolic energy, there has been interest in defining its contribution to energy expenditure. As such, if we could find a way to stimulate BAT uncoupling to an extent which could influence body weight, there may be a potential to reduce the risk of developing obesity (Nedergaard, Bengtsson & Cannon, 2007).

1.2.2 The metabolic significance of BAT in humans

The recent illustration by van Marken Lichtenbelt et al (2009) that BAT is present in a cohort of adult males, provides evidence for its metabolic contribution to energy expenditure in adulthood and therefore may play a vital part in the development of obesity (van Marken Lichtenbelt et al, 2009). Energy expenditure (EE) comprises of 3 major components. Of the total energy expenditure (TEE), 5-10% of energy is required for digestion and metabolism of ingested food, up to 60% of TEE is required for the body's resting EE, energy required for compulsory cellular and organ functions, such as breathing and maintaining the ionic gradients across cell membranes. The remaining energy expenditure refers to energy required for adaptive thermogenesis for the production of heat in response to

changes in environmental temperature (i.e. cold- and diet-induced thermogenesis; CIT and DIT). Large inter-individual differences in resting EE, DIT and CIT occur in humans (van Marken Lichtenbelt et al, 2002), with DIT being lower and CIT being impaired in obese individuals (Wijers, Saris & Lichtenbelt, 2010). The efficiency of adaptive thermogenesis may therefore relate to the susceptibility to obesity. In small mammals, defective BAT function has been associated with increased fat mass (Hamann, Flier, & Lowell, 1996). In adult humans, BAT volume reduces with increasing BMI and adiposity (Vijgen et al, 2012), however, whether this is of cause or consequence remains to be fully established. The exact contribution of BAT to daily heat production is also unclear. Ouellet and colleagues (2012), claimed that in humans, approximately 60g of BAT, if maximally stimulated, may contribute up to 20% of daily energy expenditure, which would sufficiently impact energy balance (Ouellet et al, 2012). Despite such claims, human civilisation surrounds itself in an environment of thermal comfort, thus humans are rarely exposed to long periods of temperatures below thermo-neutrality (22°C) (Johnson et al, 2011). At this ambient temperature, less than 10% of humans undergoing PET scanning have detectable BAT activity (Lee et al, 2010). Such an environment may contribute to a poor metabolic profile compared to BAT positive individuals, pushing energy balance to a more positive state (Orava et al, 2011; Yoneshiro et al, 2011).

1.2.3 Characteristics of BAT

1.2.3.1 Tissue Characteristics

White adipose tissue (WAT) has traditionally been viewed as a passive store of energy and is now considered to be the body's largest endocrine organ (Greenberg & Obin, 2006), regulating an array of physiological processes through the secretion of cytokines, adipokines, peptides and growth factors. In contrast, BAT is characterised by the presence of the thermogenic mitochondrial uncoupling protein, UCP1 (Figure 2) and acts

to dissipate energy by producing heat; a functionally important tool for the regulation of heat production at birth (Frontini & Cinti, 2010).

Brown and white adipocytes are characterised by large intracellular stores of fat but are otherwise unlike in embryological origin, structure and/or function**.** The amount and distribution of mammalian adipose tissue varies between individuals according to the depot, individual age and gender, environmental and nutritional conditions (Symonds, 2013) and is generally located either subcutaneously, beneath the skin, or viscerally, around the internal organs.

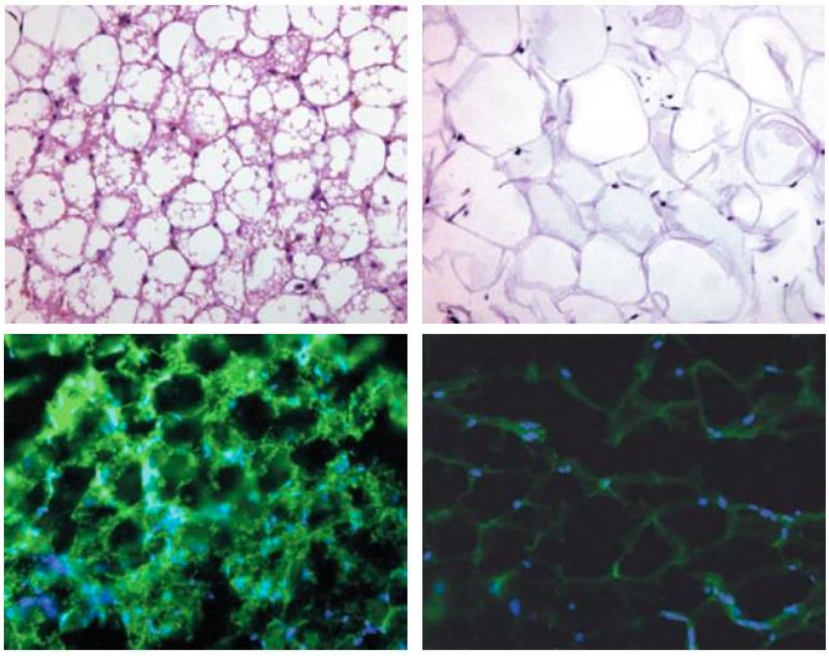

Figure 1.2. Specimens of brown and white adipose tissue from the supraclavicular region in a 46-year-old female. Top panel; Specimens stained with haematoxylin and eosin show characteristic features; BAT, granular cytoplasm containing mitochondria and multiple fat vacuoles, and WAT, a single large lipid vacuole in each white fat cell. Lower panel; Specimens stained for UCP1 using immunofluorescence assay, together with the nuclei-staining dye 4',6-diamidino-2-phenylindole, shows positive immunostaining for UCP1 (green) in BAT, but not WAT specimens. Figure from (van Marken Lichtenbelt et al, 2009).

BAT was originally identified on the grounds of its colour. This adipose tissue is brown as a result of its high vascularity and cytochrome content, reflecting high mitochondrial density, as compared to that of white adipocytes (Figure 1.3).

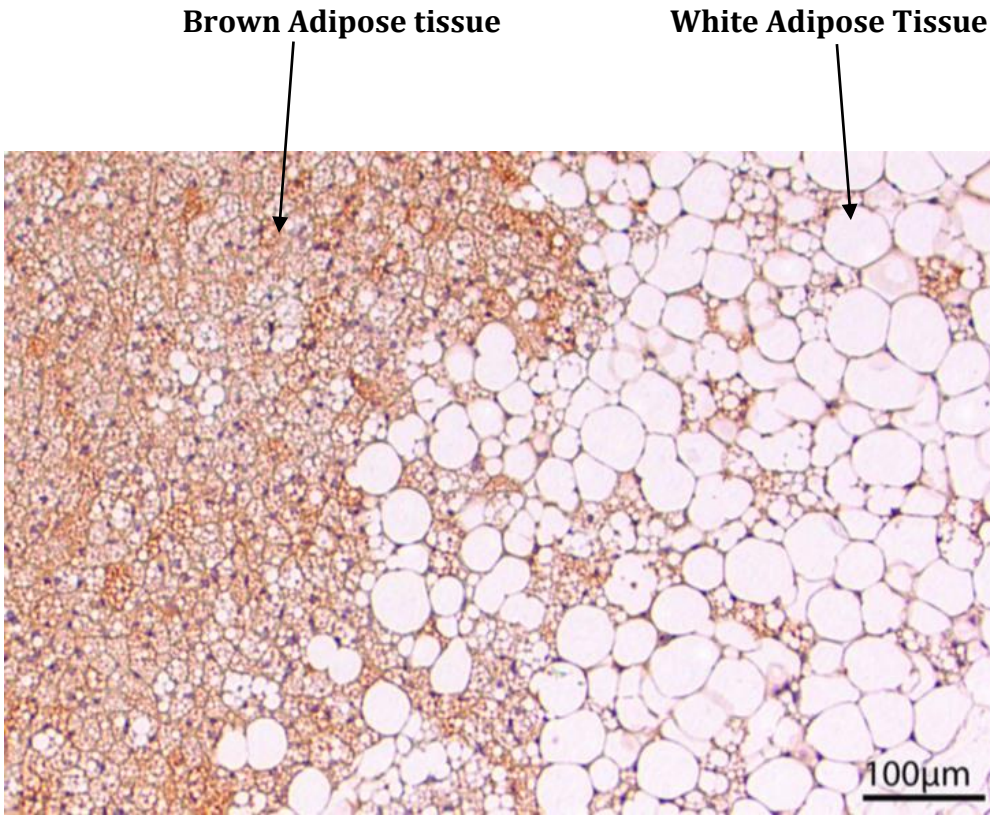

Figure 1.3. Histological representation of brown and white adipose tissue
A section of paraffin-embedded interscapular BAT was treated with haematoxylin to stain nuclei in blue. UCP1 was immunodetected and is indicated by a brownish colour. Typical multilocular brown adipocytes positive for UCP1 can be seen in the left half of the picture, while unilocular white adipocytes devoid of UCP1 dominate the right half. Figure from (Klingenspor & Fromme, 2014).

Histological studies have confirmed variation in the shape of the lipid droplets and mitochondria between brown and white adipocytes (Cinti, 2006; Frontini & Cinti, 2010). Mature white adipocytes are large spherical cells that store energy-providing lipids (triglycerides) in the form of a unilocular droplet that occupies approximately 90% of the cell volume

(Giordano et al, 2016). In contrast, brown adipocytes are multilocular, are of a polyedrical shape and smaller in size; only 50% of the volume occupied by lipids. Further, the presence of UCP1 enables brown adipocytes to dissipate heat rather than store energy.

To enable BAT to function as a heat producing tissue, the brown adipocytes in both humans and rodents are densely innervated by noradrenergic parenchymal fibres that penetrate deep into the plasma membranes, but only circulate on the surface of the capillary walls in white adipocytes (Cinti, 2006) (Figure 1.4). Parenchymal fibres are directly in contact with brown adipocytes through synaptic junctions; responsible for the functional activation of BAT thermogenesis. Gap junctions among adjacent brown adipocytes may amplify the noradrenergic stimulus that is selectively delivered to a few cells, enabling simultaneous, syncytial- like activation of large numbers of brown adipocytes, including those not directly reached by noradrenergic nerves (Giordano et al, 2016).

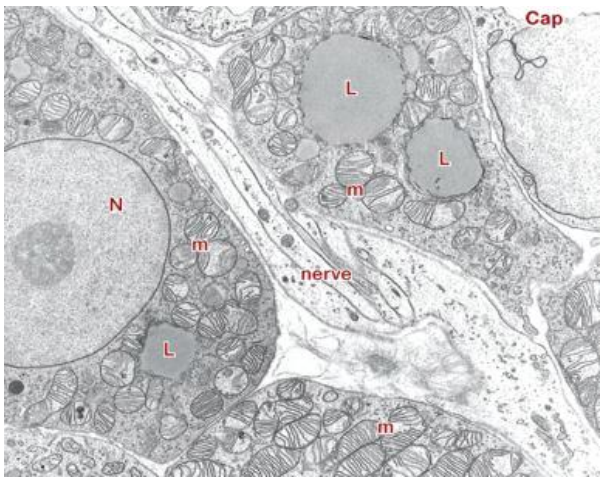

Figure 1.4. Transmission electron microscopic appearance of BAT
Of relevance is the cytoplasm filled with numerous large mitochondria packed with cristae (m), the small lipid droplets (L), part of the nucleus (N) and a parenchymal nerve amongst the adipocytes. Cap, capillary. Figure from (Frontini & Cinti, 2010).

1.2.3.2 BAT's specific Uncoupling Protein (UCP)1

The identification of the UCP1, or earlier known as thermogenin or the GDP-binding protein, as BAT's unique protein, the driver of non-shivering thermogenesis (NST), has enhanced our understandings of the function of BAT. Such discovery was made following the observation that the inner mitochondrial membrane of isolated brown adipocytes possesses high ion permeability (Nicholls et al, 1978). Further proof of concept that UCP1 is indeed essential for BAT thermogenic function was delivered by the discovery that UCP1 knockout mice are cold-sensitive (Enerback et al, 1997). The biochemical purification of UCP1 from BAT of cold-acclimated rodents demonstrated that approximately 5% of mitochondrial protein is UCP1 (Lin & Klingenberg, 1980; Stuart et al, 2001). UCP1 is exclusively found in the inner mitochondrial membrane of brown adipocytes and is the only protein which can mediate adaptive NST (Golozoubova et al, 2001).

1.2.3.3 UCP1 is the catalyst of 'Uncoupling' respiration

Stimulated BAT produces heat by 'uncoupling respiration' in the adipocytes, catalysed by UCP1 (Figure 1.5). According to Mitchell's chemiosmotic hypothesis, the electron transport chain in the mitochondria transfers reducing equivalents (electrons, hydrogen atoms) to molecular oxygen. In this process, the oxidation of nutritional substrates is coupled to adenosine triphosphate (ATP) generation by the movement of electrons through an array of electron transporters embedded in the inner mitochondrial membrane (Mitchell, 1961). This movement establishes a proton electrochemical gradient which is eliminated when hydrogen ions (H^+) move back into the mitochondrial matrix by the F_0/F_1 ATP synthase. As the H^+ ions pass, the ATP synthase complex rotates and the rotational forces catalyse the generation of ATP from adenosine diphosphate (ADP) and inorganic phosphate.

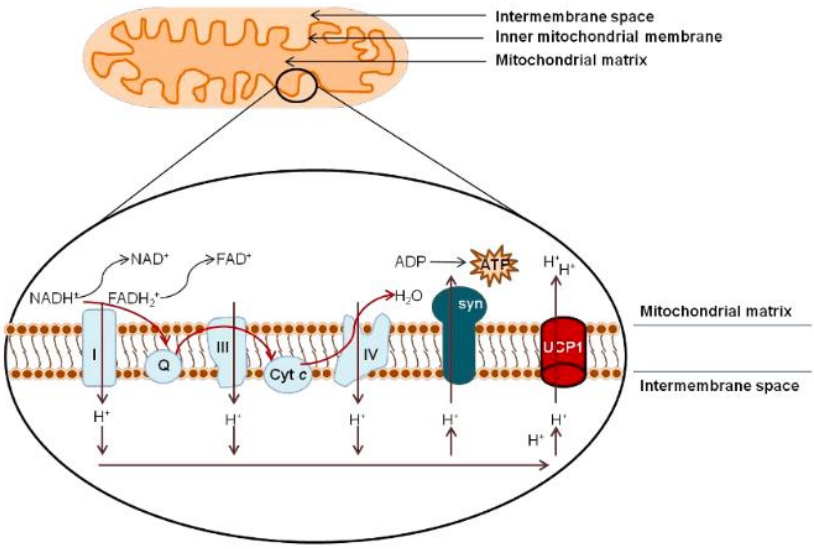

Figure 1.5. The uncoupling of respiration in the mitochondria of BAT, catalysed by the actions of UCP1.
Electron transport chain (ETC) complex I: ETC complex II, ETC complex III, ETC complex IV; NAD: nicotinamide adenine dinucleotide; NADH: nicotinamide adenine dinucleotide dehydrogenase; FAD: Flavin adenine dinucleotide; FADH: Flavin adenine dinucleotide dehydrogenase; H^+: hydrogen ion; Q: cofactor Q; ADP: adenosine diphosphate; ATP: adenosine triphosphate; syn: ATP synthase; H_2O: water; Cyt c: cytochrome c. Figure from Ojha, Budge and Symonds (2014).

In BAT mitochondria, substrate oxidisation and ATP synthesis is uncoupled by UCP1, allowing the protons to traverse from the intermembrane space (Frayn, 2010) to the mitochondrial matrix through an alternative channel, thus, dissipating the proton-motive force without generation of ATP (Figure 1.5). Subsequently, metabolic energy is displaced as heat.

Studies investigating whether UCP1 is essential for the activation of non-shivering thermogenesis have found that in UCP1 ablated mice, thermogenesis cannot be induced by norepinephrine in the brown adipocytes (Matthias et al, 2000) and such depletion vastly augments diet-induced obesity (Feldmann et al, 2009). The right hand section of the Figure 1.5. illustrates how an uncoupling protein facilitates the transfer of fatty acid anions out of the mitochondrial matrix, due to the anion possibly combining with a proton on either side, the net effect is equivalent to the discharge of the proton gradient (Ojha, Budge and Symonds, 2014).

1.2.4 Ontogeny of BAT

1.2.4.1 Developmental origins of adipose tissue

Adipose tissue depots are established in-utero and undergo active remodelling throughout life (Peirce et al, 2014). Rodent lineage-tracing studies have established brown adipocytes to be derived from myoblast precursors that are positive for the myogenic factor 5 (Myf5) gene (Kajimura et al, 2009), a completely separate linage from white adipocytes or those described as brown-in-white (brite or beige) cells and present in WAT depots, which differentiate from mesodermal stem cells that are not positive for Myf5 (Figure 1.6). Beige adipocytes are unique in the way they are formed from either the transdifferentiation from WAT in response to cues such as Irisin, or from recruitable brown pre-adipocytes (Berry et al, 2013). Consequently, there are three distinctive types of adipocyte; brown, white or brite, that result from separate lineages. The relative distribution of adipocytes, mixed or individual, varies significantly between fat depots in the body, reflecting their contrasting functions and thus, respective responsiveness to external challenges, such as cold exposure (Frontini & Cinti, 2010).

However, the overall role of beige adipocytes in the regulation of energy balance remains to be fully established, seeing as the relative abundance of UCP1 in this adipocyte cell type is known to be less than the "classical" brown adipocyte (Peirce et al, 2014).

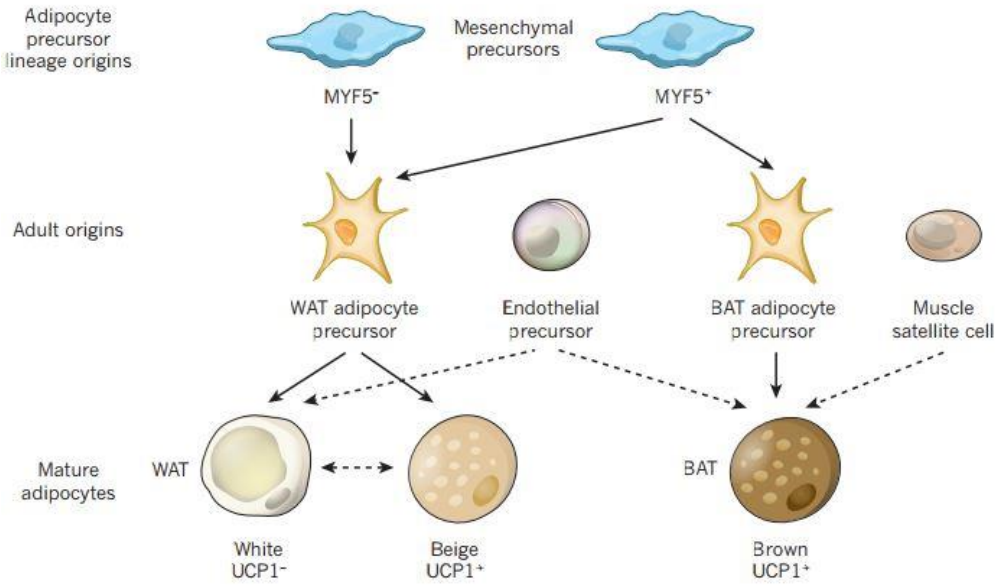

Figure 1.6. Origins of adipose tissue development
WAT adipocyte precursors can derive from both MYF5+ and MYF5– lineages, whereas BAT adipocyte precursors derive exclusively from a MYF5+ lineage. Figure from (Peirce et al, 2014).

1.2.4.2 Ontogeny of BAT in Precocial Species

BAT development in the neonate is best represented in newborn sheep, for which this process has been most extensively studied. Brown fat in precocial species born after a long gestation, is active from birth and comprises of 2-4% of birth weight. In parallel, a matured hypothalamic-pituitary-adrenal (HPA) axis enables NST to rapidly occur due to the inability to huddle with littermates', in order to maintain body temperature (M. Symonds, Mostyn, & Stephenson, 2001). Adipocytes with a multilocular appearance are visible to the naked eye from mid-gestation (Pope, Budge & Symonds, 2014) and possess a dense histological cellular structure, but at this stage, do not express UCP1 (Clarke et al, 1997). In human fetuses, brown adipocytes are initially detected histologically at 20 weeks' gestation, fully forming by 35 weeks (Moragas & Torán, 1983).
Approaching full-term-gestation, the depot size increases as adipocytes become mature and encompass both lipid filled unilocular cells and multilocular cells, which are abundant in mitochondria and highly express UCP1

(Clarke et al, 1997). At this stage, the development of white adipocytes occurs as a result of an increase in size of the pre-existing fat lobules (Poissonnet, Burdi & Garn, 1984). As the foetus grows and develops within a hypoxic and hypoglycaemic environment, it has little need to thermoregulate as its body temperature is primarily determined by that of the mother (Symonds et al, 2012). It is therefore not unexpected that adipose tissue growth is greatest over the final few weeks of gestation. Succeeding birth, a pronounced reduction in the number of white adipocytes occurs coincidentally with maximal reduction in UCP1 abundance. Lastly, the gradual disappearance of brown adipocytes occurs through the postnatal period, culminating in only white adipocytes being discernible by one month of age (Pope et al, 2014).

As a result of the multitude of sheep studies investigating adipose tissue development, four distinct phases of fetal/postnatal adipose tissue development have been constructed, and are as follows:

1.2.4.2.1 A proliferative stage in mid-gestation

The initial appearance of fetal adipose tissue coincides with a proliferative cellular stage in mid gestation, characterised by rapid cellular multiplication, in accordance with the maximal expression of KI-67, a marker of cellular proliferation (Winking, Gerdes & Traut, 2004). Adipose tissue depots are therefore established from precursor cells and the replication of pre-adipocytes increases cell pool and depot size. The transition from pre-adipocyte to a mature adipocyte in this stage is driven by triggers for cellular development, such as bone morphogenic protein (BMP) signalling and homeobox (HOX) families, including BMP4, BMP7, HOXA1, HOXC9, all highly expressed, indicative of developmental transition (Harms et al, 2014).

In mid to late gestation, the acceleration in the growth of BAT depots is primarily driven by PR domain containing 16 (PRDM16) and CCAAT-enhancer-binding protein β (C/EBPβ), which form a transcriptional complex, essential for adipogenesis (Harms et al, 2014).

1.2.4.2.2 Preparatory phase for thermogenesis in late gestation

The secondary stage of adipose tissue development is characterized by the maximal expression of UCP1, driven by an array of endocrine stimulatory factors to maximize both the amount and thermogenic capability of UCP1 (Symonds et al, 2012).

The concomitant rise in BAT specific genes prior to birth ensues maximal heat production following cold exposure into the extra-uterine environment (Symonds, 2013). One such gene, peroxisome proliferator-activated receptor c coactivator (PGC1α), is suggested to be the ''master regulator'' of mitochondrial biogenesis across species and is a prerequisite for NST at birth (Harms et al, 2014). The simultaneous peak in expression of the β3-adrenergic receptor (β3AR) and peroxisome proliferator-activated receptor (PPARγ) also facilitate thermogenesis. The peak expression of these genes prior to birth is driven by the prolactin receptor (PRLR), which is high expressed in this stage, a role that is confined to birth (Mostyn et al, 2004), as the rapid loss of this gene post birth, precedes the decline in UCP1 that continues postnatally. Adipose tissue depot size peaks just prior to birth, alongside the reduction in KI-67 to basal levels, indicating that the cells are committed to terminal differentiation (Winking et al, 2004).

1.2.4.2.3 Birth and non-shivering thermogenesis

Maximal stimulation of NST at birth is achieved by the peak expression of UCP1 (Symonds, 2013). This process is accompanied by significant reductions in the expression of WAT marker genes such as leptin, adiponectin, and corepressor receptor-interacting protein 140 (RIP140) (Kajimura et al, 2009). However, the increased expression of genes involved in adipogenesis; C/EBPβ and BMP4, in this stage indicates the beginning of the transition from brown to a white adipocyte phenotype (Harms et al, 2014).

1.2.4.2.4. Loss of UCP1 and accumulation of lipid

The final stage of adipose tissue development occurs postnatally and is characterized by the loss of BAT phenotype as UCP1 expression declines following birth, and shivering replaces NST as the primary response to cold exposure (Symonds et al, 2012). The concomitant rise in the expression of WAT marker genes, such as adiponectin, leptin, RIP140, PPARγ, HOXC9 and the glucocorticoid receptor (GR) significantly promote postnatal WAT growth by increasing cell size (Frontini & Cinti, 2010). Conversely, the loss of UCP1 over the first month of postnatal life, is accompanied by a decline in the expression of BAT genes, such as PGC1α and PRLR, whilst a linear rise in RIP140 with age is in accordance with its repressor action on UCP1 and PGC1α activity (Kiskinis et al, 2014). Furthermore, the decline in BAT genes post birth, may be facilitated by the rise in the transcriptional repressor, TWIST1, which interacts directly with PGC1α to suppress mitochondrial and thermogenic transcription factors (Jun, Gettys & Chang, 2012).

1.2.4.3 Ontogeny of BAT in Altricial Species

Altricial offspring, such as mice and rats are born after a short gestation (21 days) with an immature HPA axis, and lack the capacity to thermoregulate, thus, body temperature is regulated by huddling their litter mates (Symonds & Lomax, 1992). The first few days following birth is therefore critical for the recruitment of BAT in the altricial newborn as BAT matures postnatally in parallel with the maturation of the HPA axis (Cannon & Nedergaard, 2004; Giralt et al, 1990). There are two known phases of BAT thermogenesis, an immature phase critical for extra-uterine survival accompanying the transition to a fat-based diet and a mature phase that is regulated by the combined actions of sympathetic and circulating signals.

1.2.4.3.1 Immature phase

The expression of UCP1 in BAT occurs in the final few days prior to birth (Vinter, Hull & Elphick, 1982), driven by hormones highly expressed and released at parturition, such as, catecholamines (Skala, 1984), GCs (Mastorakos & Ilias, 2003) and prolactin (Viengchareun et al, 2008), which act either by direct effects on BAT or by activating autocrine factors such as insulin growth factor (IGF2) (Viengchareun et al, 2008). Post birth, the transition to lactation exposes the neonate to fatty acids and ketone bodies (Yubero et al, 2004), both factors promote the expression of fibroblast growth factor 21 (FGF21) by the liver (Domouzoglou & Maratos-Flier, 2011). FGF21 can be detected in plasma within 2-days post birth and is maximal at day 6 post birth. Hondares and colleagues in 2010 concluded that FGF21 treatment in neonates is sufficient to increase thermogenic genes and core body temperature (Hondares et al, 2010).

1.2.4.3.2 Mature Phase

Sympathetic nerves begin to innervate BAT of the newborn pups at 6 days post birth (Hull & Vinter, 1984), which coincides with the expansion in catecholaminergic innervation of BAT parenchyma (Berry & Daniel, 1970) enabling maximal cold induced thermogenesis between 10 and 15 days post birth. Further, UCP1 reaches adult levels by day 16 (Xiao et al, 2007). Together these observations are consistent with the idea that factors driving autonomic innervation of BAT between 5 and 15 days' post birth, are major determinants of thermogenic activity.

1.2.4.3.3 Endocrine regulation of BAT thermogenesis at birth

Birth is a time of acute stress for the fetus and the collective action of endocrine signals such as, catecholamines (Symonds et al, 2000), cortisol (Clarke, Heasman & Symonds, 1998), thyroid hormones (Heasman, Clarke, & Symonds, 2000), prolactin (Pearce et al, 2005) and leptin (Mostyn et al,

2002), ensure the rapid stimulation of non-shivering thermogenesis (Clarke et al, 1997; Taga et al, 2012), following the initiation of the HPA axis in the brain (Symonds et al, 2003). The secretion and plasma concentrations of these hormones gradually decline thereafter for the first few days and weeks of life (Bispham et al, 2002; Symonds et al,1995), as shivering succeeds non-shivering thermogenesis as the dominant response to cold-exposure (Bispham et al, 2002).

The above highlighted endocrine signals are closely inter-related and it has been suggested that the prenatal rise in the body's stress hormone, cortisol, has the greatest influence on brain maturation and adipose tissue development (Mostyn et al, 2003).

1.2.5 The stress response system and cortisol

1.2.5.1 Neuronal circuits controlling cortisol release in response to stress in immature and adult brains

Stress is defined as any condition including an adverse environment, experience, or perceived threat to an organism's homeostasis which activates the autonomic nervous system and hypothalamic– pituitary–adrenal (HPA) axis (van Bodegom, Homberg & Henckens, 2017). The subsequent initiation of the following cascade results in the release of GCs; release of corticotropin releasing hormone (CRH) from neurons in the paraventricular nucleus (PVN) of the hypothalamus, increases the secretion of pituitary corticotropin (Adrenocorticotropic hormone [ACTH]) (Avishai-Eliner et al, 2002). ACTH induces the secretion of GCs from the adrenal glands, which readily cross the blood-brain barrier (BBB) to influence brain function through the binding to two receptors: glucocorticoid receptors (GRs) and mineralocorticoid receptors (MCs) in the hypothalamus and hippocampus, respectively, to restore a steady state (Maniam, Antoniadis, & Morris, 2014; McEwen, 2000; van Bodegom, Homberg & Henckens, 2017) (Figure 1.7).

Adequate functioning of the HPA axis negative feedback loop, is critical for handling of acute stress exposure and the avoidance of adverse metabolic effects which are consequential to chronic GC exposure (Bhutta & Anand, 2002; McEwen, 2000; Welberg & Seckl, 2001). There is longstanding recognition that recurrent or persistent activation of the HPA axis, particularly during prenatal and early postnatal periods, has been associated with alterations in brain function and the development of adverse health outcomes later in life (McEwen, 1992; Pruessner et al, 2010). However less is known regarding the mechanisms underpinning such dysfunction. The following section will discuss how exposure to GCs both pre- and postnatally, may alter metabolic disease susceptibility in later life.

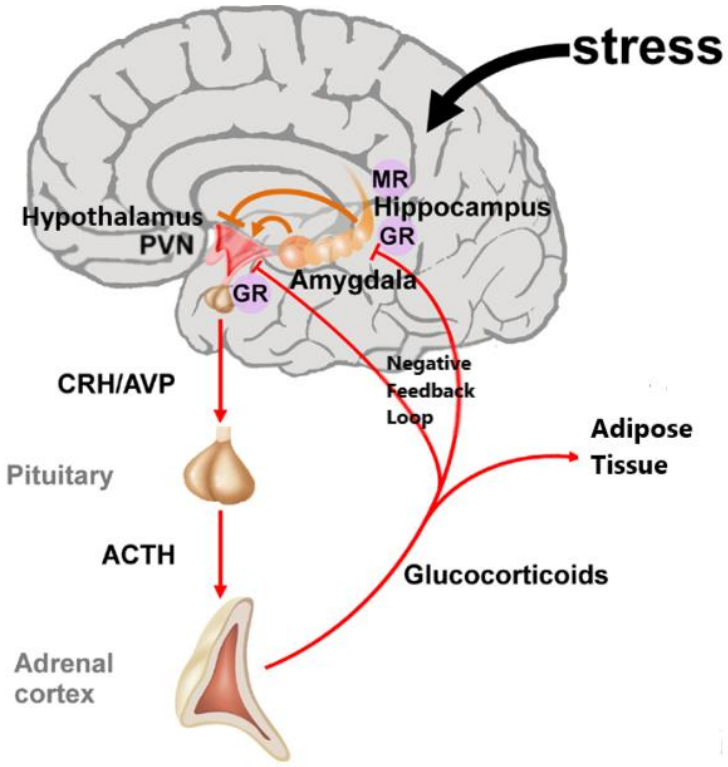

Figure 1.7. The hypothalamic-pituitary-adrenal (HPA) axis mediates the stress response

The perception of real of presumed physical and social threats causes the activation of the hypothalamic-pituitary-adrenal (HPA) axis. The paraventricular nucleus (PVN) in the hypothalamus releases hypothalamic neuropeptides; corticotrophin releasing hormone (CRH) and arginine vasopressin (AVP) which promote the synthesis and secretion of adrenocorticotropin (ACTH) from the pituitary. ACTH promotes the secretion of glucocorticoids from the adrenal glands. These hormones circulate the brain and throughout the body to bind to intracellular nuclear steroid receptors. Hippocampal mineralocorticoid (MR) receptors act to the onset of stress response, whereas glucocorticoid receptors (GR) in the hippocampus, PVN and anterior pituitary, act to terminate the stress response. GCs also mediate effects in adipose tissue. Modified figure from (Raabe & Spengler, 2013).

1.2.5.2 Effects of glucocorticoids on the programming of HPA functionality, BAT and disease risk in later life

1.2.5.2.1 Prenatal glucocorticoid exposure

Fetal development is a precarious, highly sensitive period. Fetal exposure to GCs is vital for adequate development, associated with organ maturation, which is critical for extra-uterine life. The association of GCs with accelerated tissue-maturation is important in infants at risk of preterm birth (Lunghi et al, 2010). The administration of GCs during pregnancy is not uncommon and has been widely used to treat inflammatory disorders of pregnant women (asthma or systemic lupus), for congenital problems of the foetus (adrenal or lung malformations) or to induce rapid surfactant production in the lung, thereby improving neonatal viability (Novais et al, 2017).

The fetal brain is protected from excessive cortisol exposure by the type 2 isoform of the enzyme; 11β-hydroxysteroid dehydrogenase (11β-HSD) in the placenta. Its type 1 isoform converts inactive 11-dehydrocorticosterone to active corticosterone in rodents (cortisone to cortisol in humans) (Stimson et al, 2009), whilst type 2 catalyses the reverse conversion of active GCs (corticosterone in rats, cortisol in humans) to their inactive 11-keto derivatives (11β-dehydrocorticosterone in rats, cortisone in humans) (Fernando et al, 2013). The extent of GC mediated effects depends on the balance between the two 11β-HSD isoforms. Edwards and colleagues demonstrated the protective role of placental 11β-HSD2 in a study demonstrating that offspring from pregnant rats with reduced 11β-HSD2 activity, are low birth weight (LBW) when born (Edwards et al, 1993).

Prolonged fetal exposure to maternal GCs or exogenous antenatal GC administration (Edwards et al, 1993; Stimson et al, 2009), can result in saturation of available 11β-HSD. Synthetic GCs such as such as dexamethasone, have a low affinity for 11β-HSD and can readily cross the placenta (Seckl & Holmes, 2007). Indeed, subsequent downstream consequences involve the

negative interference with fetal growth and maturation, leading to prematurity and LBW (Edwards et al, 1993; Nyirenda et al, 2004). Barker and colleagues coined the term 'intrauterine growth restriction (IUGR)', to refer to adverse factors which affect gestational growth and ultimately determine birth weight (Barker, 1992). This theory postulates that LBW predicts increased disease risk in later life, including metabolic dysfunction (Mi et al, 2000). Indeed, premature infants born less than 37 weeks' gestation (Andrews et al, 2018) and LBW infants (a birth weight of less than 2500g, regardless of gestational age), will demonstrate an accelerated catch up growth period in the first 6–12 months of life, which can raise the susceptibility for programming postnatal metabolic consequences, such as increased intra-abdominal fat and insulin resistance in infancy (Modi et al., 2006; Ravelli et al, 1998; Regan, 2006). Further, infants who exhibit catch-up growth, have been demonstrated to carry a higher proportion of body fat, particularly abdominal fat, as children and adults (Modi et al, 2006).

The mechanisms driving stress effects to lower birth weight remain largely unknown, but have been directed towards alteration in HPA axis activity and the function of the enzyme 11β-HSD. Indeed, in rodent models, rat pups born from dams prenatally exposed to GCs demonstrate hyperactivity of the HPA axis (Seckl & Holmes, 2007) and a lower expression of GR in the hippocampus, impairing the HPA axis negative feedback loop during adulthood (Barbazanges et al, 1996).

1.2.5.2.2 Early life postnatal glucocorticoid exposure

Early postnatal life is a critical developmental period for HPA axis and BAT maturation and its undisturbed development is and is sensitive to environmental challenges, such as stress stimuli (Lee, Yamaguchi & Goto, 2015), essential for adequate functioning of the stress-response system and cortisol mediated effects on metabolism during adulthood (Schmidt et al, 2003). The effects of excess cortisol in early life in rodents are protected by a period of low circulating corticosterone levels, termed the

stress hypo-responsive period (HRP) (Levine, 1994, 2002; Schmidt et al, 2003) in the first two weeks of life (Walker et al, 1986; Walker et al, 1991). This protective strategy favours optimal central nervous system (CNS) development in an environment of low responsiveness to stressors (Sapolsky & Meaney, 1986).

Humans, particularly in preterm infants exposed to IUGR, also demonstrate a period of suppressed HPA-axis responsiveness and low circulating GCs during the neonatal period (Huysman et al, 2000; Watterberg, Gerdes & Cook, 2001). These infants subsequently demonstrate hyper-responsiveness of the HPA axis up to 18 months of age (corrected age for prematurity), with levels of cortisol in preterm infants, greater than that of healthy full-term infants (Gunnar & Donzella, 2002). Given that healthy full-term infants exhibit a state of HPA axis responsiveness to stress in the first months of life, followed by a similar HRP period to rodents, between 6 and 12 months of age (Gunnar & Donzella, 2002; van Bodegom et al, 2017), prematurity consequential to intrauterine stress, may alter regulation of the HPA axis (Tu et al, 2007).

Both humans and rodents are dependent on adequate maternal nourishment and care during this HRP period to ensure normal development (Maniam et al, 2014). Alterations in maternal care induce a state of early life stress and can impact neurobiological development, since mother-offspring interactions such as licking and feeding, provide a critical input for HPA axis maturation (Suchecki, Rosenfeld & Levine, 1993). Maternal separation induced prior to weaning, has been demonstrated to significantly elevate GC exposure and over-ride this GC feedback inhibition (Rosenfeld et al, 1991; Walker et al, 1991) and alter HPA axis function (Ivy et al, 2008; Sapolsky & Meaney, 1986), which can subsequently promote weight gain and food intake in rats during adulthood (Jahng, 2011; Kalinichev et al, 2002).

1.2.5.2.3 Effects of glucocorticoid exposure on BAT

Given the vital functionality of BAT for postnatal thermoregulation, few studies have explored the biological characteristics of BAT upon early life stress. The development of rodent models enables insight into whether excess GC exposure can affect risk for later life metabolic deficit, as the direct examination of early life stress is not feasible in newborns.

The subcutaneous administration of corticosterone has been demonstrated to reduce the mRNA expression of essential BAT thermoregulatory genes including UCP1 and β3-AR (Feve et al, 1992; Garrel, 1997; Soumano et al, 2000; Strack at al, 1995; Viengchareun et al, 2001), potentially through mechanisms involving the interference with sympathetic adrenergic signalling (Collins and Surwit, 2001). Further, Miki and colleagues demonstrated that maternal separation of female rats for 3 hours per day, during postnatal days (PND) 10-15, resulted in a significant reduction in β3AR mRNA expression, whilst UCP1 mRNA remained unchanged relative to control at 10 weeks of age (Miki et al, 2013). These authors also demonstrated an upregulation of WAT prohibitin; a proliferative marker, relative to control and suggested that early life stress experienced in the first weeks of life, may begin to alter adipose tissue profile, favouring the transition to WAT characteristics. These data are in accordance with the demonstrations that stress during this early developmental period, has been associated with the development of insulin resistance (Regan, 2006) and increased BMI during infancy (Modi et al, 2009). Certainly in adults, chronic hypercortisolism is the pathophysiologic underpinning of Cushing's syndrome (Nieman and Turner, 2006) and excess circulating GCs have been demonstrated to reduce the UCP1 activation (Ramage et al, 2016; Soumano et al, 2000) and drive lipid accumulation (Bjorntorp & Rosmond, 2000; Vicennati et al, 2009). Excess GCs therefore may result in the development of metabolic disease, including obesity, type 2 diabetes mellitus and dyslipidaemia (Macfarlane, Forbes & Walker, 2008).

However, acute GC excess in humans increases cold-induced glucose uptake into BAT and stimulates BAT thermogenesis through UCP1 (Robinson et al, 2016). In 2016, Ramage and colleagues were the first to report that the GC, prednisolone, acutely increased $^{[18]}$F-Fluorodeoxyglucose ($^{[18]}$F-FDG) uptake by BAT and increased SCR skin temperature, alongside energy expenditure during cold exposure in 6 healthy male volunteers. Additionally, the incubation of human brown adipocytes with cortisol (100nM) for 24 hours, increased UCP1 levels, alongside other BAT responsive genes including PGC1α, PPARα and β3-AR (Ramage et al, 2016). The mechanisms underpinning metabolic dysfunction when exposed to chronic levels of circulating GCs is unclear, but the enzyme 11β-HSD1 may, in part, mediate these consequences. Indeed, Doig et al (2017) suggested that the overexpression of 11β-HSD1 in murine brown adipocytes as a consequence of GC excess, results in BAT dysfunction and can also impair mitochondrial biogenesis (Doig et al, 2017).

Avishai-Eliner et al (2002), suggested that GCs may also mediate effects through their receptors situated on the BAT membrane. Viengchareun et al (2001) proposed that the GR, by interacting with c-Jun and binding to the proximal Cyclic AMP (cAMP) response element (-139/-122), may inhibit catecholamine-induced UCP1 expression and thus, inhibits BAT function (Viengchareun et al, 2001). Further experiments are required to clarify the mechanistic validity of the mechanisms involved in GCs regulation of BAT in acute and chronic situations, particularly as GCs are vital for stimulation of BAT at birth and in the first weeks of life, in order to maintain body temperature. At this crucial time, adequate BAT development and function is imperative, especially as the failure to develop active BAT in young children, has been shown to correlate highly with an increased BMI (Drubach et al, 2011). The long-term challenge will be to target the long term effects of exposure to GCs, with the beneficial effects seen from acute GC exposure protocols.

1.2.5.3 Acute stimulation of BAT thermogenesis by catecholamine release from the hypothalamus

The regulation of BAT activity and its mediation by the sympathetic nervous system (SNS) has intensively been studied in human and rodent models which have experimented with environmental temperature. Sympathetic drive is augmented by cold exposure, nutrition and pharmacological stimulation, which results in almost a two-fold increase in plasma noradrenaline concentrations (Celi, Le & Ni, 2015). The rate of brown adipocyte thermogenesis is orchestrated by a pathway initiated in the preoptic area (POA) in the rostral hypothalamus (Morrison, Nakamura & Madden, 2008), which coordinates thermoregulatory information and integrates thermoregulatory responses. Stimulation of postganglionic sympathetic neurons which innervate each brown adipocyte disseminate the excitatory signal through the release of the neurotransmitter, norepinephrine (NE) (Cerri & Morrison, 2005) (Figure 1.8). At thermoneutrality, efferent inhibitory neurons projecting from the POA to the dorsal medial hypothalamus and the brain stem, block sympathetic outflow to BAT (Nakamura & Morrison, 2008).

Norepinephrine release activates and signals through the β_3–ARs situated in the plasma membrane of brown adipocytes (Celi, Le & Ni, 2015). The intracellular signal is transmitted through the β-adrenergic signalling cascade (Figure 1.9), where there is subsequent activation of the Gs protein (Gs). This G-protein coupled receptor activates adenylyl cyclase (AC), an enzyme that converts ATP to the second messenger molecule cAMP. Signal transduction proceeds to the protein kinase A (PKA) complex that releases its catalytic subunit to phosphorylate target proteins in response to increased cytosolic cAMP levels (Cannon & Nedergaard, 2004).

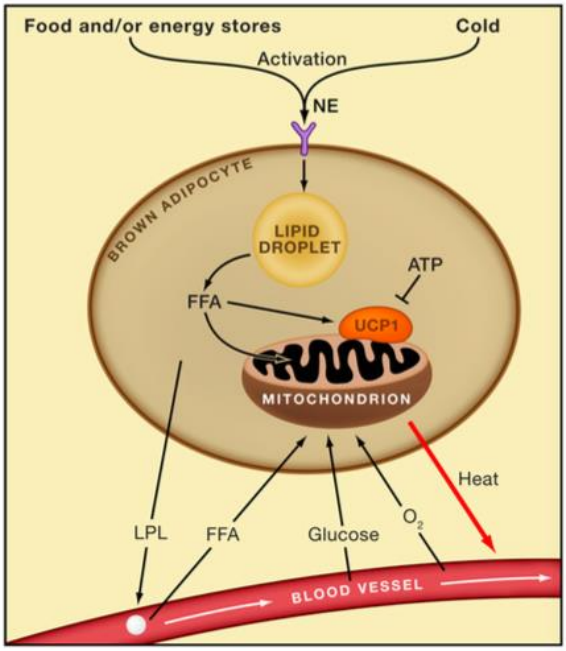

Figure 1.8. Sympathetically stimulated BAT thermogenesis
The requirement to produce heat for the defense against regulated body temperature (thermoregulatory thermogenesis) or to combust excess energy intake (metaboregulatory thermogenesis) is coordinated in an area of the brain named the ventromedial hypothalamic nucleus (VMN). From thereon, a signal is transmitted by the sympathetic nerve fibers which innervate the individual brown adipocytes. They release the transmitter, norepinephrine (NE) which signals through β-adrenoreceptors placed on the plasma membrane. The intracellular signal is transmitted via cAMP and protein kinase A, leading to the release from triglycerides (TG) of fatty acids (FA) that are both the acute substrate for thermogenesis and (in some form) the regulators of the activity of uncoupling protein-1 (UCP1). Combustion of the fatty acids in the respiratory chain (RC) leads to extrusion of H^+ and UCP1 thus allows for mitochondrial combustion of substrates, uncoupled from the production of ATP. The outcome is that an increased fraction of the food and the oxygen available in the blood is taken up by the tissue and combusted therein, leading to an increased heat production. Figure from (Nedergaard & Cannon, 2010).

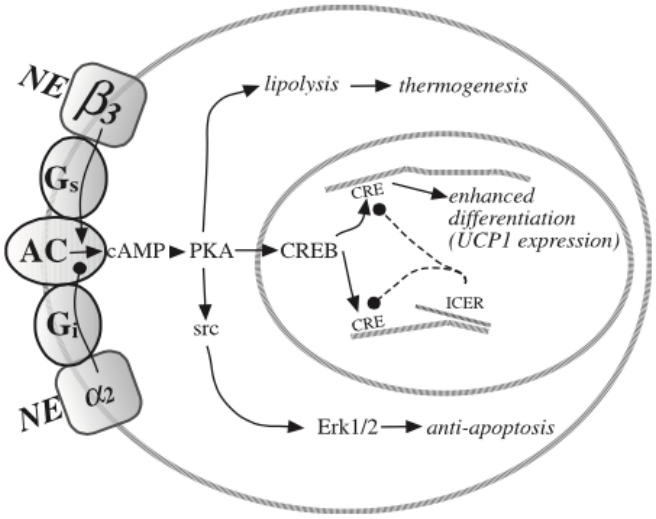

Figure 1.9. The pathway for β-adrenergic stimulation of thermogenesis. Figure from (Cannon & Nedergaard, 2004)

Activation of PKA in the β-adrenergic signalling cascade leads to an increased rate of lipolysis at the surface of lipid droplets of the brown adipocyte (Figure 1.10). The liberation of free-fatty acids (FFA), by phosphorylation of direct PKA targets perilipin and hormone sensitive lipase (HSL) (Klingenspor & Fromme, 2014), provide the acute substrate for non-shivering thermogenesis and FFA thus, regulate of the activity of UCP1 (Matthias et al, 2000; Reed & Fain, 1968).

In addition to this well understood mechanism, the β3 –AR may activate a second, extracellular signal regulated kinase (ERK) mediated signalling cascade, to reach maximal lipolytic activity in the presence of high ligand concentrations (Klingenspor & Fromme, 2014). The mechanisms involved in this process are poorly understood but it has been suggested that ERK signalling further augments maximal PKA-mediated lipolysis by approximately 20% (Robidoux et al, 2006).

Brown adipocytes abundantly express both heart-type and adipose tissue-type fatty acid binding proteins, to shuttle lipophilic fatty acids through the cytosolic compartment. Esterified to coenzyme A, fatty acids are shuttled as a metabolic fuel into the mitochondrial beta-oxidation pathway,

while in their unbound non-esterified anion form they are potent activators of UCP1 (Frayn, 2010). The degraded end products such as hydrogen ions (H^+), are then oxidized by the mitochondrial electron transport system (Cannon & Nedergaard, 2004). Thus, UCP1 allows for mitochondrial combustion of substrates, uncoupled from the production of ATP. As a consequence, there is an increase in the fraction of food and oxygen availability in the blood, which is taken up by the tissue and combusted thereafter, resulting in an increase in heat production (Cannon & Nedergaard, 2004).

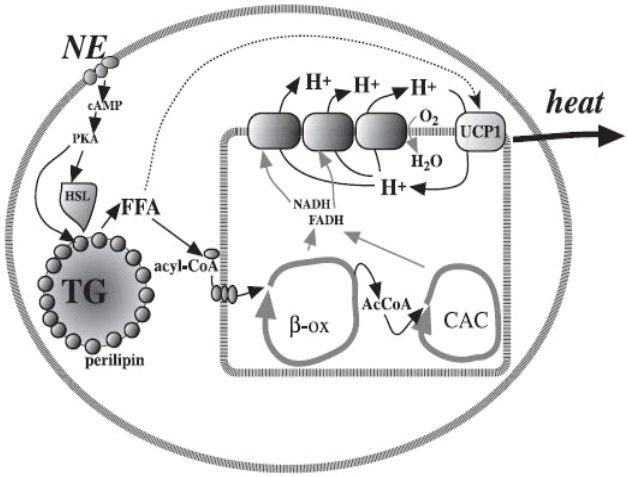

Figure 1.10. Norepinephrine-induced stimulation of thermogenesis in brown adipocytes: events downstream of the protein kinase A (PKA) activation illustrated in Figure 1.9
HSL, hormone-sensitive lipase; TG, triglyceride droplet; AcCoA, acetyl CoA. Free fatty acids (FFA) activated to acyl CoAs by acyl-CoA synthetase are first transferred to acyl-carnitine by the highly expressed muscle form of carnitine palmitoyl transferase I (M-CPT I), which is the CPT I form found in both brown and white adipose tissue (205) and which is very sensitive to inhibition by malonyl CoA. The acyl-carnitine enters the mitochondria through the carnitine transporter and is reconverted to acyl CoA by CPT II. The ensuing ß-oxidation (ß-ox) of the fatty acids (acyl CoAs) as well as the activity of the citric acid cycle (CAC) lead to the formation of the reduced electron carriers FADH and NADH, which are then oxidized by the electron transport chain (respiratory chain; here indicated by the series of 3 grey boxes), ultimately through oxygen consumption. This results in a pumping out of protons from the mitochondria and the formation of a proton-motive force that drives the protons back into the mitochondrial matrix through the uncoupling protein UCP1. The energy stored in the proton-motive force is then released as heat. Figure from Cannon and Nedergaard, (2004).

1.2.6 The Identification and assessment of BAT

1.2.6.1 Original histological identification of BAT deposits in humans and rodents

The major human BAT depot was originally identified by post-mortem tissue analysis, as the SCR region, under the sternocleidomastoid and trapezius muscles, running laterally and in parallel with the neck (Hatai, 1902). The proximity of this depot to major blood vessels supplying the brain is an adaptation for ensuring that the temperature of the brain is not compromised, especially after birth (Symonds et al, 2011). BAT in humans has also been identified around the kidneys, along the large blood vessels and trachea, and as finger-like projections following the intercostal arteries. In infants, BAT has been described to represent a shape akin to a thin kite-shaped sheet of BAT between the shoulder blades (Figure 1.11). Axillary and perirenal or adrenal BAT represents almost 50% of total BAT mass in an infant. It was once thought that with increasing age, BAT diminishes and ultimately becomes indistinguishable from WAT. However, in the 1970s, Heaton and colleagues performed the first histological examination of BAT which comprehensively assessed the effects of age on BAT abundance. Eighteen regions of BAT in 52 humans aged 0 to 80 years of age were analysed, finding that interscapular BAT was present in 80% of infants and children under 10 years of age, with the prevalence declining thereafter (Heaton, 1972). In contrast, perirenal, periadrenal, cervical and perivascular BAT depots all contained brown adipocytes well into the eighth decade, albeit in smaller quantities. The persistence of the perirenal and axillary BAT depots into adolescence was later confirmed by smaller studies showing BAT in 75% to 100% of perirenal (Cunningham et al, 1985; Ito et al, 1991; Lean et al, 1986) and axillary depots (Lean et al., 1986) across individuals aged 1 – 86 years. Despite the reports that the aforementioned BAT depots existed throughout life, the absence of the interscapular BAT in these studies, overshadowed such findings and circulated the belief that BAT diminished in adult humans.

However, several post-mortem investigations have reported that BAT does indeed persist into adulthood in many of the sites in which it occurs in infancy (Heaton, 1972), especially in those individuals exposed to a cold environment (Huttunen, Hirvonen & Kinnula, 1981).

The proceeding studies further highlight the difference in the anatomical location of BAT between humans and rodents. In rodents, BAT is most abundantly located similarly to that of a human infant, in the interscapular region throughout life. Further, BAT depots have been found to be located in the axillary, cervical and paravertebral regions, as well as in proximity of thoracic and abdominal viscera (Figure 1.12).

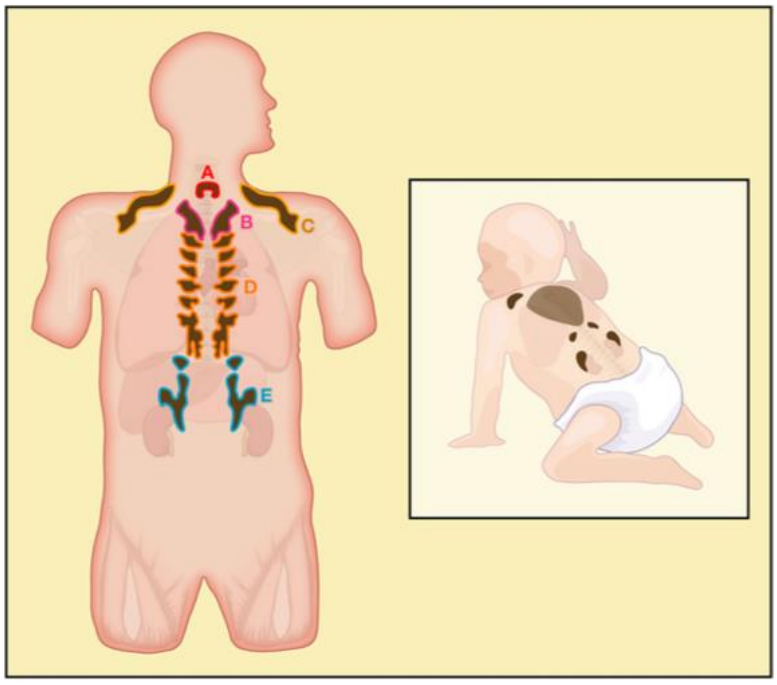

Figure 1.11. The main locations of human BAT
A) thyroid/tracheal, (B), mediastinal, (C) supraclavicular, (D) parathoracical, (E) perirenal. In the infant, a kite shaped thin layer of BAT has been described (in light brown). Figure from (Enerbäck, 2010).

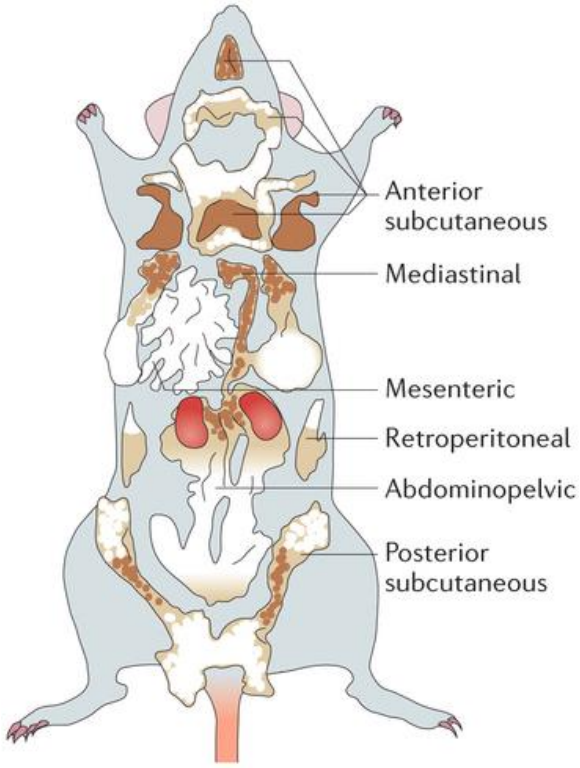

Figure 1.12. The adipose organ of an adult mouse kept at 28°C. Figure from (Giordano et al., 2016).

1.2.6.2 Imaging modalities to measure BAT

1.2.6.2.1 PET-CT

Static positron emission tomography-computed tomography (PET-CT) with ^{18}F-FDG imaging has been instrumental to the re-discovery and identification of BAT in adults in 2009 (Cypess et al, 2009; van Marken Lichtenbelt et al, 2009). PET-CT imaging is a functional technique, widely used for the anatomical localization of BAT (Nedergaard et al, 2007) and tissue-specific estimations of glucose metabolism. Such technique was originally used in the 1990s, mainly in oncology, to detect tumours and metastases, which have a higher metabolic rate than normal tissue and therefore high glucose uptake, allowing for the discrimination of tissues according to metabolic activity. ^{18}F-FDG uptake is typically reported in the literature as a maximal or mean standard uptake value (SUV; SUVmax

or SUVmean), which estimates ^{18}F-FDG bio-distribution in a specified region of interest (ROI) in relation to the injected radiotracer dose and distribution volume in a subject (i.e. body weight) (Muzi et al, 2012). Hadi et al (2007) detected BAT in 22% of 59 patients with a pheochromocytoma; rare tumour of adrenal gland tissue, who also had a greater ^{18}F-FDG uptake than in the 21 patients without pheochromocytoma (BAT was detected in 9.5% of these patients) (Hadi et al, 2007). This technique thus allows for the visualisation of BAT depots within adipose tissue, highlighting the presence of BAT in adulthood.

Indeed, PET-CT scanning has revealed BAT to be localised to a fascial plane descending from the cervical to the mediastinal and SCR regions, constituting the largest depot across varying age groups. Smaller BAT depots have been found in the epicardial, paravertebral, axillary, perirenal and periadrenal regions (Figure 1.11). The anatomical locations of BAT depots reported by PET-CT scanning have remarkable concordance with the Heaton report, over 40 years ago. However, there are discrepancies in reporting some depots. The intercostal, trachea-oesophageal and mesenteric depots have been identified histologically but have been failed to be detected by PET scanning. It is likely that such depots identified histologically, are inactive or are insufficiently active to be detectable by PET-CT. After all, BAT can be confirmed histologically, whereas PET-CT scanning indirectly detects BAT through differential ^{18}F-FDG uptake (Lee, Swarbrick & Ho, 2013).

This modality has been invaluable in the understanding of human BAT under cold-stimulated conditions in adult populations (Holstila et al, 2013; Koskensalo et al, 2017; Orava et al, 2011; Ouellet et al, 2012; Salem et al, 2016; van der Lans et al, 2013; Virtanen et al, 2009).

However, this technique has notable limitations. Most significant is the assumption that glucose uptake reflects BAT activity, since studies have indicated that fatty acids from intracellular triglyceride lipolysis, not glucose, are the primary substrate for activated BAT (Blondin et al, 2017; Labbe et al, 2015). Thus, BAT metabolic activity may be underestimated, which may result in inconsistency in findings across studies (Blondin et al, 2017; Chen

et al, 2016). A challenge with ^{18}F-FDG tracer is its relatively short half-life and rapid clearance from tissues acquisitions (Jadvar & Parker, 2005). Thus, studies have assessed BAT metabolism by utilising an alternative PET tracer such as, the long-chain fatty acid analogue, ^{18}F-fluoro-6-thi-aheptadecanoic acid [^{18}F-FTHA), to estimate NEFA uptake by BAT (Carpentier et al, 2018; Ci et al, 2006). This tracer has the same radioactive half-life (~110 min) as ^{18}F-FDG, accumulates into intracellular metabolic pathways, similarly to ^{18}F-FDG and may therefore be used in both static and dynamic imaging (Jadvar & Parker, 2005). The potential to use a combination of various radiotracers with dynamic PET-CT imaging may increase the precision in the assessment of BAT metabolic activity.
Further limitations to static ^{18}F-FDG measurements include, the reliance on a single time frame to represent overall tracer metabolism, despite the known variation in tissue glucose responsiveness (Blondin et al, 2015; Chen et al, 2017). Therefore, this method is highly influenced by both inter- and intra-subject dissimilarities in the concentrations and clearance of plasma glucose (Muzi et al, 2012).

1.2.6.2.2 The development of non-invasive techniques for the detection and monitoring of BAT function

The unexpected discovery of human BAT quantification by metabolic imaging is a major advance in BAT research and today ^{18}F-FDG PET-CT scanning stands as the current gold standard technique to quantify BAT in adult humans (Saito et al, 2009; van Marken Lichtenbelt et al, 2009). However, this technique is expensive, is unable to provide indices of BAT function in real-time, requires the administration of radiopharmaceuticals and involves ionizing radiation making it difficult to justify its use in young children and neonates. In 2011, it was reported that the level of radiation exposure from a standard PET-CT, exceeds radiation safety guidelines for medical research in healthy volunteers (Moores & Regulla, 2011). Intervention studies involving repeated scanning protocols are therefore lim-

ited to small sample sizes and healthy individuals. Furthermore, the interpretation of findings from PET-CT measurements are challenging as $^{[18]}$F-FDG signal can represent differences in BAT activation and / or volume. As only 10% of BAT uptake comes from glucose and 90% from fatty acids, the sensitivity of such glucose uptake method may be low (Nedergaard et al, 2007). It therefore lends itself to the development of novel non-invasive imaging methods that are capable of detecting BAT volume and activity separately, which could complement PET-CT scanning.

1.2.6.2.2.1 Infrared Thermography

Recently developed imaging methods such as Infrared Thermography (IRT) have been used to detect temperature changes in the skin overlying BAT. To date, the recording of surface skin temperature changes in the SCR region of adults and children has been performed using IRT (Ang et al, 2017; El Hadi et al, 2016; Lee, Ho & Greenfield, 2011; Robinson et al, 2016; Symonds et al, 2012) and has been proposed to substitute PET-FDG in research (Carter et al, 2011; Jang et al, 2014). Its principle is based on the simple understanding that BAT is a heat producing organ, causing the overlying skin to be warmer than elsewhere on the body. Such heat producing function cannot be captured by the measurement of substrate utilisation, as in PET-CT.

Current thermal imaging cameras are highly sensitive and are capable of detecting temperature differences as little as 0.1°C (Law et al, 2018). IRT has successfully detected skin temperature increases over the SCR region, compared with a control region (the mediastinum) in humans exposed to cold challenges (El Hadi et al, 2016; Jang et al, 2014; Lee et al, 2011; Robinson et al, 2016; Symonds et al, 2012). Studies have begun to examine whether this technology is feasible for large scaled investigations in humans of varying ages. Symonds et al (2012), showed that even a mild cooling challenge of placing an extremity into tap water (19-21°C) for 5 minutes, caused a significant increase in the temperature overlying the SCR BAT depot in children compared with adolescents and adults (3-8

years, 0.62± 0.14°C (P<0.05); 13-18 years, 0.25± 0.08°C; 35-58 years, 0.20 ± 0.08°C) (Symonds et al, 2012). These observations have been confirmed in further investigations reporting localised increases in temperature within the SCR in humans from 3 to 58 years of age (Jang et al, 2014; Lee et al, 2011; Scotney et al, 2017; Symonds et al, 2012). More recent investigations in support of the use of IRT, have demonstrated a significant anatomical overlap (29.5 ± 5.1%) between the surface skin temperature of the major BAT depot, as detected by IRT and the area of maximum glucose uptake, as identified by $^{[18]}$F-FDG PET-CT scans in both humans (Law et al, 2017) and in mice (Carter et al, 2011).

Although this method is currently unable to determine BAT volume, the potential sensitivity, added safety, low cost, portability and the repeatability of skin temperature measurements for measuring BAT activity in real-time, open up its potential to examine whether this technology could be utilised in vulnerable populations such as infants in early life. The use of IRT in newborn infants could propose a useful detection tool for changes in BAT function and its potential for the development of disease in later life, consequential to BAT dysfunction.

1.2.6.2.2.2 Near Infrared Spectrophotometry (NIRS)

Near Infrared Spectrophotometry (NIRS) is a non-invasive optic imaging technique, sensitive to tissue hemodynamic changes (i.e. fluctuations in blood flow, volume and oxygenation) (Ferrari, Mottola & Quaresima, 2004; Jobsis, 1977) and has been speculated to complement the use of IRT in assessing BAT activity non-invasively (Nakayama et al, 2003).

Continuous wave (cw) NIRS systems estimate blood chromophore concentrations by near infrared light (Jobsis, 1977). Light in the near-infrared spectrum penetrates several centimetres of tissue and the amplitude decay of the light intensity due to absorption is analysed, which allows for the measure of oxygenated haemoglobin, principally in the venous bed (Bozkurt et al, 2005; Muzik et al, 2013). This procedure has been used by

clinicians for over two decades to monitor cerebral haemodynamics and oxygenation and its use has recently been demonstrated clinically, to benefit neonates (Greisen et al, 2016).

Investigations into the use of NIRS to measure BAT oxygenation in humans is scarce, and the rationale for its use is based on original experiments in the 1970's, which demonstrated that oxygen delivery limits BAT oxygen consumption (Foster & Frydman, 1979). BAT is known to be highly vascularised, with blood flow providing oxygen for its mitochondria and for the transfer of heat from BAT to other locations in the body. As such, perfusion rate matches the rate of tissue oxygen consumption (Segal, 2005), and in the case of BAT, determination of perfusion rate can be used to estimate thermogenesis (Orava et al., 2011). Cold stress is known to increase the oxidative metabolism in BAT depots. Evidence from rodent studies has shown oxygen consumption to increase by as much as 81% upon cooling the POA of the hypothalamus to 28°C (Banet & Hensel, 1976). In humans, Orava and colleagues reported BAT perfusion increased by more than 50% in response to cold, whilst no changes were observed in WAT ($P = 0.18$) or in muscle ($P = 0.08$), highlighting the dense vasculature of BAT (Orava et al., 2011). In 2013, Muzik and colleagues performed a direct measurement of oxidative metabolism in the subclavicular BAT depot of healthy adult volunteers and reported that mild cold stress decreases venous oxygenation during BAT activation, as the median oxygen consumption of this depot increased to 7 kcal/d/100 g for a typical subject with 60 g of BAT (Muzik et al, 2013). The cold induced increase in subclavicular BAT blood flow was similar to that reported by Orava et al (2011) and confirms that although NIRS is capable of detecting changes in BAT oxygenation, acutely activated human BAT contributes very little to cold-induced energy expenditure (Orava et al, 2011).

NIRS systems are low-powered and practical, which allow for the non-invasive, indirect and real-time monitoring of SCR BAT oxygen consumption for extended periods without the exposure of ionising radiation (Muzik et al, 2013). Further, although this technique can be used in healthy adult volunteers as an indirect measure of oxidative metabolism, studies are yet

to provide evidence of its complementary use with IRT, which could provide greater insights into BAT metabolic activity.

1.2.7 Utilisation of protocols for acute BAT stimulation

1.2.7.1 Cold exposure

Estimations of detectable BAT (determined as the measurement of $^{[18]}$F-FDG uptake) in retrospective studies in adults at ambient temperatures, has been demonstrated to range between 2-8.5% (Au-Yong et al, 2009; Cypess et al, 2009; Ouellet et al, 2011; Yeung et al, 2003). In 2009, Cypess and colleagues analysed 3640 $^{[18]}$ F-FDG PET-CT scans (1013 women, 959 men) taken to detect neoplasms, demonstrated gender differences in prevalence estimates, finding metabolically active areas suggestive of BAT in 7.5% of women and 3.1% of men (Cypess et al, 2009). These authors further reported that age, BMI and outdoor temperature were inversely related to PET positive imaging. Indeed, when subjects are exposed to the cold, the prevalence of BAT has been demonstrated to increase to between 20-100% (Au-Yong et al, 2009; Blondin et al, 2015; Cypess et al, 2009; Saito et al, 2009; van Marken Lichtenbelt et al, 2009; Yoneshiro et al, 2011). Van Marken Lichtenbelt and colleagues reported BAT positivity in 96% of PET-CT scans in 24 individuals exposed to cold (16°C) for two hours (Figure 1.13). An inverse relationship between the level of uptake measured in kilobecquerels and body fat mass was also reported (van Marken Lichtenbelt et al, 2009). The large variation in prevalence between subjects and across studies could be due to subjective decisions about BAT definitions used in early retrospective studies of the visual examination and reporting of BAT in small sample (Cunningham et al, 1985), which could preclude individuals who are likely to have some active BAT when exposed to cold.

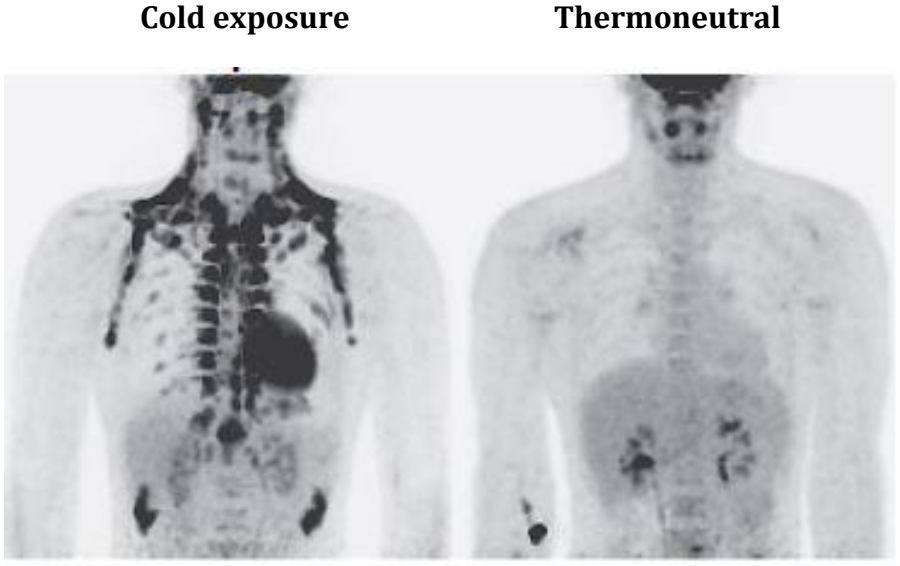

Figure 1.13. PET-FDG scans performed in the same subject after cold exposure to 16°C and under thermoneutral conditions (21-22°C) (Wouter D. van Marken Lichtenbelt et al, 2009)

Cold exposure protocols have primarily been used to activate BAT in humans, given the risk of adverse side effects often experienced in the study participants under high doses of sympathomimetics (i.e. Ephedrine) (Carey et al, 2013; Cypess et al, 2012) or β adrenergic agonists (Cypess et al, 2015; Vosselman et al, 2012). However, variability in exposure protocols has been a significant barrier to comparing findings between studies (Blondin et al, 2015; Chen et al, 2016; van der Lans et al, 2014).
Protocols for acute BAT stimulation have been shown to vary, primarily due to the chosen imaging modality (Symonds et al, 2012; Yoneshiro et al, 2017). Static PET-CT imaging requires at least a 60 minute cold exposure period after $^{[18]}$F-FDG injection, to enable the visualisation of glucose uptake into BAT (Chen et al, 2016), whilst IRT imaging can detect a significant increase in temperature overlying the SCR region, in a matter of 5 minutes after hand immersion in ice water (Robinson et al, 2016). The most commonly used cooling protocols for BAT stimulation include exposure of an extremity (hands and/or feet) to cold water (El Hadi et al, 2016; Law et al, 2017; Peterson et al, 2017; Ramage et al, 2016; Robinson et al, 2014; Symonds et al, 2012), water perfused vests or blanket covering a

limb (Salem et al, 2016) or whole-body cold exposure using a temperature controlled room (16-20℃) (Jang et al, 2014). Some studies have used these protocols in combination, such as whole-body cold exposure in a room cooled to 16℃ for up to 2 hours, with the addition of immersion of a single limb in to cold water, prior to the injection of $^{[18]}$F-FDG injection (van Marken Lichtenbelt et al, 2009).

In order to obtain reliable results between cooling protocols, it is important that cold-induced measures of whole body heat generation such as indirect calorimetry, alongside changes in mean skin temperatures over BAT locations be taken as standard BAT measurements (Blondin et al, 2017; Blondin et al, 2015). In this way, studies can contribute to the collective insights into BAT's relevance to whole-body expenditure and potential disease contribution.

1.2.7.2 Pharmacological stimulation of the β-adrenergic system

Norepinephrine action on β_3-ARs in mature human brown adipocytes is one of the most studied pathways of BAT function (Celi, Le and Ni, 2015). β-Adrenergic receptors (ARs) are G-protein-coupled receptors distributed throughout the human body (Ursino, Vasina, Raschi, Crema, & De Ponti, 2009); β_1- and β_2-ARs are expressed in the heart and smooth muscle, respectively and have well established roles in increasing the rate and contractile force of the heart and smooth muscle (Celi, Le and Ni, 2015). Furthermore, the discovery of an additional β_3-AR gene has resulted in the detection of human β_3-AR mRNA in the gallbladder, colon, bladder and most abundantly on the surface of BAT (Cypess et al, 2013; Virtanen et al, 2009).

In rodents, all three AR subtypes are present in BAT, leading to investigations exploring the effects of AR specific agents both in vivo and in vitro. The administration of a selective β_1-agonst (Ueta et al, 2012), β_2 -agonist (Preitner et al, 1998), or β_3- agonist (Preitner et al, 1998) has shown to increase BAT mass. Furthermore, in β_3-AR knockout mice, BAT structure

and function was preserved (Ueta et al, 2012). Thus, β_1 and β_2 – ARs may be sufficient for BAT recruitment and proliferation.

In humans, the roles of the AR subtypes have been studied less extensively. The understanding that β_3-AR stimulation promotes UCP1 expression in BAT and stimulates non-shivering thermogenesis (Celi, Le and Ni, 2015), has led to a promising target for weight loss or for weight maintenance after weight loss (Bonet, Oliver & Palou, 2013; Broeders, Bouvy, & van Marken Lichtenbelt, 2015; Chechi, Nedergaard & Richard, 2014). As the potential to increase energy expenditure resulting in a large amount of weight loss in the short term may be limited, BAT stimulation may mitigate the physiological decrease in energy expenditure that follows weight loss (Halpern, Mancini & Halpern, 2014). A further potential pharmacological target would be those capable of "browning" mature white (or "predisposed" brite/beige) adipocytes, promoting brown adipocyte-like features/characteristics (Bonet et al, 2013).

Unfortunately, non-specific sympathomimetic drugs cannot stimulate human BAT without marked effects on the cardiovascular system (Cypess et al, 2015; Vosselman et al, 2012). First-generation β_3-AR agonists were inadequately selective (Celi, Le and Ni, 2015) and although the second generation were more selective and demonstrated improved glucose disposal, decreased plasma triglycerides, and increased resting metabolic rate (RMR) (Cawthorne et al, 1992; Larsen et al, 2002; Redman et al, 2007; Weyer et al, 1998), they still exhibited poor oral bioavailability and pharmokinetics, not discounting the substantial cross-reactivity with the β_1-AR that caused undesirable cardiovascular effects (Arch, 2011; Cypess et al, 2015).

Mirabegron, a drug which induces smooth muscle relaxation, is the only β_3-AR compound that has advanced to phase III clinical trials, but only for the treatment of an overactive bladder (Celi, Le and Ni, 2015); Yamaguchi et al, 2014). In addition to having satisfactory bioavailability (Malik et al, 2012), Mirabegron has a higher in vitro binding affinity for the human β3-AR compared to other members of its class (Malik et al, 2012). Although its effects on weight loss have not been investigated, Cypess et al

(2015) found that Mirabegron induced BAT activation and increased energy expenditure ($P<0.05$) in 12 healthy male subjects, making this drug a potential future candidate for the treatment of obesity (Cypess et al, 2015), with its potential still to be explored.

Isoprenaline (ISO) is a non-selective β-adrenergic agonist, approved by the U.S. Food and Drug Administration (FDA) agency and used in clinical practice as a bronchodilator, cardiac stimulant and β-sympathomimetic agent. Vosselman et al (2012) measured BAT activity by $^{[18]}$F-FDG PET-CT imaging in 10 lean men during systemic infusion of ISO and compared this with cold-activated BAT activity (2hr of mild cold exposure). The authors concluded that although ISO successfully mimicked sympathetic stimulation as shown by increased cardiovascular activity, there were similar increases in energy expenditure after 55 min infusion of ISO (highest; 19.7 ± 7.2% during 24 ng/kg fat-free mass^{-1} min^{-1}) and cold exposure (16.9 ± 7.8% 24 ng/kg fat-free mass^{-1} min^{-1}) (Vosselman et al, 2012).

In summary, the AR subtypes appear to have interchangeable roles, particularly in rodents and it remains unclear to what extend humans can tolerate non-selective β-AR agonists in order to stimulate BAT thermogenesis to an extent which increases energy expenditure without inducing negative cardiovascular side effects.

1.2.7.3 Diet-induced thermogenesis and BAT

Evidence for the induction of diet-induced thermogenesis (DIT) in BAT has stemmed from early experimental investigations in rodents in the 1970s, which reported chronically feeding rats a “cafeteria-diet” (composed of a high energy value diet, rich in fat and carbohydrates and poor in protein) over a 21 day period, disproportionally increased energy expenditure, that could not be attributed to the energy cost of food alone (Rothwell & Stock, 1979). Although these animals consumed around twice as many calories, they produced twice as much heat and only gained 30% more weight, as their net efficiency of weight gain was around 30% lower than controls. Thus, it was suggested that the excess unaccounted calories were being

burned off by the induction of DIT. After euthanasia, tissue analysis confirmed a 260% increase in BAT mass compared with control rats fed a standard chow diet, suggesting that the dissipated heat derived from BAT recruitment and activation (Rothwell & Stock, 1979). Additionally, the consumption of a cafeteria-diet resulted in an enhanced thermogenic response to noradrenaline administration. In support, a number of further studies in rats show that following a defined period of food withdrawal, feeding a low-protein/high-carbohydrate diet raised norepinephrine turnover in BAT (Glick & Raum, 1986), whilst simultaneously stimulating the GDP binding resulting in an increase in the thermogenic capacity of UCP1 (Lupien et al, 1985).

In humans, the relationship between DIT and BAT remains uncertain. Seeing as meal ingestion stimulates insulin secretion, investigations involving insulin administration have provided insight into its relationship with BAT. Orava et al (2011) observed that insulin stimulated almost a 5-fold increase in FDG uptake in BAT during a hyperinsulinemic-euglycemic clamp in 27 individuals (Orava et al, 2011). Conclusions from this study imply that BAT may indirectly contribute to postprandial energy metabolism. Vrieze et al (2012) compared $^{[18]}$F-FDG uptake upon cold exposure in the fasted state or after a high-fat meal in 10 subjects, concluding that FDG uptake in BAT was observed in 6 of 10 subjects, which were found to have a higher maximal standardized uptake value (SUV) when fasting (median, 13.1 g/mL; range, 6.1–27.6 g/mL) compared to in the postprandial state (median, 6.8 g/mL; range, 2.1–13.4 g/mL) (P = 0.03) (Vrieze et al, 2012). Despite these findings, insulin was not measured in this study, even though it may be eluded to that the lower SUV in the post-prandial state can be explained by an increased insulin-stimulated glucose uptake into muscle (Vrieze et al, 2012). More recently, Peterson et al. examined the thermic response to a 50% overfeeding diet following a 4-week cold intervention. Despite increases in cold-induced thermogenesis and SNS activity, DIT was unchanged in response to 50% overfeeding (Peterson et al, 2016).

Although dismissed by some (Kozak, 2010; Maxwell et al, 1988), there is currently mixed evidence relating to the contribution of BAT to DIT, which may vary with subject population and/or macronutrient content. Thus, the notion that BAT may dissipate excess calories as heat and make weight gain difficult in some individuals supports further investigation.

1.3 Experimentation outlined in this thesis

Given the potential for GC-mediated effects on BAT function, pilot and experimental studies were conducted to assess the utility of non-invasive techniques to detect changes in BAT activity during situations of acute stress in adults and newborn infants. Due to ethical reasons, it is not possible to use invasive experimental techniques in newborn infants, so rodent models provide the opportunity to assess the genetic profile of BAT. A rodent model of early life stress was therefore developed, to examine the effects of acute stress on key BAT genes essential for thermogenesis during critical stages of brain and BAT maturation. These investigations were conducted primarily at The University of Nottingham and at the University of Birmingham, to utilise expertise in the immediate fields. IRT imaging protocol was under continual development by my current laboratory group throughout the duration of the data collection. In this sense, investigations conducted in humans were not only to explore the potential effects of stress-mediated BAT activity, but also to investigate the ability of novel non-invasive methods to quantify BAT function.

1.3.1 Endocrine stimulation of BAT thermogenesis

1.3.1.1 Human studies

Situations of acute stress provoke the activation of the HPA axis, which induces BAT activity in humans, through the release of catecholamines and subsequent binding to β3-ARs. The pharmacological administration of non-selective β-agonists such as ephedrine in high doses, increases BAT activity in humans (Carey et al, 2013). However, such agonists are unable to stimulate BAT to the same extent as cold exposure without significant adverse cardiovascular effects. ISO is a non-selective β-agonist, found to stimulate thermogenesis to the same extent as cold exposure, without the aforementioned adverse cardiovascular side effects (Vosselman et al, 2012). Thus, experimentation with ISO dosage will enable the exploration

of the extent of BAT stimulation that allows for a tolerable level of cardiovascular effect.

The simultaneous release of cortisol from the adrenal glands, alongside catecholamine's during situations of stress, is vital in order to promote adaptation and recovery through a negative feedback loop (Avishai-Eliner et al, 2002). Acute elevations in cortisol (corticosterone in rodents) have been shown to negatively interfere with BAT function in rodents, reducing the expression of UCP1 and β3-AR. However, in humans, these effects are reversed. Robinson et al (2016) confirm that acute anticipatory stress from a psychological stress test can stimulate BAT activity in healthy female adult volunteers, as assessed by IRT (Robinson et al, 2016). The molecular mechanisms underpinning these findings in humans are unclear, so too is the disparity in BAT function between rodents and humans. Indeed, circulating hypercortisolism in excess of normal circadian rhythm (i.e. Cushing's syndrome), is considered to be detrimental to human health (Nieman & Turner, 2006), resulting in the development of excess adiposity and obesity (Nedergaard & Cannon, 2010; Ramage et al, 2016). Mechanisms of altered adipose characteristics have been directed towards species-specific regulation of UCP1 and certainly in chronic situations, cortisol's activating enzyme, 11β-HSD1. However, there is limited evidence investigating the effects of hypercortisolaemia on BAT function in humans. My thesis, therefore examined the effects of hypercortisolaemia in healthy adult males. As we did not conduct PET-CT scanning to determine BAT volume in the subjects, the pharmacological stimulation of BAT during conditions of hypercortisolaemia, using the non-selective β-agonist, ISO, was conducted to ensure the brown adipocytes were active.

1.3.1.2 Rodent study

BAT plays a vital thermoregulatory role at birth and during early life, for which excess GC exposure experienced prenatally and postnatally alters BAT characteristics alongside HPA axis regulation and its end-point cortisol (corticosterone in rodents), It is unclear why elevated corticosterone levels inhibit UCP1 expression and BAT function in rodents (Soumano et

al, 2000; Strack et al, 1995; Viengchareun et al, 2001). But it is clear that early postnatal stress, influences disease risk during infancy and in later life. Rodents provide an opportunistic model for assessments of acute early life stress on metabolism and as such, my study developed a rodent model to assess the effects of stress exposure during early critical developmental stages on BAT transcription and control.

1.3.2 Non-invasive BAT quantification and monitoring

The unexpected discovery of human BAT quantification by metabolic imaging is a major advance in BAT research and currently $^{[18F]}$F-FDG PET-CT scanning stands as the gold standard technique to quantify BAT in adult humans (Saito et al, 2009; van Marken Lichtenbelt et al, 2009; Virtanen et al, 2009). However, this technique is limited by its sheer cost and radiation exposure, meaning that repeated scanning is restricted to a small number of subjects. Further, the interpretation of findings from PET-CT scanning can be challenging as $^{[18]}$F-FDG signal can represent changes in BAT activation or volume, and as only 10% of BAT uptake comes from glucose and 90% from fatty acids, the sensitivity of such glucose uptake method may be low (Nedergaard et al., 2007). Thus, alternative non-invasive techniques that are capable of continually assessing BAT function and/or volume separately would be more advantageous and potentially more applicable studies in babies and children.

Several lines of evidence from our research group in Nottingham, have proven IRT imaging to be a highly sensitive and promising modality in assessing BAT function in real time, both in children and adults, in a safe and non-invasive manner (Jang et al, 2014; Law et al, 2014; Law et al, 2017; Robinson et al, 2016; Scotney et al, 2017; Symonds et al, 2012). The imaging modality provides a measure of surface skin temperature, for which, when stimulated, the overlying skin of particularly the SCR BAT depot, is warmer than other reference parts of the body. Inferences can subsequently be made about BAT activity after its stimulation. Proposals that IRT may substitute for PET-FDG scanning in research (Carter et al, 2011;

Law et al, 2014), particularly in young children, have stemmed from recent PET-IRT correlative investigations reporting an anatomical overlapping between the increase in $^{[18]}$F-FDG uptake and the rise in the temperature overlying the SCR BAT (Carter et al, 2011; Law et al, 2017). Further investigations have reported highly localised increases in temperature over this region of BAT, compared to elsewhere, upon cold stimulation in healthy humans from 3 to 58 years of age (Jang et al, 2014; Lee et al, 2011; Scotney et al, 2017; Symonds et al, 2012). This non-invasive technique may well have the capability of assessing BAT function in healthy individuals, or in combination with other non-radioactive techniques, however, whether IRT can be successfully conducted in younger subjects below 3 years of age to assess BAT function is unknown.

The technique of NIRS may complement the use of IRT in the non-invasive assessment of BAT activity, due to its ability to determine tissue oxygenation (Nakayama et al, 2003). Seeing that the blood flow to BAT provides oxygen to its mitochondria and is able to transfer heat from the stimulated adipocytes to the overlying skins surface (Foster & Frydman, 1979), determination of perfusion rate can be used to estimate thermogenesis (Janne Orava et al, 2011). BAT perfusion rate increases in response to acute cold stress stimuli (Muzik et al, 2013; Orava et al, 2011) in combination with a decrease in venous oxygenation during BAT activation (Muzik et al, 2013). Thus, NIRS may allow for the non-invasive, indirect and real-time monitoring of SCR BAT oxygen consumption during acute cold stimulation, without the exposure of ionising radiation (Muzik et al, 2013). Seeing as BAT dysfunction in children is correlated with an increased BMI (Drubach et al, 2011; Robinson et al, 2016), safe and appropriate methods that can be employed to assess BAT activity in early post-natal life will be advantageous. Therefore, this thesis incorporated two proof-of-concept studies which utilized IRT alone, to determine its utility in detecting changes in SCR skin temperature over known BAT regions in newborn infants. In a further study, IRT was combined with NIRS to assess the feasibility of detecting alterations in BAT function during acute cooling stimulation, which may

provide an insight into the regulation of BAT function and more information about BAT function and subsequent implications for metabolic health.

1.4 Main hypothesis and aims

The introduction has discussed the potential for the deleterious effects of excess GCs upon BAT function in both humans and rodents. However, greater insights into GC-mediated effects on BAT activity in humans, has been restricted by current imaging modalities. To further elucidate the mechanisms pertaining stress-induced alterations in BAT function and characteristics during early life and in adulthood, four studies were used in the course of my PhD.

Chapter 3

The aim of this study was to examine the effects of hypercortisolaemia on BAT activity in healthy adult males. My primary hypothesis was that chronic infusion of the GC, hydrocortisone would stimulate BAT and increase surface skin temperature over the SCR BAT depot, assessed by IRT.

Chapter 4

Given the increasing popularity of IRT as a surrogate assessment tool for BAT function, its complementary use with NIRS, may collectively provide a greater understanding of BAT, through a non-invasive means. The primary aim of this chapter was to assess BAT activity during forearm cold stimulation in healthy adults, utilising a combination of non-invasive techniques. These methods were used to acquire an understanding of tissue oxygen saturation and blood flow within the SCR region with respect to BAT heat production.

Chapter 5

Given the importance of BAT during birth, assessments of BAT function in early post-natal life, may become a valuable tool for the initial detection of changes in BAT characteristics and the development of metabolic disorders in later life. However, IRT imaging has not been utilised in children younger than 3 years of age, due to the challenges surrounding neonatal thermoregulation. This pilot study was conducted in newborn infants, in two phases and aimed initially to develop an IRT imaging protocol and secondly; the exploration of IRT imaging to measure skin temperatures over previously identified brown fat regions in full-term infants.

Chapter 6

To model the effects of excess GCs on BAT gene expression during early postnatal life, a rodent study was conducted. The primary aim was to assess the short-term effects consequences of early postnatal stress on parameters of; HPA axis activation, including plasma levels of corticosterone and; biological characteristics of BAT in female pups, including the mRNA expression of UCP1, ADRB3, PRDM16, PPARγ, FGF21 and 11β-HSD-1 at PND 7 and PND 21.

Chapter 2

Materials and Methods

This chapter describes the scientific concepts and implementation of experimental procedures used throughout this thesis.

2.1 Procedural and legislative declaration and ethical approvals

2.1.1 Approvals for human studies

The effects of acute hypercortisolaemia on the thermogenic function of human brown adipose tissue

This study was approved by the Edgbaston NRES Committee, UK (REC reference 14/WM/1085). All *in-vivo* measurements taken and serum samples collected were obtained from participants upon providing written informed consent. After collection, serum samples were stored for future analysis by Dr Manolopoulos.

A multimodal approach for the non-invasive detection of brown adipose tissue activation in healthy adults

This study was conducted in two parts; Study A, the initial feasibility, between 25/04/16 – 19/05/16 and Study B, between the dates of 20/02/17 – 09/03/17. All measurements for this study were carried out once ethical approval was granted by the University of Nottingham ethical committee, UK (part A REC reference, l16022016; part B REC reference, F14112016) and only when participants provided written informed consent.

Infrared Thermography Imaging for the identification and quantification of newborn brown adipose tissue

This pilot study was conducted between 28/10/16 and 15/08/17. IRT imaging in newborn infants in this study, assessed skin temperature changes over the interscapular BAT region (Chapter 5). Ethical approval for this study was granted by the Yorkshire & the Humber–Sheffield Research Ethics Committee 15/YH/0522 and informed parental content was obtained prior to the beginning of the study.

2.1.2 Approval for rodent study

All animal experimental procedures performed in the studies included in this thesis attained ethical approval from the University of Nottingham and were conducted under Home Office approval, in accordance to the regulations of the UK Animals (Scientific Procedures) Act, 1986. Laboratory procedures were carried out in accordance with the Control of Substances Hazardous to Health (COSHH: SI No 1657 1988) regulations and following Good Laboratory Practice guidelines (University of Nottingham Safety Office). Unless otherwise stated, all chemicals and reagents were purchased from Sigma- Aldrich Company Ltd., and laboratory plastics and equipment from Scientific Laboratory Supplies. Details for all suppliers are located in Appendix B.

2.2 Human studies

2.2.1 Infrared thermography imaging in adults

To apply the use of infrared thermography in assessing BAT function, an in-house protocol had previously been devised (Symonds et al, 2012). This procedure had been carefully designed to help optimize results and ensure high quality data. Since the beginning of my studies, the original protocol has been continually improved. The following sections refer to the current methodological procedures for IRT imaging in adults and subsequently,

the development of a novel IRT protocol to assess changes in skin temperature over the interscapular BAT region in newborn infants.

2.2.1.1 Image acquisition

Human studies using IRT imaging should preferably take place in a controlled environment where an ambient room temperature can be maintained consistent between participants. During all human imaging studies carried out in the current work, imaging was conducted in a thermoneutral environment (21-22℃) (Law et al, 2018) and participants were not exposed to drafts or convection currents, which could've affected the measurement of surface skin temperature.

Previous IRT imaging studies in Nottingham, have devised an imaging protocol to assess changes in skin temperature over the SCR BAT region in humans (Law et al, 2018; Robinson et al, 2016; Symonds et al, 2012). These studies collectively detail recommendations for the effective acquisition of images in adults, which has helped to improve the inconsistency in IRT imaging protocols across studies assessing BAT function.

The protocol states that a thermal imaging camera (FLIR B425 2.3 Megapixel Infrared Camera; FLIR Systems AB, Danderyd, Sweden) should be mounted onto a tripod at a recommended distance of 1m vertically from the ground and 1m horizontally from the participant. The participant's shoulders should be clearly seen in the thermograms, alongside the neck and upper chest region, incorporating the SCR BAT depots (Figure 2.1)

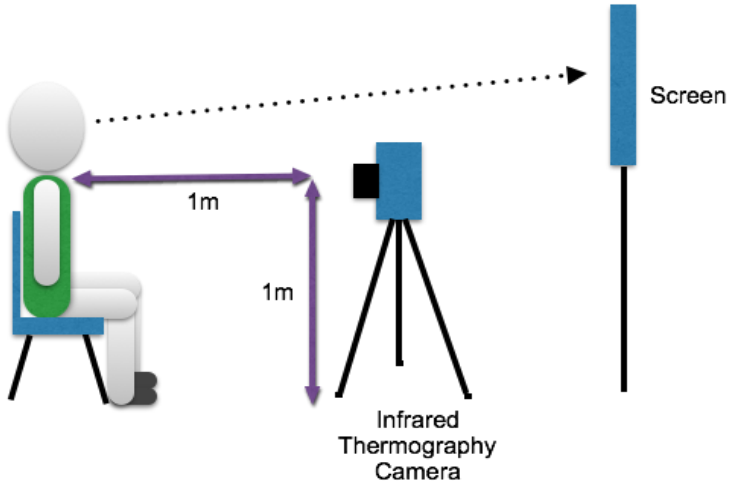

Figure 2.1. Schematic diagram demonstrating the setup of thermal imaging of BAT in adult humans
The suggested distance of the camera to the participant is 1m and 1m from the ground. A screen is placed behind the camera so the participant can look straight ahead to expose the SCR region and to maintain a stable head and shoulder position.

Prior to obtaining thermal images, it is recommended that participants change into a loose fitted cotton vest (provided by the department), exposing the shoulders. Long hair should be tied back to ensure that no strands cross the region of interest and all necklaces and long earrings should be removed. Participants should be sat comfortably on the chair directly facing the camera, ensuring that they are sat in an upright position, with shoulders symmetrically aligned. There should be no supporting cushions behind the shoulders which may aid heat transfer off the shoulders to distort the image.

One of the difficulties with imaging participants is that they are encouraged to remain as still as possible throughout the entire imaging study, so that images do not become distorted or loose resolution. Thus, in the human imaging studies in this thesis, a computer screen monitor displayed the participant and was positioned directly behind the camera. Markers were placed on to the screen to indicate the position of the participant's eyes, chin and shoulders which helped to minimise any movement between images.

Assessments of room temperature, humidity and camera-to-participant distance were made prior to the commencement of the study and entered into the camera.
Prior to beginning each study, it was essential that there was a period of acclimation to the thermoneutral environment to ensure that core and skin temperatures has plateaued. The study then commenced and a series of thermal images could be obtained at a chosen rate.

2.2.1.2 Image analysis

Thermograms provide visual pictures of temperature distribution throughout the surface of an object under study. FLIR thermal imaging cameras sequentially saved labelled images in Joint Photographic Experts Group (JPEG) format, with encoded radiometric metadata. The analysis software program utilised to assess BAT function in the current studies provides a quantitative temperature or photon count for each pixel beneath the cursor as the cursor scans over the image on the computer.
In order to analyse the thermal images, the files were firstly converted to a Matlab file format (.mat). Thermograms were opened in the ThermoCam professional software (ThermaCAM researcher Pro 2.1), in conjunction with an Autohotkey script. The software opened and viewed each image, whilst the coded script stated that by pressing the key "F12", the JPEG files would be converted into ".mat" files. The converted files were exact replicas of the original images and all were counted to ensure that the correct number had been converted. The thermograms could subsequently be analysed.
The sequence of images was processed with an automated analysis program (MATLAB™, [Version R2013a]). The software's "area tool" was used to define a region of interest (ROI) encompassing the upper thorax and neck, using five apices each corresponding to the right and left acromion, the angle where the jaw meets the neck on the left and right side, and the sternum. A non-adipose tissue reference region was located directly below the central apex of the ROI. This process was repeated for all thermograms. The resulting output created was one black and white '.png' image

for each thermogram, which displays the left and right ROI (Figure 2.2). The hottest 10% of data points within each ROI were identified and the median values of these points were calculated as previously reported (Robinson et al, 2014; Symonds et al, 2012) and was subsequently analysed for statistical significance in GraphPad (Prism version 7.0c for Mac OS X, GraphPad Software, La Jolla California USA, www.graphpad.com).

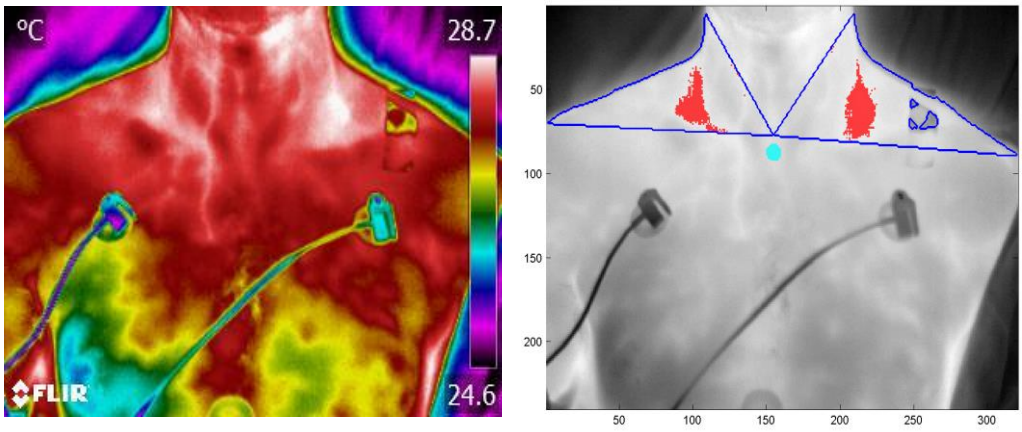

Figure 2.2. Thermogram output in Matlab software program
For each thermogram (displayed on the left), black and white '.png' images displaying the left and right 'region of interest' (ROI) are produced. The figure represents one participant. The pixels within each ROI comprise of the radiometric temperature data in the 10% of values and are highlighted by the red colouring in right image.

2.2.1.3 IRT imaging in newborn infants

IRT imaging of the major SCR BAT depot has been conducted in infants as young as 3 years of age (Symonds et al, 2012). However, a new protocol was specifically developed for IRT imaging in healthy, full-term infants and is explained in Chapter 5. Broadly speaking, the major differences in acquiring images in IRT protocols between adults and clinically-stable newborns are highlighted in Table 1.

Table 2.1. Major differences in the acquisition of thermograms between adults and healthy newborns

	Adult	Healthy Newborn
Major BAT depot	SCR	Interscap
Imaging platform	Participant sat on a chair facing IRT camera	Infants laid prone on a resuscitaire or in an Incubator
Ability to remain still throughout IRT	Yes	No
Analysis method	Median of ROI (reference) and hotspot (SCR) calculated using UoN MATLAB™ algorithm.	Define ROI in FLIR Tools+ software and export as CSV for calculation of median of hotspot.

CSV, comma separated value; Interscap, interscapular; IRT, infrared thermography; ROI, region of interest; SCR, supraclavicular.

2.2.1.4 Near Infrared Thermography in adults

Near-infrared light (in the NIR spectrum 700 to 1000 nm wavelengths) can be used to measure the regional tissue oxygen saturation (rSO_2) of an area of interest. NIRS systems comprise a NIRs monitor, a hub, signal processors and light source (e.g. a LED) within the rSO_2 sensors, which are usually attached cutaneously to the skin overlying the tissue of interest (Figure 2.3).



Figure 2.3. Near-infrared system set up, supplied by Nonin Medical Inc. (Plymouth, Mn, USA)
NIRS system comprises of a monitor, hub, signal processors and NIRS sensors to assess tissue oxygenation.

Respective stickers of the probes serve to stabilize the sensor's position over long study periods and can also act to restrict entrance of ambient light into the measurement photon pathway (Figure 2.4). In the present work, NIRS technology was used to acquire a trace of rSO_2 during a cold exposure challenge, in the SCR region potentially containing BAT deposits; in the deltoid muscle region acting as a reference position, which is separated from the BAT deposits on the left side and; in a peripheral site, using the superficial tissue of the forearm.

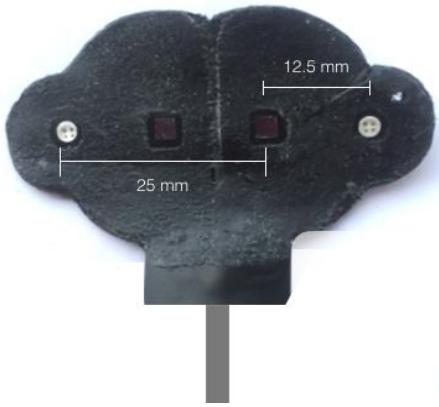

Figure 2.4. The smallest (neonatal) dual-emitter and dual-receiver probe used in the Nonin Medical Inc. Near-infrared system.

The correct choice of rSO_2 sensor is crucial, seeing as the distance between the source of NIR light (point of light entry) and the receiver of the reflected light (exit), determine the depth and volume of the trans-illuminated tissue underneath the sensor (Davie & Grocott, 2012). The penetration depth varies, usually in the range of 1 to several centimetres, under the assumption of a 'banana-shaped' pathway of the light from the superficial emitter through the tissue of interest and back to a superficial detector (MacLeod et al, 2012). In essence, the greater distance between the light source and the detector, the greater the light penetration. Using a 15mm probe, penetration is 7.5mm, thus, the measurement will be influenced by subcutaneous oxygen consumption and will undoubtedly not reflect skeletal muscle oxygenation. Using deep penetrating probes of ≥25 mm means NIRS light can trans-illuminate tissues of up to several centimeters and can even penetrate the skull, which allows for the most common application of NIRS in the real-time assessment of regional cortical oxygenation (Epstein and Haghenbeck, 2014).

Additionally, the NIRS Nonin technology (Nonin Medical, Inc. Plymouth, MN, USA) used in this work utilises dual emitters of light and dual receivers to collect the fraction of light returning to the tissue's surface, integrated into each NIRS probe. This is advantageous as firstly, the source-to-detector distance in the probes used varied at two lengths: 12.5 and 25 mm, respectively. Therefore, the measurements attained at either the SCR

region potentially containing BAT deposits, or at the skeletal muscle level will be representative of oxygenation at these sites. Secondly, the probes containing dual emitters and receivers enable the measurement of rSO_2 without significant signal contamination from shallow tissue that interferes with the measurement accuracy seen with the use of rSO_2 sensors of other companies (Covidien [Dublin, Ireland]) (Figure 2.5).

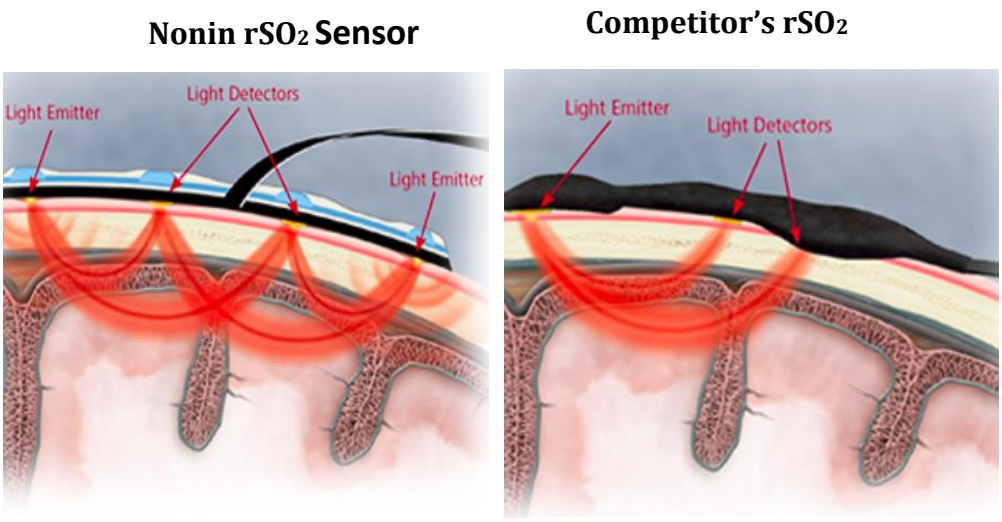

Figure 2.5. Differences in regional tissue oxygen saturation (rSO_2) sensors between Nonin Medical Inc. and other companies (Covidien [Dublin, Ireland])
Nonin rSO_2 sensors use two emitters and two detectors that are minimally affected by intervening tissue. Whereas, other sensors use one emitter and two detectors, which have a greater signal contamination from shallow tissue. Figure taken from http://www.nonin.com/equanoxtechnology.

The simultaneous recording of up six channels can be made by the Nonin Medical Inc. device, which also includes the use of pulse oximetry to measure pulse rate. Oximetry data for each channel (rSO_2 and pulse rate) is sampled and recorded in memory once every 4 seconds. Oximetry data is sampled and recorded once every 4 seconds. Using a computerized algorithm based on the principles of the Beer-Lambert law, oxygen saturation values are stored in 1% increments in the range of 0 to 100% (Tosh & Patteril, 2016). The accuracy of the Nonin Medical Inc. to assess tissue oxygen saturation within the range of 70-100% is ±2% (Nonin Medical, 2014).

2.2.1.4.1 Study set up

The NIRS set up follows that described in the Nonin technology manual provided with instrumentation. Illustration of the NIRS components is previously described in Figure 2.3. NIRs probes were attached to the relevant skin sites; SCR BAT, Deltoid muscle, forearm and a pulse oximeter on the Digitus Medius (Diagrammatic representation shown in Chapter 4.2), ensuring that the sensor surface adheres to the skin to prevent any emitted light from travelling along the surface between emitters and detectors. Sensors were additionally secured using tegaderm tape (3M™ Tegaderm™, Bracknell, United Kingdom) to help prevent ambient light from entering. Data recording began as soon as the sensors were firmly secured to the skin when there was ample signal conductivity and recording ceased when the Nonin monitor was switched off. The recorded data were automatically saved and stored on the device. Each participant's data were transferred from the Nonin monitor to a computer using Bluetooth connectivity once the adjoining software for the oximetry system had been opened (SenSmart software) and data were exported into Microsoft excel for subsequent analysis.

2.2.1.5 Laser Doppler Flowmetry in adults

Laser Doppler Flowmetry (LDF) estimates blood perfusion in the microcirculation (Bakker et al, 2014). LDF uses continuous wave helium-neon (He-Ne) laser, at a 640 nm wavelength, as a light source which illuminates a tissue sample, directed by an optical fibre to the probe head, applied to the skin surface. The light will penetrate to a depth of approximately 1.5 to 2 millimetres. All red blood cells traversing this volume will be struck by laser light, partly reflecting it, where the light undergoes a doppler shift; the frequency shift that arises in light that has been scattered by moving red blood cells. The illuminating light is back-scattered from the tissue and picked up by two optical fibres which convey the back-scatter fraction to photo-detectors and an estimate of the blood perfusion can be achieved (Figure 2.6) (Bakker et al, 2014).

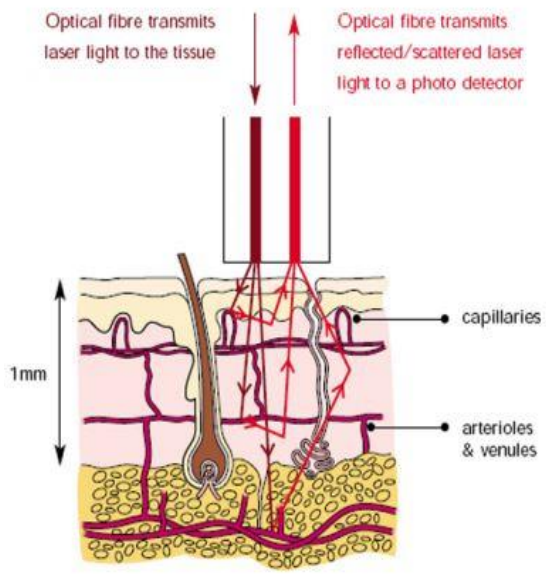

Figure 2.6. Mechanistic properties of laser doppler flow
An illustration of a laser light being directed to the tissue surface by an optic fibre and the resultant Doppler shift causes scattered light to be reflected from the tissue and transmitted by an optical fibre to a photo detector where an estimate of the blood flow can be achieved. Figure taken from http://www.moor.co.uk/ckfinder/userfiles/files/Moor_Laser_doppler_theory_Issue_1.pdf.

The doppler shifted signal is shown as a concentration and velocity (flux) of red blood cells using an arbitrary term 'perfusion units' (PU), where the conversion of 2.5 volts of blood flow is equivalent to 250 PU, calculated by the software used by each Doppler device. As red blood cells represent a majority of moving objects within a blood vessel, the measurement of the Doppler shifted back-scattered light generates the PU values. However, commercially available LDF devices cannot currently determine absolute blood flow perfusion values (e.g. blood flow in 100g tissue: mL min^{-1}/100 g^{-1}/tissue) (Limjeerajarus, 2014).

2.2.1.5.1 Instrumentation set up

An optical probe was connected to the instrument and attached to the surface of the skin on one side of the SCR region by a double sided-adhesive ring by firmly applying pressure for 15 seconds. The probe has an integrated memory chip to save calibration constants. A USB cable connected the instrument to the study laptop containing the Moor-VMS PC software (Moor Instruments Ltd.). The instrument was switched on and allowed to reach a steady state for 5 minutes prior to making any measurements. A new blank recording file was created, where the participant's study number and the study date were entered, alongside the study time. Immediately prior to the commencement of the study, the 'record' icon was pressed, which then began the measurement period and remained in the recording phase until the completion of the study. To reduce signal noise, the PC software allowed for the smoothing of data every 0.5 seconds and running averages of data for every 30 seconds. Data were subsequently extrapolated into Microsoft excel, allowed for analysis.
Throughout the study, special attention was paid to the participant with regards to their ability to control for relative movements of the area in which the probe was attached (i.e. induced by breathing, etc.) to reduce artefact in the perfusion signal.

It was also important to ensure that there was no direct illumination of the measurement site from external lighting sources and/or direct sunlight, as excessive ambient lighting at the probe site can disturb the blood perfusion reading. To control for any erroneous readings due to excessive ambient lighting levels, the attached probe and measurement area was covered with a light piece of opaque material.

2.3. Rodent study

Pregnant female Sprague Dawley rats were housed at the University of Nottingham's Biomedical Science Unit, Medical School. Dams were housed at 1 week prior to their predicted birthing date and housed thereafter with their pups. Dams had free access to chow and pups to maternal milk. All rats had free access to water at all times. Rat pups at the age of 7 and 21 days' post birth were entered into the study. Environmental temperature was maintained at 21°C, with the light/dark exposure regulated to minimise the effects of circadian rhythm (Bedrosian & Nelson, 2017; Fonken & Nelson, 2014). All experimental studies were conducted in accordance with the UK Animals (Scientific Procedure) Act of 1986 (Project licence, PPL 40/3560). Pups at postnatal (PND) days 7 and 21, experienced acute whole body vibration (WBV), to examine the effects of early life stress on selected BAT gene expression, some 21-hours later. Details of vibration stress are explained in Chapter 6.2.

2.3.1 Collection of serum samples

All blood samples were taken by Dr Lara Shipley and Dr Ian Bloor according to the serum preparation method set by Thermo Fisher Ltd (United Kingdom). A needle was introduced into the intracardiac muscle under the sternum. For any samples where blood failed to be collected in this area, particularly in the 7 day old rodents, serum was collected from the external jugular vein in the neck upon decapitation. Upon collection the whole blood was allowed to clot for 30 minutes by leaving undisturbed at room

temperature. Blood samples were then centrifuged at 2000g for 30 minutes. The resultant supernatant is the designated serum. Following centrifugation, the serum was aspirated into a clean polypropylene tube using a Pasteur pipette. During this process, samples were maintained at 2-8°C whilst handling. Serum was portioned into 0.5mL aliquots and stored at -80°C until later analysis.

2.3.2 Collection of Tissue Samples

Tissue and blood samples were collected by Dr Lara Shipley and Dr Ian Bloor, as soon as possible after humane euthanasia of the rat pup by cervical dislocation and death was confirmed by decapitation as stated by the guidelines in Schedule 1 of the Animal Scientific Procedures Act, 1986. WAT and BAT tissues were taken and included interscapular and perirenal BAT depots, alongside, inguinal WAT. Organs including the brain, lungs, heart, liver and kidneys were also dissected out carefully and weighed prior to either being snap frozen or fixated in in 10% formaldehyde, depending upon the intended analysis. Samples were subsequently stored at -80 °C.

2.3.3 Analysis of Tissue Samples

Prior to any molecular bench work, all surfaces and instruments were cleaned with RNAse Zap® (Ambion, California, USA), or 1% Virkon disinfectant (Antec International, Suffolk, UK) and 70% denatured ethanol (Ecolabs, Surrey, UK). Experimental work was performed on ice, using autoclaved and sterile equipment including filter pipette tips, whilst wearing a laboratory coat and latex gloves (Fisherbrand™, Loughborough, UK). These practices were followed to eliminate the possibility of contamination and to preserve the integrity of all samples throughout the performed experimental procedures. The selected tissues were removed from -80°C storage and transferred to dry ice for sampling.

2.3.4 Ribonucleic acid extraction from rodent tissue samples

Total Ribonucleic (RNA) extraction from tissue can be achieved using the widely utilised and published single step acidified phenol-chloroform homogenisation method (Cox and Arnstein, 1963), alongside an RNA extraction kit. Through lysing the desired samples and homogenising in a phenol and guanidine isothiocyanate monophase buffer solution, this causes the denaturing and dissolution of all proteins and inhibition of any RNase activity, ensuring that the intact RNA will be obtained at the end of the procedure. The addition of chloroform gives rise to the formulation of three phase layers; the top clear aqueous phase with RNA dissolved exclusively in it; the intermediate phase containing dissolved DNA; and the organic lower phase containing dissolved proteins. Upon separation, the upper aqueous phase is treated with ethanol to provide appropriate binding conditions to the RNA centrifuge column where total RNA (>100mg) binds to the membrane. A subsequent series of washing steps with ethanol and guanidium salt-based buffers removes any contamination and the final elution of RNA can be performed using nuclease-free water.

2.3.4.1 RNA extraction procedure

The interscapular BAT depot was used for analysis in this study. Each interscapular BAT sample was assigned an animal number and transferred into a dry ice box. An adequate amount of tissue (50-60mg) was chopped from each sample and placed into the corresponding labelled Dispomix tube (Medic Tools, Zurich, Switzerland) on dry ice.
Five hundred microliters (500µl) of TRI® reagent (Sigma Chemical Co. Poole, UK) was added to each sample and all samples were then homogenised at 3000 rpm for 40 seconds using a Dispomix homogeniser (Medic Tools, Zurich, Switzerland). The homogenate was then centrifuged at 3220g for 1 minute at room temperature (22°C) and transferred to a new labelled, sterile 1.5ml Eppendorf tube. One hundred microliters of analytical-grade chloroform (Fisher Scientific, Leicestershire, UK) were added,

vortexed and samples were left at room temperature for 10 minutes. Following incubation, the samples were centrifuged at 12000g for 15 minutes at 4°C, to allow for phase separation, after which, the top aqueous layer (~300µl), containing the RNA, was carefully aspirated and pipetted into a genomic deoxyribonucleic acid (gDNA) column and centrifuged for 8000g for 1 minute at room temperature, to remove any remaining gDNA contamination. An equal volume of 70% ethanol to the amount of RNA in the top aqueous layer previously aspirated was added to each sample and mixed by vortex.

RNA was extracted using the RNeasy Plus Universal extraction kit (Qiagen, West Sussex, UK) by transferring 700µl of each sample into an RNeasy mini-spin column and centrifuging at 8000g for 15 seconds at room temperature, discarding the flow through, with all RNA being retained in the column. This step was repeated until the total sample volume (700 µl aliquots) passed through the column. The membrane in the RNeasy spin column bound all the RNA and contaminants were washed away in the flow through. Seven-hundred microliters of buffer RW1 was added to each column and samples were centrifuged at 8000g for 15 seconds at room temperature, to wash the spin column membrane, the flow through was discarded. Five-hundred microliters of buffer RPE was then added and samples centrifuged at 8000g for 15 seconds, again at room temperature. The flow through was discarded and this step was repeated but samples were centrifuged for 2 minutes at 8000g. The RNeasy column was then transferred to a sterile, 2ml collection tube and samples were centrifuged at 8000g for 1 minute to eliminate any chance of buffer RPE carryover, which may interfere with future RNA applications. The mini-spin column was then transferred to a sterile 1.5ml Eppendorf tube, 50µl of RNAse-free water was added and samples were centrifuged at 8000g for 1 minute at room temperature. The eluted sample was then pipetted back into the column and samples were centrifuged for a final time at 8000g for 1 minute, in order to obtain a higher concentration of RNA.

2.3.4.2 Determination of RNA concentration purity and integrity

RNA concentration and purity measurements were determined using a NanoDrop ND-1000 (NanoDrop Technologies, Wilmington, USA) spectrophotometer (Desjardins and Conklin, 2010). Upper and lower optical surfaces of the microvolume spectrophotometer sample retention system were cleaned by pipetting 2-3µl of deionized water onto the lower optical surface. The NanoDrop software was opened and a blank measurement was performed by dispensing 1µl of buffer onto the lower optical surface using a calibrated pippetor. Both optical surfaces were cleaned with a dry, lint-free lab wipe. For each nucleic sample, 1µl was dispensed onto the lower optical surface for measurement to be made. The ratio of the optical density (OD) of RNA at 260 and 280 nm was quantified and an absorbance ratio between 1.7 and 2.2 was considered an acceptable indicator of good RNA quality without contamination (Desjardins and Conklin, 2010) (Figure 2.7). All extracted RNA samples were stored in a freezer at -80˚C until further use.

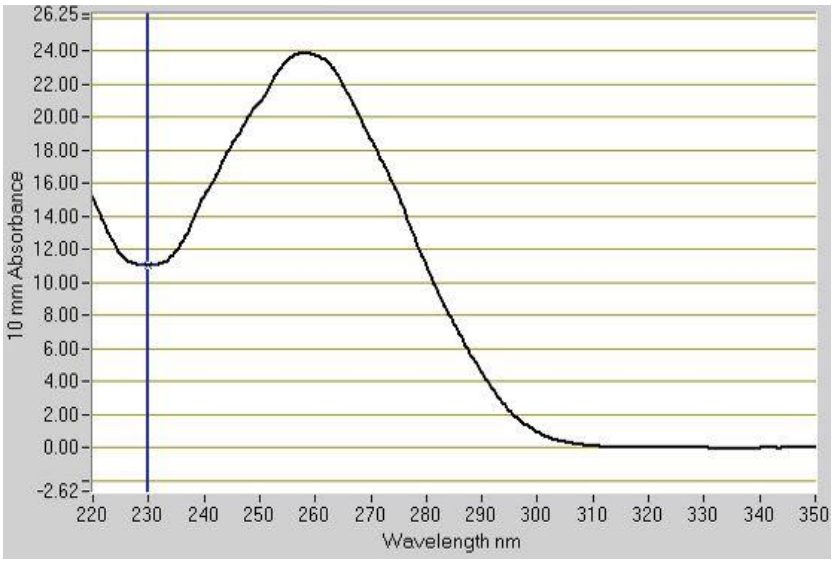

Figure 2.7. Determination of RNA concentration purity and integrity. The typical nucleic acid sample holds a characteristic profile. Pure nucleic acids typically yield a 260/280 ratio of ~1.8 and a 260/280 ratio of ~2.0 for DNA and RNA, respectively. Information from https://mlz-garching.de/files/nanodrop_2000_user_manual.pdf.

2.3.4.3 Reverse Transcription Polymerase Chain Reaction (RT-PCR)

Reverse Transcription -Polymerase Chain Reaction (RT-PCR) is a sensitive and useful technique for detecting cell specific gene expression, evident by the presence of specific mRNA (Powell, Ferguson, Bowman, & Snape, 2006). RNA itself cannot serve as a template for PCR, so must firstly be transcribed into complimentary DNA (cDNA), which can subsequently be amplified by PCR to produce numerous copies of cDNA.

The process of reverse transcription where RNA is transcribed into cDNA, is catalysed by the enzyme reverse transcriptase. Initiation of the reaction by annealing the oligo-dT primer to its complimentary sequence on the mRNA strand, is subsequently followed by the action of reverse transcriptase which acts to elongate and transcribe the first cDNA strand. The template strand of mRNA is then removed by RNAse and the cDNA strand can then be utilised and amplified by PCR (Figure 2.8).

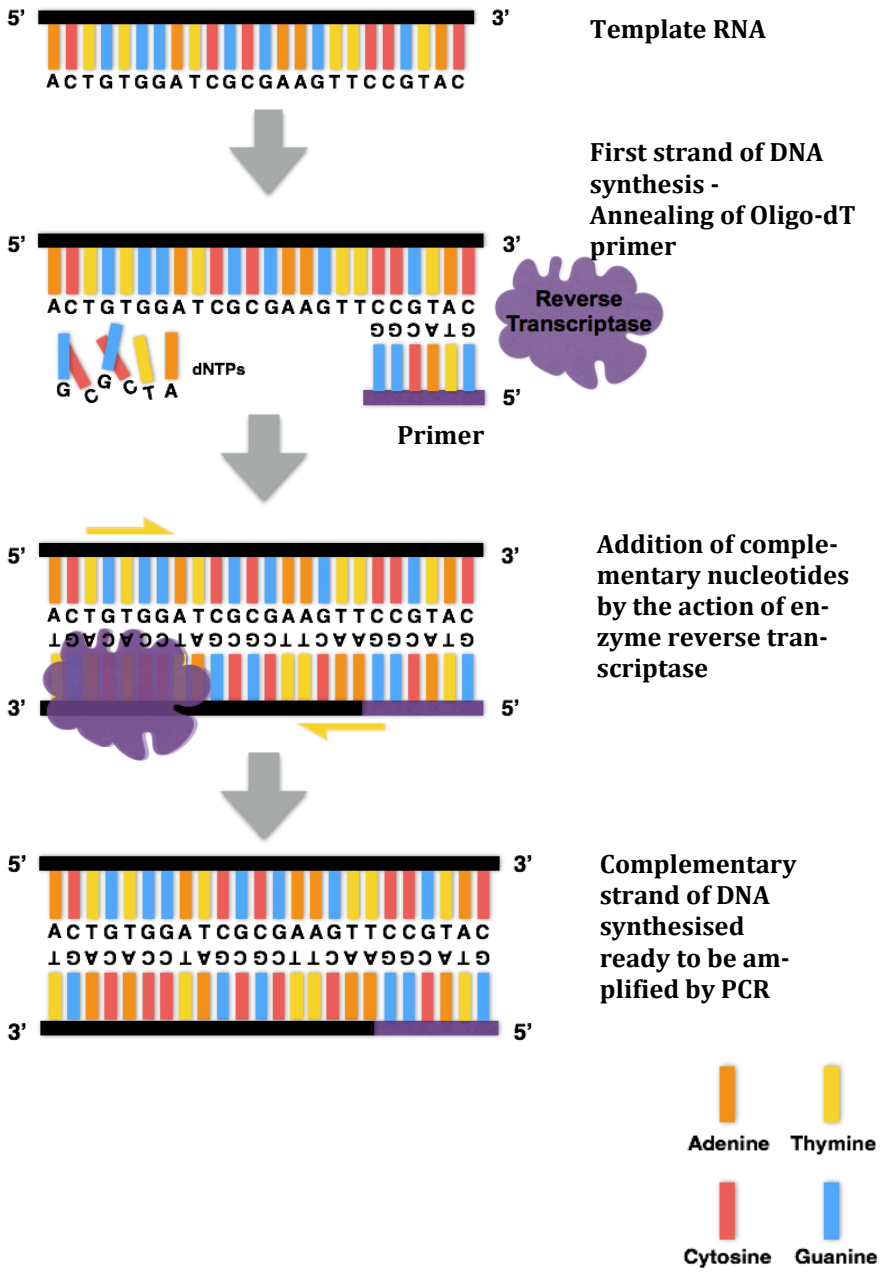

Figure 2.8. The process of Reverse Transcription Polymerase Chain Reaction

A primer binds to the single stranded messenger RNA (mRNA) and the sequence is elongated by the addition of complementary nucleotides by the enzyme reverse transcriptase to synthesize a complementary DNA (cDNA) strand. The double stranded cDNA is then amplified by polymerase chain reaction.

2.3.4.4. Procedure for Reverse Transcription Polymerase Chain Reaction

RT-PCR was performed using sterile equipment, on an uncluttered hygienic bench. Benches were wiped down using 70% ethanol and RNases prior to beginning the procedure. RT-PCR was performed using a High Capacity RNA-to-cDNA kit (Applied Biosystems, Warrington, UK), which encompassed a 2X RT Buffer and 20X enzyme mix. Components were stored in a -20°C freezer and were placed onto ice (4°C) alongside each sample to thaw prior to reactions. Sterile 0.2ml Eppendorf tubes were labelled for each sample alongside a tube for a No-Template-Control (NTC) and a No-Reverse-Template-Control (NRTC).

After the determination of RNA purity for each sample using Nanodrop spectrometry, concentrations were recorded in ng per µl. RNA concentrations were then converted to µg per µl by dividing by 1000 and 1µg of RNA template made up to a maximal volume of 9µl with nuclease-free water was pipetted into 0.2ml Eppendorf tubes.
Ten microliters of 2X RT Buffer and 1µl of 20X RT enzyme mix was added to each sample and the NTC, making a total sample volume of 20µl. Ten microliters of 2X RT Buffer and 1µl of nuclease-free water was added to the NRTC tube. The reaction mixture was centrifuged for 1 minute at 4000g and incubated for 60 minutes at 37°C followed by heating to 95°C for 5 minutes and holding at 4°C in the Techne Touchgene Gradient thermal cycler (Techne Incorporate, New Jersey, USA). Upon completion, template cDNA samples were diluted to 1:10, with 10µl of cDNA in 90µl of nuclease-free water and diluted cDNA stock was stored at -20°C.

2.3.4.5 Polymerase Chain Reaction

The development of the polymerase chain reaction (PCR) was a huge breakthrough in DNA analysis (Mullis, 1990), which allowed for the isolation and amplification of a specific region of a small known quantity of DNA sequence using a pair of complementary oligonucleotide forwards and reverse primers in an enzymatic reaction. This reaction comprises the target DNA, a pair of primers that hybridize with the flanking sequences of the target, deoxy-ribonucleotide triphosphates (dNTPs), a thermostable enzyme (Taq Polymerase) and a suitable pH and ion buffer. Amplification of the target sequence occurs by repeated cycles of 3 steps; initialed by template denaturation of the double stranded DNA; annealing primers to the complimentary sequence and the extension of the annealed primers to the enzymatic reaction (Dorak, 2006). After each full cycle, the DNA product is doubled, resulting in an exponential increase of target DNA, approximately 2^n, where *n* is the number of cycles (Dorak, 2006). Figure 2.9 demonstrates the basic PCR principles resulting in the amplification of target DNA sequence.

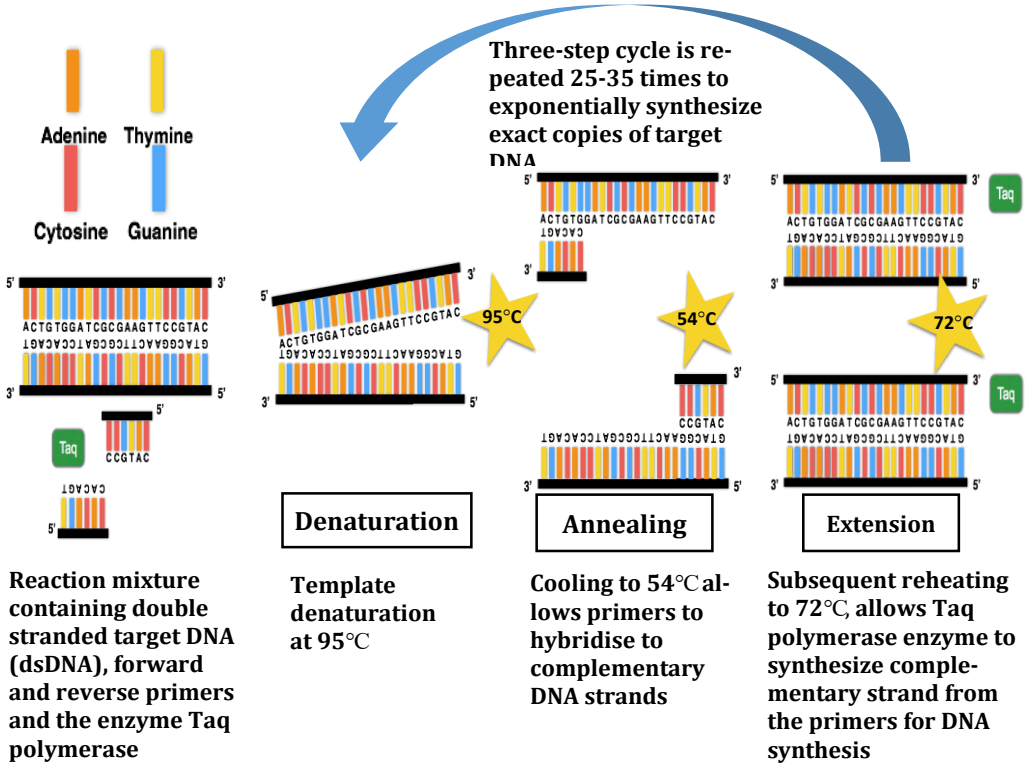

Figure 2.9. Polymerase chain reaction with Taq DNA polymerase
DNA amplification is achieved by three steps; Denaturation, in which doubled stranded DNA templates heated to 95°C denature into two separate strands; Subsequent cooling to 54°C allows for annealing, in which primers hybridise to the complementary DNA strands; Reheating the sample mixture to 72°C allows for extension, in which Taq DNA polymerase extends the 3′ end of each primer along the template strands. The cycle is repeated 'n' number of times to produce 2^n number of cDNA strands.

The primer design is a vital aspect when conducting PCR analysis, since the elongation and amplification may only occur on the DNA sequence to which the complimentary primers have annealed. Thus, poorly designed primers may result in a reduced product yield, through interaction between each other to form primer dimers and hairpins, or through dissimilar annealing and melting temperatures, which are affected by the length of the primer and sequence content (Dieffenbach et al, 1993). Table 2.2 demonstrates the guidelines for general parameters for designing the optimal PCR primer.

Table 2.2. General parameter guidelines for optimal polymerase chain reaction primer design (Dieffenbach et al, 1993)

Parameter	Optimal Values
Primer length	18-30 bases
Melting temperature (T_m)	55-72℃
Percentage guanine/cytosine (GC) content	40-60%
Distance between two primers on target sequence	<2000 bases
T_m difference between forward and reverse primer pair	≤5℃

2.3.4.6 Quantitative Polymerase Chain Reaction

Due to the advancements in PCR technology, nucleic acid analysis can be achieved in real-time to allow for the detection and quantification of a sequence of DNA or mRNA simultaneously, without the additional analysis steps of northern blotting, thus, reducing the time, expenditure and the probability of contamination (Dorak, 2006). Quantitative PCR (Q-PCR) detects and quantifies a PCR product by measuring the signal of fluorescence emitted by a fluorogenic chemical reagent, such as SYBR green, once bound to DNA or cDNA. The intensity of fluorescent signal is proportional to the amount of DNA. Fluorescent dyes emit a basal level of fluorescence, which the Q-PCR instrument calculates as PCR cycles in which a reporter fluorescent signal is accumulating, but is beneath the limits of detection of the instrument (usually between three and fifteen PCR cycles). The detector unit within the Q-PCR instrument will only detect the fluorescent signal when a certain threshold of fluorescence is crossed, also referred to as the cycle threshold (C_t) or crossing point (C_p). The C_t is the parameter used for quantification and is defined as the fractional PCR cycle number at which the reporter fluorescence is greater than the minimal detection level {Arya, 2005), or simply, the initial amount of target template. PCR amplification of a target sequence occurs at an exponential rate, the Q-PCR

instrument graphically represents such increase in fluorescent signal as a sigmoidal curve, for which the linear section of the curve is compared to signals from other samples in the same experiment (Figure 2.10).

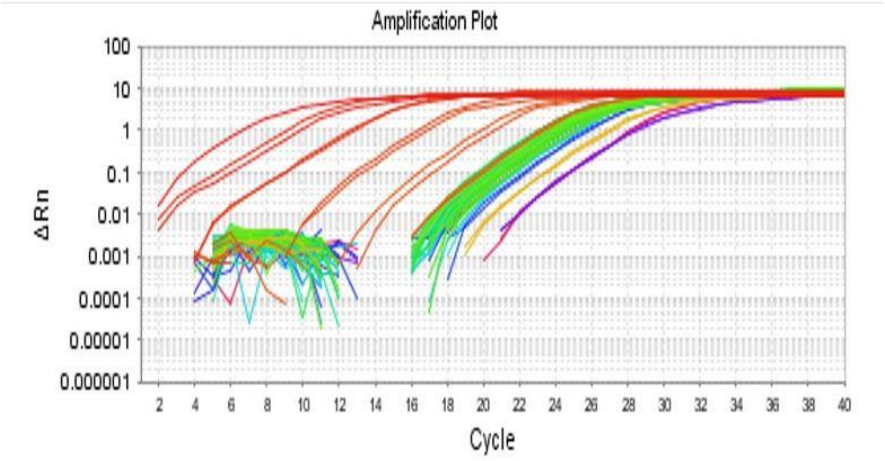

Figure 2.10. The sigmoidal curves in Q-PCR
Fluorescent signal crosses threshold and increases exponentially until plateau from expenditure of reagents or cycle number. Red lines represent external standards, green are unknown samples and blue represent negative controls.

2.3.4.7 The standard curve

Q-PCR produces a standard curve; where serial dilutions of a known concentration of target cDNA are amplified using the target sequence primers and then subsequently used to calculate the concentration of an unknown from a standard curve. The plot of the log concentration of initial target copy number for a set of known standards against cycle number when the cycle threshold is reached, is a straight line (Higuchi et al, 1993) (Figure 2.11). The generation of a standard curve enables the calculation of efficiency of the reaction (E) and correlation coefficients (R^2) of duplicate samples, which acts as a positive control for verification of the experiment. The efficiency of PCR should lay between 90-100% and may be affected by the following factors; samples may contain PCR inhibitors; PCR primer design may not be optimal; Inaccurate sample and reagent pipetting and; the standard curve may not have been properly analysed. If analyses are affected by one or more of these factors, the experiment should be repeated.

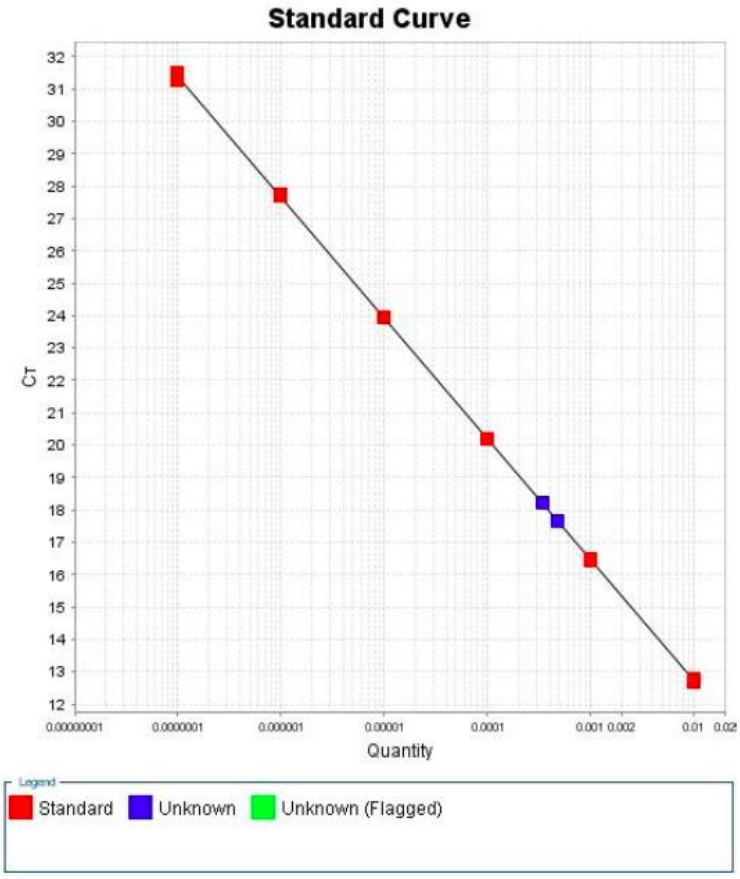

Figure 2.11. The standard curve
A standard curve produced from Q-PCR. A linear graph of exponential polymerase chain reaction is produced by plotting the cycle number at a cycle threshold against the logarithm of the known dilution series. Standard dilutions are created by using duplicated ten-fold serial dilutions of purified template of the target cDNA. The assays have a six log linear dynamic range from 10^{-2} to 10^{-7} copies of the template cDNA.

2.3.4.8 Identifying non-specific PCR products

Similarly, to standard PCR, primer design is a key component to specific region amplification of a sequence. However, fluorogenic chemical dye reagents such as SYBR green bind to the desired doubled stranded DNA molecule and also, to non-specific bound dye-DNA complexes, such as primer dimers. Thus, the assay should be optimised so that only the specific target of interest is amplified and that the non-specific products can be identified and excluded. The Q-PCR instrument generates a melt curve upon comple-

tion of the cycles by recording the loss of fluorescence signal, as the temperature is raised from 60°C to 95°C, resulting in denaturation of the PCR product at given melting temperature. Melting temperatures are dependent upon length and sequence base composition, but denaturation at a specific temperature should produce a single peak (Figure 2.12). Further, the presence of non-specific products can be identified as multiple of broader melting curve peaks.

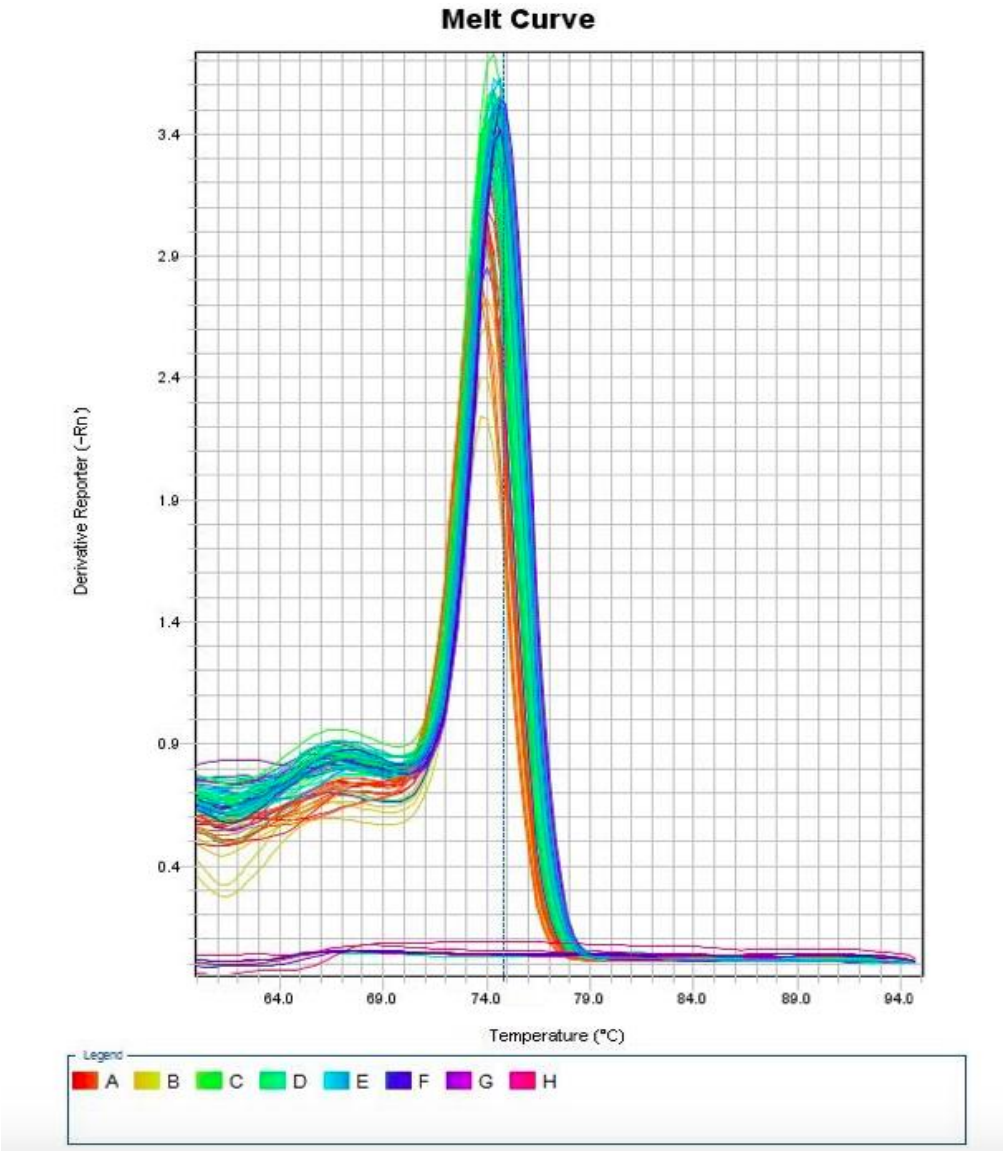

Figure 2.12. A typical melt curve produced as a result of Q-PCR
The single peak indicates specificity of product amplified.

2.3.4.9 Quantification of gene expression

To quantify gene expression of a given sample, it is imperative to normalise for any variation in starting RNA abundance. The relative quantification of gene expression can be determined by the comparison of the expression of the reference gene against the gene of interest, by using a mathematical model known as the comparative threshold ($2^{-\Delta\Delta Ct}$) method (Livak and Schmittgen, 2001). This model by PE Applied Biosystems, where Δc_t = [average C_t of target gene – average C_t of reference gene (of sample)], gives the amount of the target gene in the sample, normalised to an endogenous reference gene. To attain reliable results from such mathematical calculation, the amplification efficiencies of target and reference genes must be above 90% (Arya et al, 2005).

2.3.5 Selection of a reference gene

A reference gene acts as an internal control against which the target RNA values are normalised. The use of a reference gene can reduce the chance of errors occurring during the Q-PCR reaction due to minor differences in the quality or starting amount of RNA, or differences in the efficiency of cDNA and PCR amplification. The housekeeping genes such as RPLPO, TBP and YWHAZ are most commonly recommended as BAT reference genes (Zhang et al, 2016). In theory, these genes are constantly highly expressed across all cells. However, in reality, none are perfectly ideal. Based on the Minimum Information for Publication of Quantitative Real-Time PCR Experiments (MIQE) guidelines, multiple reference genes can be utilised to increase the validity of data (Bustin et al, 2009).

GeNorm software v3.5 (Primer Design, Ltd, Southampton, UK) is one of the most commonly-used algorithms utilised to evaluate reference gene expression stability, by a pairwise comparison between one reference gene and each other (Vandesompele et al, 2002). A stability value (M) is calculated for each gene and the software determines the two most suitable

genes for use as a reference gene, i.e. the two genes with the lowest M value for normalisation (Vandesompele et al, 2002).

2.3.6 Development of oligonucleotide primers for Q-PCR

Primer sequences used in this study were either taken directly from previously published studies or designed by myself using rat genome sequences from the National centre for Biotechnology Information (NCBI) online database. This database allows for the correct primer design, based on the desired amplicon and were chosen if they flanked exon boundaries in the intron sequence and have optimum annealing temperatures; guanine-cytosine base pair content and length were chosen to achieve the most desired reaction conditions. The NCBI nucleotide Basic Local Alignment Search Tool (BLAST) database was used to check all designed primers against the sequence and genome of interest to ensure amplification of the correct sequence. Primers were manufactured by and acquired from Sigma Aldrich as lyophilised powder and stored in nuclease free water at a stock concentration of 100µmol/l. Correct product design was confirmed by agarose gel. The following primer sequences were developed / predesigned TaqMan gene expression assays (Bio-Rad Laboratories Ltd.) were ordered for this study and are detailed in Table 2.3.

Table 2.3. PCR primer sequences and TaqMan probe identification numbers for rodent investigation

Gene	Oligonucleotide Sequence (5'-3') /Assay ID		Reference
TBP	Forward	5'- TGGGATTGTACCACAGCTCCA	Developed in house
	Reverse	5'- CTCATGATGACTGCAGCAAACC	
B2m	Forward	5'- ATAC CCGGCACCCGGCTGAG	Developed in house
	Reverse	5' -AGAGAGGTCCGACTGCTCGACT	
UCP1	Forward	5'- GCCTAGCAGACATCATCACCT	Developed in house
	Reverse	5'- GTTTCGGCAATCCTTCTGTC	
PRDM16	Forward	5'- CAGCACGGTGAAGCCATTC	Developed in house
	Reverse	5'- GCGTGCATCCGCTTGTG	
PPARγ	Forward	5'- GCGATCAAAGTAGAGCCTGC	Developed in house
	Reverse	5'- TGCATCCTTCACAAGCATGG	
11β-HSD 1	Bio-Rad TaqMan probe	Assay ID: qRnoCEP0023342	
β3-ADR	Bio-Rad TaqMan probe	Assay ID: qRnoCEP0028144	
FGF21	Bio-Rad TaqMan probe	Assay ID: qRnoCEP0024589	

Abbreviations: B2m, Beta-2-Microglobulin; TBP, TATA-Box Binding Protein; UCP1, Uncoupling protein 1; PRDM16, PR (PRD1-BF1-RIZ1 homologous)-domain-containing protein; PPAR, peroxisome proliferator-activated receptor gamma; 11β-HSD 1, Hydroxysteroid 11-Beta Dehydrogenase 1; ADR, adrenergic receptor beta 3; FGF21, Fibroblast Growth Factor 21

2.3.7 Procedure for Polymerase Chain Reaction

2.2.7.1 Hot Start PCR

PCR was conducted for the creation of cDNA Q-PCR standards and for primer optimisation using the cDNA produced in the reverse transcription step, as described in section (Chapter 2.2.4.4). Eppendorf tubes were labelled accordingly and a PCR master mix was prepared and added to each tube as described in Table 2.4.

Tubes were centrifuged for 1 minute at 13,500 rpm and subsequently loaded in to the thermal cycler (Techne) and were set to run on a 60℃ hot start PCR programme (Table 2.5). Upon cessation of the programmer, PCR products were stored at -20 °C until gel electrophoresis.

Table 2.4. Classical PCR reaction mix

Step	Volume per Tube
cDNA template or Nuclease-free water for negative control	2 µl
1:40 dilution forward primer	4 µl
1:40 dilution reverse primer	4 µl
PCR master mix (One Taq™ Hot Start Quick Load 2X Master Mix with standard buffer (New England BioLabs inc. USA))	10 µl
Total mixture volume	**20µl**

Table 2.5. Hot Start PCR programme conditions
Second phase of the program repeats for 35 cycles.

Process	Temperature (℃)	Duration (minutes)
Initiation	105	4
Enzyme activation	96	15
Repeated for 35 cycles:		
Denaturing of cDNA strands	94	0.5
Primer annealing	60	0.5
Primer extension	72	1
Final extension	72	7
Hold	4	∞
The second phase of cDNA denaturation, primer annealing and extension is repeated for 35 cycles		

2.3.8 Agarose Gel Electrophoresis

Agarose gel electrophoresis was carried out in order to assess the size and abundance of the PCR product. A 2 % (w/v) tris-acetate (TAE) agarose gel (2 % (w/v) made up to volume with 1g of agarose and 50ml of TAE was prepared and 0.5µl of Ethidium Bromide (EB) per ml of TAE was pipetted in to the mixture. To create the gel, the mixture was heated for up to 2 minutes, in order for the agarose to completely dissolve and become opaque in colour. The gel was briefly left to cool and then poured into a gel caster containing a comb which formed 10 wells. The gel was left to set in a fume hood for 15 minutes. Once set, the comb was removed and the gel placed in an electrophoresis box filled with TAE buffer, so that the buffer covered the top of the gel by at least 2mm.

Twenty microliters of each sample was loaded into individual wells alongside 10µl of a base pair marker (DNA 100 base pair ladder, Promega). Positive and negatively charged leads were attached to the electrophoresis power box and the gels were set to run at 80 volts, 400 mA for 35 minutes, this ensured that the dye face would have enough time to travel to at least 1cm from the end of the gel.

The ladder and PCR products were visualised under an ultraviolet (UV) illumination using a CCD camera (Fugi; Luminescent Image Analyser LAS-1000) to ensure equal loading and that no degradation had occurred. The fluorescent Bands were cut out of the gel and cPCR products extracted and purified using the QIAquick Gel Extraction Kit (Qiagen, West Sussex, UK). The gel bands were weighed and dissolved in Buffer QG solution by heating at 50°C for 10 minutes. Three volumes of Buffer QG to one volume of gel (assuming 100mg of gel = 100µl). One gel volume of isopropanol was added to the dissolved gel and mixed by vortex. The sample was then pipetted into a 2ml QIAquick spin column and centrifuged at 10,000g for 1 minute. Discarding the flow-through, 500µl of Buffer QG was added to the spin column, and again centrifuged at 10,000g, for 1 minute, followed by discarding of the flow through for the second time. Subsequently, 750µl of

Buffer PE was added to the spin column, which was again, centrifuged for 1 minute, discarding the flow through. The spin column was further centrifuged once more and any remaining flow through was discarded to remove any residual ethanol. To elute the PCR product, the QIAquick column was placed in a clean 1.5ml Eppendorf tube and 30µl of Buffer EB was directly pipetted into the center membrane of the column. The column rested for 4 minutes, which helps to increase DNA extraction rates, and was then centrifuged for 1 minute at 10,000g. The integrity and concentration of DNA was subsequently assessed using the Nanodrop® ND-1000 (Nanodrop Technologies, Wilmington, USA) spectrophotometer. The extracted cDNA samples were diluted to 1ng/µl and stored at -20°C until required. An example agarose gel for UCP1 and PRDM16 genes from interscapular BAT depot in rat pups, is demonstrated in Figure 2.13.

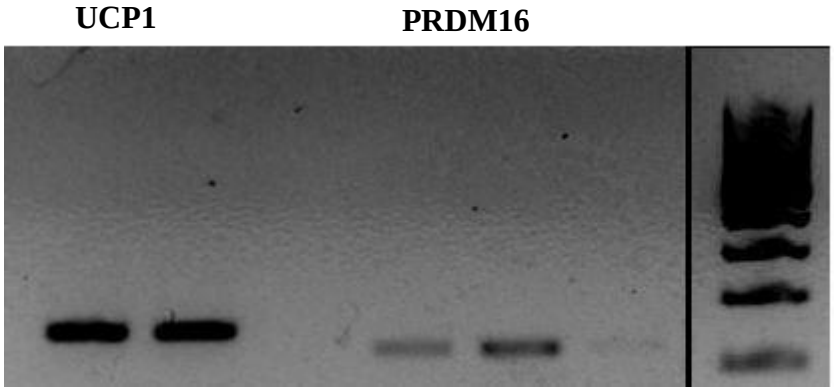

Figure 2.13. Agarose gel from UCP1 and PRDM16 genes

2.3.9 QPCR procedure

2.3.9.1 Standard curve

For each gene of interest, serial 1:10 dilutions were prepared from 1ng/µl template cDNA obtained from cPCR and gel electrophoresis. Dilutions up to and including $1x10^{-8}$ were prepared. Samples were tested in duplicate on a 96-well QPCR plate (Abgene, Thermo Fisher Scientific Inc. UK), with a negative (nuclease-free water) and positive, to verify the efficiency of the experiment.

2.3.9.2 Q-PCR of unknown samples

Samples and standards with a negative control were run in duplicate in 10µl aliquots. The QPCR reaction mixture is given in Table 2.5.

PCR plates were sealed with an Abgene plate sealer and thermal seals (Alpha Laboratories, Hampshire, UK) and plates were placed in the StepOne Plus Real Time PCR system (Applied Biosystems, Warrington, UK) and QPCR programme was run as stated in the programme outline in Table 2.6.

Table 2.6. Q-PCR reaction mixture

Reagent	Volume
SYBR Green (Applied Biosystems, Warrington, UK)	5 µl
1:40 dilution forward primer	1 µl
1:40 dilution reverse primer	1 µl
cDNA sample	3 µl
Total mixture volume	**10 µl**

Table 2.7. Q-PCR programme conditions

Process	Temperature (°C)	Duration
Initial denaturing of the cDNA strand	95	15 minutes
Denaturing of cDNA strands	95	15 seconds
Primer annealing	58-62	30 seconds
Above steps repeated for 45 cycles		
Melt curve analysis	65 to 95 in 1°C incre-ments	15 minutes
Above step repeated for 31 cycles		
Hold	95	10 minutes

2.3.9.3 Taqman Probes

2.3.9.3.1 Preparation of PCR reaction mix

Reagents were thawed on ice, re-suspended by gentle vortexing and subsequently centrifuged. Working in duplicates, 2µl of each cDNA sample was pipetted into a 0.5mL Eppendorf tube. For each sample, the following master mix components were added (Table 2.7).

Table 2.8. PCR reaction mix

PCR reaction mix component	*Volume*
20X TaqMan™ Gene Expression Assay	0.5µl
2X SsoAvanced™ Universal Supermix	5µl
cDNA sample	2µl
RNase-free water	2.5µl
Total mixture volume	**10 µl**

2.3.10 Analysis of Serum Samples

2.3.10.1 Corticosterone

Plasma Corticosterone levels were determined using the assay protocol supplied by the ordered enzyme immunoassay kit (K014-H1 ArborAssays™). This assay has been validated for serum analyses across all species other than human and has an accuracy and limit of detection was determined as 16.9 pg/mL (Assays, 2018).

Standards or diluted samples are pipetted into a clear microtiter plate coated with an antibody. A corticosterone-peroxidase conjugate is added to the wells. The binding reaction is initiated by the addition of a polyclonal antibody to corticosterone. After an hour incubation the plate is washed and substrate is added. The substrate reacts with the bound corticosterone-peroxidase conjugate. After a short incubation, the reaction is read at 450 nm wavelength. The concentration of the corticosterone in the sample is calculated using software available with most plate readers.

2.3.10.2 Corticosterone Assay Procedure

Reagents were kept at room temperature and plasma samples were thawed on ice (4°C). The assay buffer was diluted to 1:5 in deionised water and wash buffer diluted to 1:20 in deionised water. A serial dilution of Corticosterone stock solution for an 8-point standard curve was subsequently prepared. Eight Eppendorf tubes were sequentially labelled and 450µl of the diluted assay buffer was pipetted into the first tube and 250µl pipetted into tubes two to eight. As the Corticosterone solution contains an organic solvent, the pipette tip was rinsed several times to ensure accurate delivery. Fifty microliters of corticosterone stock solution were added to tube one and gently vortexed. Two-hundred and fifty microliters of corticosterone solution were taken from tube one and added to tube two and then vortexed. Dilutions were repeated for tubes three to eight. Standards were kept on ice (4°C). The concentrations of corticosterone in tubes one to eight are demonstrated in Table 2.8.

Plasma samples were pre-diluted to 1:100 in dissociation reagent and assay buffer; 5µl of Dissociation Reagent was pipetted into a 1.5mL Eppendorf tubes; 5µl of each sample was pipetted into the Dissociation Reagent in the tube and subsequently incubated at room temperature for 5 minutes. Four-hundred and ninety microliters of diluted assay buffer were finally added to each tube.

Fifty microliters of each sample or standard was then pipetted into duplicate wells of the 96 well microtiter plate. Seventy-five microliters of the diluted assay buffer were pipetted into the Non-specific binding (NSB) wells. Fifty-microliters of the diluted assay buffer was then pipetted into each well except for the NSB wells. Twenty-five microliters of Detect X Corticosterone Peroxidase Conjugate were pipetted into each well, subsequently followed by 25µL of Corticosterone Antibody to each well except for the NSB wells and the plate was incubated at room temperature on a shaker for 60 minutes. All wells were then aspirated and washed 4 times with 300µL of wash buffer. The plate was tapped well to dry.

One-hundred microliters of TMB substrate was pipetted into each well and the plate was incubated for 30 minutes at room temperature without shaking. Fifty microliters of stop solution were pipetted into each well and the plate was read at 450 nm.

The concentration of Corticosterone was calculated from the standard curve with a 4 point fit, after subtracting the mean optimal density (OD) of the NSB.

Table 2.9. Concentrations of corticosterone for standards

	Std 1	***Std 2***	***Std 3***	***Std 4***	***Std 5***	***Std 6***	***Std 7***	***Std 8***
Assay Buffer (µl)	450	250	250	250	250	250	250	250
Addition	***Std 1***	***Std 2***	***Std 3***	***Std 4***	***Std 5***	***Std 6***	***Std 7***	***Std 8***
Vol of Addition (µl)	50	250	250	250	250	250	250	250
Final concentration (pg/mL)	10,000	5,000	2,500	1,250	625	312.5	156.25	78.125

2.3.11 Statistical Analysis

The statistical tests applied to all results are described in the methodology section of each respective chapter. Analyses were performed using SPSS for Mac package (v21-22) and GraphPad Prism for Windows and Mac version 6.05. Additional details of statistical analysis will be included in the individual chapters.

Chapter 3

The effects of acute hypercortisolaemia on the thermogenic function of human brown adipose tissue

---

3.1 Introduction

The re-discovery of BAT in adult humans using $^{[18]}$F-FDG-PET/CT scanning (Saito et al, 2009; van Marken Lichtenbelt et al, 2009; Virtanen et al, 2009), advocates the tissues physiological importance far beyond that of thermoregulation in newborn infants and rodents (Cypess et al, 2012; Ouellet et al, 2012). Due to its high metabolic capacity to oxidize both glucose and lipid, BAT is an important regulatory tissue for whole-body energy expenditure (EE) and core body temperature (Cannon and Nedergaard, 2004) and is of great interest in the current worldwide obesity epidemic. Attention has therefore turned to its involvement in the pathogenesis of obesity and the exciting possibility of activating BAT to enhance energy expenditure, providing a therapeutic target for obesity and the metabolic syndrome (Nedergaard and Cannon, 2010).

BAT is characterised by the presence of its unique uncoupling protein UCP1, which mediates the uncoupling of mitochondrial substrate oxidation from adenosine triphosphate (ATP) production, resulting in the release of energy as heat from the oxidation of the primary substrate, free fatty acids (Cannon and Nedergaard, 2004). The activation of this tissue is very much dependent upon UCP1 expression and the induction of the β_3-AR signalling pathway by the SNS (Bachman et al, 2002), for which i*n vitro* studies have confirmed the presence of β3-AR in brown adipocytes (Cypess et al, 2013; Virtanen et al, 2009).

The stimulation of the SNS through a variety of stressful means, such as cold, pharmacological targets, and diet, have therefore become an attrac-

tive prospect which may help to explain how BAT can contribute to adaptive thermogenesis (van Marken Litchenbelt et al, 2011). The pharmacological stimulation of the β-AR in rodent BAT is one of the most-commonly explored pathways of BAT regulation, however, human investigations are scarce, likewise are the investigations into clarifying the role of BAT in diet-induced thermogenesis. This concept remains controversial with some authors demonstrating an enhancing level of diet induced thermogenesis and postprandial insulin sensitivity (Hibi et al, 2016; Lee et al, 2014) and others indicating an unchanged response to overfeeding by 50% (Peterson et al, 2016). Thus, BAT may play a role in postprandial thermogenesis to produce heat from fatty acid oxidation, but this has yet to be proven directly.

The role that other endocrine factors play in the regulation of BAT thermogenesis also remains largely unknown. The pre-partum elevation of cortisol is pivotal in the initiation of non-shivering BAT thermogenesis at birth (Mostyn et al, 2003). GCs are known powerful regulators of energy metabolism and have been proposed to increase cold-induced glucose uptake into BAT (Ramage et al, 2016) and to regulate BAT activity in healthy adult females, as assessed by thermal imaging (Robinson et al, 2016). However, chronic circulating hypercortisolism results in weight gain and thus, the potential for the development of obesity and type 2 diabetes mellitus (Macfarlane, Forbes and Walker, 2008). Little is known about the role that this endocrine factor plays in human BAT thermogenesis and the mechanisms that may underpin its action, which in part, may be due to the technical limitations of assessing BAT function in vivo. The field's gold standard method for BAT function analysis is $^{[18]}$F-FDG-PET/CT scanning, however the constraints of the exposure to ionizing radiation and the unsuitability for real-time tracking of BAT activation has directed the search for a non-invasive method of BAT assessment.

3.1.1 Main Aim

The aim of this study was to investigate the effects of hypercortisolaemia in healthy adult males. Since the presence of active BAT was not assessed prior to the study, the pharmacological stimulation of BAT using the non-selective β-agonist, ISO, was conducted to ensure activation of brown adipocytes. It was hypothesised that the acute infusion of the GC, hydrocortisone, would stimulate BAT and increase the temperature of the skin overlying the SCR BAT depot.

3.3 Materials and Methods

This study was approved by the Edgbaston NRES Committee, UK (REC reference 14/WM/1085). All subjects provided written informed consent. All parts of this study were conducted in a temperature controlled room at the National Institute for Health Research (NIHR)/Welcome Trust Clinical Research Facility (CRF) of the University of Birmingham at the Queen Elizabeth Hospital Birmingham, UK. Room temperature was held constant at 23-26°C and was monitored using an ambient temperature probe.

Subjects

Upon obtaining written informed consent, eight healthy male volunteers participated in this randomised, double-blind, placebo controlled study, conducted between January and March 2015. Individuals were recruited using print and electronic advertising at the University of Birmingham and the University Hospitals Birmingham NHS trust and none was selected or screened on the basis of presence of any active BAT. All subjects underwent a medical evaluation during a screening visit to ensure they were healthy. No subject had any significant past medical history, smoked tobacco or took any regular medications that could affect the study's outcome measures.

Anthropometric Measurements

Measurements were taken during the screening visit. Body composition was determined by waist circumference, measured midway between the lower margin of the last palpable rib and the top of the iliac crest, and hip circumference at the level of the greater trochanters. Total and regional fat masses were measured by dual-energy x-ray absorptiometry (DXA; type Discovery A; Hologic). Visceral fat mass was estimated by DXA using a proprietary algorithm provided by the manufacturer (Kaul et al, 2012). Core temperature was measured with a tympanic thermometer. Eight subjects met the inclusion criteria of the study (Table 3.1).

Table 3.1. Inclusion and exclusion criteria to the study (n=8)

Inclusion criteria	Exclusion criteria
Healthy, lean, young male participants No current medical condition No drug therapy	Age <18 years or >36 years of age BMI <18 or >25 kg·m^2 Any medical condition or drug therapy Current smoker Unsuitable blood vessels for cannulation (i.e. veins too small or arterial plaques)

Experimental Design

The experimental protocol for this study is illustrated in Figure 3.1. Study visits were identical, except for the nature of overnight infusion, and were at least 2 weeks apart. Subjects were admitted to the CRF in the afternoon, and a cannula for infusion purposes was inserted into a right antecubital fossa vein. At 1800 hours, they were served a standardized calorie-controlled meal (vegetable lasagne; total energy 2634 kJ; typical nutri-

tional values per 100g of product: 1.9g fat, 12.2g carbohydrates, 3.3g protein, 1.5g fibre), and then fasted until study completion the next day. Thermal imaging of the SCR region potentially containing BAT deposits, was performed for 30 minutes immediately before and after the meal, which was ingested within 20 min and was accompanied by tap water. During thermal imaging, two iButtons (iButton DS1922L, Maxim Integrated, Winnersh, UK) otherwise referred to as digital thermometers, recorded skin temperature every minute and were taped over the SCR fossa (main site of BAT) and lateral of the umbilicus (reference point; RP). At 1900 hours, a constant infusion of either hydrocortisone (HC, 0.2 $mg.kg^{-1}.h^{-1}$) or saline (S, control study visit) was started and given until study completion the following day. This dosage is equivalent to 209.1 to 277.1 mg/day and greatly exceeds the weighted daily dosage given chronically to Addison's patients as steroid replacement therapy; at 12 to 20 mg/day (Nieman & Turner, 2006). Infusions were administered in a double-blind, randomised fashion, away from the subject's and study investigators. Research nurses based in the CRF who were not directly involved in the study, prepared the infusions after a random number generator on the computer was used to randomise in the order of infusions for each subject. At 2200 hours, lights were switched off for night rest.

The following morning, cannulations for blood sampling purposes were performed; a venous catheter was placed into the superficial epigastric vein using a red light source (Schott, KL2500 LCD)**,** and an arterial catheter was inserted into the left radial artery using ultrasound guidance (Philips iE33). For the purposes of white adipose tissue blood flow (ATBF measurement), ^{133}Xe (Xenon) was injected into abdominal adipose tissue and measured continuously with a radioactivity monitor (GMS411, John Caunt Scientific, Summerseat, UK). Subjects were left to relax for 45 minutes in order to allow equilibration of ^{133}Xe and during this period iButtons were fixed to the same anatomical locations as the evening prior. After a period of 45 minutes, a baseline period of 45 minutes was under-

taken, in which thermal imaging began in the final 15 minutes of this period. Blood samples were drawn simultaneously from both sites (artery, superficial epigastric vein) at 15 minute intervals for the baseline period. At 45 minutes (0900 hours), a one-step ISO infusion (25 ng.kg fat-free mass^{-1}.min^{-1}) commenced for 60 minutes (1 ng·kg fat-free mass^{-1} min^{-1} more than that reportedly used by Vosselman et al (2012). A previous study also reported that it takes approximately 8 minutes for each ISO dose to reach a steady-state concentration in the body (Martinsson et al, 1989). Thus, the extended duration of this dose was necessary to obtain a stable period for energy expenditure with continued interval blood sampling. After the end of the infusion, BAT thermogenic activity was measured for a further 15 minutes and blood sampling was continued for 30 minutes. For the duration of the study, participants were wearing a hospital gown, with their torso exposed for the duration of all measurements.

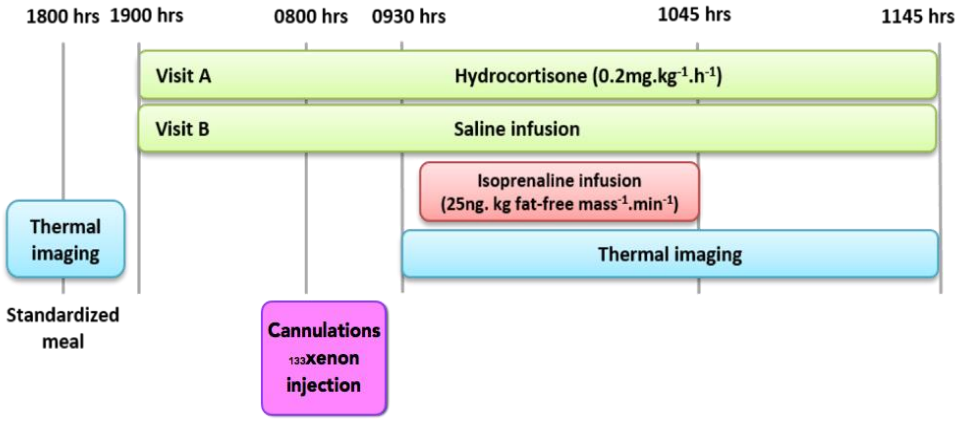

Figure 3.1. An illustrated overview of the experimental study design for Chapter 3 (n=8).

Infrared Thermography

Each subject rested in a bed in a quiet room, maintained at a constant temperature (23°-26°C). Subjects rested comfortably in a steady state, sat in a semi-supine position, with arms adducted and head positioned in a neutral position, so the subject could look straight ahead. The upper torso from the chest area to neck region was exposed. A thermal imaging camera (FLIR b60 2.3 Megapixel Infrared Camera; FLIR Systems AB, Danderyd,

Sweden) was used to acquire images of the anterior neck and upper chest region, which were sequentially processed and analysed offline by an automated analysis program, as described in the Materials and Methods chapter of this thesis (Chapter 2.2.1.1).
The camera was fixed on a tripod and positioned on a table over the hospital bed, at the level of the neck at a distance of 1m from the subject's face and from the floor. This positioning ensured comfort as well as the optimum position for visualisation of the SCR BAT depots. IRT was performed on all subjects for 15 minutes pre-ISO infusion, for the 60-minute duration of the infusion and for 15 minutes' post-infusion, at a rate of 4 images per minute (1 per every 15 seconds) for the baseline and infusion period and then 2 per minute for the post-infusion period (2 per every 30 seconds). Areas of interest were the temperature over the SCR region (T_{SCR}) representing BAT, and a non-adipose tissue reference point (T_{REF}) on the chest, close to the xiphoid.

Additional Skin Temperature Measurements

During the periods of infrared thermography, two skin contact temperature sensors (iButton DS1922L, Maxim Integrated, Winnersh, UK) recording skin temperature every minute were taped within the SCR fossa (main BAT site) and lateral to the umbilicus (white adipose tissue). For skin contact temperature measurements, data were collected every minute, and analysis was performed using 5-minute averages.

Laboratory Procedures

Blood samples were drawn into heparinized syringes, and plasma was prepared rapidly at 4°C and immediately frozen at -80°C prior to analysis. Systemic metabolites were analysed by Dr Konstantinos Manolopoulos at the Institute of Metabolism and Systems Research, University of Birmingham. Plasma glucose and NEFA concentrations were measured enzymatically using commercially available kits on an ILAB600 or ILAB650 clinical analyser (Instrumentation Laboratory UK, Warrington, UK). Cortisol was

measured by a colorimetric assay (R&D Systems, Abingdon, UK). Insulin and C-peptide concentrations were measured by ELISA (Invitron, Monmouth, UK) at a reference laboratory (Diabetes Research Unit Cymru, Swansea University, UK). Thermal imaging was conducted and analysed by myself, based in the Department of Child Health, Obstetrics and Gynaecology, University of Nottingham.

Statistical Analysis

Comparisons between groups were analysed using one way ANOVAs or t-tests for parametric data or non-parametric tests for data that were not normally distributed.

The temperature changes over the SCR region compared with a reference area during ISO infusion, measured by IRT were categorised and averaged into 6 different time points; baseline, 15, 30, 45, 60 minutes and post-infusion. One-way repeated measures ANOVAs were conducted to compare the temperature differences between basal and maximal T_{SCR} and $T_{REF.}$ SCR temperature was also compared to control chest areas for each of the time points during ISO infusion under saline and hydrocortisone conditions. Paired t-tests were conducted to compare the absolute change in cardiovascular responses from baseline between saline and hydrocortisone conditions. Further, to examine postprandial T_{SCR} after ingestion of a standardised meal.

Indexes of β-cell function and insulin resistance were calculated according to the homeostatic model assessment (HOMA) method, whereby the mean of three consecutive plasma glucose and insulin post-absorptive measurements were used. Energy expenditure was calculated based on heart rate, age and weight as previously described (Keytel et al, 2005).

Statistical significance was set at $p<0.05$. The sample size was calculated based on a similarly designed experimental study (Manolopoulos, Karpe, & Frayn, 2012). This randomised cross-over design study with an estimated sample size of n=8, with an 85% power, would detect a difference of 0.75 standard deviations at the 5% significance level for metabolic parameters. Data were analysed using IBM Statistics for Windows v21 and GraphPad

Prism for Windows version 6.05. All data are presented as mean ± standard error of mean (SEM), unless stated otherwise.

3.4 Results

3.4.1 Anthropometric and Metabolic Characteristics

The baseline anthropometric and metabolic characteristics of participants prior to the beginning of the study are shown in Table 3.2. The study was conducted in eight healthy male individuals with an average age of 20 years, average weight of 75kg and BMI of 23 kg/m^2. Three of the eight participant's systolic blood pressures were classed as being in a healthy range, three were pre-hypertensive (121–130mmHg) and two had high basal systolic blood pressures (145–146mmHg), according to the definition set by the American Heart Association (2017). However, as all eight participants' diastolic blood pressures were classed as being in a healthy range, the average basal blood pressure reading was deemed satisfactory for entry into the study. All participants who entered into the study were of a healthy body mass index (WHO, 2016).

Indoor room temperature was constantly monitored and maintained to as close to thermoneutral as possible, ensuring no significant difference between subjects (Table 3.3). Further, the study was conducted within a short time frame to minimise any effects of seasonality. In support, there were no differences in indoor room temperature (P = 0.703) or outdoor temperatures (P = 0.774) between saline and hydrocortisone experiments. (Table 3.3).

Table 3.2. Anthropometric and metabolic characteristics of male adult participants entered into the study (n=8)

Characteristic	
Age (years)	20 (18 – 34)
Weight (kg)	75.0 (61.5 – 81.7)
BMI (kg/m^2)	23.0 (20.6 – 24.2)
WHR	0.84 (0.78 - 0.9)
Trunk fat (kg)	7.7 (5.1 – 9.2)
Leg fat (kg)	5.5 (4.3 – 7.5)
Visceral fat (kg)	0.2 (0.1 – 0.4)
Systolic BP (mmHg)	124 (105 – 145)
Diastolic BP (mmHg)	72 (59 -79)
Heart rate (bpm)	58 (53 – 62)
Fasting glucose (mmol/L)	6.3 (4.9 – 7.2)
Fasting insulin (pmol/L)	30.6 (14.4 – 68.5)
Fasting NEFA (μmol/L)	707 (450 – 873)

Median and range shown. BMI, body mass index; WHR, waist-to-hip ratio; BP, blood pressure. Data presented as mean (range)

Table 3.3. Indoor and outdoor environmental temperatures between participants throughout the study, prior to and after saline (A) and hydrocortisone (B) infusions

Environmental outdoor temperature; data obtained from the Meteorological office based on temperatures in Birmingham, UK for each study day (Metoffice.gov.uk, 2015). Date of study represents the evening of which participants began study.

(A)	**Saline infusion**				
Participant	**Date of study**	**Environmental room temperature (°C)**		**Environmental outdoor temperature (°C)**	
		Infusion start	Infusion end	Infusion start	Infusion end
1	13/01/2015	23.7	25.2	6	4
2	24/02/2015	22.8	25.8	6	5
3	11/02/2015	24.4	24.0	5	5
4	21/01/2015	24.2	24.6	4	4
5	22/01/2015	24.1	23.9	4	4
6	26/02/2015	24.2	23.2	5	5
7	26/03/2015	25.2	25.2	7	7
8	24/03/2015	24.1	24.6	7	7
Mean ± SEM		**24.1 ± 0.2°C**	**24.6 ± 0.3°C**	**5.5 ± 0.4°C**	**5.1 ± 0.4°C**

(B)	Hydrocortisone infusion				
Participant	**Date of study**	**Environmental room temperature (°C)**		**Environmental Outdoor temperature (°C)**	
		Infusion start	Infusion end	Infusion start	Infusion end
1	10/02/2015	23.7	23.9	4	5
2	14/01/2015	24.0	25.3	4	5
3	15/01/2015	22.2	23.5	5	4
4	25/02/2015	25.5	26.2	5	5
5	12/02/2015	24.0	24.8	5	4
6	25/03/2015	25.2	23.6	7	7
7	11/03/2015	25.1	25.2	6	6
8	12/03/2015	25.3	23.6	6	5
Mean ± SEM		**24.4 ± 0.4°C**	**24.5 ± 0.4°C**	**5.3 ± 0.4°C**	**5.1 ± 1.0°C**

3.4.2 Effects of acute hypercortisolaemia on systemic metabolites

As expected, plasma cortisol concentrations were found to be significantly higher upon an overnight infusion of HC compared to the infusion of saline ($P = 0.001$) (Figure 3.2). Basal plasma non-esterified fatty acids (NEFAs) were elevated in both conditions due to fasting, and HC significantly increased plasma NEFA concentrations, compared to saline ($P = 0.001$) (Figure 3.3).

The infusion of HC also significantly increased basal glucose ($P = 0.01$) and insulin concentrations, compared with saline infusion ($P = 0.025$) (Figure 3.4). Consistent with this, hypercortisolaemia was seen to induce peripheral insulin resistance, as shown by the increases in HOMA IR ($P = 0.016$) and reduction in insulin sensitivity ($P = 0.004$) (Table 3.4).

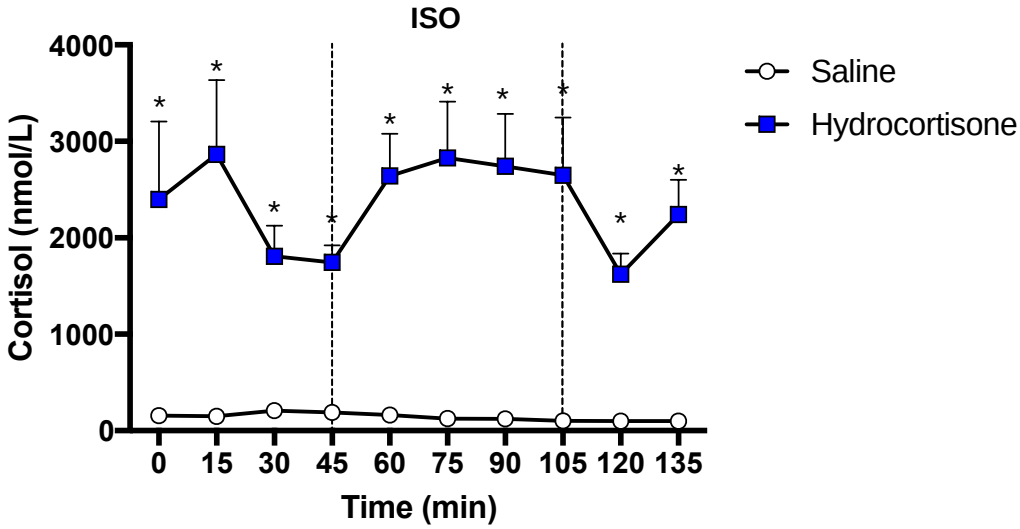

Figure 3.2. Plasma cortisol concentrations following saline infusion or hydrocortisone infusion at baseline and during an isoprenaline infusion (ISO, dotted lines indicate infusion period) in healthy male subjects (n=8)

Data are shown as mean ± standard error of mean. *$p < 0.05$ vs. control.

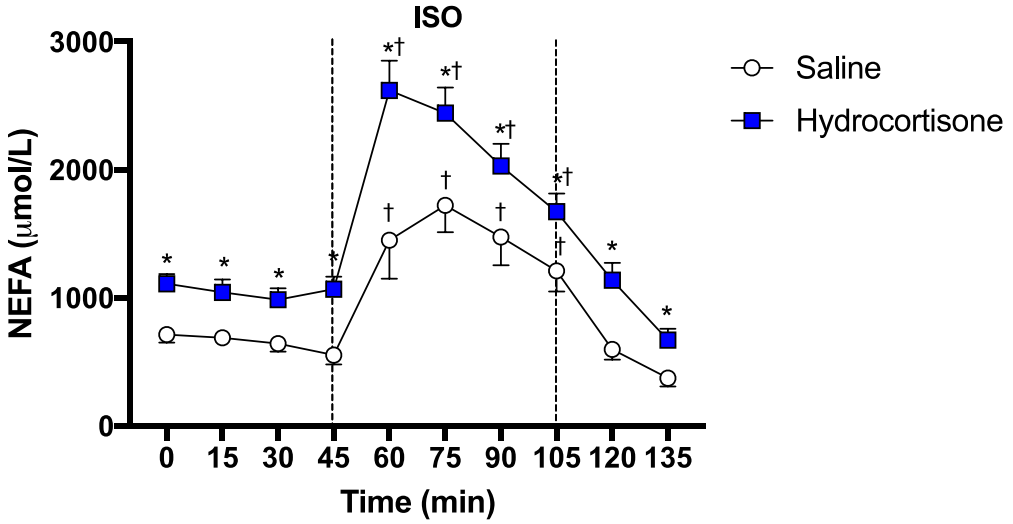

Figure 3.3. Non-esterified fatty acid concentrations (NEFA) following saline infusion or hydrocortisone infusion at baseline and during an Isoprenaline infusion (ISO, dotted lines indicate infusion period) in healthy male subjects (n=8)

Values are mean ± standard error of mean. *$p < 0.05$ vs. control, †$p < 0.05$ vs. baseline.

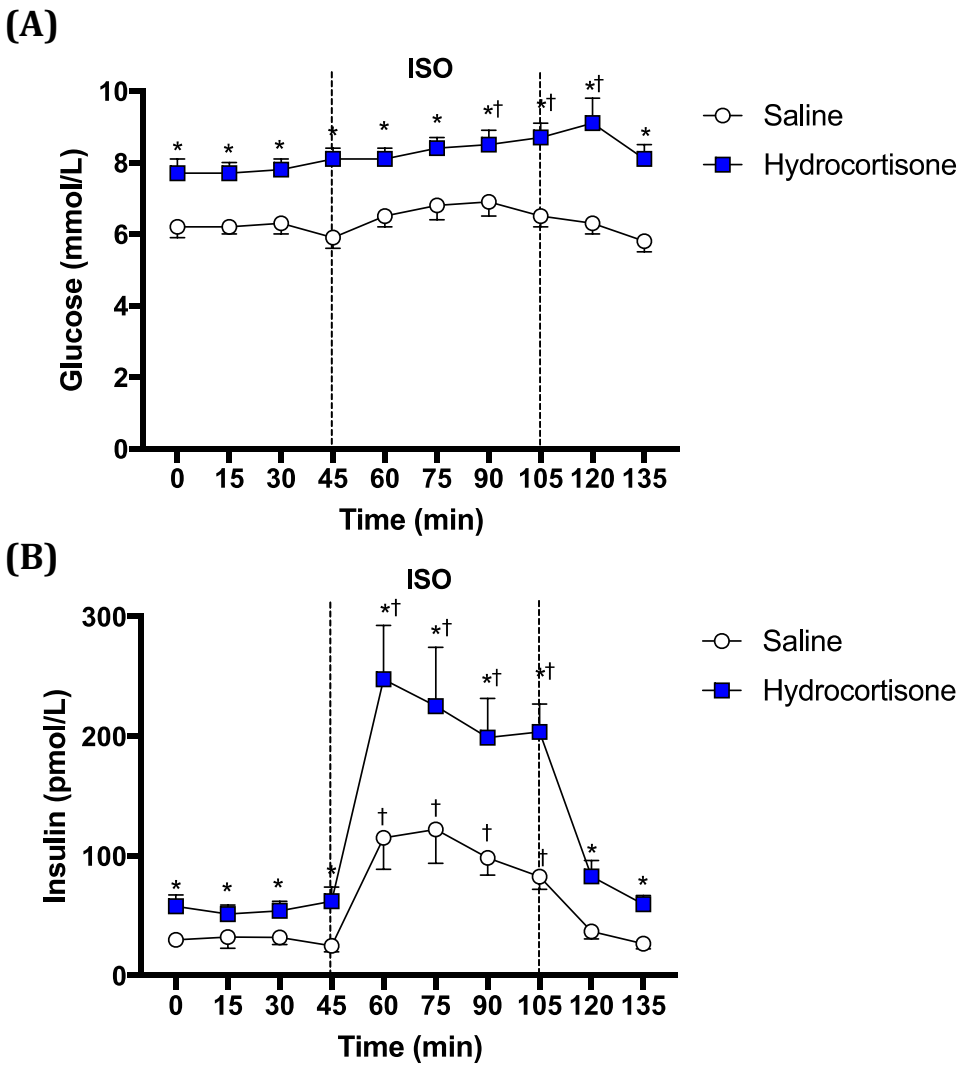

Figure 3.4. Glucose (A) and insulin (B) concentrations following saline infusion or hydrocortisone infusion at baseline and during an isoprenaline infusion (ISO, dotted lines indicate infusion period) in healthy male subjects (n=8)

Values are mean ± standard error of mean. *$p < 0.05$ vs. control, †$p < 0.05$ vs. baseline.

Table 3.4. Anthropometric and metabolic characteristics of adult male participants entered into the study (n=8)

Comparison of homeostatic model assessment (HOMA) indexes during basal and isoprenaline-stimulated conditions in healthy adult males (n=8)			
	Saline	**Hydrocortisone**	***P* value**
HOMA %B	42.2 ± 5.9	40.5 ± 4.5	0.731
HOMA %S	192.2 ± 29.5	105.9 ± 19.2	0.004
HOMA IR	0.62 ± 0.11	1.11 ± 0.16	0.016
%B, estimate of steady state beta-cell function; %S, estimate of steady state insulin sensitivity; IR, Insulin Resistance (the reciprocal of %S [100/%S]). Mean and SEM presented.			

3.4.3 Metabolic responses to acute β-AR stimulation

From a metabolic perspective, ISO infusion was seen to significantly increase systemic NEFA concentrations, both under control and hypercortisolaemia conditions ($P = 0.001$) (Figure 3.3). The rise in plasma NEFA was of similar magnitude between hydrocortisone and control conditions (delta change Δ AUC 953 ± 155 vs. 979 ± 175 μmol/L; $P = 0.926$ compared to control). Subsequent to the initial rise in NEFA, plasma concentrations sharply decline thereafter, despite continued ISO infusion. β-AR stimulation also increased plasma insulin (Figure 3.5a) and C-peptide concentrations (Figure 3.5b).

Finally, stimulation of BAT through ISO, increased whole body energy expenditure (Figure 3.6). Energy expenditure was closely correlated with maximal temperature over the SCR region during hypercortisolaemia conditions ($R = 0.87$, $P = 0.005$).

(A)

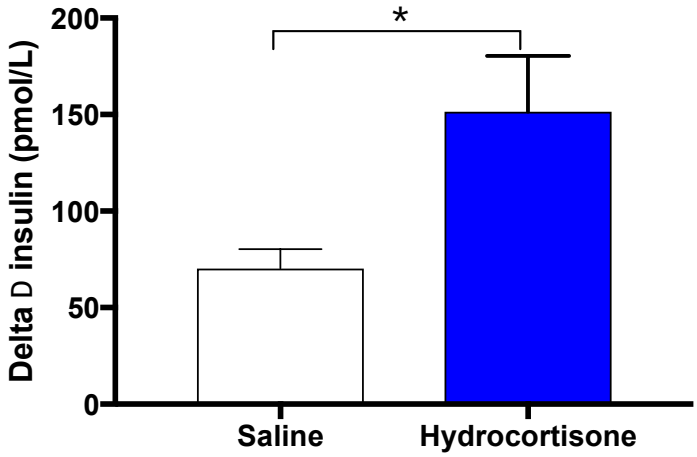

(B)

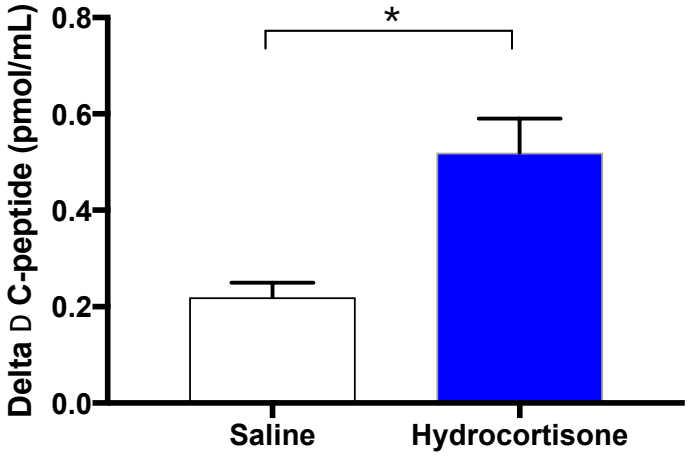

Figure 3.5. Delta change in systemic metabolites; insulin (A) and C-peptide (B) during basal and isoprenaline stimulated conditions, after an overnight infusion of saline or hydrocortisone (n=8)
Values are mean ± standard error of mean. *p<0.05 vs. saline.

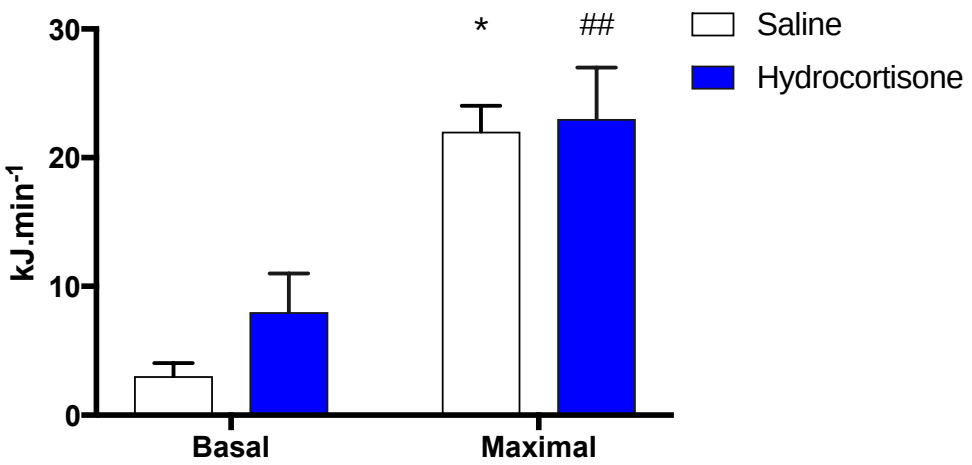

Figure 3.6. Whole body energy expenditure under saline conditions and following an overnight infusion of hydrocortisone, at baseline and after isoprenaline infusion (maximal) in 8 adult male subjects
Data are shown as mean ± standard deviation**.** *$p \leq 0.05$ compared to basal control. ##$p \leq 0.05$ compared to basal hydrocortisone. Energy expenditure calculated based on heart rate, age and weight using the equation as previously described by Keytel et al, 2005: EE = gender x (-55.0969 + 0.6309 x heart rate + 0.1988 x weight + 0.2017 x age) + (1 - gender) x (-20.4022 + 0.4472 x heartrate - 0.1263 x weight + 0.074 x age).

3.4.4 Acute hypercortisolaemia increases basal thermogenic activity of brown adipose tissue

Elevations in basal plasma cortisol concentrations following the overnight infusion of HC (P =0.001), were seen to raise the threshold for basal BAT activity, indicated by the increased T_{SCR} in the basal state by (P = 0.049). All individuals were seen to respond to a greater extent after HC infusion compared to saline (P = 0.001) (Figure 3.7). This was accompanied by an observed increase in basal core temperature (P =0.042) (Figure 3.8), but no effect was seen on blood pressure (P = 0.596) and heart rate (P = 0.171) (Figure 3.9).

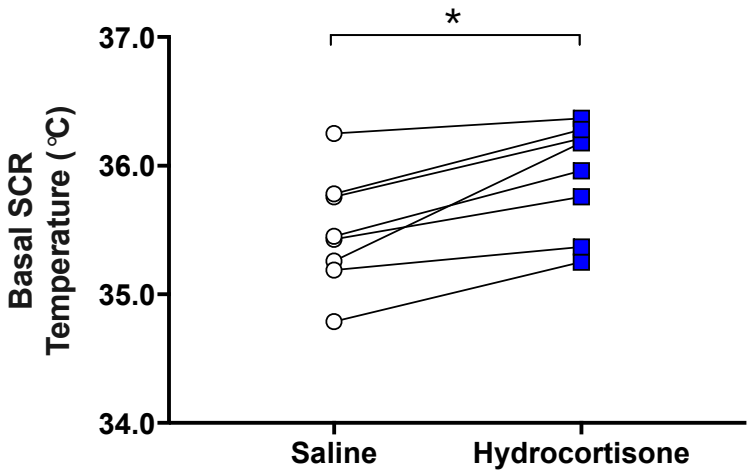

Figure 3.7. Supraclavicular BAT temperature responses at baseline following saline or hydrocortisone infusion in healthy males (n=8)
All responses were greater upon hypercortisolaemia. Values are mean ± standard error of mean. *$p < 0.05$ vs. control.

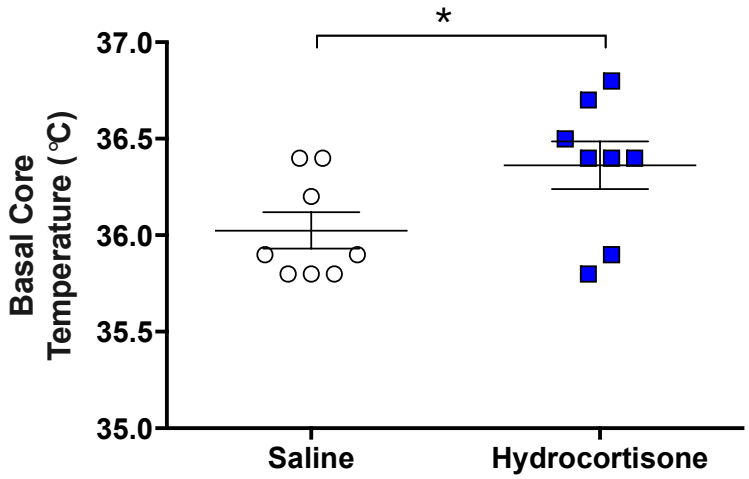

Figure 3.8. Core temperature responses at baseline following saline or hydrocortisone infusion in 8 healthy adult males
Values are mean ± standard error of mean. *$p < 0.05$ vs. control.

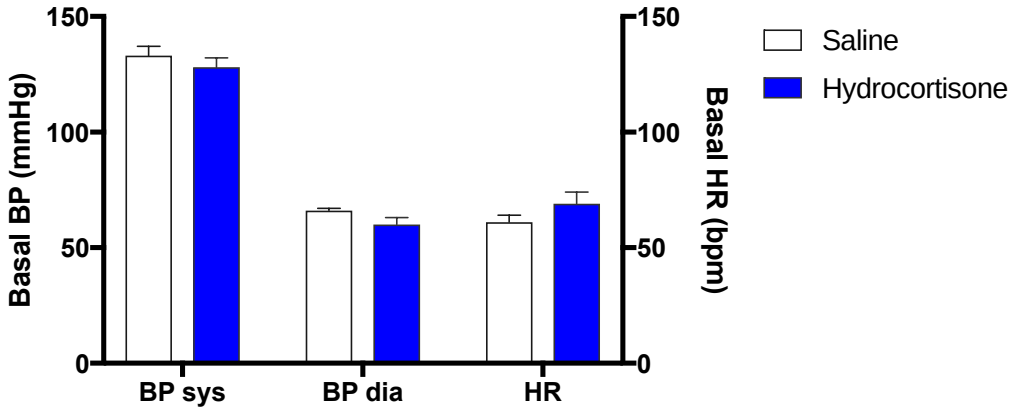

Figure 3.9. Basal cardiovascular responses following saline or hydrocortisone infusion in 8 male subjects
Values are means ± standard error of mean. sys, systolic; dia, diastolic blood pressure (BP); HR, Heart Rate.

3.4.5 Acute β-AR stimulation increases the thermogenic activity of brown adipose tissue during both control and hypercortisolaemia conditions

Pharmacological adrenergic stimulation of brown adipose tissue with the β-AR agonist, ISO, resulted in a highly localised increase in the temperature of the skin overlying the SCR BAT region representative of BAT activity, both under control and hypercortisolaemic conditions (P = 0.001) (Figure 3.10). SCR skin temperature was seen to rise in response to ISO in all participants across both experimental conditions (Figure 3.11a, Saline, P = 0.001; Figure 3.11b, Hydrocortisone, P = 0.009).

Under control conditions, the 60-minute infusion of ISO stimulated a significant increase in T_{SCR} which then plateaued and returned to baseline thereafter. Such responses followed a similar pattern upon HC infusion, where maximal T_{SCR} was significantly greater (P = 0.020) (Figure 3.12). However, there were no significant differences in the delta change in T_{SCR} between saline and hydrocortisone conditions (P = 0.472) (Figure 3.13). Further, the skin temperature over the SCR region using iButtons demonstrated similar results upon saline and hydrocortisone infusions (Figure 3.14).

Maximal core temperature was found to be similar between control and hypercortisolaemia conditions upon ISO infusion (P = 0.367) (Figure 3.15).

Non-selective β-AR stimulation with ISO significantly stimulated heart rate (P = 0.001) and systolic blood pressure (P = 0.001), however responses were not significantly affected by hypercortisolaemia (P = 0.061) (Figure 3.16).

(A) Saline

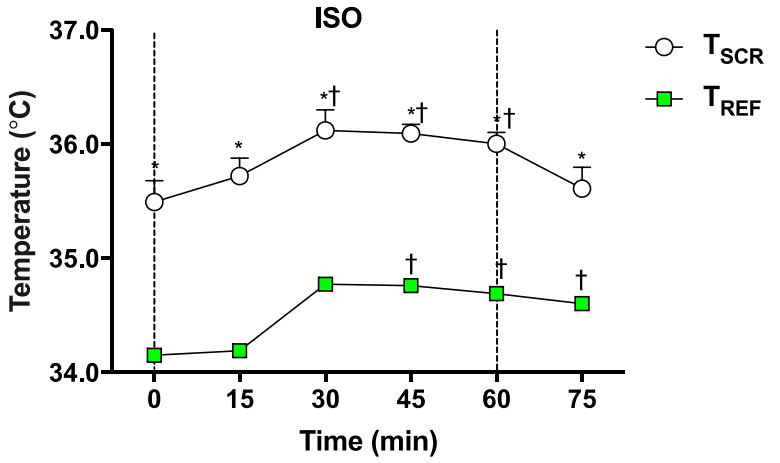

(B) Hydrocortisone

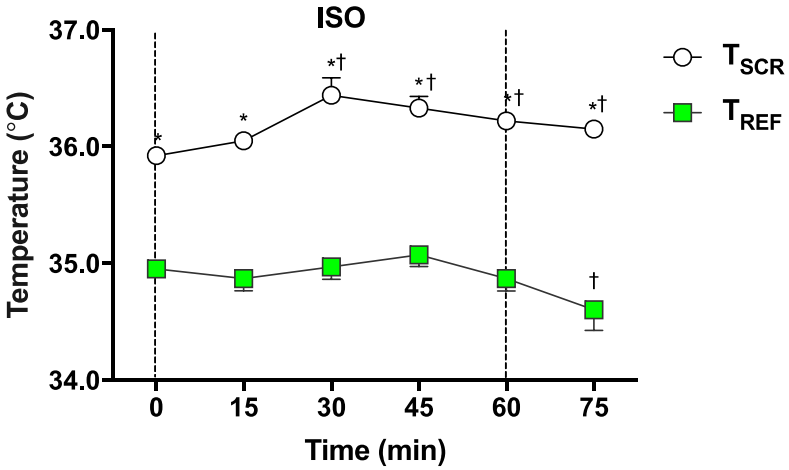

Figure 3.10. The thermogenic responses of brown adipose tissue. Supraclavicular temperature (T_{SCR}) and a non-adipose tissue reference point (T_{REF}) following saline infusion (A) or hydrocortisone infusion (B) during and post Isoprenaline stimulation (ISO, dotted lines indicate infusion period) in 8 healthy adult males

Supraclavicular temperature (T_{SCR}; open circles), Reference temperature (T_{REF}; green squares). Values are mean ± standard error of mean. *$p < 0.05$ vs. Control, †$p < 0.05$ vs. baseline.

(A) Saline

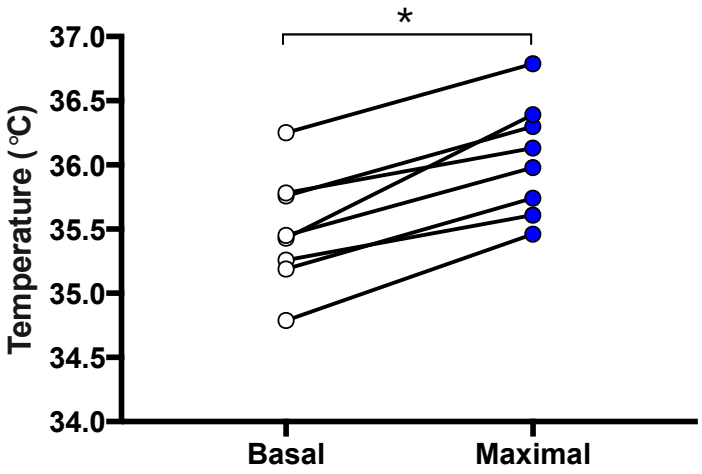

(B) Hydrocortisone

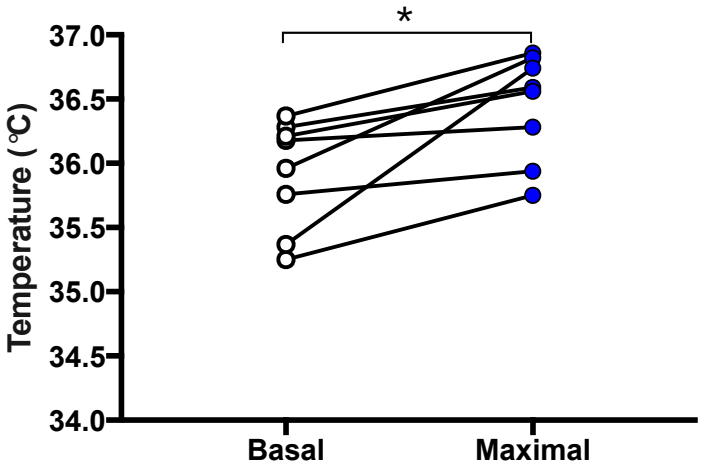

Figure 3.11. Individual basal and maximal T_{SCR} responses during Isoprenaline infusion following an overnight infusion of saline (A) or hydrocortisone (B) in eight healthy male subjects
*$p < 0.05$ vs. baseline.

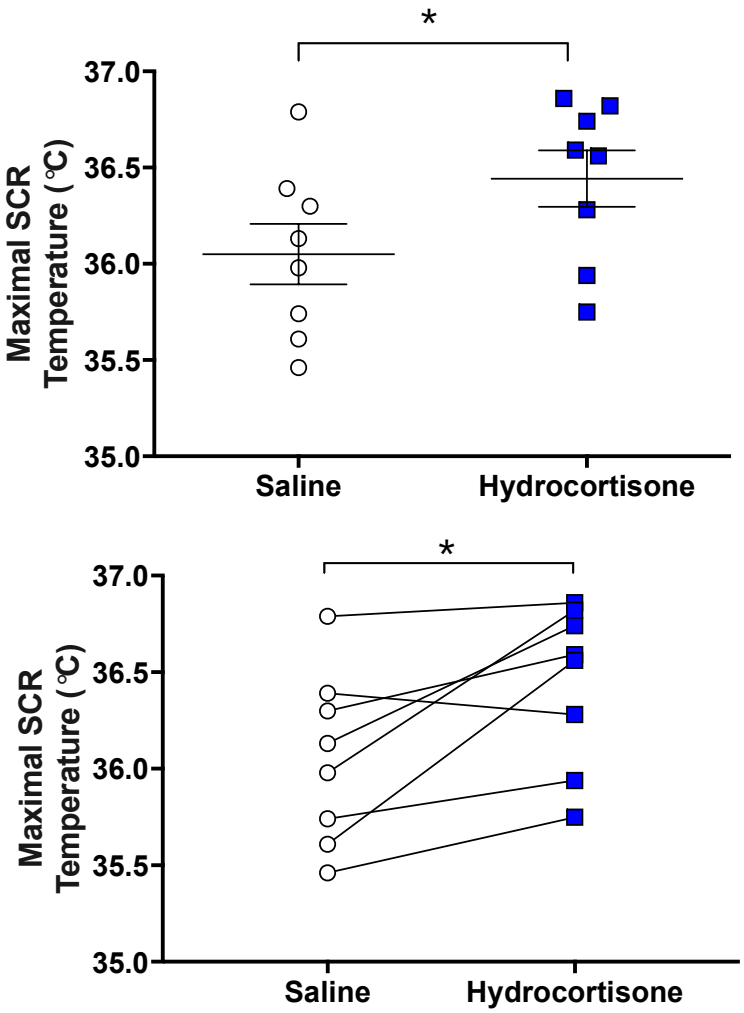

Figure 3.12. Individual maximal supraclavicular skin temperatures during Isoprenaline infusion following an overnight infusion of saline or hydrocortisone in eight healthy adult male subjects
Values are means ± standard error of mean. *$p < 0.05$ vs. control.

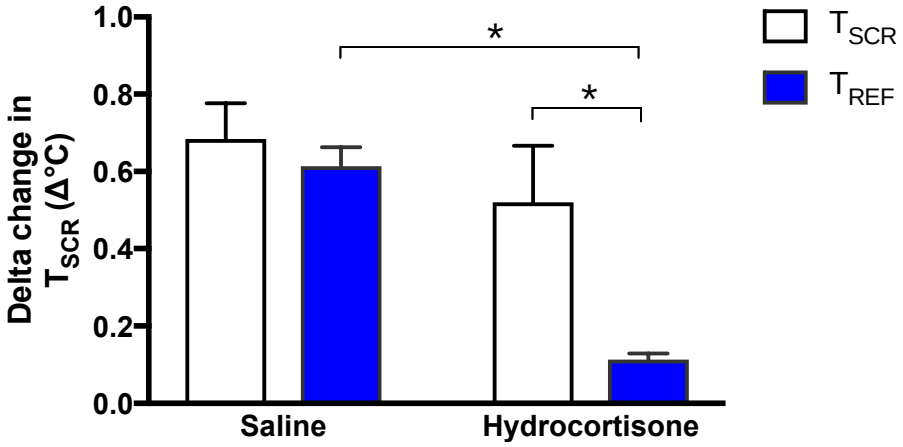

Figure 3.13. Delta change in supraclavicular temperature during isoprenaline infusion after an overnight infusion of saline or hydrocortisone in 8 healthy adult male subjects
Values are mean ± standard deviation. *p < 0.05 vs. supraclavicular temperature.

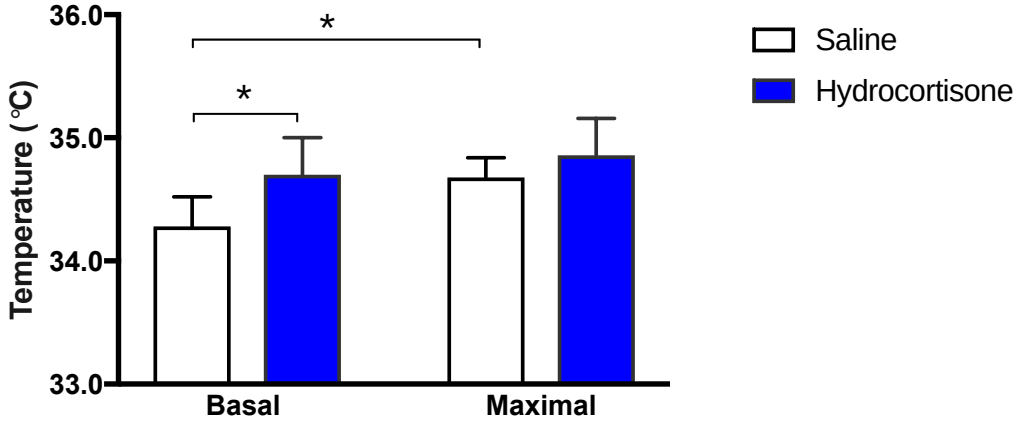

Figure 3.14. Mean basal and maximal skin temperature responses to isoprenaline during saline and hydrocortisone infusions, using skin contact temperature sensors placed over the supraclavicular BAT region (n=8)
Values are mean ± standard deviation. *p <0.05 vs. baseline.

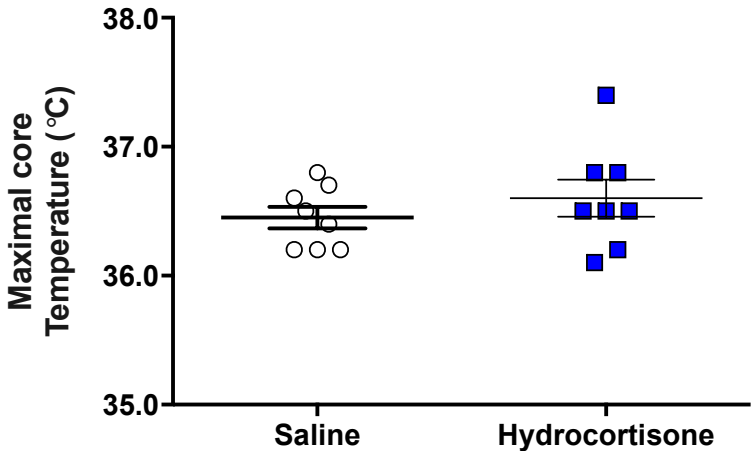

Figure 3.15. Individual maximal core temperature responses during isoprenaline infusion following an overnight infusion of saline or hydrocortisone (n=8)

Data are shown as mean ± standard error of mean.

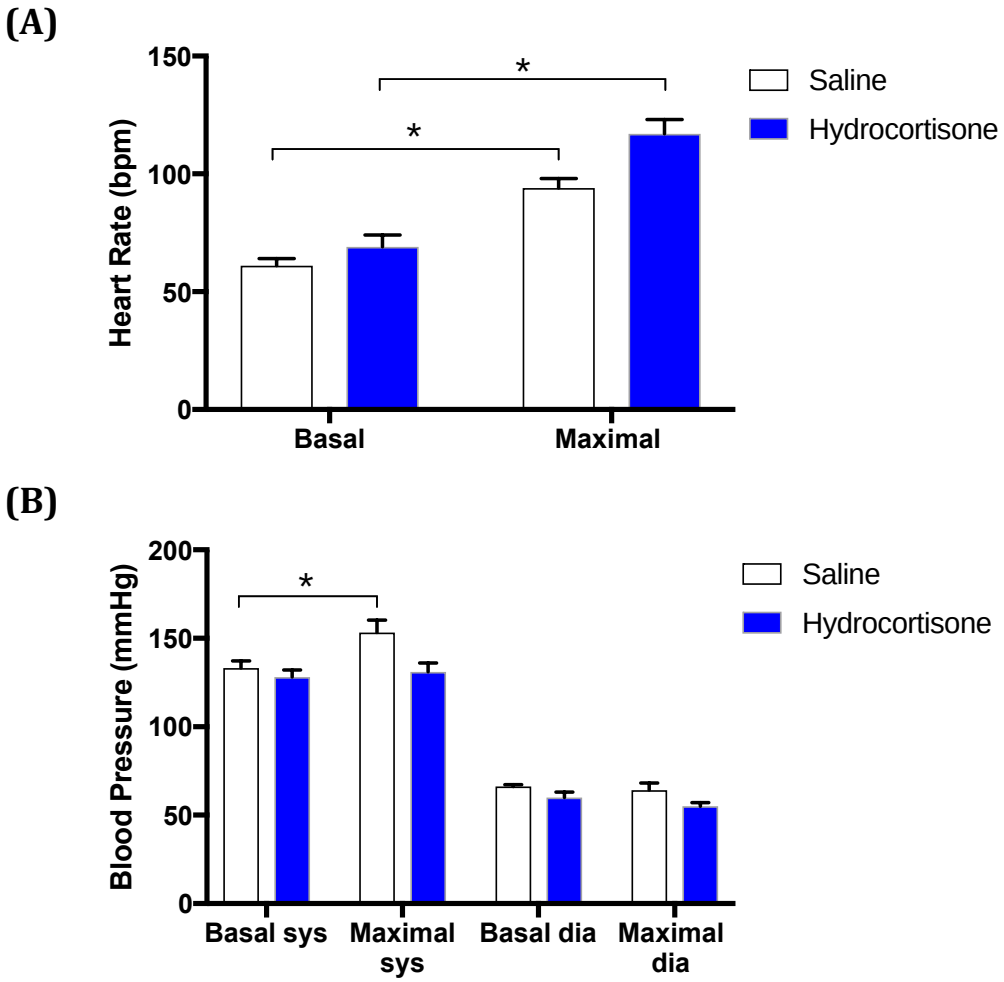

Figure 3.16. Basal and maximal heart rate (A) and blood pressure (B) responses during isoprenaline infusion in control and hydrocortisone conditions (n=8)

Values are mean ± standard error of mean. *p <0.05 compared to baseline.

3.4.6 The thermogenic effect of meal ingestion

Ingestion of a single, calorie-controlled meal, resulted in a significant increase in postprandial SCR skin temperature within 5 minutes, compared to a reference region identified below the clavicle (T_{SCR} 0.4 ± 0.05°C vs. T_{REF} -0.3 ± 0.01°C) (Figure 3.17a) (P = 0.001). Findings were accompanied by a significant increase in Core temperature upon meal ingestion (Pre-ingestion, 36 ± 0.3°C vs. Postprandial, 36.2 ± 0.3°C) (Figure 3.17b) (P = 0.049).

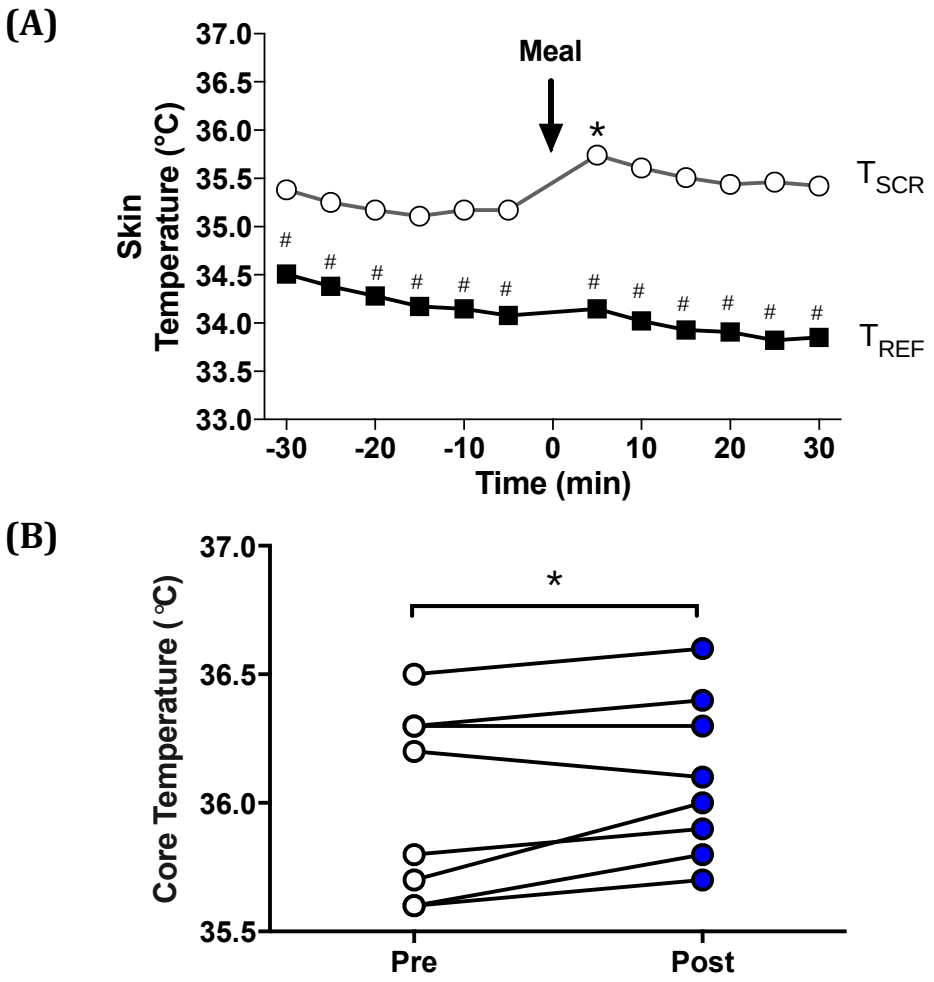

Figure 3.17. Thermogenic (A) and core temperature (B) responses of ingesting a single calorie controlled meal in healthy adult males (n=8)

Meal was ingested at time point '0'. Pre, pre-ingestion; Post, postprandial; Supraclavicular temperature (T_{SCR}); Reference temperature (T_{REF}). Values are mean ± standard deviation. *p <0.05 compared to pre-ingestion. #p <0.05 compared to T_{SCR}.

3.5 Discussion

BAT holds a unique thermogenic function due to its mitochondrial protein UCP1, with a respiratory capacity far greater than that of white fat (Cannon and Nedergaard, 2004). A range of endocrine factors regulate BAT function around the time of birth. The suggestion that cortisol has the greatest influence on the ability of BAT to become maximally stimulated (Mostyn et al, 2003) has provoked interest into our understandings of the effects of plasma hormones on the metabolic capabilities of this tissue. In this study I investigated BAT in vivo under hypercortisolaemic and dietary conditions to determine the relative importance of plasma hormones to BAT thermogenic function in humans.

3.5.1 Effect of acute hypercortisolaemia on basal thermogenic and metabolic responses

The stress hormone, cortisol, exerts species specific effects on BAT function (Ramage et al, 2016). Whilst cortisol promotes adipose tissue UCP1 abundance at the time of birth in sheep (Mostyn et al, 2003; Symonds et al, 2012), GCs are known to inhibit the activity of BAT in adult rodents (Beukel et al, 2014), by impeding β-adrenergic signalling (Martinez-deMena et al, 2016; Soumano et al, 2000). In contrast, human data suggest that the administration of the synthetic GC prednisolone in vivo, stimulates BAT activation (Ramage et al, 2016).

In this study, hydrocortisone was chosen to model a physiological acute surge of cortisol, as seen at birth and at times of acute stress. An infusion duration of approximately 18 hours was selected in order to allow for GC mediated genomic effects to take place (Biddie, Conway-Campbell & Lightman, 2012). While the achieved plasma cortisol concentrations were in excess of those typical for acute stress (Wong et al, 2010), it is important to note that tissue-responsiveness can be determined by tissue-specific GC metabolism rather than absolute plasma concentrations (Morgan, Hassan-Smith & Lavery, 2016). The current data indicate that the induced hypercortisolaemia was sufficient enough to produce an elevated

temperature response in the SCR region at baseline, upon cortisol infusion, compared to saline. This evidence is in support of a physiological role for cortisol in activating BAT, as there were no additional effects observed on blood pressure or heart rate.

Collectively, these data indicate that supra-physiological concentrations of cortisol excess cortisol increases BAT temperature as assessed by infrared thermography, which supports previously published data by Robinson et al (2016) in small sample of healthy adult females (Robinson et al, 2016).

3.5.2 Pharmacological activation of BAT thermogenesis in humans

Since the activation of BAT is facilitated by sympathetic efferents predominantly through β-adrenergic receptors in the adipose tissue (Cannon and Nedergaard, 2004), sympathomimetic drugs are of interest in targeting its activation. However, studies have reported extreme adverse cardiovascular side effects (Astrup et al, 1985; Yoneshiro et al, 2012) or no observed effects on BAT activity (Cypess et al, 2012; Vosselman et al, 2012). Only recently has human BAT activation been shown by the administration of the pharmacological β-adrenergic receptor agent, epinephrine (Carey et al, 2013). In the current study, I observed a localised increase in SCR temperature during ISO infusion both under control and hypercortisolaemia conditions. The temperature change was limited to the duration of the 60-minute infusion only, which suggests underlying BAT activation. The temperature responses for the SCR region were seen to increase within the first 5 minutes in all subjects, which is in line with acute cold exposure on BAT (Symonds et al, 2012). In accordance, given that BAT primarily utilizes NEFA for the generation of heat (Cannon and Nedergaard, 2004), the concentration of NEFA increased within the first 30 minutes of ISO infusion, driving BAT activation, which coincided with the peak increase in T_{SCR}. The finding of a slightly higher peak SCR temperature during hypercortisolaemia suggests a minor synergistic effect between cortisol and β-AR stimulation. Rozansky and colleagues suggested that the two pathways are intrinsically connected as catecholamine synthesis is under GC control

(Rozansky et al, 1994). The observed subsequent plateau in SCR temperature is suggestive of a threshold to BAT thermogenesis in vivo. The concomitant sharp decline in NEFA concentrations during the later stages of the infusion is consistent with β-AR desensitization due to maximal receptor stimulation (Manolopoulos et al, 2012).

3.5.3 Acute hypercortisolaemia induces peripheral insulin resistance

BAT is known to be one of the most insulin-responsive tissues with respect to glucose-uptake and is mediated by GLUT4, similar to that in white adipocytes (Shimizu et al, 1993). The uptake of glucose into BAT is thus, both insulin-mediated (mainly during non-thermogenic conditions) and norepinephrine-mediated (in thermogenic conditions) (Shimizu et al, 1996). Human experimental studies using PET/CT scanning have shown that insulin-mediated glucose-uptake into BAT may increase by 5 fold in comparison to WAT, and gene expression of GLUT4 was greater in BAT compared to WAT (Orava et al, 2011).

The current study indicated that even though acute elevations of plasma cortisol concentrations signify an adaptive stress response to increasing BAT thermogenesis, an 18-hour surge of GCs received in excess began to signify the induction of peripheral insulin resistance. In support, Ramage et al (2016) reported that GC treatment for 48 hours in human brown adipocytes, reduced UCP1 and PET-CT scanning revealed that chronic GC excess suppressed BAT activation in 6 lean males (Ramage et al, 2016). Although clear mechanisms have yet to be determined, the suggestion that stress is involved in the development of insulin resistance stems from the knowledge that the HPA regulates plasma circulating levels of GCs and hyper-stimulation of the HPA results in insulin resistance (Heim et al, 2008). Further, hyperinsulinaemia has been shown to induce apoptosis of endothelial cells in rat BAT, thus reducing BAT mass (Markelic et al, 2011). This may explain the reduced activity of BAT seen in insulin-resistant states such as obesity and type 2 diabetes mellitus in humans (Cypess et al, 2009; Ouellet et al, 2011). Additionally, the effects of surplus GC concentrations

on insulin activity for a period of 18 hours, as seen in this study, may partly explain why chronic GC excess results in weight gain, insulin resistance, and dyslipidaemia (Macfarlane, Forbes and Walker, 2008).

3.5.4 Infrared thermography can assess thermogenic changes in brown adipose tissue

The identification of BAT in adults using PET-CT scanning, reignited interest in the understandings of the function of this tissue in humans of varying ages. BAT has been shown to vary between sex and decline with age and obesity status (Symonds et al, 2012; Yoneshiro et al, 2013). In the current study, healthy, lean adult males under the age of 35 years were studied to control for the effects of hormones and aging. Using IRT, BAT activity was studied to evaluate the temperature changes in the SCR region and over a defined region of non-adipose tissue. This study confirmed that the temperature overlying the SCR region; main BAT region, increased upon BAT activation (Boon et al, 2014; van der Lans et al, 2016), as assessed by the use of IRT, which enables real-time tracking of temperature changes. These data support that of previously published data reporting highly localised increases in temperature over this region of BAT, compared to elsewhere, upon cold stimulation in healthy humans from 3 to 58 years of age (Symonds et al, 2012). Further, these data complement other research demonstrating IRT as a reliable alternative for the in vivo assessment of BAT activity (Symonds et al, 2012), through PET-IRT correlative studies reporting the anatomical overlapping between the increase in $^{[18]}$F-FDG uptake and the rise in the temperature overlying the SCR BAT (Carter et al, 2011).

Confusing this picture is the contention that BAT temperature may be influenced by subcutaneous adipose tissue thickness (Gatidis et al, 2016). Gatidis et al (2016) reported a negative correlation between mean SCR skin temperature and BMI ($r = -0.65$). The authors suggested that the higher SCR skin temperature in the subjects with a lower BMI could be explained by a relatively thin layer of isolating adipose tissue (Gatidis et al,

2016). Seeing as large blood vessels are located in this anatomic region, principally the subclavian and carotid arteries, thermal energy may be conveyed from the body core to the extremities which might result in an improved detection in lean compared to obese individuals. In the current study, the subjects were lean (average BMI 23kg/m^2) and dynamic SCR skin temperature was continually monitored throughout the study, as opposed to a single, static measurement, as conducted in the aforementioned study. Adrenoreceptor-induced vasodilation, both as a result of hydrocortisone and ISO infusions, might increase skin blood flow and interfere with IRT measurements. However, compared to SCR skin temperature, there were clear differences in the change in temperature of the non-adipose tissue reference point, which showed a later initial increase and a sustained increase post-infusion. Overall, this study demonstrates a BAT-specific thermogenic and vasodilation response to both hydrocortisone and ISO clearly differentiated from non-BAT reference areas, confirming that the temperature responses we measured are likely confined to BAT.

My findings support previous studies showing β-AR stimulation as a means of activating BAT in humans (Carey et al, 2013; Cypess et al, 2015), confirming IRT as a sensitive, non-invasive method for the in vivo assessment of BAT function in humans under thermoneutral conditions (Ramage et al, 2016; Symonds et al, 2012). This is particularly important when comparing the results reported in the current study with those studies using glucose tracer uptake as an index of BAT activity. Similar ISO doses have been shown not to have any significant BAT glucose tracer uptake, most likely due to competition between the tracer and NEFAs from ISO-induced lipolysis combined with increased insulin resistance (Vosselman et al, 2012). As BAT's primarily fuel source comes from NEFAs to generate heat (Cannon and Nedergaard, 2004), it is possible that $^{[18]}$F-FDG-PET-CT scanning underestimates the amount of active BAT in humans. This limitation has led to the development of alternative BAT assessment methods, in addition to IRT, either using different PET-CT tracers (Hwang et al, 2015), or based on magnetic resonance imaging techniques (Holstila et al, 2013). This study demonstrates that temperature changes in the SCR area upon

β-AR stimulation are indicative of localised BAT activity in a cohort of randomized young male individuals, maintained at room temperature. This supports the prospect of harnessing BAT activity and the associated increase in energy expenditure as a potential treatment for metabolic diseases. The study provides further evidence that in humans, in contrast to rodents, acute hypercortisolaemia does not inhibit BAT function, but results in BAT activation (Ramage et al, 2016). In spite of this, there is a threshold of activity that cannot be overcome even during maximal short-term β-AR stimulation.

3.5.5 BAT and Diet Induced Thermogenesis

The concept that energy expenditure may be increased in response to overeating in some individuals has sparked debate as to the association between diet-induced thermogenesis and BAT in humans. In favour, original studies have demonstrated that in wild-type rats, BAT is known to waste excess calorie intake, as demonstrated by increased BAT recruitment and enhanced norepinephrine-induced thermogenesis during high-fat feeding and voluntary overeating (Rothwell & Stock, 1979).
Several rodent studies have demonstrated that a single meal enhances BAT activity to waste a fraction of the ingested energy as heat through facultative diet-induced thermogenesis (Glick & Raum, 1986; Glick, Teague, & Bray, 1981; Glick et al, 1985; Lupien et al, 1985; van Baak, 2008). Such evidence is lacking in humans. The SNS may play an important role in facultative DIT seeing as macronutrients such as carbohydrates are potent stimulators (van Baak, 2008). Glucose uptake into BAT reportedly increases upon a single carbohydrate-rich (Vosselman et al, 2013). However, overfeeding for 24 hours on a 60% fat, 20% protein, 20% carbohydrate diet at 200% of energy requirements, seemingly had no effect on BAT glucose uptake, when assessed by a singular PET-CT scan post-feeding (Schlogl et al, 2013). In the current study, selective temperature changes over SCR region only were observed immediately after the meal, suggesting direct BAT activation and not a thermic effect of food. This is in line with evidence by Lee et al (2011) demonstrating increased skin temperature over

SCR BAT depots after a single meal (Lee et al, 2011). Clearly further work is required to investigate the mechanisms regulating postprandial BAT activation in humans versus rodents.

3.5.6 Study Limitations and Strengths

The current study has several limitations within its experimental design, including the small sample size. However, for such a complex, novel and invasive study, the sample size calculation revealed that the sample number was enough to achieve statistical significance, for which the sample size is typical for a healthy volunteer study of this type. The 17-hour infusion of hydrocortisone was deemed as an acute bout of stress, thus, inferences from the conclusions drawn from this study, cannot be made in relation to states of chronic GC excess that are associated with profound metabolic changes, i.e. metabolic conditions such as Cushing's syndrome. The associated induction of peripheral insulin resistance in this short period of stress could have masked the true effects of GCs on BAT function, particularly as there is a multifaceted relationship between insulin mediated glucose uptake and BAT function in vivo.

The study would have been strengthened by the addition of PET-CT scanning to detect the presence of BAT in the subjects prior to the commencement of the study, which could have been used to correlate the location of BAT in the SCR region and given substantial support for the use of IRT imaging to assess BAT activity (Law et al, 2018). A further assessment of blood flow in this region, would have helped to deter criticism regarding the potential for IRT to detect superficial blood flow in this region as opposed to solely the heat generated by BAT.

The current study was the first of its kind to touch upon the endocrine regulation of human brown adipose tissue, assessed by IRT. The assessment of BAT thermogenic activity by this imaging modality enabled the real-time tracking of BAT function in response to the experimental stimuli. Further, the randomized double-blind design of the infusion protocol in addition to the short time frame in which the study was conducted, reduced

the confounding effect of variations in seasonal temperature, and thus endogenous BAT activity.

3.6 Conclusion

In conclusion, this was the first study in males to show that an acute exogenous influx of GCs, regulates supraclavicular skin temperature, inferring increased BAT activity. This may represent an important thermoregulatory mechanism during short-term stress in humans, particularly as acute stress in rodents negatively influences BAT function. Such heat inducing stimuli could potentially be utilized to improve body weight regulation and metabolic homeostasis.

Chapter 4

A multimodal approach for the non-invasive detection of brown adipose tissue activation in healthy adults

4.1 Introduction

A number of studies using IRT to assess BAT activation in response to cold exposure, have demonstrated significant changes in localised skin temperature overlying the SCR region in both children (Symonds et al, 2012) and adults (Lee et al, 2010; Robinson et al, 2016; Symonds et al, 2012; van der Lans et al, 2016). Indeed, recent correlative investigations have demonstrated an overlap between the increase in $^{[18]}$F-FDG uptake and the rise in T_{SCR} on (Carter et al, 2011)**,** and thus promote the use of IRT in assessing BAT heat production.

Interest in the exploration of BAT activity through non-invasive methods is becoming increasingly prevalent (Hartwig et al, 2017; Hu et al, 2013; Law et al, 2017), particularly those methods which could be implemented alongside IRT to study BAT activity.

BAT is densely vascularised, to enable the continuous supply of sufficient amounts of blood delivering oxygen and macronutrients to the tissue to meet its demands, with subsequent heat dissipation towards the skins surface overlying the SCR region (Abreu-Vieira et al, 2014). NIRS oximetry has been proposed as an attractive assessment tool to study BAT (Nakayama et al, 2003; Orava et al, 2011), due to its ability to provide a non-invasive estimation of tissue oxygen saturation (StO_2) (Jobsis et al, 1979). However, data on the application of NIRS in the assessment of BAT activity is scarce. Muzik et al (2013) used ^{15}O-PET imaging in combination with NIRS to estimate BAT blood flow and oxygen consumption in response to cold stimulation. The authors demonstrated a significant correlation be-

tween PET derived O_2 uptake (indicative of BAT perfusion rate) and oxygen saturation assessed by NIRS in 25 healthy subjects with activated BAT (Muzik et al, 2013). Whilst one recently published pilot study combined non-contact NIR spectroscopic two-dimensional (2D) imaging with IRT in a small group of healthy and obese adults, demonstrating adrenergic-stimulated increases in temperature over the SCR region, were not matched by changes in StO_2 in same region (Hartwig et al, 2017). However, the lack of any change in StO_2 over the SCR region could be due to the limited depth of sensitivity using NIRS 2D imaging (Beekvelt et al, 2001). Additionally, the oxygen saturation values were extracted from an ROI that did not directly correspond to the SCR area where BAT is located. Therefore, studies should consider the application of NIRS using contact sensors placed directly over BAT (Davie and Grocott, 2011).

4.1.1 Main Aims

The primary focus of this chapter was to assess BAT activity during forearm cold stimulation in healthy adults, utilising a combination of non-invasive techniques. These methods were used to acquire a greater understanding of the responses of tissue oxygen saturation and blood flow within the SCR region with respect to BAT heat production.

To achieve this aim, this chapter comprises of two feasibility studies both utilising the following technology:

- Contact NIRS to assess BAT tissue oxygen saturation
- IRT to assess superficial skin temperature over the SCR BAT region
- Laser Doppler (LD) to assess localised skin blood flow over the SCR BAT region

This chapter further aimed to assess whether NIRS could be used to support IRT as a measure of BAT activity.

4.2 Materials and Methods

Subjects

The study was approved by the University of Nottingham ethical committee (REC l16022016 QUANT-BAT). Potential subjects were recruited using printed advertisement posters placed around the University of Nottingham University Park Campus and Medical School. Subjects were provided with an electronic version of the participant information sheet or sent a paper version by post. Eligible subjects were provided with the information leaflet for at least 24 hours to ensure familiarisation and were asked to attend one screening session and one study session. All subjects provided written informed consent and none were selected or screened on the basis of presence of any active BAT. Exclusion criteria included an age of <18 or >35 years, a BMI of >25 kg/m^2, pre-diabetes or diabetes, metabolic disorders, ingestion of medications and smoking. No subject had any significant past medical history, smoked tobacco or took any regular medications that could affect the study's outcome measures.

Study A was conducted between the months of May – September 2016; Study B was conducted between February and June 2017. All subjects who participated in the initial feasibility study (Study A), were re-contacted by email to enquire whether they would like to take part in Study B. All subjects were re-screened for their eligibility and study information was provided in the same manner as conducted previously.

Experimental protocol

Screening visit

All subjects attended a screening session prior to the commencement of the studies. Subjects completed a medical screening questionnaire (followed by the recording of age (years), height (cm) and weight (kg) measurements. A BMI score was calculated using the equation stated in Chapter 1.1.

Study visit

Experimentation was conducted within the thermoneutral zone (22 - 24°C) (Law et al, 2017) in Academic Imaging Suite at the Queens Medical Centre, University of Nottingham. All subjects were fasted from midnight and had abstained from caffeine and alcohol ingestion for 24 hours prior and excessive exercise for 48 hours prior. Study sessions commenced between 0800h and 0900h. Upon arrival, subjects changed into a cotton pair of trousers and a vest provided by the department, to ensure adequate exposure of the neck and upper thorax for infrared thermography imaging.

Both studies consisted of an acclimatisation period of 30 min during which subjects were asked to sit comfortably at rest with their SCR region exposed, in order to achieve stability of blood pressure and skin temperature. During this time, the standardised placement of NIRS sensors over the SCR region and a non-adipose tissue reference region (deltoid muscle; reference, Ref), alongside the placement of an LD sensor within the SCR region. This enabled the continuous measurement of tissue oxygen saturation and localised skin blood flow, respectively, throughout the duration of study commencing in the baseline period of 15 minutes. Thereafter, acute BAT stimulation was achieved by the cooling of the forearm using a cooling blanket for 15 minutes (at 16°C), followed by a post-stimulatory period of 15 min. To assess presumed BAT heat production, IR imaging of the subject's SCR region was conducted throughout resting, cold-stimulation and post-stimulation periods in both studies (Figure 4.1). In addition, a pulse oximeter was attached to the digitus medius of the same hand to assess pulse rate throughout the duration of study.
Tympanic membrane temperature was measured in triplicate immediately before and on cessation of IR imaging, using a Braun Thermoscan Pro 4000 (Welch Allyn, Skaneanteles Falls, New York). Measurement accuracy of the ear thermometer was ± 0.2°C (Specification sheet on WelchAnn.com, 2015).

In order to strengthen the methodology to improve data acquisition, a number of amendments to the study protocol were introduced in study B:

1) In study A, tissue oxygenation was assessed over SCR and Ref sites only. In study B, the placement of an additional NIRS sensor on the forearm, which received the cooling stimulus, offered the potential to measure oxygenation in an isolated upper extremity muscle compartment, known to be a sensitive in detecting circulatory stress (Cole et al, 2012). Thus, this sensor would be informative in attaining an understanding of cold-induced changes in blood perfusion through the induction of peripheral vasoconstriction.
2) In order to accurately determine the resting state of skin temperature prior to the commencement of the study, the addition of thermal skin probes over the SCR and cooled forearm, enabled the real-time tracking of SCR skin temperature, recorded every minute.
3) In study A, to achieve BAT thermogenic stimulation, a cooling blanket (Cincinnati Sub Zero CSZ Blanketrol II) was cooled to 16°C, then applied to the forearm after the baseline period. Since this was thought to induce an acute anticipatory stress response, in study B, the cooling blanket was wrapped and fixed around the subject's forearm in a 'switched off' state prior to subject acclimation and basal periods. The blanket roll blanket was then allowed to cool to 16°C, before the stimulation period began.

An illustration of the overview of the two study set-ups incorporating the protocol variations, are shown in Figure 4.2a-b.

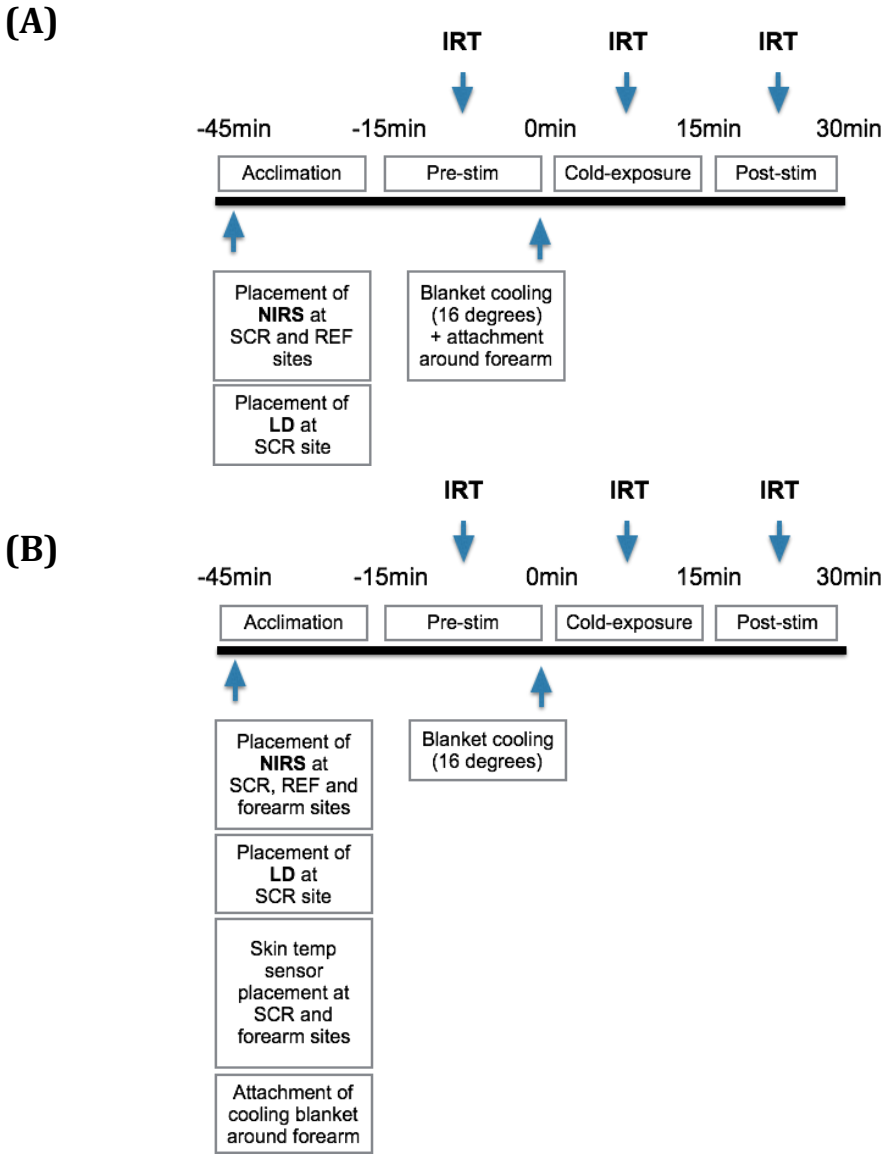

Figure 4.1. Study assessment protocols for the assessment of brown adipose tissue activation in healthy adults Chapter 4
Protocols of the assessments conducted prior to and after cooling in study A and the refinements added to study B. During the single study visit, BAT heat production was measured based on IR thermography imaging (IRT) of the SCR region, alongside the continuous assessment of blood flow (NIRS and LD) in this region, prior to, during and post- a 15-minute cold-exposure intervention. IRT Imaging was captured at 2 images per minute during resting pre-stimulatory and post-stimulatory periods and at 4 images per minute during cold-stimulation. Vascular assessments were continuously recorded throughout the study visit.

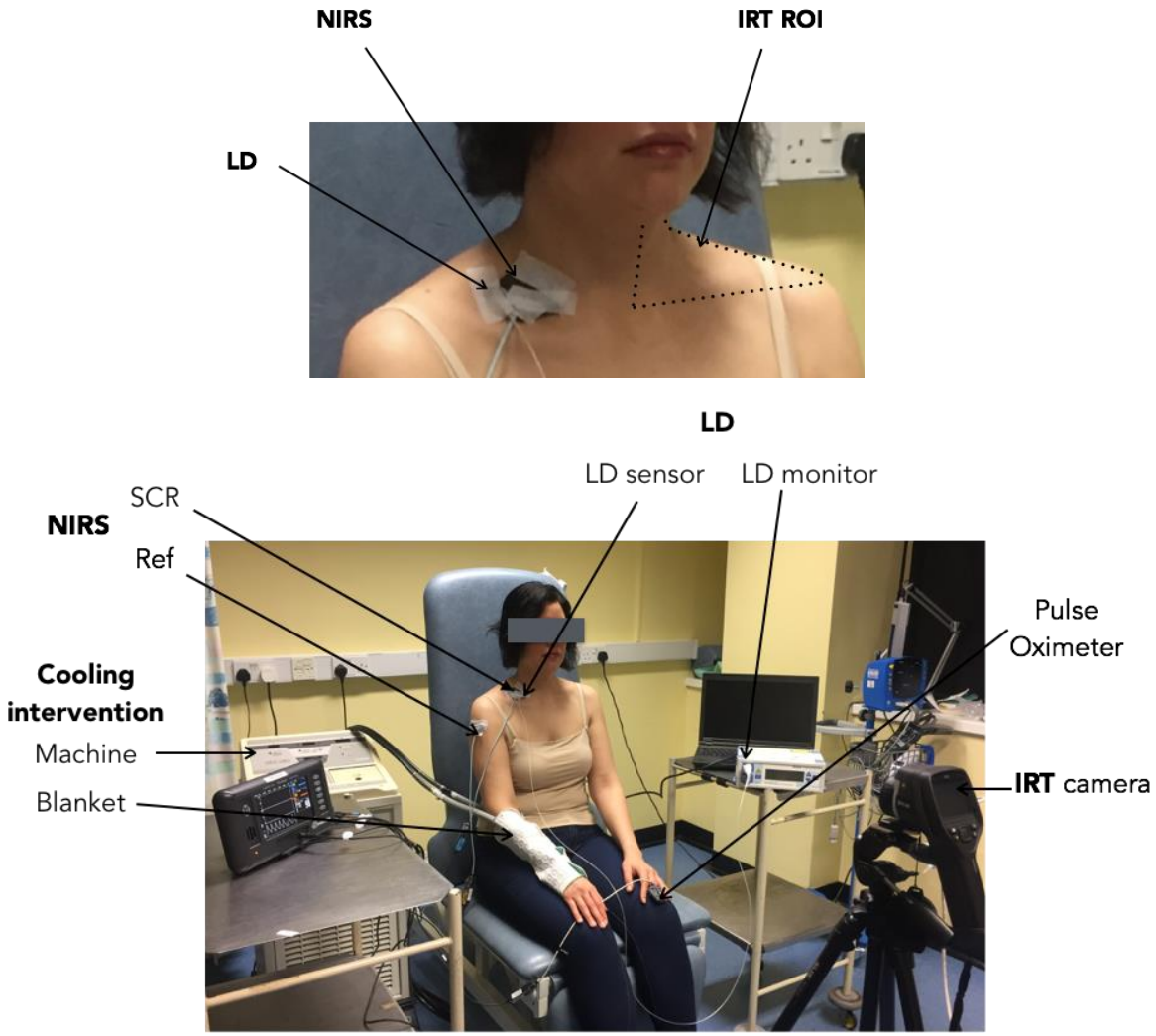

Figure 4.2a. Experimental set up for study A, Chapter 4
Each subject received the same placement of sensors. NIRS sensors measured oxygenation of BAT and of a non-adipose tissue site; deltoid muscle (Ref). A single LD sensor which measured dermal blood flow was placed next to the BAT NIRS sensor in the SCR region. Cold-stimulated (16°C) heat production in the SCR region was assessed by IRT prior to, during and post the cooling challenge.

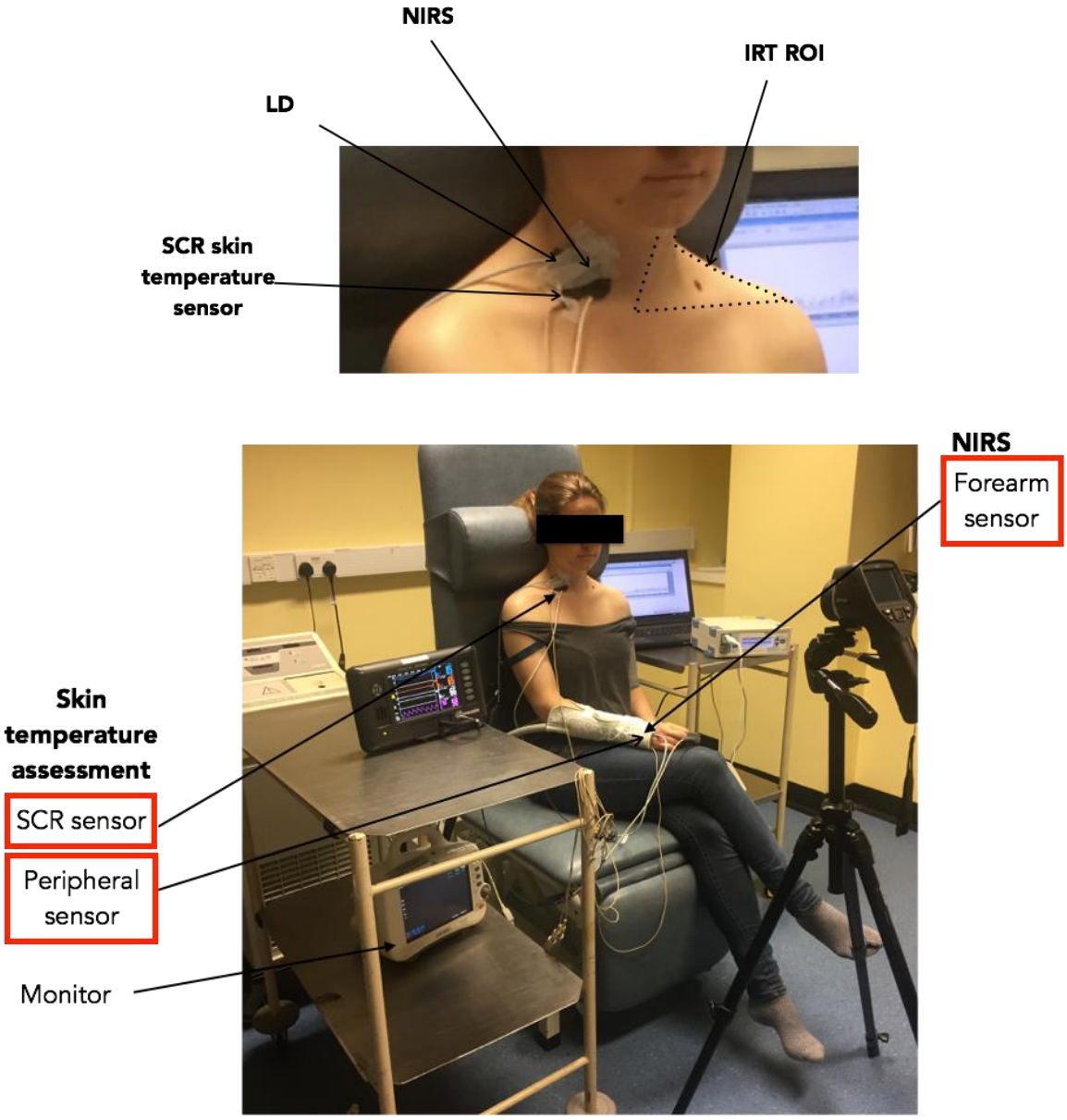

Figure 4.2b. Experimental set up for study B, Chapter 4
In study B, the addition of the following sensors (highlighted in the red boxes) included; skin temperature sensors which were placed on the on the forearm being cooled and in the SCR region and; a NIRS sensor, placed on the forearm receiving cold-stimulation in order to assess oxygenation during presumed vasoconstriction. Cold-stimulated (16°C) heat production in the SCR region was assessed by IRT prior to, during and post the cooling challenge.

Infrared Thermography of SCR region

In both studies, subjects were seated relaxed in the upright position, with arms adducted, and head positioned neutrally looking straight ahead. The subject was positioned away from all heat-emitting objects at a distance of 1.0m from the infrared thermal imaging camera. Prior to imaging, recordings of relative humidity, emissivity, ambient room temperature and distance of the camera to the subject were made. Thermographic images of the neck in the SCR fossa region were acquired by using a FLIR E60 2.3 Megapixel Infrared Camera (FLIR Systems AB, Danderyd, Sweden) which was fixed onto a tripod (model FLIR T440; FLIR Systems AB, Ta¨ by, Sweden). The camera was positioned perpendicular to the region of interest (ROI) (i.e. SCR fossa) at the level of the subject's larynx, ensuring that the ROI was as large as possible within the field of view whilst ensuring that the deltoid muscles are close to the border of view, maintaining the necessary anatomical landmarks, which maximises the amount of infrared radiation measured (Figure 4.2).

Analysis of thermograms

The FLIR thermal imaging camera continually saved labelled images in JPEG format as they were acquired from each 15-minute period of the study. Each thermogram was encoded with radiometric metadata. Thermograms were sequentially processed and analysed by an automated analysis program containing a complied binary code file (MATLAB™.mex file), by the method described in the Methodology section of this thesis (Chapter 2.2.1.2). Parts of the analysis protocol had been updated since the beginning of this work, so any amendments to the original protocol are now described.

Initially thermograms were required to be converted from their JPEG format to non-proprietary Portable Network Graphic format (.png) using the in-house custom built Thermal Imaging Technical Conversion Hub (TITCH), as described by Law et al (2017), for subsequent analysis in

MATLAB™. Such method for converting the raw radiometric data to temperature data produces indistinguishable results to that obtained by FLIR's exclusive software (Law et al, 2017). Thermograms were opened in MATLAB™ where a region of interest was defined for the left or right ROIs labelled with five key points corresponding to the apices of the ROIs. Medial and inferior borders of the ROI were drawn automatically by the software and defined as straight lines between the apices of the right or left acromion to the sternum and the angle where the jaw meets the neck on the left and right side. The method to identify the lateral contour of the neck had been improved from previous published methods where such border of the ROI was approximated to a simple straight line (Gatidis et al, 2016) or by visual identification by plotting points (Symonds et al, 2012). Thus, the developed method for identification of the lateral border of the ROI was defined programmatically by identifying the temperature gradient between the individual and the background (Law et al, 2017).

Following processing of the ROIs within each thermogram in MATLAB™ , the data was exported as a comma-separated value (.CSV) file to calculate the average value of the BAT "hotspot" within the ROI (Symonds et al, 2012; Robinson et al, 2014). Unilateral analysis for the assessment of surface skin temperature was conducted. The hottest 10% of data points within each ROI were identified and the median values of these points were calculated as previously reported (Robinson et al, 2014; Symonds et al, 2012). A non-adipose tissue reference region comprising of a circle with a diameter of 10 pixels, located directly below the central apex of the ROI was analysed for comparison. Outcome measures for IRT included: resting T_{SCR} (mean of the final 5 minutes of the pre-stimulatory period); maximal T_{SCR} (within a given time period during forearm blanket cooling); and ΔT_{SCR} from resting (maximal T_{SCR} – resting T_{SCR}), calculated over the first 10 minutes of cold-stimulation relative to the reference region (Robinson et al, 2016).

Near Infrared Spectroscopy

The non-invasive measurement of tissue oxygen saturation of haemoglobin (StO_2) by NIRS is based on the relative transparency of human tissue to light in the near-infrared region (700–1000 nm), in which 4 wavelengths of light penetrate several centimetres of tissue and the amplitude decay of the light intensity due to absorption of chromophores (oxy- and deoxy-haemoglobin) is analysed. The result allows for the measure of oxygenated haemoglobin, principally in the venous bed (Niwayama et al, 2006). The final StO_2 percentage value is displayed on a monitor and is calculated as oxyhaemoglobin concentration / total oxyhaemoglobin and deoxyhaemoglobin concentration (oxy-deoxyhaemoglobin) (Epstein and Haghenbeck, 2014). For the purpose of this thesis, StO_2 will used to refer to changes in tissue haemoglobin oxygen saturation.

In the present studies, a Nonin Equanox oximeter device and sensors (Nonin Medical Inc. Minnesota, USA) was used to acquire information about localised blood oxygen saturations over the SCR region and two non-adipose tissue regions (Hartwig et al, 2015). These particular sensors use dual emitters/detectors to create pairs of reflected light paths capable of penetrating superficial and deeper layers of tissue, producing measurements that are minimally affected by intervening tissue or surface effects. More detailed information about the NIRS instrumentation is detailed in the methodology section of this thesis (Chapter 2.2.1.4).

Prior to the commencement of the study, soft, non-invasive oximetry sensors were attached to the sites of interest on each subject as described above. Data were continuously measured throughout the experiment ensuring adequate contact of the sensor to the skin at all times. Upon cessation of the study, the NIRS recording for each sensor was saved and subsequently downloaded as an excel spreadsheet. Data were produced every 4 seconds (based on the manufacturer's output software) throughout the study. Resting, maximal and the change in oxygenation values over the SCR region was calculated in the same way as that described above for IRT data.

Laser Doppler Flowmetry

LD is well established non-invasive technique of assessing blood flow in the microcirculation (Frederickson, Fors and Johansson, 2007). This method uses continuous wave helium-neon (He-Ne) laser, at a 640 nm wavelength, as a light source that irradiates intravascular red blood cells and the reflected light is subsequently analysed. The light is reflected back within irradiating fibre glass. The intensity of such reflected light alongside the discrepancies in the wavelength phase of the reflected and irradiated light are determined and red blood cell mass and velocity are determined. More detailed information about the use of LD instrumentation in this study is provided in the methodology chapter of this thesis (Chapter 2.2.1.5). In this study, a Moor Co. (UK) LDI2-IR LD instrument was used and the LD sensor was placed within the subjects' SCR fossa region directly next to the NIRS sensor, to non-invasively assess superficial skin blood flow at a depth of 1-2mm below the skins surface. From the "flux" values obtained from the measurement, a perfusion unit (PU) in the range of 0-100 was calculated every 30 seconds throughout the study and was considered to reflect regional tissue blood flow in this region (Wellhoner et al, 2006; Fredericksson, Fors and Johansson, 2007). Data were saved and downloaded from the Moor Co. measurement monitor as an excel file and to make inter-individual comparisons, blood flow was demonstrated as a change from resting.

Statistical Analysis

Statistical analysis was performed using IBM Statistics for Windows v21 and GraphPad Prism for Windows 2016a (The Mathworks Inc., Natick, MA, USA). To test for differences, comparisons at resting and after cold-exposure were drawn by using two-way repeated measures ANOVA, *t* test or non-parametric tests for data that were not normally distributed. Spearman's correlation tests were used to analyse correlations. A $P < 0.05$ was considered statistically significant. All data are presented as mean ± SD,

unless otherwise stated. Data were categorised and averaged into 7 time points; resting was defined as the average of the final 5 minutes of the pre-stimulatory period from time point – 5 to 0 (time point '0'); for cold-stimulatory period, data were averaged and graphically presented every 5 minutes for 15 minutes; and the post-stimulatory period was defined from 30 to 45 minutes, again data are presented as 5 minute averages.

4.3 Results

4.3.1 Subjects

The initial feasibility study (Study A) comprised of 15 healthy, lean [body mass index (BMI) of <25 kg/m^2] adults aged 18-36 years, recruited between the months of May and September 2016 (Table 4.1). Of the original 15 subjects who participated, 9 returned to repeat the study between February and June 2017 (Study B; Table 4.1). The basic characteristics of subjects from both pilot studies are given in Table 4.2. There were no significant differences in age, height, weight and BMI characteristics between study A and study B.

Table 4.1. The time of year in relation to the outside environmental temperature for each individual participating in study A (*n* = 15) and study B (*n* = 9)

	Date of study		Environmental temperature (°C)	
Participant	Study A	Study B	Study A	Study B
1	**26/04/16**	**28/02/17**	7	5
2	**26/04/16**	**01/03/17**	7	5
3	**27/04/16**		8	
4	**28/04/16**	**02/03/17**	8	5
5	**05/05/16**		11	
6	**10/05/16**	**02/06/17**	11	14
7	**11/05/16**	**09/03/17**	11	4
8	**12/05/16**		12	
9	**12/05/16**		12	
10	**13/05/16**	**05/05/17**	11	13
11	**16/05/16**		11	
12	**17/05/16**	**19/02/17**	12	7
13	**18/05/16**	**02/06/17**	13	16
14	**19/05/16**		15	
15	**19/05/16**	**03/03/17**	15	4

Table 4.2. Characteristics of study subjects

Characteristic	**Study A**	**Study B**	***P* value**
Recruited n	15	9	
Age (years)	28.8 ± 6.2	29.1 ± 7	$P = 0.895$
Male: Female ratio	6:9	6:3	
Height (cm)	172 ± 11.7	171 ± 9.3	$P = 0.941$
Weight (kg)	69.4 ± 12.4	70.1 ± 10.7	$P = 0.725$
BMI (kg/m^2)	23.3 ± 2.5	24.1 ± 1.6	$P = 0.289$

Abbreviations: BMI, Body mass index
Data are shown as mean ± SD
No significant differences in subject demographics was observed between either investigation.

4.3.2 Study A

Cold-induced adrenergic stimulation resulted in a localised increase T_{SCR} compared to a reference region ($T_{SCR,}$ 0.3 ± 0.2°C vs. T_{REF}, 0.2 ± °C; P = 0.453), representative of BAT thermogenic activity (Figure 4.3a; $P < 0.05$). Cold exposure increased T_{SCR}, plateaued and then returned to baseline after stimulation. A similar response was observed for T_{REF} (P = 0.378).

Relative to baseline, maximal increases in T_{SCR} occurred between 5 and10 minutes during cooling, with all individuals responding to the cold-exposure with an increase in BAT temperature (Figure 4.3b; $P < 0.05$). As expected, cold-induced cold-exposure through assumed β-AR stimulation, increased heart rate, systolic blood pressure and core temperature (Figure 4.4; $P < 0.05$). Furthermore, increases in SCR skin temperature, measured by IRT, can be seen in the ROI of the thermograms (Figure 4.5).

Since blood flow provides oxygen for BAT mitochondria, and also transfers heat from BAT to other parts of the body, I quantified tissue oxygenation directly over the SCR BAT depot and blood flow in the SCR region. In response to cold, localised tissue oxygen saturation within the SCR region increased by 8%, with responses peaking at 10 minutes (Figure 4.6a; P = 0.040). Adrenergic stimulation resulted in an increase in SCR oxygen saturation in all individuals (Figure 4.6b; P = 0.001). No changes in oxygenation were observed during the cold stimulation over a non-brown adipose tissue region of the deltoid muscle (Ref) (Figure 4.6a; P = 0.476). In line with the aforementioned cold-induced increases in SCR tissue oxygenation and skin temperature overlying BAT, blood flow localised to the SCR region, subsequently increased, with maximal responses in the final 5 minutes of cold-stimulation compared to resting PU values (Figure 4.7; P = 0.002).

Since cold exposure was shown to induce increases in T_{SCR} indicative of BAT heat production, SCR tissue oxygenation compared to a non-adipose tissue reference region and superficial blood flow over the SCR region, I sought to understand the dynamic pattern of these responses every 30 sec

throughout the 15 min BAT stimulatory period.

Analysis revealed sharp rises in T_{SCR} and tissue oxygenation were initiated in the first minute of stimulation (Figure 4.8) which continued to increase gradually. Maximal responses of tissue oxygenation over the SCR region occurred over 3 and a half minutes earlier than the maximal increases in BAT thermogenesis (9.1 mins) (Figure 4.8). In all subject's, increases in tissue oxygenation occurred prior to maximal increases in T_{SCR} (Figure 4.9). Further, blood flow over the BAT SCR region increased maximally at the end of cold-stimulation, subsequent to the aforementioned peak responses (P = 0.001).

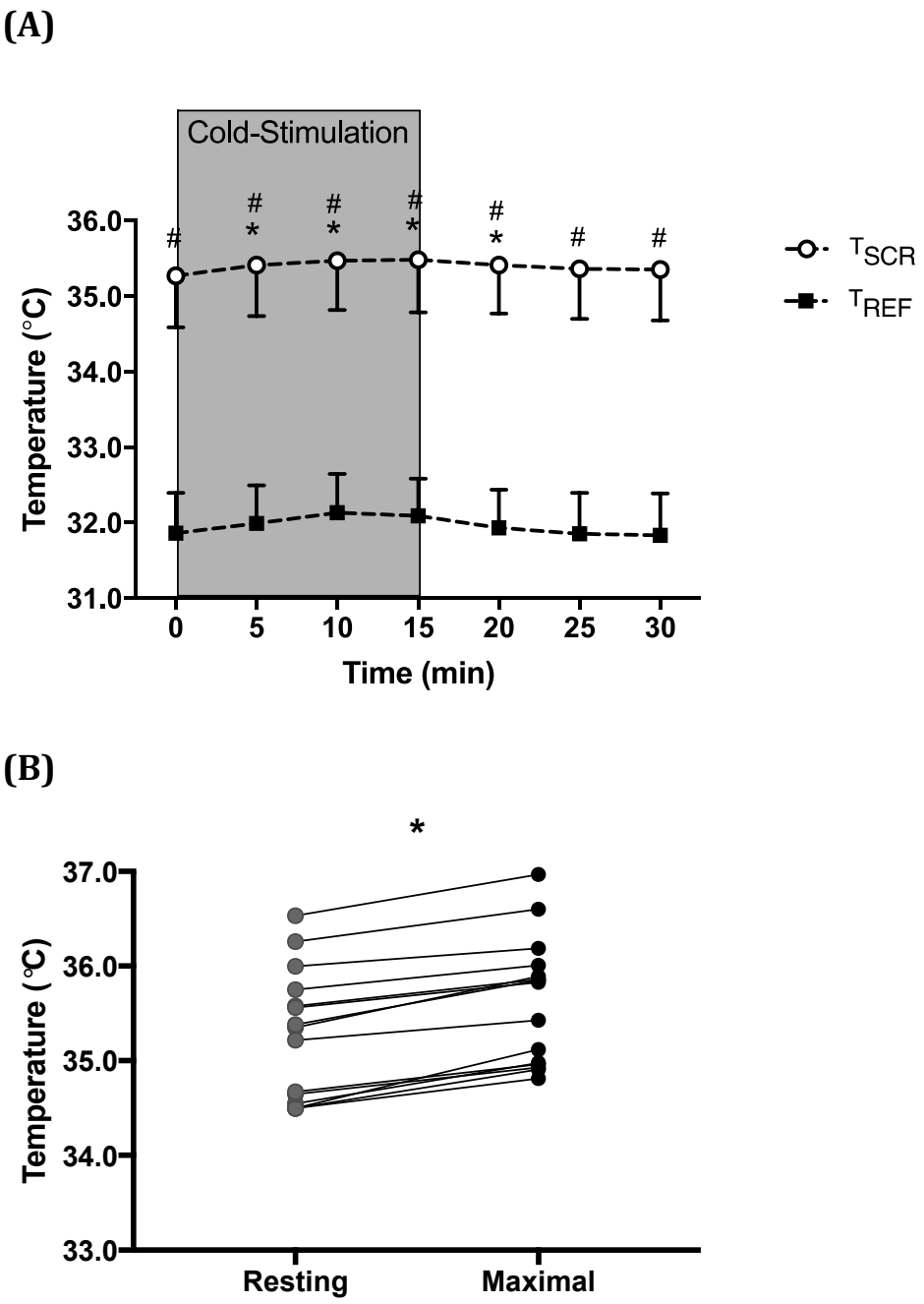

Figure 4.3. Cold-induced thermogenic responses, assessed by IRT
Mean ± standard deviation BAT thermogenic responses to cold-exposure (white circles) compared to a non-adipose tissue reference region (T_{REF}) (A) and mean values of T_{SCR} at resting (grey circles) vs. maximal thermogenic responses (black circles) during cold-stimulation (B). Asterisk (*) denotes a significant difference compared to resting T_{SCR} ($P < 0.05$). Hashtag (#) denotes a significant difference compared to a non-adipose tissue reference region at that time-point ($P < 0.05$).

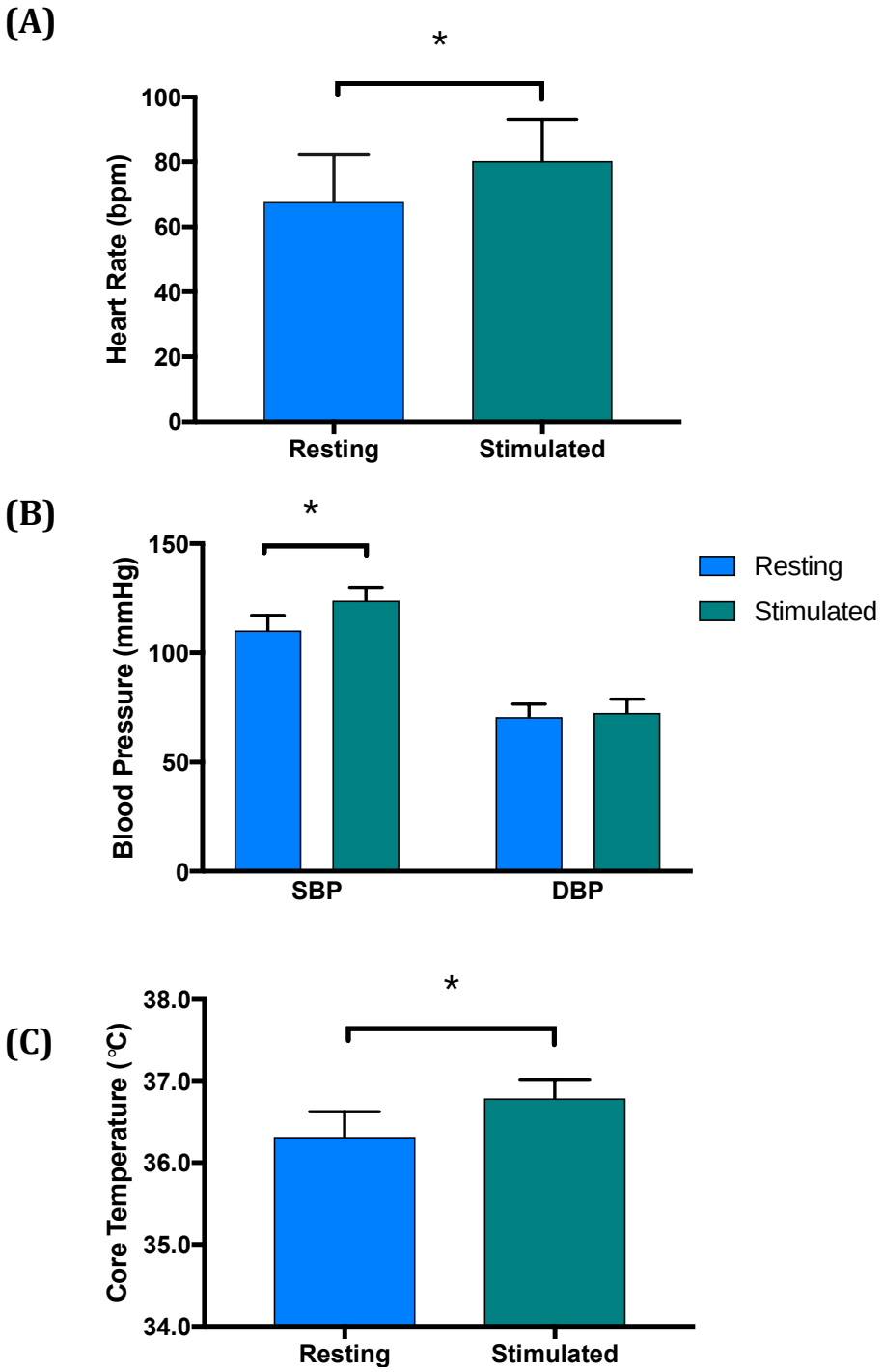

Figure 4.4. Cold-stimulated SNS responses to cold-stimulation
Acute sympathetic nervous system responses to 15 minutes of cold-exposure in 15 subjects in study A; (A) Heart rate (B) Blood pressure and (C) Core temperature. Asterisk (*) denotes a significant difference compared to resting ($P < 0.05$). SBP, systolic blood pressure; DBP, diastolic blood pressure. Data are shown as mean ± standard deviation. *$p < 0.05$ vs. resting.

(A)

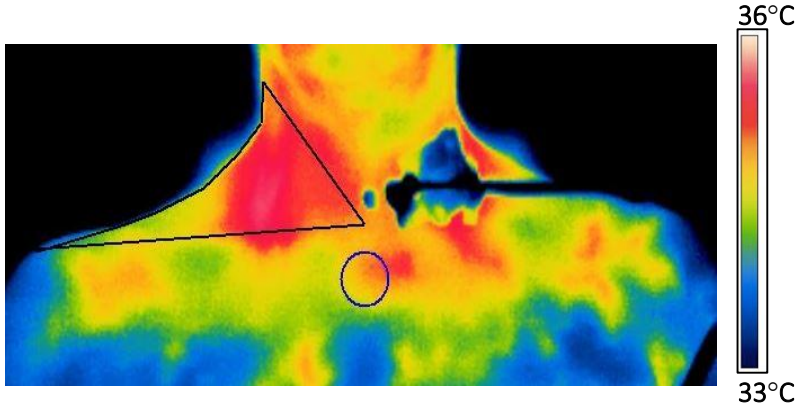

(B)

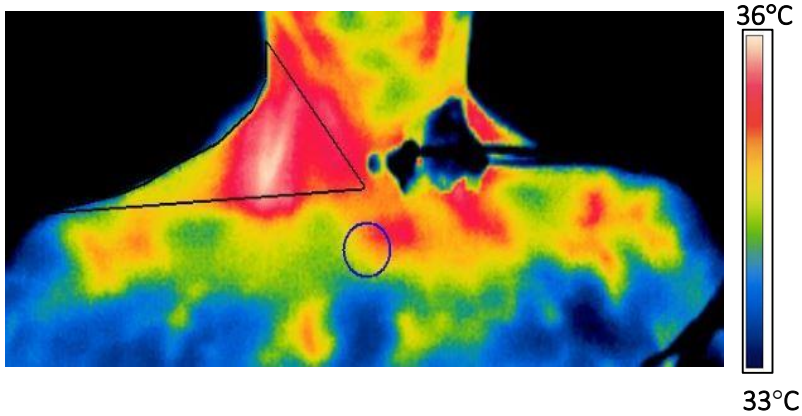

Figure 4.5. Anterior thermal images of the neck and upper thorax
Representative example of thermograms of the skin overlying the ROI located at the SCR (black triangle) and sternal (blue circular reference region) in the same individual at resting (A) and during cold-stimulation at 16°C for 15-minutes (B).

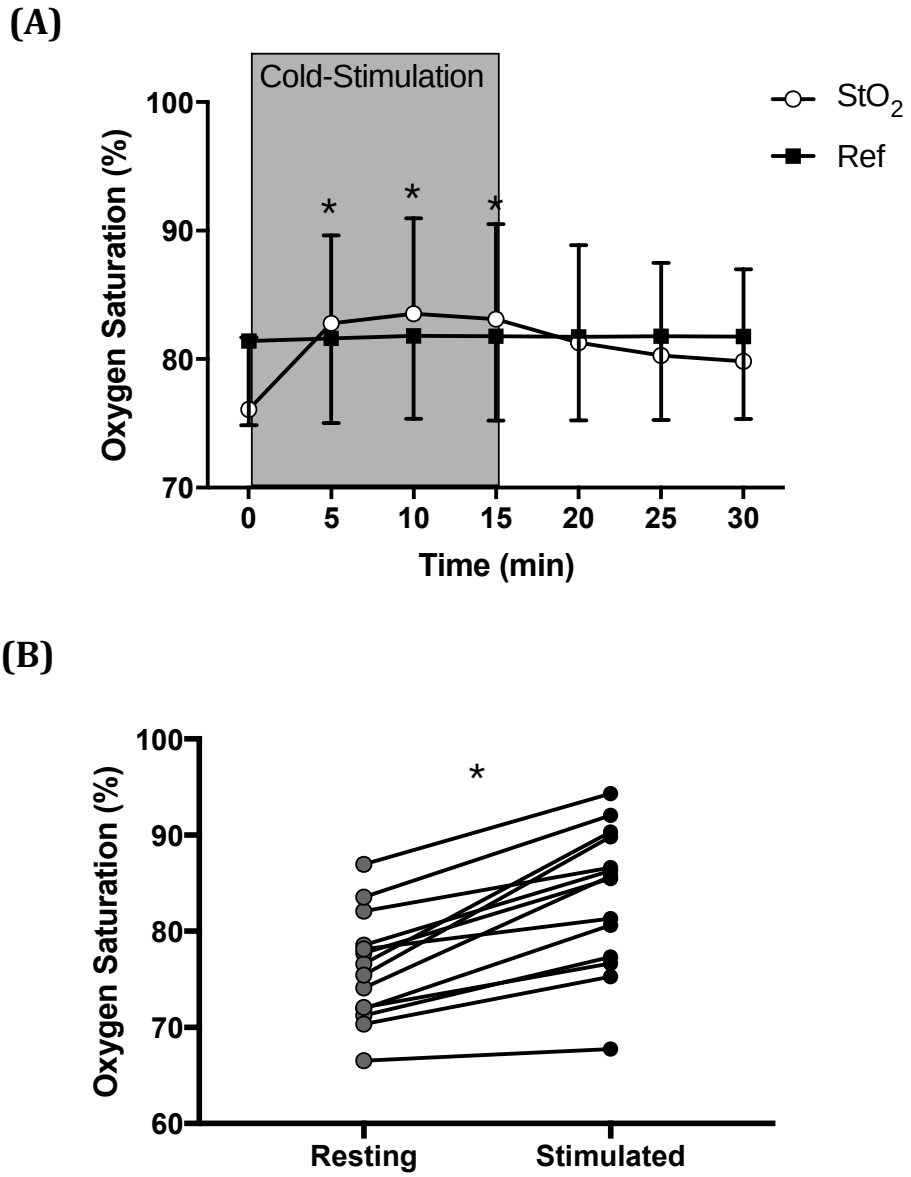

Figure 4.6. Localised tissue oxygen saturations upon cold-stimulation

Cold-induced stimulation of mean (± standard deviation) BAT SCR oxygenation values, over the SCR region (white circles) compared to over a non-adipose tissue reference site (Ref; black squares) (A) and mean values of SCR temperature at resting (grey circles) vs. maximal tissue oxygenation responses over the SCR region (black circles) during cold-stimulation (B). Asterisk (*) denotes a significant difference compared to resting SCR oxygenation ($P < 0.05$).

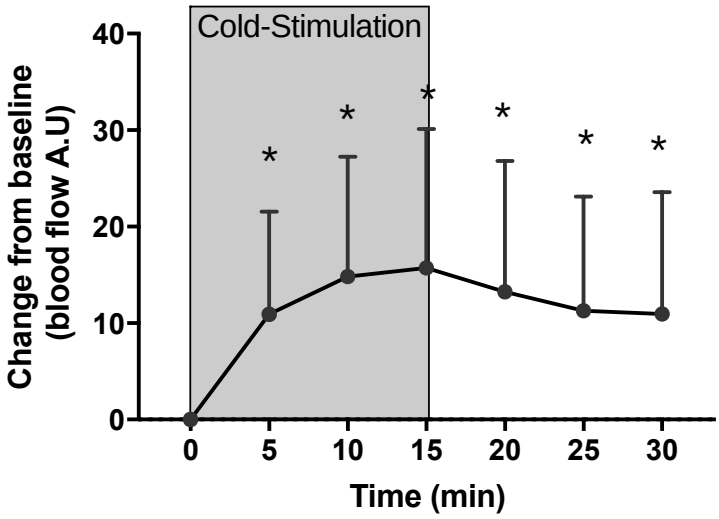

Figure 4.7. Cold-stimulated blood flow over SCR region
Mean (± standard deviation) change in blood perfusion over the SCR region in response to 15 minutes of cold-insult to the forearm in 15 subjects in study A. Asterisk (*) denotes a significant difference compared to resting SCR oxygenation ($P < 0.05$).

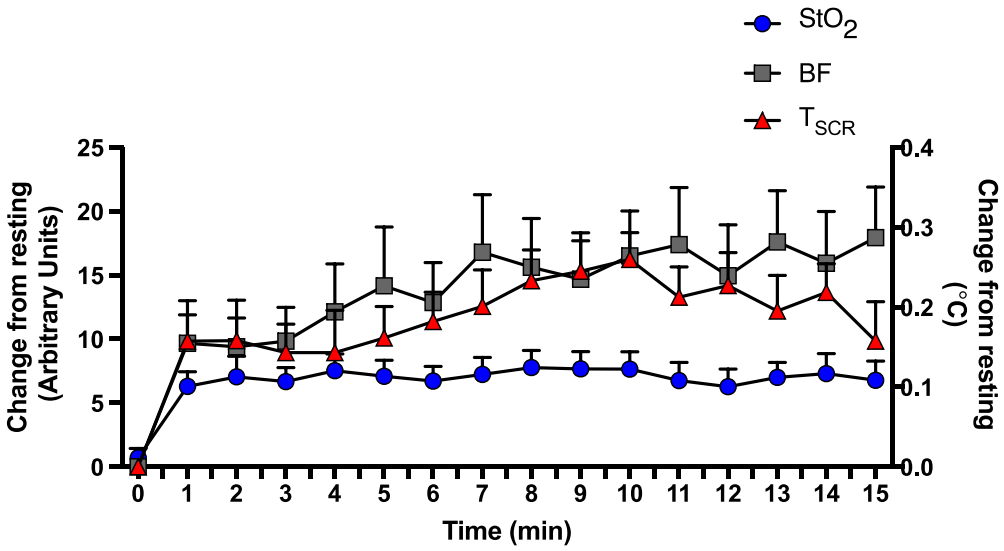

Figure 4.8. Cold-stimulated responses during cold-stimulation
Mean (± standard deviation) changes from resting (time point '0') every minute during cold-stimulation of the forearm only, in 15 participants; BAT thermogenic responses (T_{SCR}; orange triangles; right axis); SCR tissue oxygenation (StO_2; blue circles; left axis); and SCR blood flow (BF; grey squares; left axis) (n=15).

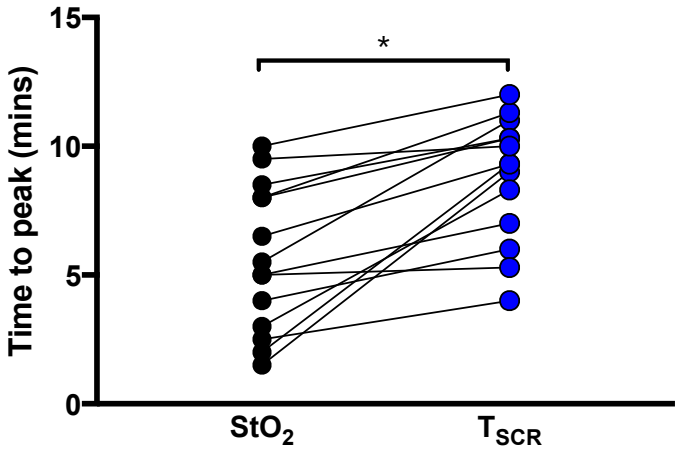

Figure 4.9. Maximal tissue oxygenation responses relative to peak BAT heat production during forearm cold-stimulation
Individual maximal tissue oxygenation (StO_2) responses and SCR skin temperature responses (T_{SCR}) to cold stimulation. The greatest increments StO_2 occur precede maximal BAT thermogenesis in all subjects (n=15).

4.3.3 Study B

In the 9 participants who returned to complete the revised experiment, there was a similar pattern of response demonstrating cold-induced increases in T_{SCR}, representative of BAT thermogenic activity (Figure 4.10a; $P = 0.001$). Again relative to baseline, a maximal change in T_{SCR} of 0.28 ± 0.21°C occurred between 5-10 minutes during stimulation, with all participants responded to the cold-exposure with an increase in BAT temperature (Figure 4.10b; $P = 0.001$). There was no effect of season on BAT thermogenic responses between the 6 participants who completed study B in the winter and the remaining 3 completing study B in the spring season (resting T_{SCR}; 34.91 ± 0.2°C vs. 35.14 ± 0.34°C, $P = 0.999$; maximal change in T_{SCR} from resting; 0.36 ± 0.07°C vs. 0.36 ± 0.04°C, $P = 0.999$). Confirming cold-induced β-AR stimulation were the observed in increases heart rate ($P = 0.003$), systolic blood pressure ($P = 0.001$) and core temperature ($P = 0.001$) (Figure 4.11). The addition of skin temperature probes over the SCR region and the cooled forearm, correspond with these observations, demonstrating a simultaneous increase in SCR skin temperature and reduction in peripheral skin temperature, evidenced by a 6°C gradient

change in the skin temperature between these two locations (Figure 4.12). Further, coinciding with the reductions in peripheral skin temperature, a drop in peripheral oxygenation was also observed during cold-stimulation (Figure 4.13; $P = 0.001$), indicative of the initiation of cutaneous vasoconstriction.

Similarly, to study A, in response to cold-exposure, increases in T_{SCR}, as assessed by IRT occurred concomitantly with the highly localised increase in tissue oxygen saturation also within the SCR region (10%; $P = 0.001$), with responses peaking at between 5-10 minutes (Figure 4.14a). Oxygen saturation of the SCR region increased in all individuals (Figure 4.14b; $P = 0.001$). No changes in oxygenation were observed during the cold stimulation over a non-brown adipose tissue region of the deltoid muscle (Ref) (Figure 4.14.1; $P = 0.492$). Superficial blood flow over the SCR region subsequently increased, again with maximal responses in the final 5 minutes of cold-stimulation compared to resting PU values (Figure 4.15, $P = 0.001$). There was no effect of season on tissue oxygenation responses over the SCR region between the 6 participants completing study B in the winter and the remaining 3 in the spring season (resting ; $72 \pm 4\%$ vs. $69 \pm 4\%$, $P = 0.381$; maximal change in StO_2 from resting; $13 \pm 6\%$ vs. $16 \pm 7\%$, $P = 0.714$).

Analysis of the dynamic responses to cold-stimulation over 15 minutes revealed on this occasion, gradual increments in SCR tissue oxygenation, skin temperature and blood flow over the SCR region (Figure 4.16). Blood perfusion over the BAT SCR region increased maximally subsequent to the changes in SCR oxygenation and BAT thermogenesis, peaking at 15 minutes during the stimulation ($P = 0.001$; Figure 4.16). Further, maximal responses of tissue oxygenation over the SCR region occurred concomitantly with maximal increases in BAT thermogenesis (Figure 4.16- Figure 4.17; $P = 0.791$). In 7 of 9 subjects, increases in tissue oxygenation occurred prior to maximal increases in T_{SCR}.

(A)

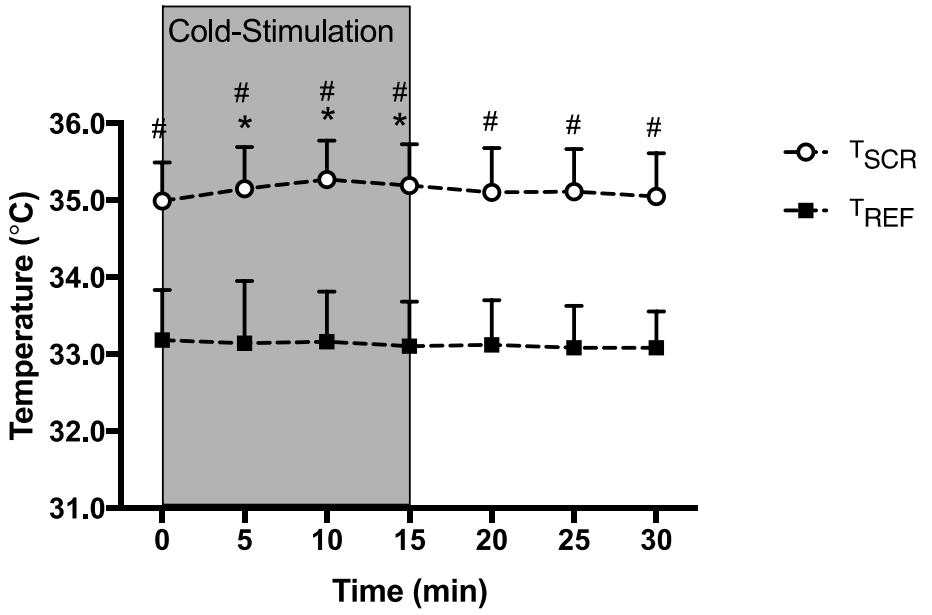

(B)

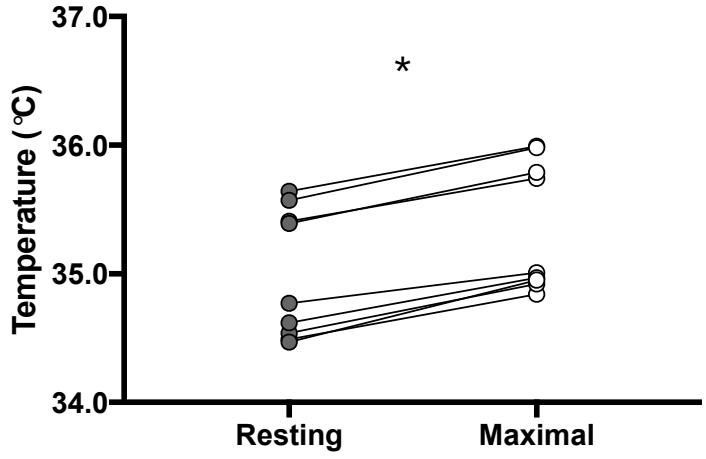

Figure 4.10. Cold- stimulated thermogenic responses, assessed by IRT

Mean (± standard deviation) BAT thermogenic responses to cold-exposure (white circles) compared to a non-adipose tissue reference region (T_{REF}) (A) and mean values of T_{SCR} at resting (grey circles) vs. maximal thermogenic responses (black circles) during cold-stimulation (B). Asterisk (*) denotes a significant difference compared to resting T_{SCR} ($P < 0.05$). Hashtag (#) denotes a significant difference compared to a non-adipose tissue reference region at that time-point ($P < 0.05$).

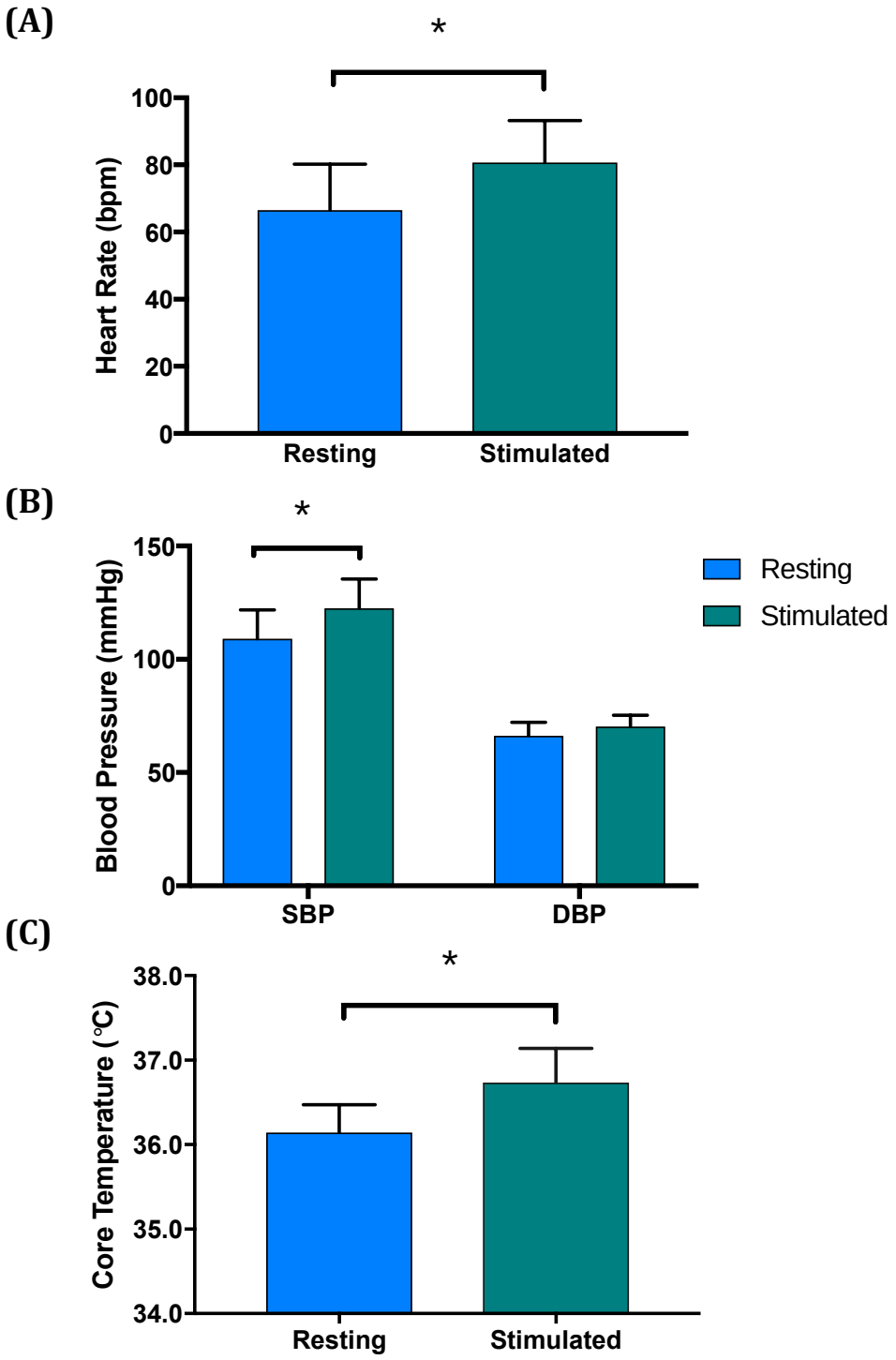

Figure 4.11. Cold-stimulated SNS responses to cold-stimulation

Mean (± standard deviation) sympathetic nervous system responses to 15 minutes of cold-exposure in 9 subjects in study B; (A) Heart rate (P = 0.003) (B) Blood pressure (P = 0.001) and (C) Core temperature (P = 0.001). Asterisk (*) denotes a significant difference compared to resting (P < 0.05). SBP, systolic blood pressure; DBP, diastolic blood pressure.

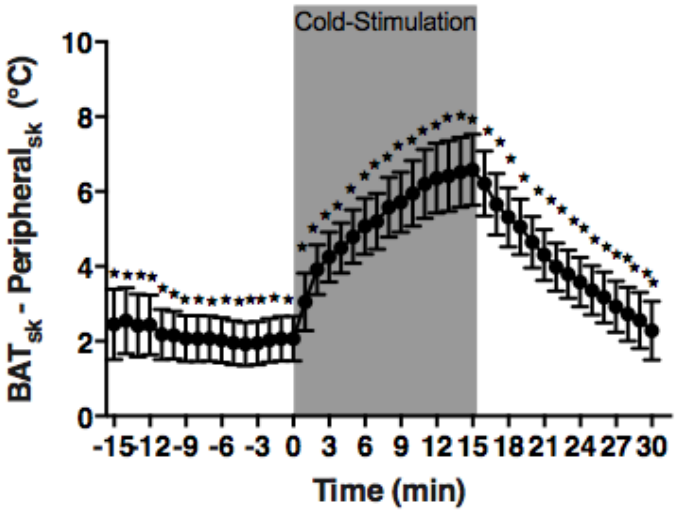

Figure 4.12. Cold-stimulated skin temperatures over SCR and peripheral regions

Gradient of skin temperature change between the skin temperature sensor placed over the SCR BAT region (BAT_{SK}) and the peripheral skin temperature sensor placed over the cooled forearm prior to, during and post-cold stimulation in the 9 subjects participating in study B. Asterisk (*) denotes a significant difference between BAT_{SK} and $Peripheral_{SK}$ temperatures ($P < 0.05$). Data are shown as mean ± standard error of mean.

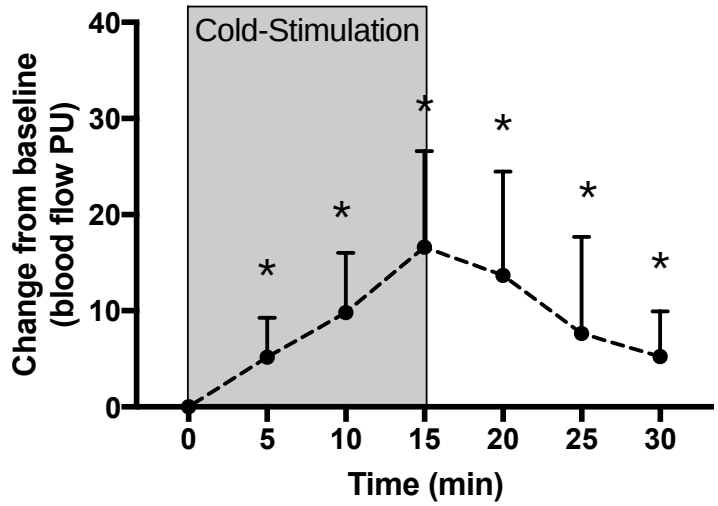

Figure 4.13. Oxygen saturation of the cooled site during cold-stimulation

Mean (± standard deviation) change in peripheral oxygenation over the forearm receiving the cooling stimulus in the 9 subjects in study B. Asterisk (*) denotes a significant difference compared to resting SCR oxygenation ($P = 0.001$).

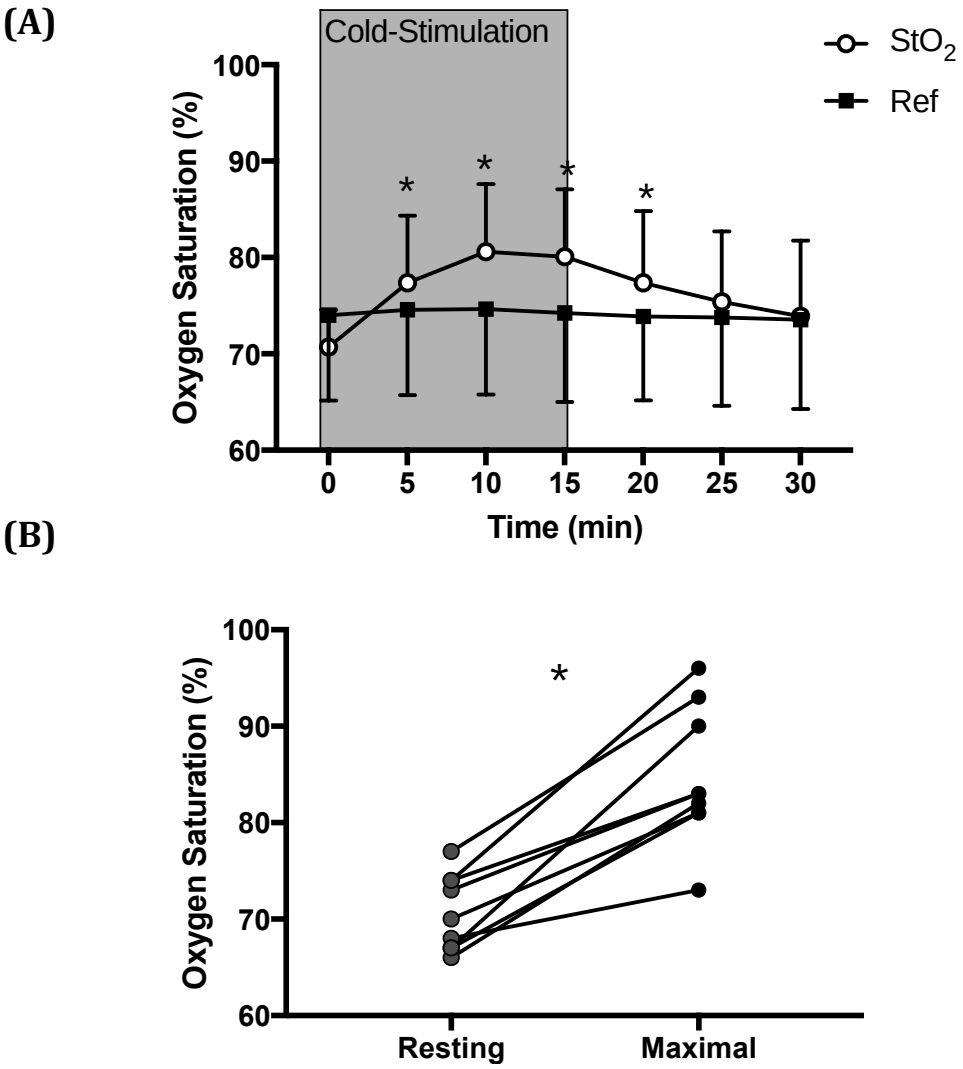

Figure 4.14. Oxygen saturations of the SCR region upon cold-stimulation

Cold-induced stimulation of mean BAT SCR oxygenation values, over the SCR region (white circles) compared to over a non-adipose tissue reference site (REF; black squares) (A) and mean values of SCR temperature at resting (grey circles) vs. maximal tissue oxygenation responses over the SCR region (black circles) during cold-stimulation (B). Values are shown as mean ± standard deviation. Asterisk (*) denotes a significant difference compared to resting SCR oxygenation ($P < 0.05$).

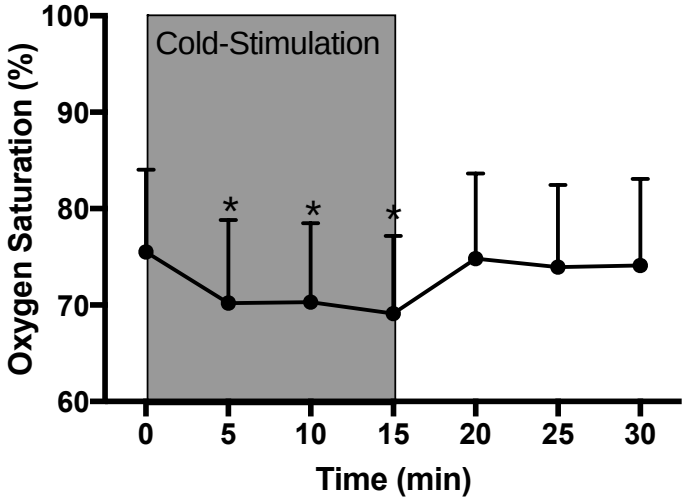

Figure 4.15. Cold-stimulated oxygen saturation over the forearm
Mean (± standard deviation) change in oxygenation in response to 15 minutes of cold-insult to the forearm in 9 subjects in study B. Asterisk (*) denotes a significant difference compared to resting SCR oxygenation ($P < 0.05$).

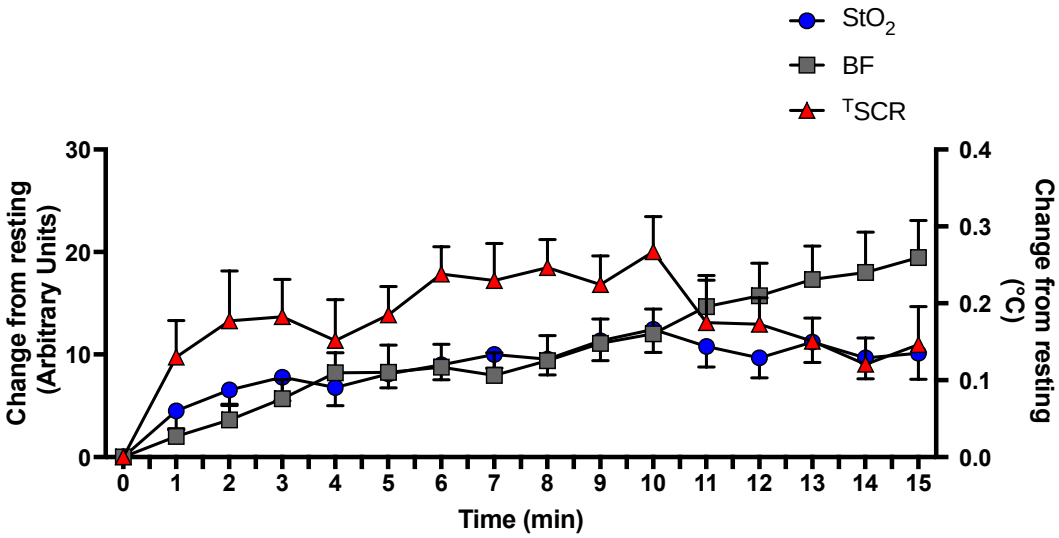

Figure 4.16. Cold-stimulated responses during cold-stimulation
Mean (± standard deviation) changes from resting (time point '0') every minute during cold-stimulation of the forearm only, in 9 subjects in study B; BAT thermogenic responses (T_{SCR}; orange triangles; right axis); SCR tissue oxygenation (StO_2; blue circles; left axis); and SCR blood flow (BF; grey squares; left axis) (n=9).

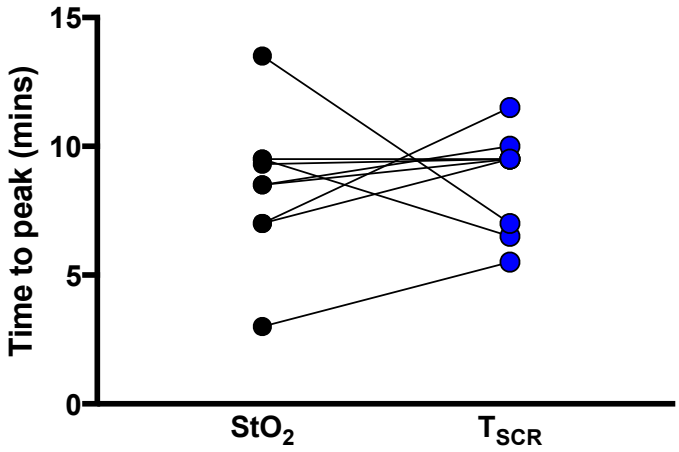

Figure 4.17. Maximal tissue oxygenation responses relative to peak BAT heat production in 9 healthy adult subjects during cold-stimulation
Individual maximal tissue oxygenation (StO_2) responses and SCR skin temperature responses (T_{SCR}) to cold stimulation. The greatest increments StO_2 occur precede maximal BAT thermogenesis in 7 of 9 subjects.

4.3.4 Differences between subjects in study A and study B

Prior to cold-stimulation, resting T_{SCR} assessed by IRT, indicative of BAT thermogenic activity, was not found to be significantly different in the 9 subjects who participated in study A and B (P = 0.932; Figure 4.18a). Likewise, intra-subject differences demonstrated no disparity in the maximal change from resting between studies (P = 0.445; Figure 4.18b). Interestingly, in all but one participant, resting T_{SCR} vs. the magnitude of maximal change, revealed a trend towards a greater resting SCR skin temperature corresponding to a lower change from resting (Table 4.3).

Mean resting SCR tissue oxygenation was observably lower in study B compared to study A (P = 0.023; Figure 4.19a), whilst there were no significant differences in the maximal change from resting for SCR tissue oxygenation (Study: A, 8 ± 5% vs. B, 10 ± 5%, P = 0.199; Figure 4.19b). Further, there were no differences in the magnitude of change in blood flow over the SCR region in the 9 subjects completing both study A and study B (Figure 4.20; P = 0.199).

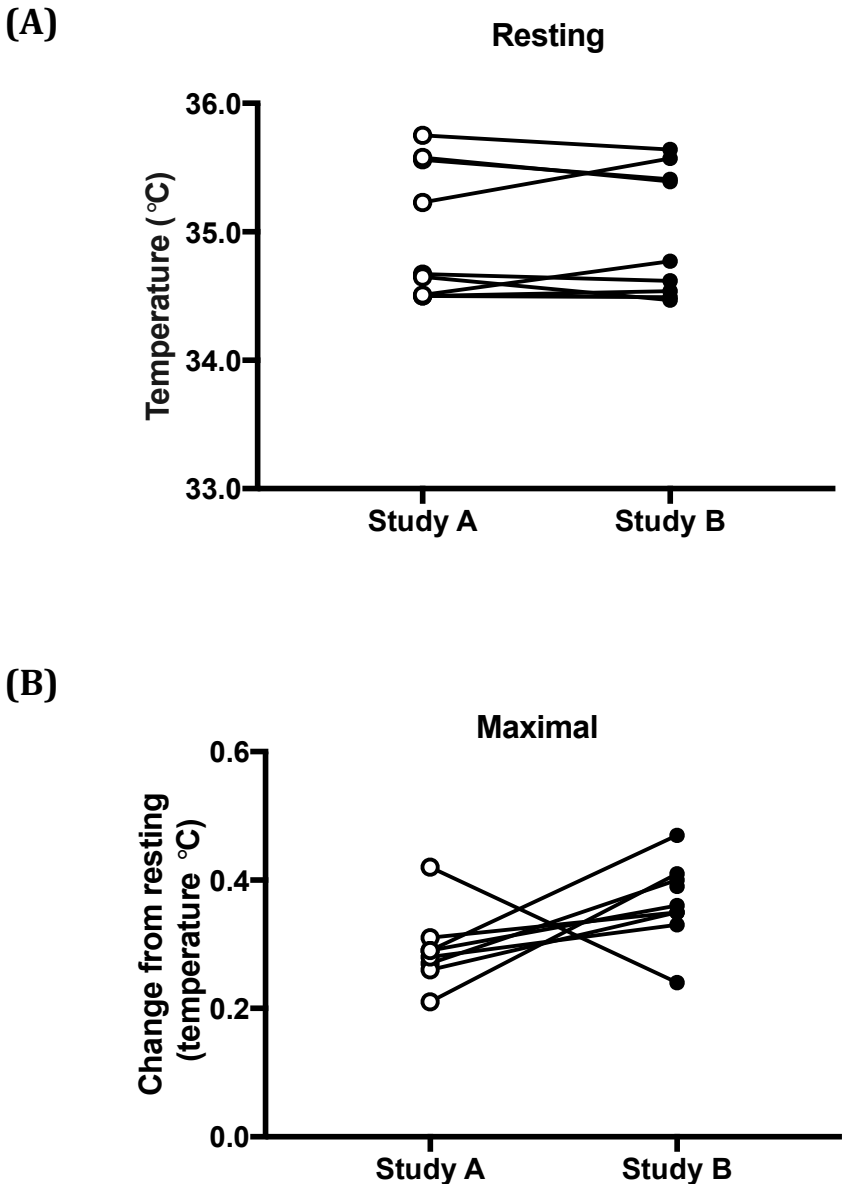

Figure 4.18. SCR skin temperature responses to forearm cold-stimulation between study A and study B
Intra-subject differences demonstrated no significant difference in mean resting TSCR (A) and maximal change from resting between studies (B).

Table 4.3. Intra-subject comparisons of resting T_{SCR} and its magnitude of change (n=9)

Participant	Resting T_{SCR}		Change from resting (T_{SCR})	
	Study A	Study B	Study A	Study B
1	35.56	35.41	0.28	0.33
2	34.50	34.49	0.31	0.35
3	34.50	34.54	0.62	0.39
4	34.49	34.77	0.42	0.24
5	34.67	34.62	0.29	0.36
6	35.75	35.64	0.26	0.35
7	34.65	34.47	0.29	0.47
8	35.58	35.39	0.27	0.40
9	35.23	35.57	0.21	0.41

(A)

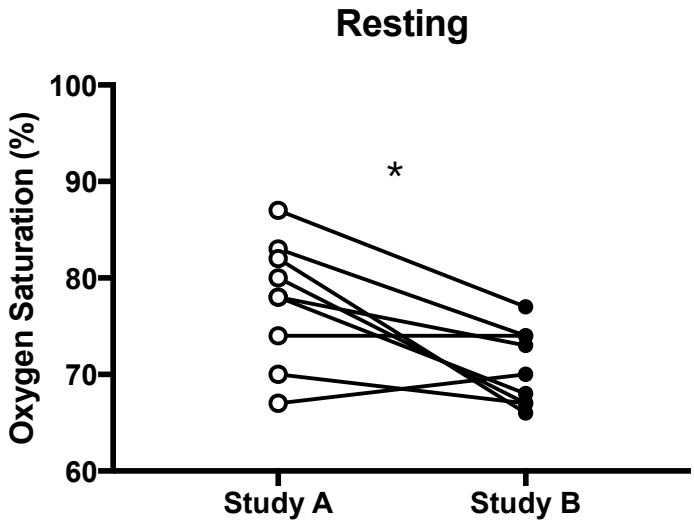

(B)

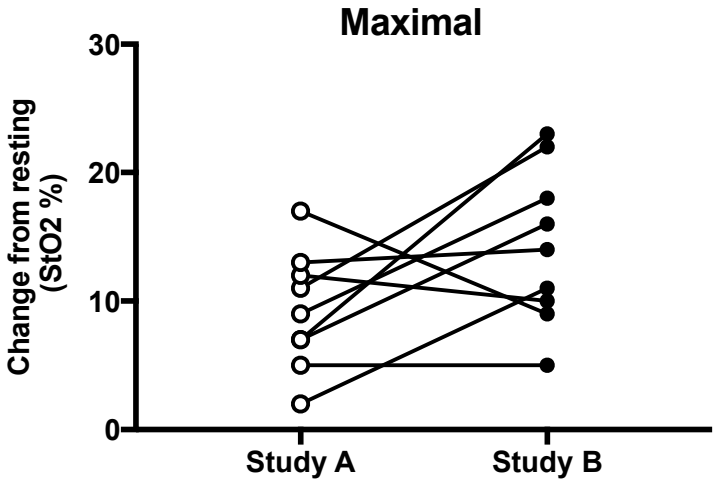

Figure 4.19. SCR tissue oxygenation responses to forearm cold stimulation between study A and study B
Intra-subject differences demonstrated no significant difference in mean resting StO_2 (A) and maximal change from resting between studies (B).

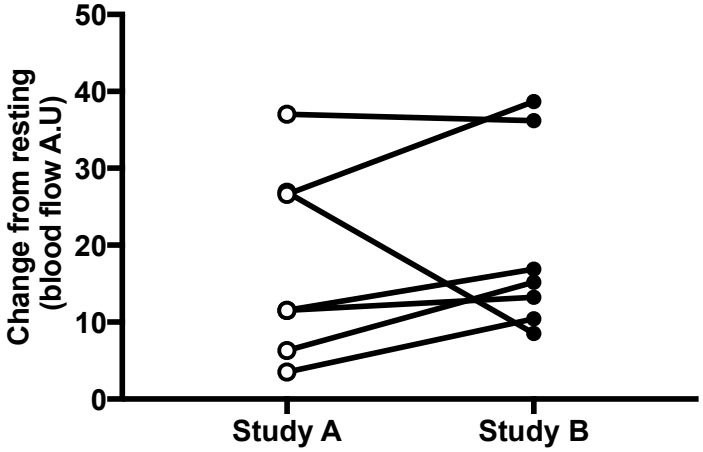

Figure 4.20. SCR blood flow responses to forearm cold-stimulation between study A and study B

Intra-subject differences demonstrated no significant difference in the magnitude of change in blood flow from resting between studies.

4.4 Discussion

The thermogenic function of BAT and its substrate disposal during cold exposure is increasingly being explored by various means of assessment, since BAT may hold the potential for weight loss management (Marlatt, Chen and Ravussin, 2018).

Since the current gold-standard for the assessment of BAT metabolic activity ($^{[18]}$F-FDG PET-CT) involves the use of ionising radiation and is expensive to conduct, the development of harmless methods for quantitative measurement of BAT activity can change the outlook of studying metabolism in this tissue *in vivo*. A step towards advancing the understandings of the metabolic capabilities of BAT *in vivo* by using non-invasive methods, has been the successful demonstration of cold-induced increases in skin temperature directly over the main BAT depot in humans, assessed using IRT, indicative of BAT activity (Ang et al, 2017; Din et al, 2016; El Hadi et al, 2016; Jang et al, 2014; Lee et al, 2011; Peterson et al, 2016; Ramage et al, 2016; Salem et al, 2016; Symonds et al, 2012). Studies implementing alternative safe techniques such as that of NIRS; a straightforward measure of tissue oxygenation, have highlighted its potential to understand BAT activity (Muzik et al, 2013), but are yet to demonstrate its use in supporting IRT as an effective tool to study BAT metabolic activity in humans (Hartwig et al, 2017).

In this feasibility study, on two occasions, a non-invasive multimodal approach (using NIRS, IRT and LD) was used to understand tissue oxygenation and local skin blood flow in relation to BAT heat production during cold-exposure in healthy adults. The major findings drawn from these experiments were the demonstration that in response to acute cold-exposure, NIRS detected increases in SCR tissue oxygenation (7-10%) which paralleled the increases in T_{SCR} (0.22-0.26°C) assessed by IRT. Interestingly, maximal SCR oxygenation responses preceded the peak responses of T_{SCR}, indicative of BAT thermogenesis. Subsequently these responses began to decline, whilst blood flow responses over the main SCR BAT depot

continued increasing until the cessation of the cold-stimulation. These findings are one of the first attempts to investigate the dynamic activity of BAT under cold-stimulation utilising NIRS and display enormous promise for the complementary use of NIRS with IRT for the assessment of acute BAT activity, at least in human adults.

4.4.1 Acute cold exposure stimulates SCR BAT Thermogenesis

Cold-induced sympathetic β-AR stimulation in a cohort of unselected, healthy, lean subjects, resulted in a localised increase in SCR temperature relative to a non-adipose tissue reference region, indicative of BAT activity in both pilot experiments. The temperature response was temporally limited for the duration of cold-insult, suggesting underlying BAT activation. Temperature responses over the SCR region for all subjects increased within the first 5 minutes which is in accord with the multitude of IRT studies reporting increases in local SCR skin temperature in response to cold stimulation (Ang et al, 2017; Din et al, 2016; El Hadi et al, 2016; Jang et al, 2014; Lee et al, 2011; Peterson et al, 2016; Ramage et al, 2016; Salem et al, 2016; Symonds et al, 2012). However, sharp increments in the responses of SCR tissue oxygenation and blood flow were observed within the first minute of cold-stimulation in study A, demonstrated in figure 4.8, for which responses only increased gradually thereafter. Such responses maybe attributed to methodology employed, given that the cooling blanket was cooled to the desired temperature (16°C) next to the subject, prior to its placement on the forearm at time point '0'. Responses suggest an acute stress response attributable to anticipatory stress (Robinson et al, 2016). In study B, the cooling blanket was placed on the subject's forearm during the acclimation phase prior to the commencement of the study and gradually cooled once the baseline period was complete. Thus, the stimulatory phase commenced (at time point '0') once the blanket cooled to 16°C. Responses spiked quickly within the first minutes, with tissue activity remaining constant but SCR temperature continued to increase, as heat travels to the surface of the skin, which subsequently increased blood flow.

Since there were no significant variations in the maximal change in T_{SCR} from resting between study A and B, a more severe cold-insult at a temperature below 10°C, may have provoked a significant change, since evidence has demonstrated changes of between 0.4-0.9°C with water cooling interventions between 5-8°C (El Hadi et al, 2016; Salem et al, 2016). Indeed, at such low temperatures, an assessment of the contributions of shivering thermogenesis to heat production, if any, must be made.

Additional skin temperature measurements using thermal skin probes have also been used to assess BAT activity. In the second pilot experiment, skin temperature probes were placed over the SCR area adjacent to NIRS sensor, and over the forearm receiving the cooling stimulus. SCR skin temperature recorded by the overlying probe also revealed significant increases in response to cooling in all participants, supporting the demonstration that skin temperature over known BAT depots is higher compared to other non-BAT related areas using IRT (Jang et al, 2014; Robinson et al, 2016) and thermal skin probes (Boon et al, 2014; van der Lans et al, 2016; Chondronikola et al, 2016a).

Despite the advantages of these methods including their low cost and lack of radiation exposure, which make serial measurements of large numbers of individuals, feasible and ethical, IRT has been criticised. Gatidis and colleagues (2016) demonstrated a significantly greater SCR skin temperature in adults with active BAT compared to those with no detectable active BAT, with SCR temperature found to be negatively correlated with SCR adipose tissue thickness (SCAT) (P <0.01, r = 0.65). The authors demonstrated how BMI, thus SCAT, affects SCR temperature and proposed that the observed increases in SCR temperature in lean individuals were due to large blood vessels (mainly carotid artery and jugular vein) located in the supraclavicular fossa region which may have resulted in an improved detection in lean compared to obese individuals. Law and colleagues have recently highlighted (unpublished data) 'hot spots' following the path of the carotid vessels, for which an increase in blood flow in such major vascula-

ture may confound IRT measurements (Law et al, 2017). Thus, the demonstration in the current pilot investigations that superficial blood flow over the SCR BAT gradually increased throughout cold-stimulation until its cessation, even though SCR skin temperature and oxygenation began to decline, suggests thermal energy being transferred away from BAT into the systemic circulation (Foster and Depocas, 1980), supporting IRT in measuring localised BAT heat production. These results are particularly important since, a recent study has now compared the use of IRT against the current gold-standard BAT assessment tool, PET-CT imaging, providing evidence of an anatomical overlapping between the increase in $^{[18]}$F-FDG uptake and the rise in SCR skin temperature overlying the main BAT region, upon water jacket cooling (8°C) in 8 healthy males shown to be BAT positive (Law et al, 2017). Thus strong evidence currently supports IRT as a sensitive, non-invasive method for the real-time tracking of temperature changes in humans (Gatidas et al, 2016; Symonds et al, 2012). However the contention suggested by Gatidas et al, is still valid, given that my study did not assess lean vs. overweight individuals and thus, further investigation is necessary.

4.4.2 Detection of cold-induced increases in BAT oxygenation by NIRS

BAT displays a basal oxidative capacity of approximately 300% greater than that of subcutaneous WAT (Matthias et al, 2000; Vijgen et al, 2012). In response to cold-exposure, BAT perfusion using [^{15}O] H_2O has been demonstrated to increase by 200% and glucose uptake using $^{[18]}$F-FDG by 600%, with no change in these parameters in WAT (Orava et al, 2011). Since the use of in the radiotracer $^{[18]}$F-F-FDG can underestimate BAT metabolic activity (Bauwens et al, 2014), as thermogenesis is largely fuelled by mitochondrial beta-oxidation of fatty acids, Ouellet et al. used [^{11}C]-acetate PET, a surrogate marker of tissue oxygen consumption and demonstrated increased [^{11}C]acetate uptake by approximately 150% in BAT in response to cold exposure (Ouellet et al, 2011). Thus, BAT holds a poten-

tial to influence energy expenditure for targeting anti-obesity therapeutics.

The rationale for the use of NIRS is centred around the ability of light in the near-infrared spectrum (700-1300nm wavelengths) to penetrate several centimetres of sampled tissue which allows for the non-invasive assessment of changes in oxygen saturation of haemoglobin molecules, based on the absorbance of near-infrared light by this chromophore (Bakker et al, 2012). The majority of haemoglobin-related NIRS signal reflects venous and capillary oxygenation since these micro-vessels compose the largest portion of vascular volume believed to be proportioned in the ratio of 70:20% respectively (Mozina and Podbegar, 2015; Mesquida, Gruartmoner and Espinal, 2013). The arteriolar vessels make up the final 10% of blood compartmentalisation, however vessels >1mm can be excluded from StO_2 determination as photons would be entirely absorbed (Mozina and Podbegar, 2015). Thus, in the current study the SCR tissue oxygenation reported here as a NIRS value of StO_2, represents BAT haemoglobin oxygen saturation primarily in the venous bed (Mesquida, Gruartmoner and Espinal, 2013). In the current study, in response to cold-exposure, the observed increases in maximal StO_2 (oxygenated and deoxygenated haemoglobin) in the SCR region peaked prior to the maximal SCR skin temperature changes. In addition, intra-subject comparisons demonstrate a trend towards the greatest change in SCR oxygenation values coupled to the highest change in SCR skin temperature, independent of study (Table 4.3). Together, these findings are interesting given that BAT is highly vascularised and heat production is achieved by the continual supply of a sufficient amount of blood delivering oxygen and macronutrients to the tissue to meet its demands, whilst removing carbon dioxide and warm blood into the systemic circulation (Nagashima et al, 1994). Thus, my findings imply that within each subject in response to cold-exposure, adequate delivery of oxygen resulted in increases in BAT heat production, since there were no changes in localised oxygenation over the reference site (deltoid muscle). These findings support the successful use of NIRS in

the metabolic assessment of BAT activity (Muzik et al, 2013; Nirengi et al, 2015).

However, tissue oxygen saturation reflects the balance between local oxygen delivery and consumption (Mesquida, Gruartmoner and Espinal, 2013) and any measured change in StO_2 could thus be interpreted as either a change in microcirculatory blood flow or the simultaneous change in oxygen consumption to support BAT oxidative metabolism (Simonson and Piantadosi, 1996). The assumption that NIRs estimates tissue perfusion, is based on studies using vascular occlusive testing (VOT) to assess the dynamic changes in microcirculation in conjunction with StO_2 monitoring (Suhaimi et al, 2013; Gomez et al, 2008). VOT provides an ischemic challenge to peripheral tissues allowing identification of tissue hypo-perfusion and the analysis of issue response when occlusion is released (Gomez et al, 2008; Epstein and Haghenbeck, 2014). When tissue hypoxia occurs, the compensatory vasoconstriction that occurs in peripheral tissues will be signalled by a decrease in the StO_2 (Mesquida, Gruartmoner and Espinal, 2013). Indeed, in my second experiment, the application of NIRS to the forearm which was exposed to cooling as a thermogenic stimulus, resulted in a reduction in StO_2, which returned to baseline upon cessation of cold-insult, implying reperfusion. Thus, decreases in StO_2 suggest reduced skeletal muscle perfusion to shunt blood flow away from the periphery to centrally and changes in StO_2 therefore act as a surrogate marker for perfusion.

Considering the well-documented use of NIRS in the assessment of cerebral haemodynamics (Grocott et al, 2012; Jobsis et al, 1977; Murkin et al, 2011), it is surprising that there few published studies to date which have adapted the technique for investigating BAT activity in humans. In two studies, BAT activity has been assessed by the combined use of NIRS with FDG-PET/CT scanning (Muzik et al, 2013; Nirengi et al, 2015), although this approach allows for accurate quantification of oxygen consumption in BAT by the comparison NIRS against $^{[18]}$F-FDG-PET or $^{[15]}$O-PET, the intravenous administration of radioactive compounds does not allow for a non-

invasive, continuous assessment of BAT metabolic activity. Muzik and colleagues (2013) used non-invasive $^{[15]}$O-PET imaging in combination with NIRS (INVOS 5100C somatic oximeter) to estimate BAT blood flow and oxygen consumption in response to cold stimulation, successfully demonstrating a significant correlation between O_2 uptake, indicative of BAT perfusion rate assessed by PET scanning and regional tissue oxygenation assessed using NIRS, in 25 healthy subjects with activated BAT. Whilst Nirengi and colleagues utilised time-resolved spectroscopy to assess the optical characteristics of the SCR BAT against $^{[18]}$F-FDG-PET, reporting BAT haemoglobin concentration and scattering coefficient (μ'_s, an index of mitochondrial concentration) both correlated with $^{[18]}$F-FDG uptake (Nirengi et al, 2015).

In contrast, Hartwig and colleges (2017) were the first authors to combine IRT with NIRS 2D-imaging producing an imaging protocol which can monitor the dynamic activity of BAT. Although the authors reported adrenergic-stimulated increases in temperature over the SCR region, responses were not matched by any corresponding change in tissue oxygenation over the same region, in 10 lean and overweight female subjects. The lack of any change in StO_2 over the SCR region could be due to numerous methodological inaccuracies. The assessment of oxygen saturation was made by the use of NIR spectroscopic two-dimensional (2D) imaging, which as a non-contact method, has so far only offered the possibility of visualizing superficial StO_2 distribution in large heterogeneous tissues, for the assessment of microvascular dysfunction of the whole hand (Hartwig et al, 2015). Considering the short acquisition time of NIRS imaging and IRT, which allow for the continuous assessment of responses to cold-stimulation, only three consecutive NIRS/IRT images were acquired at hourly intervals (basal, 60′, 120′, and 180′) upon glucose administration and subsequently after cold stimulation. The mean of three consecutive images was then reported as the value of oxygen saturation or temperature. Thus, minimal data was collected throughout the study where changes in SCR temperature and oxygenation could have been overlooked. In both pilot

experiments of the current study in this chapter, SCR tissue oxygenation, temperature and blood flow responses were analysed every 30 seconds upon cold-stimulation. This ensured the dynamic nature of BAT responses to thermogenic stimulation were captured. Additionally, visual examination of the ROI chosen for NIRS analysis of the neck by Hartwig et al (2017), demonstrate the ROI to correspond to an area over the sternocleidomastoid; a superficial muscle of the neck and external jugular vein, not directly over SCR BAT. This study may also be confounded by the relatively shallow penetration depth of light using NIRS 2D imaging, which may restrict its applicability for the assessment of BAT metabolic activity, particularly in the SCR region of adults (Hartwig et al, 2017). The limited penetration depth is due to the majority of backscattered photons predominantly being sampled from the very superficial layers of tissue, whereas fewer photons travel deeply and manage to return to the surface (Hillman et al, 2007). Adipose tissue thickness at the site of measurement is known to influence NIRS signal intensity from the target tissue, through its effect on the scattering properties of the tissue (Beekvelt et al, 2001), with optical path length increasing with an increase in fat content (Hamaoka and McCully, 2007). Gatidis et al (2017) reported in lean adults with a BMI of between 18-24.9kg/m^2, a SCR adipose tissue (SCAT) thickness; defined as the minimal distance between the vascular compartment of the neck and the skin surface in the SCR region, of up to 25mm. Whilst Nirengi et al (2015) reported subcutaneous adipose tissue thickness in young individuals in a similar BMI range, of 1.8-2.6mm (Nirengi and Hamaoka, unpublished data). Thus, the effect of adiposity and the capability of NIRS penetration depth should be considered when selecting an appropriate NIRS device and during the study design.

The NIRS device used in the current study and by other authors for the assessment of BAT activity (Muzik et al, 2013; Hartwig et al, 2017) are continuous wave instruments ($NIRS_{CW}$). This means the instrumentation is solely based on a light intensity measurement, i.e. near-infrared light is

sent into the tissue and the intensity of the re-emerging (i.e. diffusely reflected) light is measured (Murkin and Arango, 2009). The following section (4.4.3) describes the strengths of the chosen $NIRS_{CW}$ device used in the current study compared to those applied in the aforementioned studies for the assessment of BAT activity, which further reveals how it may be used to complement IRT.

4.4.3 The use of $NIRS_{CW}$ to complement IRT in the assessment of BAT activity in healthy, lean adults

$NIRS_{CW}$ is the most commonly used non-invasive spectrometer for estimating tissue oxygen saturation in a clinical (Bozhurt et al, 2005; Greissen et al, 2016) and research setting (Muzik et al, 2013; Niwayama et al, 2006). $NIRS_{CW}$ oximeters constitute the same basic components; a light source emitting two or more wavelengths of light in the near-infrared range into the tissue and a light detector to measure the intensity of light exiting the tissue after the absorption of various wavelengths of light by haemoglobin, as the photons follow a curvilinear path through the tissue before being reflected (Wahr et al, 1996).

However, each oximeter uses a different set of wavelengths of light to trans-illuminate the desired section of tissue (Macleod, 2012). The absorption and scatter of photons in the tissue is dependent on the light wavelength, with increasing wavelength reducing scatter (Bakker et al, 2012). This is an important consideration since these characteristics can impact the stability, reliability and accuracy of the oximeter in determining tissue oxygenation (Kreeger et al, 2012). Selecting a NIRS device which utilises specific wavelengths in the oxy- and deoxyhaemoglobin range, minimises the impact of the influence of other chromophores (myoglobin, melanin, bilirubin, cytochrome a,a^3), on the NIRS signal. Since the absorption spectra of deoxyhaemoglobin ranges from 650 to 1000nm and oxy-haemoglobin, 700 to 1150nm (Murkin and Arango, 2009), the use of the Nonin Equanox oximeter in the current study which utilises four wavelengths of light (730nm, 760nm, 810nm, 880nm), means the differentiation among

the different types of haemoglobin are more accurate and thus reflect the balance of oxy- and deoxyhaemoglobin specifically in their spectra, isolating single chromophores that may vary from subject to subject (MacLeod et al, 2012). This is an advantage over other commercially available $NIRS_{CW}$ devices such as the Covidion INVOS device used by Muzik et al (2013), which utilises only two wavelengths in which contamination from chromophores other than haemoglobin becomes inevitable.

Further support for the use of the Nonin NIRS oximeter for the assessment of BAT oxygenation rests within its sensor design. To distinguish between oxygen saturation and signal contamination, oximeters use a process of spatial resolution (Davie and Grocott, 2012), based on the principle that the depth of interrogated tissue is proportional to the distance between the light emitter and detector (Germon et al, 1999). Variations in the distance between the various light emitters and detectors and the number of emitters and detectors can thus affect the acquisition of oxygen saturation measurements and signal contamination. The Covidion INVOS device used by Muzik et al (2013) utilises a single emitter and 2 detectors located at 30mm and 40mm from the emitter. In comparison, the newly developed Nonin equanox sensors contain dual-emitter/dual-detector sensor technology, arranged so that the distal light detector for one light source is collocated with the proximal detector for the other. This architecture provides further accuracy by accounting for tissue variation and contamination throughout the entire curvilinear light path (Nonin Medical, 2016). The emitter to detector distances of this device were 12.5mm and 25mm, allowing the penetration of photons superficially and well as deeply into the SCR region of the neck, presumed to be BAT (Murkin and Arango, 2009).

To date there is no established gold standard for determining the precise level of tissue oxygenation, and, therefore, it is difficult to know whether an oximeter- generated StO_2 value agrees absolutely with true tissue saturation (Macleod et al, 2012; Wahr et al,1996). Commercially available oximeters have however, been accepted as relative or trend monitors, where

changes from the baseline of StO_2 values could accurately reflect the magnitude and direction of changes in tissue saturation (Bakker et al, 2006; Han et al, 2005; Kim et al, 2010; Macleod et al, 2012). The StO_2 values reported in this study can be considered reliable since published studies particularly in the past decade have shown tissue saturation can be accurately estimated against a reference value of arteriovenous saturation ($SavO_2$), calculated based on the venous saturation ($SvO2$) and arterial saturation (SaO_2), as a ratio of 70:30, from blood samples drawn from the jugular vein and carotid artery, respectively. Published studies by Macleod et al (2009) and Kreeger et al (2012), have validated the use of the Nonin Equanox oximeter system and sensors in healthy adult and diseased paediatric populations, demonstrating its use to be a valid assessment of true cerebral tissue oxygen saturation. Macleod and colleagues (2009) reported the resulting accuracy as measured by A_{RMS} (a common statistic for oximetry devices which estimates the agreement between a test device and an accepted reference value; Macleod et al, 2009) from 11 healthy subjects, was 4.1% and mean bias was 0.8 ± 4.0% (Macleod et al, 2009). Whilst Kreeger and colleagues (2012) demonstrated for an entire cohort consisting of 7 neonates, 44 infants, and 35 children, an A_{RMS} statistic of 5.4%, 0.5% (Kreeger et al, 2012). Thus, the Nonin cerebral oximeter technology can provide accurate data on regional cerebral compared with arteriovenous saturation in both adults and paediatric populations (Macleod et al, 2009; MacLeod et al, 2012).

4.5 Conclusions and summary

In conclusion, despite variations in the interpretation of NIRS data, this is the first study to combine IRT, NIRS and LD to assess BAT activity under thermogenic stimulation in healthy adults. Here I demonstrate adrenergic stimulated changes in venous tissue oxygenation of the SCR BAT region, in relation to the rise in localised SCR skin temperature. Further, this study addresses the uncertainty of whether changes in skin temperature overlying the SCR region arise from an increase in blood flow or from a thermo-

genic response in BAT. The demonstration of a continued rise in superficial blood flow upon reductions in SCR oxygenation and skin temperature until cessation of cold stimulation, with subsequent reductions in these responses, implies that the detection of heat overlying the SCR region, is due to heat dissipation from metabolically active BAT to the skin's surface. These findings may in part help to elucidate some of the mechanisms involved in the augmentation and detection of BAT heat production, as summarised in Figure 4.21. The combination of IRT, thermal probes and NIRS enables the real-time detection of small alterations in local skin temperature and BAT activity induced by cold exposure, under thermoneutral conditions. Since $NIRS_{CW}$ technology is portable, capable of sampling tissue oxygenation at a high rate and is relatively cheap to conduct, its complementary use with IRT can provide real-time functional information about BAT activity, without the exposure of ionising radiation. Thus, serial measurements of large numbers of individuals are feasible and ethical.

However, it is beyond the scope of this feasibility study to draw any definitive conclusions about the oxidative capacity of BAT. Continuous wave NIRS is only capable of oxygenation trend monitoring, which limits the ability to make detailed inferences about tissue oxygen use over its supply. Challenges remain to be overcome in the use of these harmless methods to quantify BAT function. Limitations of this study and its future directions are detailed in Chapter 7. Indeed, an attempt to address these factors will aid to advance the understandings of the metabolic capabilities of BAT in vivo in humans.

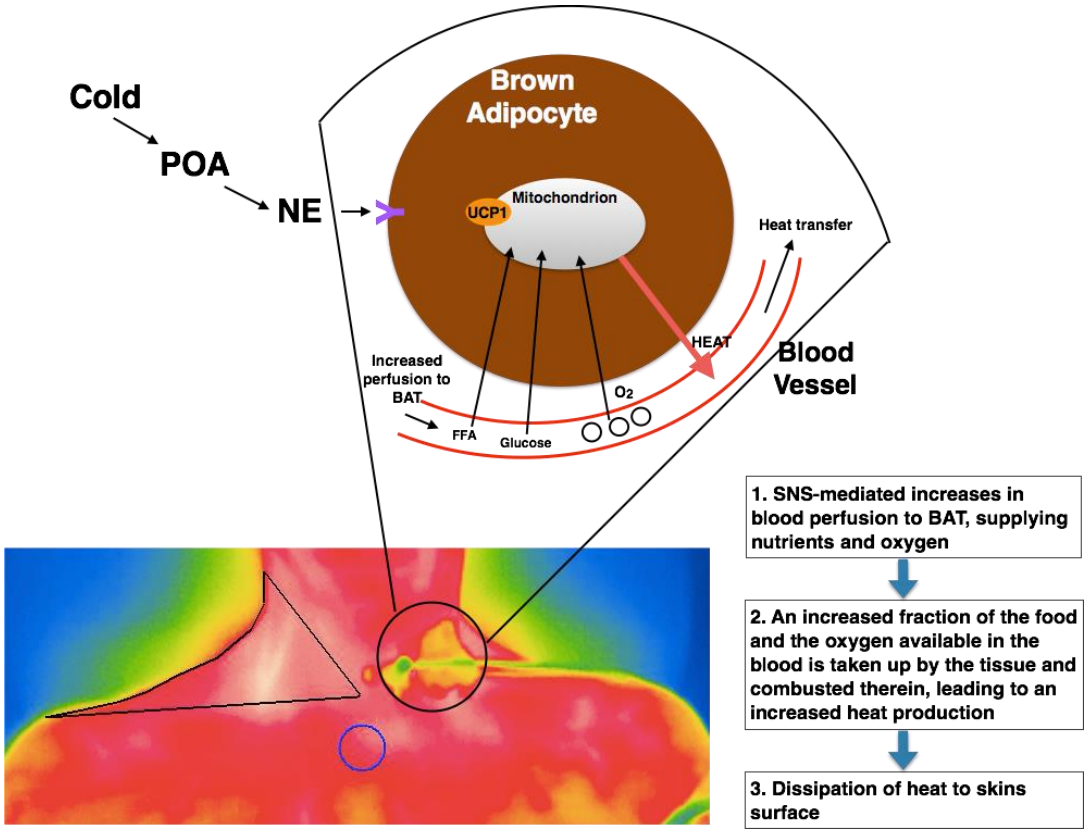

Figure 4.21. Summary diagram of cold-induced sympathetic stimulation of BAT thermogenesis in healthy, lean adults, as assessed by IRT/NIRS and LD

NE – Norepinephrine; POA - preoptic area. Blue circle is reference region for IRT analysis. Left, black triangle is ROI for IRT imaging analysis of participant's right supraclavicular (SCR) region. Right black circle provides a mechanistic view of beneath SCR region, once stimulated.

Chapter 5

Infrared Thermography Imaging for the identification and quantification of newborn brown adipose tissue

5.1 Introduction

BAT has long been established to hold a critical role in the maintenance of neonatal body temperature at the time of birth, due to its unique heat producing function (Gilsanz, Hu & Kajimura, 2013; Lidell, 2018; Nedergaard & Cannon, 2017). Once thought to disappear after infancy, recent evidence demonstrates active BAT in adult patients undergoing PET-CT scanning (Cypess et al, 2009; Saito et al, 2009; van Marken Lichtenbelt et al, 2009), which has renewed interest in the relevance of BAT in human metabolism. The development of imaging techniques that provide reliable BAT measurements has so far advanced our understandings of human BAT predominantly in adults. Less well understood are the characteristics of BAT in early postnatal life, such as its amount, activity, change over time, as well as its immediate and long-term implications for adiposity and metabolic function. Reliable methods for non-invasive BAT measurement in human infants less than 3 years of age, have yet to be demonstrated, since original techniques used to identify BAT deposits (tissue biopsies), alongside more recent advancements (CT, MRI scanning), are hampered by their harmful nature, and thus should not be used in neonates and small infants (Scheele & Nielsen, 2017).

In adults, BAT has been verified at a molecular level mainly by the use of PET-CT and/or guided biopsy, in the SCR region (Au-Yong et al, 2009; Jespersen et al, 2013; Lidell et al, 2013; van Marken Lichtenbelt et al, 2009). However, because PET-CT exposes participants to significant radiation doses, it is not suitable for research use in paediatric populations (Law et al, 2018). The morphological characterisation of BAT depots in infants and children has largely been due to original post-mortem and MRI

studies (Hu et al, 2012), identifying the main site of BAT in the infant in the interscapular (Lidell, 2018) and perirenal regions (Ito et al, 1991; Tanuma et al, 1975). MRI scanning in newborn infants has also confirmed the presence of abnormally large BAT deposits extending from the lower neck to axillary regions (Carter and Schucany, 2008) and bilateral BAT deposits in the subscapular and spinal regions (Rasmussen et al, 2013) (Figure 5.1).

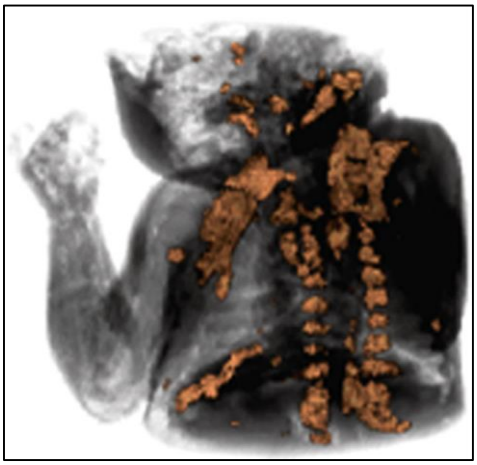

Figure 5.1. Identification of BAT deposits in the newborn using MRI
A single water-fat separated MRI scan of the neonatal back, demonstrates bilateral BAT deposits in the subscapular and spinal regions. Image taken from (Rasmussen et al, 2013). Fat- and water-based images of 22 neonates were acquired during natural sleep and the ratios of fat to the combined signal from fat and water (fat signal fraction) were calculated to quantify BAT.

There is interest in developing and refining thermal imaging protocols to assess BAT function in children (Symonds et al, 2012). The use of IRT in a paediatric population may be a preferential method to assess BAT function, over PET-CT scanning, due to its non-invasive nature (Lee et al, 2011; Symonds et al, 2012) and ability to take continuous measurements of neonatal skin and core temperatures in real-time (Abbas et al, 2011; Abbas & Leonhardt, 2014; Heimann et al, 2013). Assessments of SCR BAT activity during short imaging protocols have been made in children as young as

three years of age (Symonds et al, 2012). However, original work by Grausz (1970) provides the only evidence of the assessment of interscapular skin temperature and presumed BAT activity in newborns, within the first month of life (Grausz et al, 1970). Using skin temperature probes, surface skin temperature over the interscapular region, exposed to air temperature (26°C), was demonstrated to be up to 0.3°C greater than that of other regions of the back where brown fat is not known to be subcutaneously located. Despite these findings, there have been no further attempts to measure surface skin temperature over known BAT locations using thermogenic techniques in this population. Indeed, the relative importance of using this technique in neonatal care, has been demonstrated in the study of contactless monitoring of neonatal vital signs (Abbas et al, 2011). Infrared thermal imaging has successfully been used to explore variations in regional body temperatures in preterm infants inside neonatal intensive care unit (NICU) facilities (Heimann et al, 2013; Knobel et al, 2017). These findings give promise of the effective use of thermography imaging in neonatal medicine.

From a metabolic perspective, adipose tissue characteristics of particularly preterm infants, exposed to inter-uterine growth restriction (IUGR) through maternal undernutrition (Barker, 1992; Barker, 1997), can be altered and driven towards that of a white adipocyte phenotype (Gnanalingham et al, 2005; Sarr, Yang & Regnault, 2012; Seckl, 1997). Exposure to deficient nutrition *in utero* results in a permanent increase in the capacity to form new cells in adipose depots or to store lipid in existing adipocyte in postnatal life (Martin, Hausman and Hausman, 1998). Indeed, the pathophysiological development of visceral obesity in children (Uthaya et al, 2005; Modi et al, 2006; Modi et al, 2009) and reduction in insulin sensitivity (Regan, 2006), has been observed postnatally in preterm infants born with IUGR (Modi et al, 2006; Modi et al, 2009). Further, overexposure to GCs and 11β-HSD1 enzyme may underpin dysfunction of the HPA axis and BAT thermogenesis during infancy (Gnanalingham et al,

2005), given that elevated 11β-HSD1 mRNA expression correlates positively with BMI and adipocyte size (Engeli et al, 2004; Kannisto et al, 2004; Lee et al, 2008; Rask et al, 2002; Tomlinson et al, 2002) and has been shown to reduce the expression of BAT genes such as, UCP1 and β3-AR (Liu et al, 2013). To date, the use of IRT in clinically stable infants has yet to be made, but if successful, could propose a functional tool to monitor surface skin temperatures over known BAT locations to explore its development and potential involvement in later metabolic complications.

5.1.1 Main Aim

The aim of the present study was to explore the feasibility of IRT imaging to measure skin temperatures over previously identified brown fat regions in full-term infants. I am reporting an exploratory method, conducted in two phases; the first phase initially focussed on the development and practicality of using thermal imaging to assess skin temperature variations in full-term infants; the second phase was then conducted once standardisation had occurred, in an attempt to improve the quality of data obtained and to assess whether IRT could detect a greater skin temperature over the interscapular BAT region, compared to a reference site. The hypothesis of this study was that IRT would be capable of detecting a greater surface skin temperature over the interscapular region compared to a reference region located on the lower back, in healthy, term infants.

5.2 Materials and Methods

Study Approval

The study was granted by the Yorkshire and the Humber- Sheffield Research Ethics Committee, UK (IRAS no. 187149). The study was explained to parents of eligible infants by two members of the study team using an information leaflet and enrolment began after parental consent was approved.

Subjects

Healthy infants admitted to the postnatal ward at the Queens Medical Centre (QMC) between 28/10/16 and 05/12/16 for phase 1 and between 24/07/17 and 15/08/17 for phase 2, were chosen for trial enrolment. Inclusion criteria were; a birth gestational age of ≥37 weeks, corresponding to full term; less than 7 days of age at entry to the study, and a stable resting core temperature between 36.5°C – 37.5°C. Gestational age was assigned by obstetrical dating (based on first trimester ultrasound). Exclusion criteria included any major genetic disorder, congenital anomaly, or congenital heart disease; maternal death and a resting core temperature of <36.5°C or >37.5°C.

Thermography imaging experiment set up

The study was conducted on the postnatal ward at the QMC. Room temperature was maintained between 26.3°C and 28°C, which is an appropriate temperature for maintaining core body temperature (WHO, 1993) in fully-clothed infants at full-term (WHO, 1993). The study was conducted in infants wearing their nappy, so that their back was exposed. The transition from the warm in-utero environment (>39°C) to the cooler extra-utero environment at birth initiates BAT to increase heat production (Seron-Ferre et al, 2014). Theoretically, this could enable the detection of heatspots over the infants' back, using thermal imaging. However, the capacity of the newborn for self-protection against heat loss is limited. Without external support, newborns can readily lose heat and body temperature with the potential to become hypothermic (Seron-Ferre et al, 2014). Thus, the choice of platform from which to conduct the imaging, needed to be easily accessible to research staff; minimize the effects of heat loss through conduction, convection, evaporation and radiation; as well as to be a suitable size and depth to enable thermograms of the whole of the infant back to be captured.

Multiple types of incubator are available in neonatal care. Each is a rigid box-like enclosure in which the infant can be kept in a controlled environment for observation (WHO, 1993). Newborn age, weight, disease status and availability will influence which incubator best suits the newborn's needs (Hammarland, Strömberg and Sedin, 1986). In this study, healthy full term infants were recruited. Compared to preterm infants, term newborns possess a layer of subcutaneous fat, helping to insulate from heat loss (Hammarland, Strömberg and Sedin, 1986). Thus, imaging could therefore be conducted from an open air cot or resuscitaire (WHO, 1993).

In phase 1, non-invasive skin temperature measurements of the back, were taken whilst infants laid on a Draeger Caleo resuscitaire (Draeger Medical, Telford, PA) with an overhead radiant warmer (Hill-Rom Airshields) (Figure 5.2.1). Radiant heaters are overhead heating elements, that provide warmth locally, to maintain infant core body temperature and reduce heat loss (WHO, 1993). The temperature of the radiant heater was adjusted based on the infant's axillary skin temperature, as measured by a skin probe, to ensure the maintenance of core temperature in the range of 36.5°C – 37.5°C. The overhead radiant warmer was rotated at an angle of 45° throughout the duration of study, to enable the stabilisation of core temperature without directly affecting the measurement of surface skin temperature (Figure 4.2.2).

IRT imaging must be conducted away from air vents of moving air, given that skin temperature is affected by airflow (Law et al, 2017; Jang et al, 2014), which can increase convectional heat loss (Law et al, 2017). Drafts and sudden changes in skin temperature are also minimised by small opaque walls which enclose the resuscitaire platform. Such aspects enable the measurement of skin temperature in healthy infants from this platform.

(A)

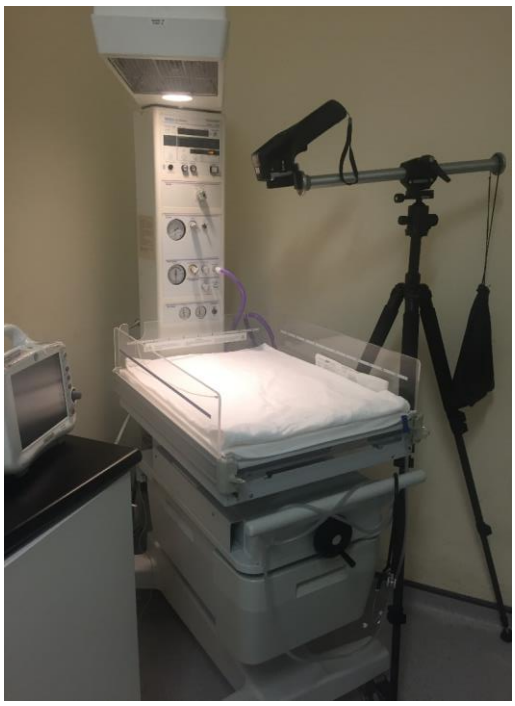

(B)

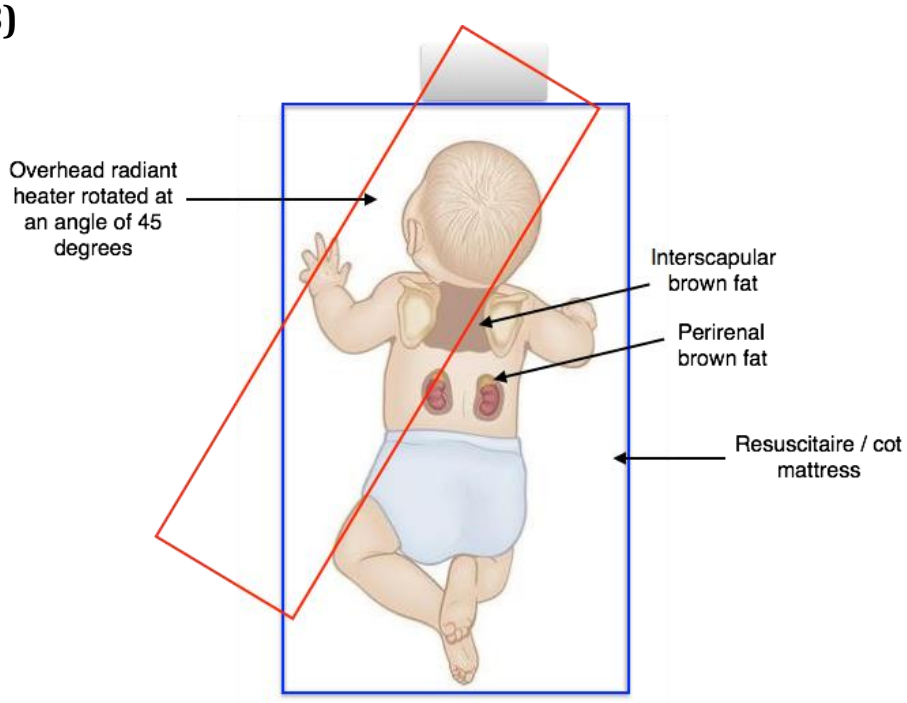

Figure 5.2. The initial thermal imaging platform used for the detection of heatspots over brown fat deposits, in clinically stable infants

Infants in phase 1 (n=9), were laid down onto an open resuscitaire (Draeger Medical, Telford, PA) (A) with an overhead radiant heater rotated to a 45° angle (B).

The imaging protocol in phase 2 was refined so that infants were imaged whilst laid down in an open babytherm 8000 cot (Drager Medical, Telford, PA) with a heat retaining lid instead of an overheat radiant heater (Figure 5.3). This alternative imaging platform ensured the maintenance of the infants' core temperature and was hypothesised to increase the number of focussed, non-distorted thermograms.

The babytherm cot has a deeper cot enclosure, with higher opaque walls compared to the resuscitaire, which further prevents changes in air-flow affecting skin temperature.



Figure 5.3. A developed imaging protocol used in phase 2 for the detection of heatspots over brown fat deposits, in clinically stable infants

Infants in phase 2 (n=6), were imaged at a height of 40cm above the infant, whilst laid in a babytherm cot, with an attachable heat retaining lid.

Experimental Protocol

In phase 1, infants were laid down onto a mat of an open resuscitaire. To avoid the risk of neonatal hypothermia, the resuscitaires overhead radiant heat source was switched on and initially set to 100%, until confirmation that axillary temperature satisfied the entry criteria of >36.5°C. The heat lamp temperature was then reduced by two-thirds prior to beginning the study.

Infants in phase 2 were laid down in a babytherm cot, where the heat source was a heated mat, set to 37°C. Once the infant was placed fully clothed in the supine position into the cot, the heated mat was subsequently switched off.

Clothing was stripped off down to the nappy. The infant was rotated from a supine to a prone position, ensuring that they remained in the centre of the mat. Using a FLIR camera (E series), four thermal images were captured 15 seconds apart at time point '0' (T0) and after 60 minutes (T60). Parents of the infant were able to remain in close proximity for reassurance. The study ended prematurely if the infant was too distressed to console.

A skin temperature probe was also placed on the infant positioned over the lower right side of the back, below the kidneys and connected to a Dash 3000 Monitor (GE healthcare, Chicago, USA). The probe was used to continuously record skin temperature every minute. Axillary temperature was assessed using an electronic thermometer (Beurer, Germany) prior to the commencement of the study, to determine if the infant was eligible to continue (an axillary temperature of ≤36.5°C resulted in the termination of the study) and every 10 minutes thereafter for the duration of the study, to ensure the infant remained normothermic.

Thermal Imaging

For IRT imaging, a FLIR E60 2.3 Megapixel Infrared Camera (FLIR Systems AB, Danderyd, Sweden) was used to acquire thermal images of the back. The camera was factory calibrated to operate at an accuracy of within 0.2°C as previously described (Knobel et al, 2009; Knobel et al, 2017; Rice et al, 2010). Manual refocusing of the lens was made after each time the infant moved. Skin temperature was measured to the nearest 0.1°C. The camera settings for emissivity remained the same for each infant. IR measurement of the skin surface is possible due to the high emissivity of the skin surface to IR, at 0.98 (Steketee, 1973). Reflective temperature and room temperature were set prior to the commencement of each study day. To minimise changes to the newborns' thermal environment during imaging and to acquire images efficiently, IRT imaging was conducted with the camera positioned from a distance of 40-60cm, directly over the newborn infant (Symonds et al, 2012) (Figure 5.4). This camera positioning allowed for the ease of image capturing in the positions of interest, without causing additional stress to the newborn. The thermal camera was suspended above the infant held by a Repro arm extension (model 131D, Manfrotto, Italy), which was attached to an Omega Carbon III tripod (Hama, Germany). To improve camera stability, a 1kg bag of weights was attached to the non-camera end of the extension arm.

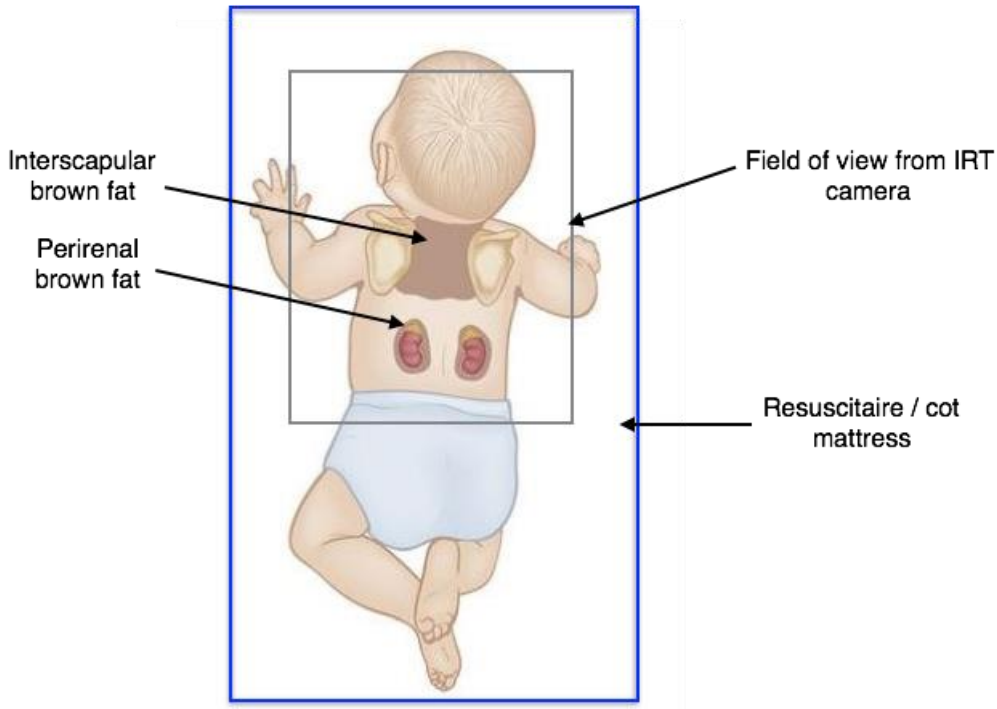

Figure 5.4. An 'overhead shot' of the infant back whilst laid in a prone position
IRT imaging from above the infant, laid on a mattress of a resuscitaire or cot.

Analysis of skin temperature over regions of interest

Thermograms encoding the radiometric data were sequentially saved by the camera to the inserted USB drive in a JPEG format. Infrared images were downloaded to a computer and analysed by the FLIR Tools+ software (FLIR, Oregon, USA) which accompanied the infrared imaging camera. FLIR tools software performs real-time image analysis to convert passive infrared radiation emitted by the target surface, to a two-dimensional image corresponding to the temperature distribution at the target surface (Knobel et al, 2017).

The in-house departmental analysis of thermal images has so far only been adopted for thermal images captured of adult SCR BAT region. Thus, to facilitate skin temperature analysis of newborn infants, the FLIR Tools+ software was used, and a previously published technique for analysing neonatal thermal images was adopted and amended (Rice et al, 2010), in order

to measure the mean skin temperature over the interscapular region of interest. The software uses the analysis tools of spot, line and area measurements to analyse a segment of pixels within the ROI, to calculate mean skin temperature, as well as additional metrics including the maximum, minimum and standard deviation of skin temperature in the ROI.

In phase 1, a grid sampling method using circular measurements, determined mean skin temperatures of 9 ROIs per image, in which the upper middle spot (El2 and El5 on analysed thermogram) corresponded to the approximate location of interscapular BAT (Figure 5.5). The ROIs were kept consistent in shape and location among newborns and were similar in size (48 ± 4 pixels, mean $\pm$ SD).

(A) **(B)**

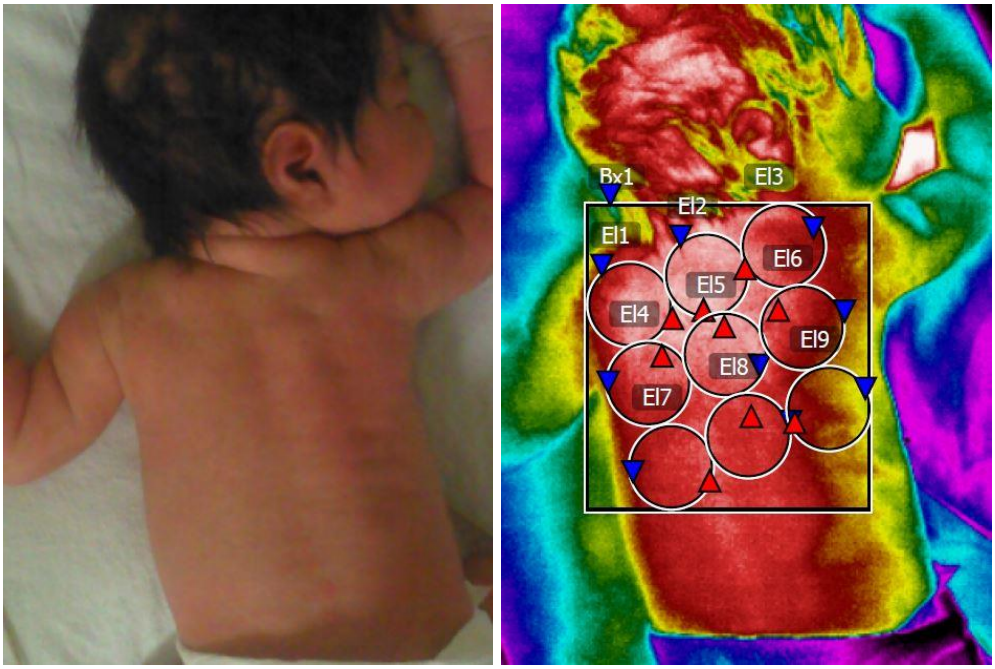

Figure 5.5. Initial analysis method of IRT thermograms taken of the interscapular BAT region in healthy newborn
An example neonatal image (A) captured in the prone position, with the corresponding thermogram (B) demonstrating the grid analysis created in phase 1. Spot measurements labelled El2 and El5 correspond to regions of the skin that overlay the interscapular BAT depot. The red and blue triangles represent areas of the hottest and coolest data points in each ROI (n=6).

An alternative method of analysis was used in phase 2. A grid sampling method using square measurements was created which incorporated all of the infant back, thus enabling greater amount of analysis for each thermogram (Figure 5.6). The grid sampling method used square regions of interest and determined the mean skin temperatures of 9 ROIs per image. Squares were placed according to the visual estimations of anatomic landmarks of the upper and lower scapular and mid-thoracic level (T6/T7) of the spine. The upper middle square aimed to correspond to the location of interscapular BAT. The ROIs were kept consistent in shape and location among newborn infants and their size did not significantly vary (P = 0.290). Once the 9 squared region of interests had been configured, radiometric data was exported to excel, where for each region of interest an

equation to determine the 95th percentile, equating to the top 10% of data, was generated. This produced a median value for each region of interest, similar to what is generated during the Matlab software when analysing human BAT function.

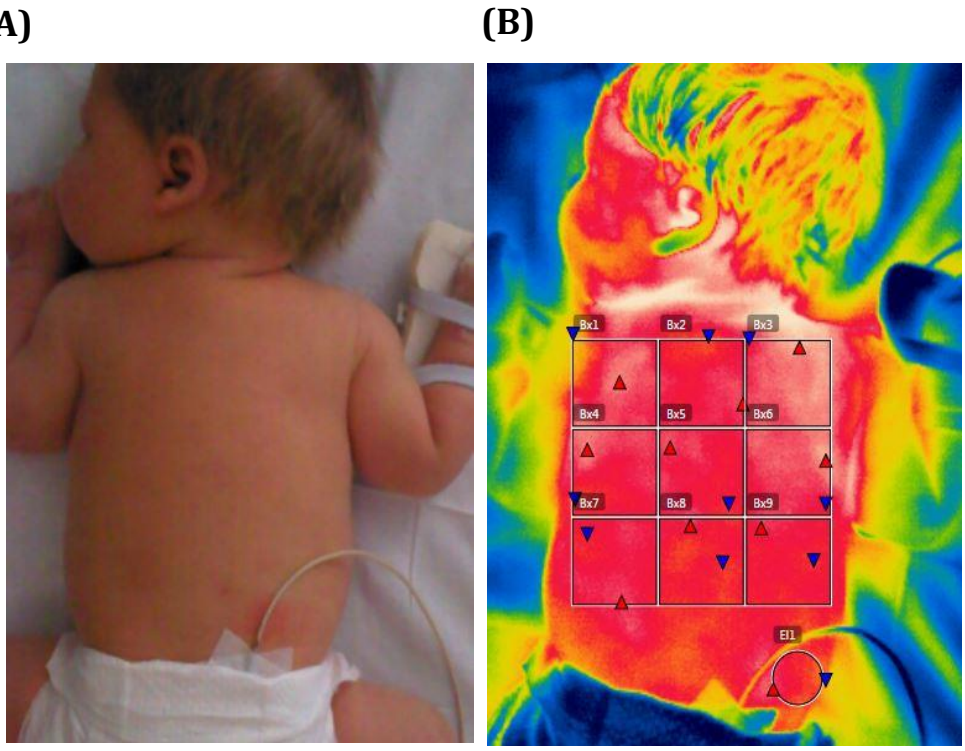

Figure 5.6. Improvement in the grid analysis method for phase 2
A neonatal JPEG image (A) captured in the prone position, with the corresponding thermogram (B) demonstrating a squared grid analysis method for phase 2, which enabled a greater amount of the back to be analysed. Spot measurements labelled Bx2 and Bx5 correspond to regions of the skin that overlay the interscapular BAT depot. The red and blue triangles represent areas of the hottest and coolest data points in each ROI (n=6).

Statistical analysis

For each neonatal thermogram, the comparison of the mean of the top 10% of data from each ROI was conducted using a one-way ANOVA with green-house geisser correction. The mean of each ROI was used to calculate the difference in temperature between each ROI of the neonatal back and a reference region, not known to harbour a BAT deposit, for which paired t-tests were used to assess significance. Paired t-tests were conducted to assess differences in interscapular skin temperatures between time 0 and time 60. All analysis considered a significant change as $P \leq 0.05$. Data were analysed using IBM Statistics for Windows v21 and GraphPad Prism for Windows v6.05. All data are presented as mean ± SD, unless otherwise stated.

5.3 Results

5.3.1 Subjects

Twenty-six families were approached and offered study enrolment, of which 11 families declined participation. Of the 9 families which accepted participation, none withdrew consent later. Gestational age of infants recruited, ranged from 37 to 41 weeks. Enrolment into phase 1 resulted in an original cohort of 9 subjects, of which 3 subjects were excluded; 1 infant completed half of the study before becoming too distressed to console; for 1 infant the study stopped after only 12 minutes due to a core temperature below 36.5°C at 36.1°C; for the third infant, the study stopped after 23 minutes due to a core temperature of 36.3°C. Thermograms obtained at T0 for these three excluded infants, were analysed for presumed BAT activity. However, images at T0 were distorted and could not be analysed. Thus, the final cohort number was 6 subjects (3 males: 3 females) for phase 1 (Figure 5.7). Six subjects (4 males: 2 females) enrolled into phase 2 and retained a core temperature of above 36.5°C, completing the study. The anthropometric characteristics of the infants in both

phases are presented in Table 5.1. There were no significant differences in the birth weight of infants between phase 1 and 2 (P = 0.198). The environmental room temperature between phases did not vary significantly (Table 5.2), nor did core temperature upon entry into the study. Captured thermograms weren't analyzed if they met the exclusion criteria detailed in Table 5.3.

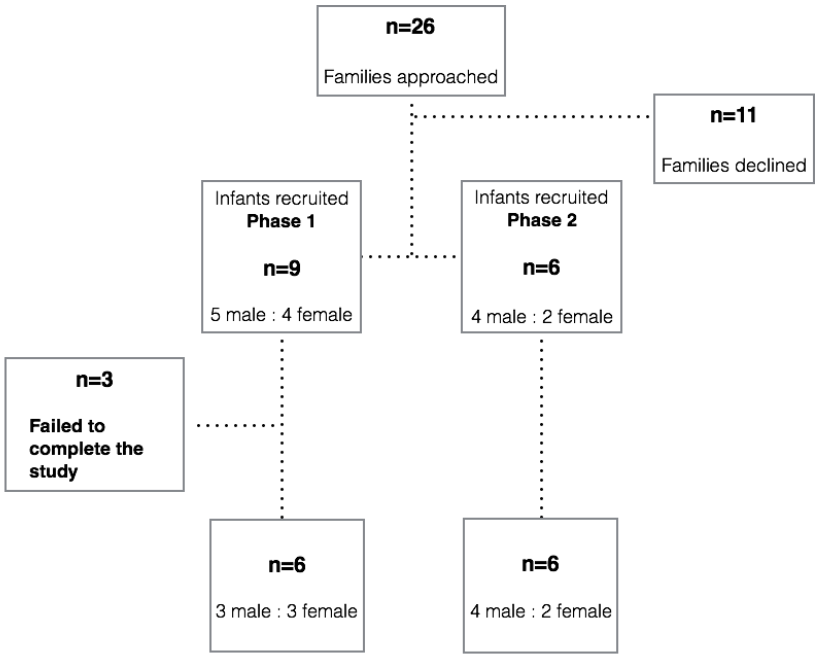

Figure 5.7. Recruitment statistics into phase 1 and phase 2 of the study
Enrolment into phase 1 resulted in an original cohort of 9 subjects, of which 3 subjects were excluded, leaving 6 subjects (3 males: 3 females) as the final study cohort for phase 1. Six subjects (4 males: 2 females) enrolled into phase 2 and retained a core temperature of above 36.5°C, all completing the study.

Table 5.1. Anthropometric and demographic characteristics of infants enrolled into phase 1 and phase 2 of the study in Chapter 5.

Characteristic	Phase 1	Phase 2
Recruited n	6	6
Male: Female ratio	3:3	4:2
Gestational age range	37-41 weeks	37-41 weeks
Birth weight (mean ± SD)	3266 ± 912 grams	3808 ± 397 grams
Age at entry into study	0-5 days	1-4 days

Table 5.2. Environmental room temperatures for phase 1 and phase 2 of the study in Chapter 5

Phase 1			
Subject	**Date of study**	**Environmental room temperature (°C)**	**Core temperature (°C)**
1	**28/10/16**	26.4	36.7
2	**29/10/16**	26.3	36.8
3	**29/10/16**	26.0	36.9
4	**01/11/16**	25.3	36.9
5	**01/11/16**	25.0	36.9
6	**02/11/16**	23.6	36.7
7	**05/11/16**	25.5	36.5
8	**05/11/16**	26.0	36.7
9	**05/11/16**	26.8	36.9
Mean ± SD		**25.56 ± 0.97**	**36.8 ± 0.1**
Phase 2			
10	**24/07/17**	24.5	36.9
11	**24/07/17**	24.5	36.7
12	**25/07/17**	24.5	36.9
13	**01/08/17**	26.0	36.7
14	**01/08/17**	26.0	37.0
15	**15/08/17**	25.0	36.7
Mean ± SD		**25.08 ± 0.74**	**36.8 ± 0.1**

Table 5.3. Exclusion criteria for thermograms which could not be analysed

Thermogram exclusion criteria
1) An unidentifiable outline of the infant in the thermal image (i.e. the image was blurred) 2) Insufficient area to apply the grid analysis, i.e. due to the distortion in imaging quality as a result of the reflective heat from the overhead heat lamp 3) Newborn laid in a curled fetal position instead of a flat prone position

The following results of the study are presented in two sections representing those obtained in phase 1 and phase 2.

5.3.2 Phase 1

5.3.2.1 Excluded thermograms

Of the 6 infants' who completed phase 1, 48 thermal images were taken in total, 10 images (21%) were excluded since they met the exclusion criteria. Two examples of thermograms which met these criteria are demonstrated in Figure 5.8.

(A) **(B)**

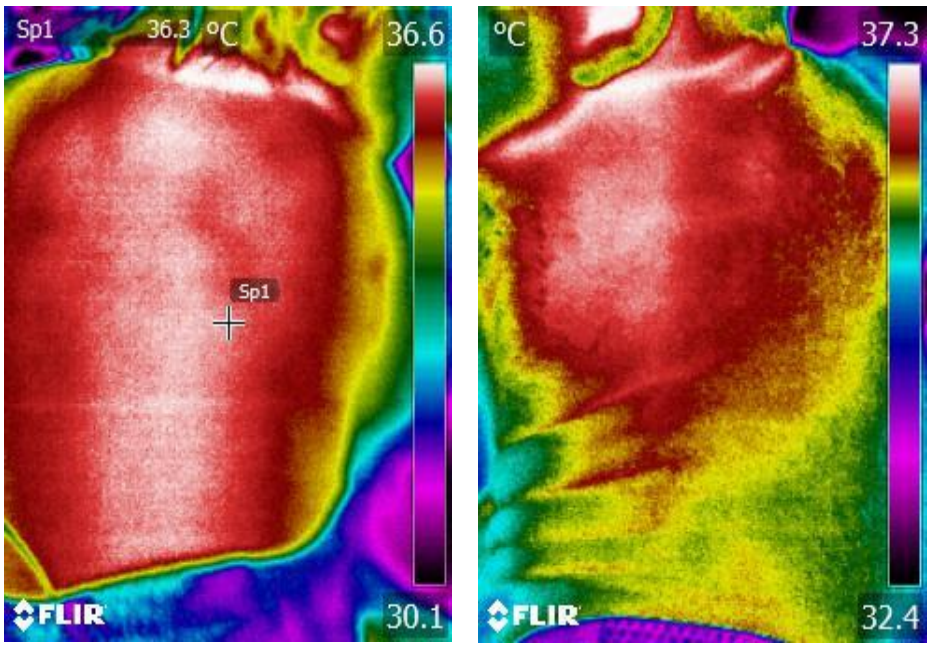

Figure 5.8. Representative examples of excluded thermograms from phase 1
Distorted thermograms from two infants, which could not be analysed due to reflective heat on the surface of the skin from the overhead radiant heater (A) and a neonate laid in a curled fetal position (B).

5.3.2.2 Assessment of skin temperature by IRT imaging

In the 38 thermograms analysed from T0 and T60, the greatest mean temperatures of the neonatal back overlaid the interscapular region. Mean interscapular temperatures were greater than those of the subscapular regions (Interscapular, 37.17 ± 0.56°C vs. left subscapular, 36.92 ± 0.53, P = 0.032; vs. right subscapular, 36.71 ± 0.62; P = 0.002). This trend continued down the back, where the temperature of the skin overlaying the lower central spinal region was significantly greater than that either side (lower spine, 37.07 ± 0.41°C vs. lower left of back, 36.77 ± 0.46, P = 0.001; vs. lower right of back, 36.60 ± 0.42; P = 0.001). Visual observations of the hotter areas of the back (white heat), shown to be in the interscapular and spinal regions are demonstrated on the thermogram in Figure 5.9. No significant difference was observed between mean interscapular skin temperature and that of the lower central spinal region (P = 0.496).

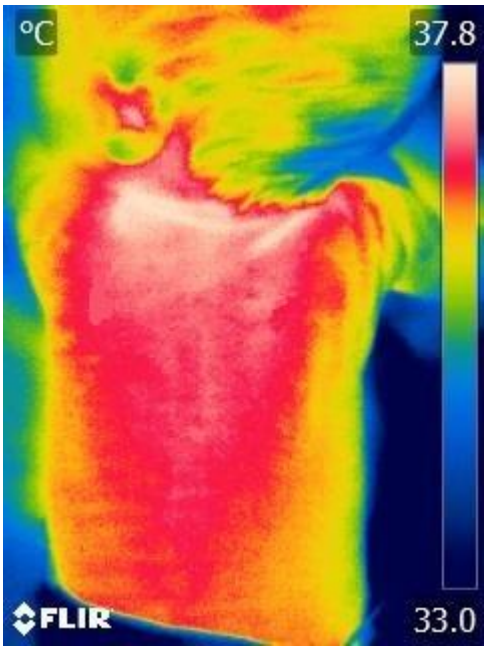

Figure 5.9. The visual observation of hotter areas of the back corresponding to the interscapular and spinal regions (white heat) in a single thermogram captured in phase 1.

5.3.2.3 Skin temperature change over time

Whether exposure of the skin to room temperature (25.5°C) for 60 minutes, would enable the detection of a change in skin temperatures over the back was unknown. Skin temperatures, analysed using the circular measurement tool, were compared between the two time points (T0 and T60), an hour apart.

In the 38 thermal images eligible for analysis, 21 were from T0 and 17 from T60. At T0, as soon as clothing had been stripped off the newborn, in 18 thermograms, the hottest region was observed to correspond with the interscapular region, compared with 3 thermograms) where the greatest temperatures were over lower central spine region (Interscapular, 37.05 ± 0.29°C vs. Lower central spine, 36.83 ± 0.11°C; $P = 0.121$). An hour later (T60), all 17 thermograms demonstrated the hottest area of the back overlaid the interscapular region (37.61 ± 0.20°C), where the temperature increased by 0.56°C after an hour ($P = 0.001$; Figure 5.10).

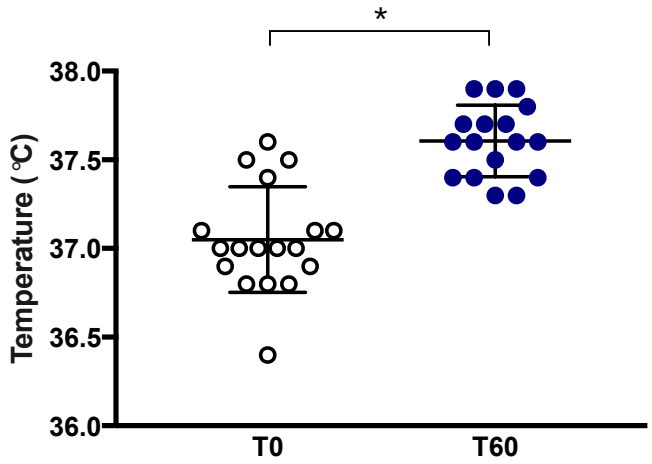

Figure 5.10. Interscapular skin temperatures of thermograms analysed in phase 1, immediately upon the removal of clothing (T0, n=18) and after an hour of exposure to room temperature (25.5°C) (n=17)
Data are shown as mean ± standard deviation. Asterisk denotes a significant difference over time ($P \leq 0.001$).

5.3.2.4 Skin temperatures

Neonatal skin temperature of the lower back as assessed by a single skin temperature probe, increased over the period of an hour from the first prone period to the second (T0, 34.9 ± 0.5°C vs. T60, 36.3 ± 0.3°C; P = 0.031; Figure 5.11).

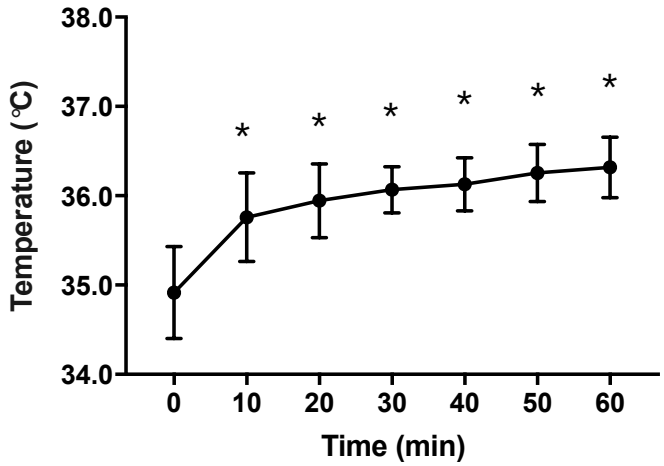

Figure 5.11. Neonatal skin temperature of the lower back as assessed by a single skin temperature probe
Skin temperature was assessed using a thermal probe after a 10-minute acclimation period at time point '0' and at 60 minutes after an hour of exposure to room temperature (25.5°C) (n=6). Data are shown as mean ± standard deviation. * denotes a significant difference over time (P <0.05).

5.3.2.5 Core temperature

The threshold for neonatal core temperature for inclusion into the study, was set at >36.5°C. After exposure to room temperature (25.5°C) for a period of an hour, core temperature remained unchanged (P = 0.773) (Figure 5.12).

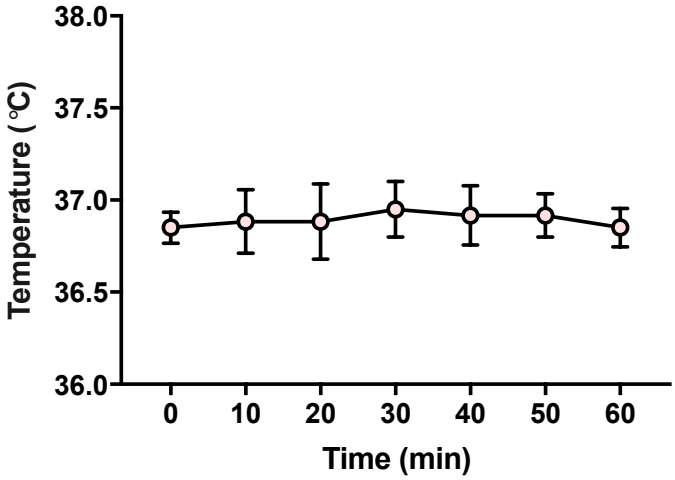

Figure 5.12. Neonatal core temperatures immediately upon the removal of clothing (time point '0') and after an hour of exposure to room temperature (25.5°C) (n=6)
No significant change was observed over the study period of an hour. Data are shown as mean ± standard deviation. $P \leq 0.05$.

5.3.3 Phase 2

5.3.3.1 Excluded thermograms

Of the 6 infants' who completed phase 2, 48 thermal images were taken in total, 8 of which (16%) were unable to be analysed due to the newborn being in an incorrect position due to distress or excessive movement instead of lying in a flattened prone position. In this phase, no thermograms were excluded due to image distortion.

5.3.3.2 Assessment of skin temperature by IRT imaging

Skin temperatures of the infant back in this phase, were analysed using a squared grid method applied to the thermograms, to incorporate a greater amount of temperature data into the analysis (Figure 5.13a-c).

(A) Neonatal Image **(B) Newborn Thermogram**

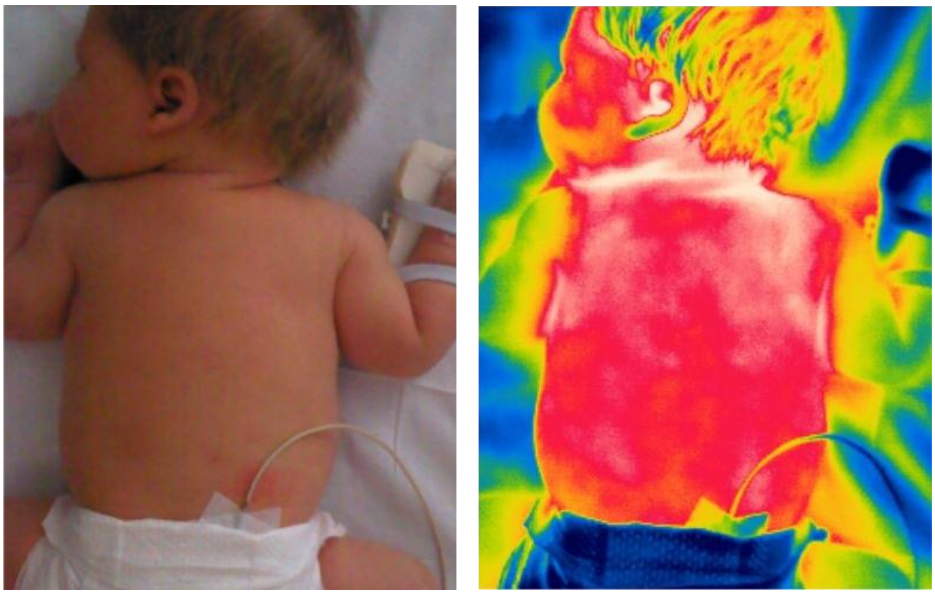

(C) Analysed thermogram

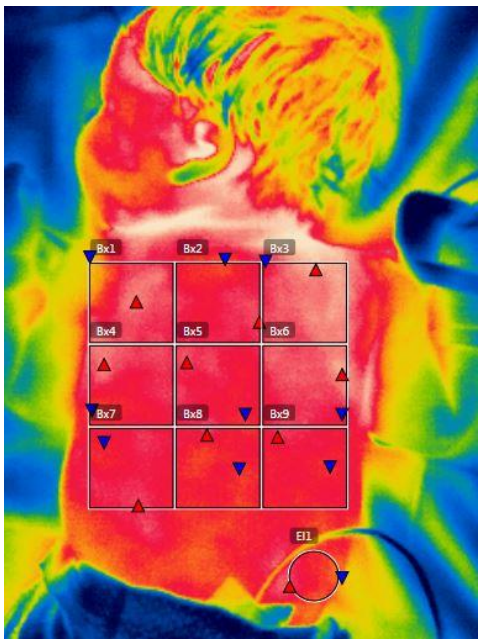

Figure 5.13. Application of the grid analysis method to the thermogram initially captured as a JPEG image
An example image of a newborn laying in the prone position (A) and the corresponding neonatal thermogram (B). Interscapular temperature (C) (Box Bx2), was greater than the temperature over a reference region (small circle located on the lower right side), with no brown adipose tissue deposits (P = 0.004).

5.3.3.3 Skin temperature change over time

Skin temperatures were compared between the two time points (T0 and T60), an hour apart. In the 40 thermograms eligible for analysis, 17 were from T0 and 23 from T60.

At T0, mean skin temperatures of the scapular region were greater than that of a reference region on the lower back (left subscapular vs. reference, $P = 0.001$; Interscapular vs. reference, $P = 0.001$; right subscapular vs. reference, $P = 0.001$) (Figure 5.14a-c).

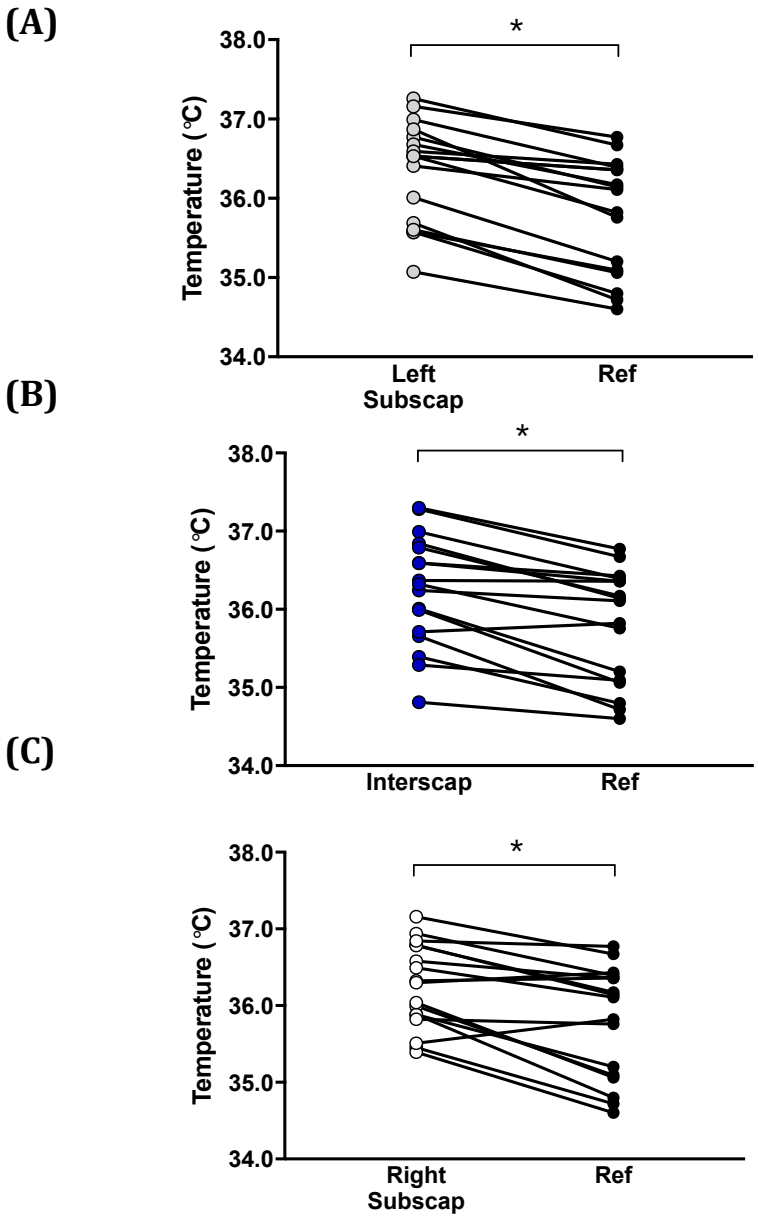

Figure 5.14. Mean skin temperatures of the scapular region at time point '0' in the 17 analysed thermograms

At T0 skin temperatures of the left subscapular (A), interscapular (B) and right subscapular (C) regions were significantly greater than the reference region in the lower right side of the infant back. * $P \leq 0.05$. Left Subscap, left subscapular; Interscap, interscapular; Right Subscap, right subscapular.

An hour later (T60), in the 23 thermograms analysed, 11 thermograms (48%) demonstrated that the hottest area of the back overlaid the interscapular region, compared to 7 thermograms (30%) over the left subscapular and 5 thermograms (22%) over the right subscapular regions (Interscapular, 36.57 ± 0.57°C vs. Left subscapular, 35.81 ± 0.69°C vs. right subscapular, 35.37 ± 0.31°C; $P = 0.002$; Figure 5.15).

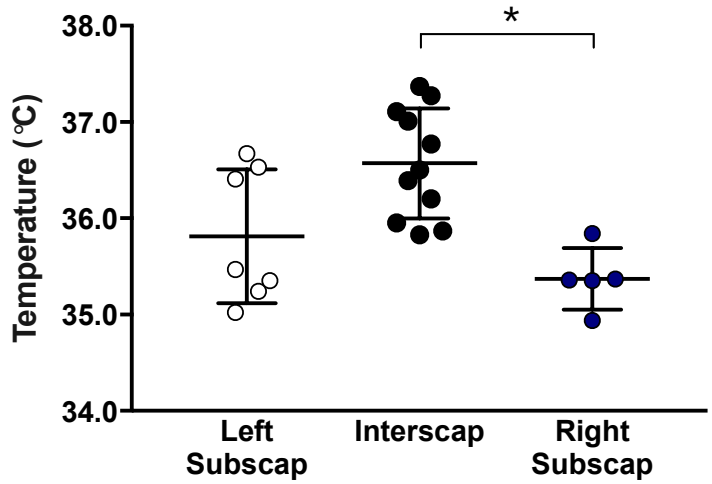

Figure 5.15. Maximal temperatures at T60 over the scapular region of the infant back

After an hour of exposure to room temperature (25°C), 11 of the 23 thermograms, demonstrated the hottest area of the back overlaid the interscapular region. * $P \leq 0.05$. Left Subscap, left subscapular; Interscap, interscapular; Right Subscap, right subscapular. Data are shown as mean ± standard deviation.

The skin temperature over the reference region remained unchanged between T0 and T60, across all 40 thermograms from the 6 newborns (P = 0.802) (Figure 5.16).

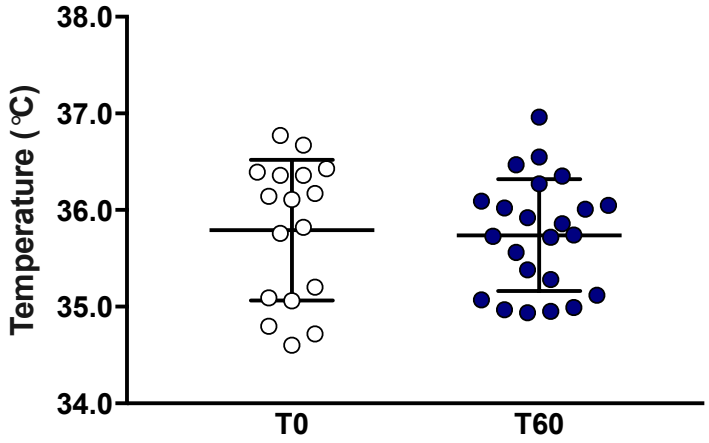

Figure 5.16. Reference temperatures of the neonatal back upon initial removal of clothing (T0) and after an hour of exposure to room temperature (25°C)
No observed difference in reference temperatures overlying a region where there are no known brown adipose deposits between T0 (17 thermograms) and T60 (23 thermograms). Data are shown as mean ± standard error of mean. ($P \leq 0.05$).

Although the greatest skin temperatures were observed over the interscapular region in a large majority of thermograms at both time points, after an hour of exposure to room temperature, mean skin temperatures of the subscapular and interscapular regions did not significantly alter (P >0.05) (Figure 5.17a-c). In addition, white heat spots were visually evident across all three of these areas (Figure 5.18).

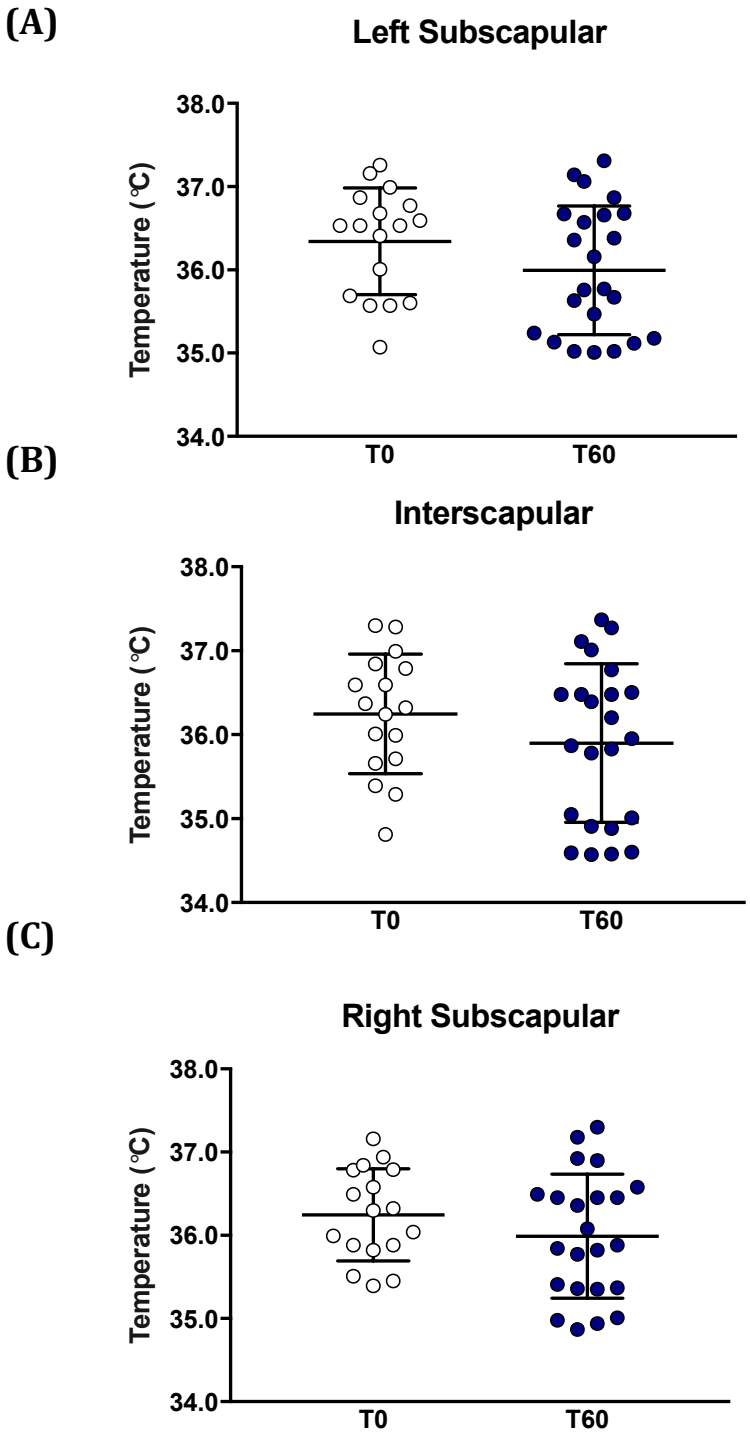

Figure 5.17. Mean skin temperatures of the scapular region throughout the duration of study, from time point '0' (T0) in (17 thermograms), to T60 (23 thermograms)

Skin temperatures of the left subscapular (A), interscapular (B) and right subscapular (C) regions did not significantly differ upon an hour exposure to room temperature (25°C). Left subscap, left subscapular; Interscap, interscapular; Right subscap, right subscapular. Data are shown as mean ± standard error of mean.

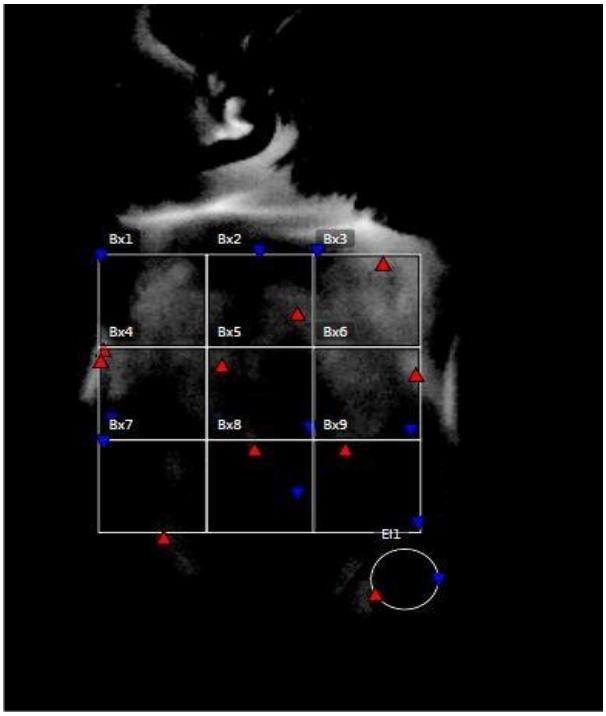

Figure 5.18. Representative example of scattered heatspots
An example thermogram demonstrating scattered heat spots observed over the subscapular and interscapular regions.

5.3.3.4 Skin temperature

Neonatal skin temperatures of the lower back assessed by a skin temperature probe, increased in all infants upon an hour of exposure to room temperature in just a nappy ($P = 0.020$) (Figure 5.19).

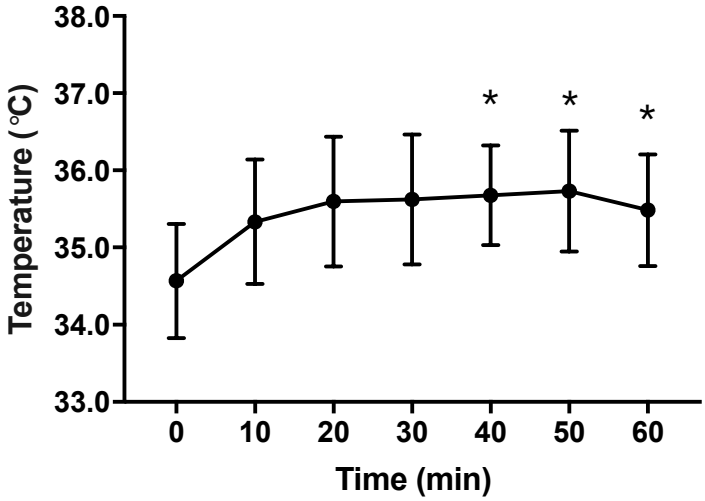

Figure 5.19. Neonatal skin temperatures of the lower back assessed by a skin temperature probe during two periods separated by 60 minutes, whereby the infant was laid on their abdomen (n=6)
Significant increases in skin temperatures were observed after 40 minutes of exposure to room temperature (25°C). Data are shown as mean ± standard deviation. *$p < 0.05$ vs. baseline.

5.3.3.5 Core temperature

A core temperature of >36.5°C satisfied entry criteria into the study. Upon an hour of exposure to room temperature core temperature remained unchanged (P = 0.159). (Figure 5.20).

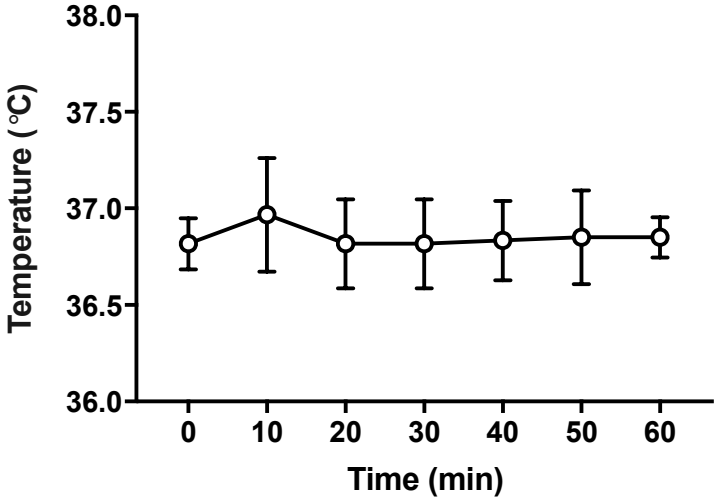

Figure 5.20. Neonatal core temperatures at baseline (time point '0') and after an hour of exposure to room temperature (25°C) (n=6)
The exposure to room temperature (25°C) for 60 minutes, had no effect on core temperature in the six clinically stable infants. Data are shown as mean ± standard deviation.

5.4 Discussion

The resurgence of interest in brown fat activity in the past decade, has been instigated by the demonstration of metabolically active BAT in a significant number of adult cancer patients undergoing PET-CT scanning (Cypess et al, 2009; van Marken Litchenbelt et al, 2009; Virtanen et al, 2009). These studies have been imperative in providing evidence that BATs role extends far beyond that of neonatal thermoregulation, since it's universally present in children and adults (Enerback et al, 2010; Heaton, 1972; Lee et al, 2011). However, significant advances in the understanding of the thermoregulatory and metabolic capabilities of brown fat alongside assessments of its amount and activity, particularly in the paediatric population, are confounded by the lack of development of safe technologies to assess its function. Although first described in neonates back in 1902 (Hatai, 1902), the characterisation of BAT in infants has relied primarily on biopsies derived from major surgical procedures, postmortem samples or more recently, MRI scanning (Hu et al, 2012; Lidell et al, 2013). This in part, has been the reason for the limited exploration of BAT in neonates. Since non-invasive IRT imaging has recently demonstrated that heatspots in the SCR region, strongly correlate with measurements of BAT activity determined by PET-CT scanning (Law et al, 2017), IRT has proven to be a practical and ethically harmless method of assessing skin temperature changes over the main BAT depot in both adults and children (Symonds et al, 2012). This pilot study, conducted in two phases, aimed to develop an imaging protocol using IRT to examine the feasibility to co-locate BAT heat spots over the neonate back region, with known BAT depots determined by MRI scanning (Hu et al, 2013; Rasmussen et al, 2013) in small groups of healthy infants in the first weeks of life. Although the study demonstrated greater temperatures over the interscapular region compared to other areas of the back in both phases, notable, but unavoidable limitations encountered particularly in phase 1, made data analysis and interpretation extremely difficult.

The challenges faced in the initial development of the imaging protocol in phase 1, in relation to the results observed, are discussed below. Phase 2 of the study aimed to demonstrate improvements in the quality of thermograms captured through amendments to the methodology.

5.4.1 Methodological challenges faced in phase 1

Several critical factors have been identified for the use of infrared thermography in neonates (Knobel et al, 2017; Rice et al, 2015). A majority of IRT studies in adults are conducted in a thermoneutral environment, where participants are sat in a position that isn't affected by overhead airflow and where there is a space between the participant and a plain wall behind them, so that there is no heat transfer (Law et al, 2017). However, the measurement of newborn superficial skin temperature is more challenging and must take account neonatal physiological development. Premature infants are at an increased risk of heat loss through immature thermoregulation as they possess very little fat, thin skin and experience greater evaporative losses (Hammarland, Strömberg and Sedin, 1986). As the skin of premature infants lacks insulative properties, it is recommended that measurements of surface skin temperature are taken with the infant in a heat preserving cot or resuscitaire (WHO, 1993). Recent evidence has demonstrated the successful use of IRT imaging in neonatal care to monitor core and body temperatures preterm infants in convective incubators for up to 20 minutes (Abbas et al, 2011; Abbas & Leonhardt, 2014). These studies conducted imaging either through a hole in the top of the incubator at a 90° angle over the infant (Rice et al, 2010) or through the incubator opening, without disturbing the normal thermal environment (Abbas et al, 2011; Abbas & Leonhardt, 2014).

In the current study, an open resuscitaire with an overhead radiant heater was chosen take thermograms of the back of healthy full-term infants, since these infants have greater amounts of subcutaneous fat and thus reduced capacity for heat loss compared to preterm infants (Knobel et al, 2017). However, ethical concerns required a factor for ensuring that the infant's core temperature would not be compromised to the extent, which

induces neonatal hypothermia, during study exposure. Thus, in phase 1, nine healthy infants were placed in a prone position on their abdomen onto an open resuscitaire, with an overhead radiant heater. The heater was switched on and positioned at a rotated angle throughout the duration of the study. However, as the study progressed, a reoccurring pattern began to emerge. It was observed that 21% of thermograms captured, could not be analysed due to either reflective heat trailing down the back of the infant or distortion of the outline of the infant. The remaining 79% of thermograms did reveal that the greatest temperatures of the back corresponded to the upper central region overlying the interscapular BAT depot and down the spinal regions. These results are in agreement with previous identifications of brown fat in these regions of the infant back (Enerback et al, 2010; Rasmussen et al, 2013). However, as the overhead radiant heater was directly over these regions, albeit at a rotated angle, it is unclear as to whether the increased surface skin temperatures in these regions, compared to a lower region of the back, is a result of direct heat from the heater. Since core temperature remained unchanged in the hour between prone periods, but skin temperatures as assessed by a skin probe, increased in all infants, it may be a plausible suggestion that the overhead radiant heat was the source of the greater skin temperatures over the upper back. Indeed, research by Abbas et al (2011) demonstrated the utility of infrared thermography video recording for respiration monitoring in premature infants (mean gestational age, 29 weeks) in neonatal intensive care. Whilst five infants were handled in an incubator, two infants were positioned in an open resuscitaire, similar to that used in the current study. The authors noted that in these two infants under radiant warmer, respiration temperature was greater than that of neonates cared inside convective incubator unit.

Thus, in clinically stable infants non-contact monitoring of surface skin temperatures based on infrared thermography as a new biomedical engineering application, could be improved by alteration of the platform to reduce radiant heat exposure. In phase 2 of the study, in an aim to improve the quality of thermograms obtained.

5.4.2 Phase 2

As evidenced in the first part of this study, obtaining high quality thermograms using infrared thermography is a challenge in this population. In an attempt to reduce the amount of distorted, blurred and unfocused thermal images due to radiant heat exposure, the methodology for phase 2 was amended so that the newborn infants were imaged whilst laid on a heat mat in an incubator with attachable heat retaining lid, which ensured a warm localised environment for the neonate. Modifying this part of the methodology improved the quality of thermograms (i.e. image distortion), and thus the amount of thermograms that were analysed. The exposure time of the camera remained the same as in phase 1, at 12 milliseconds. We were still unable to control for the amount of thermograms which were excluded from analysis due to large amounts of neonatal movement or the tendency to remain in a curled fetal position. Eight of the 48 thermograms were excluded on the premise of movement artefacts. The thermography data of similar designed studies using infrared thermography imaging of neonatal skin temperature, has also featured movements incorporating rotation of the hands, feet, and main trunk, as the neonates rotated their heads left, right, up, down, or in a random motion (Abbas et al, 2011). These movements exhibited are natural, considering are infants are born with fundamental inherent reflexes to multiple environmental stimuli which affects their movement (Slater, 2002). However, the precision of IRT imaging requires the participant to remain still throughout the imaging period (Law et al, 2017). Thus, capturing high quality thermograms in this population remains a challenge.

In the 40 thermograms which were analysed from the six infants, I examined whether thermal imaging could be used to detect regions of heat spots over previously identified brown fat locations. Since phase 1 of the study demonstrated greater skin temperatures over the interscapular region compared to lower regions of the back, it was hypothesised that the

alteration in imaging platform could further reveal this findings, without the effects of direct radiant heat exposure hampering thermograms.
The thermographic data in phase 2 demonstrate that mean scapular skin temperatures were ~0.5°C greater than that of a reference region of the lower back. Further, in approximately half of thermograms captured immediately upon the removal of clothing (9 of 17 thermograms) and after 60 minutes (11 of 23 thermograms) of exposure to room temperature, the greatest skin temperatures overlaid the interscapular region. These results are in agreement with observations over 50 years ago, which demonstrated skin temperatures in the interscapular region of the newborn during cold challenges between temperatures of 24.9 - 30°C, could increase as much as 0.5°C greater than the relative difference between this area and adjacent regions on the back, which are not known to possess brown adipose depots (Grausz et al, 1970). Further, the increases in the interscapular skin temperatures identified in this study, correspond to the main location of BAT identified from original and more recent anatomical studies in neonates (Aherne & Hull, 1966; Enerback, 2010; Rylander et al, 1972). These studies have demonstrated that neonates have an active interscapular BAT depot, shaped as a kite (Aherne & Hull, 1966; Heaton, 1972), representative of classical BAT, similar to that found in rodents (Peirce, Carobbio and Vidal-Puig, 2014; Lidell et al, 2013).
Despite these findings, caution must be taken when visually identifying BAT heatspots on the thermograms of the neonatal back, since there is a complex relationship between skin surface temperature and BAT heat output (Moreira et al, 2017). The highly vascular nature of BAT enables the transfer of heat from the activated tissue to the skins surface and around the body (Law et al, 2017). However, since superficial blood vessels disperse heat, IRT was originally found to measure changes in skin blood flow (Rothwell and Stock, 1979). This is important since the thermograms in the study demonstrated that heatspots were not only confined to the interscapular region. Over the period of an hour, between T0 and T60, the scattering of white heatspots (shown as white regions on the thermograms) covering the subscapular region was also identified. It is unclear

whether the heatspots over the subscapular region are due to brown fat heat generation. Certainly, this could be the case based on evidence by Rasmussen et al (2013), who demonstrated bilateral BAT deposits in the spinal and subscapular regions of the neonatal back, using water-fat separated MRI (Rasmussen et al, 2013). However, a more likely explanation for the scattering of white heatspots at T60, maybe as a result of heat loss at the skins surface. This theory is based on the findings that there was no change in skin temperatures over the scapular regions from T0 to T60, assessed by IRT; no changes in core temperature upon exposure to room temperature for 60 minutes and; an increased skin temperature (assessed by contact thermosensors), over an area of the lower back not known to harbour BAT deposits. Indeed, the increase in skin temperatures assessed by skin sensors, could be due the heat arising from the heated mat. Core temperature and skin temperatures over the interscapular region would be expected to increase during BAT activation as a result of sympathetic stimulation (Jang et al, 2014). Further means to support this suggestion stem from the fact that activity and environmental room temperature can affect skin perfusion (Formenti et al, 2013), which is why individuals are required to remain as still as possible throughout the duration of study and room temperature is required to remain constant (law et al, 2017; Law et al, 2018; Symonds et al, 2012). Since environmental room temperature of the study remained unchanged, this could not be the cause of such heat dispersion. However, many infants were observed to exhibit profound reflex movements resulting in restless behaviors, which could increase skin blood flow and perfusion (WHO, 1993), resulting in the observations of heat loss over the back.

5.4.3 Advantages and disadvantages of the study protocol

Although this thermal imaging has successfully been applied to assess surface skin temperature over brown fat regions in adults, this is the first time non-contact IRT imaging has been used in clinically stable, full-term

infants. Initial protocol development was based on previously devised exploratory protocols from preterm infants (Abbas et al, 2011). Selection of the open resuscitaire with overhead heat source used in phase 1, enabled the imaging protocol to be conducted with ease, since the camera could be positioned at a height of 1m, directly above the infant, whilst the rotated overhead heat source provided enough heat to ensure core temperature remained above 36.5°C. The selection of clinically stable infants imaged from this open platform, enabled thermograms to be captured of the whole infant back without interference from additional neonatal support i.e. blankets or breathing apparatus. Previously reported investigative studies of preterm skin temperatures have been conducted with infants in incubators and thus, thermal imaging has been conducted from the incubator openings, with a smaller field of view (Abbas & Leonhardt, 2014; Heimann et al, 2013). This approach could not have been taken in this study, since the infants would have needed to have been rotated to one side and held in positon by a member of research staff. Additionally, imaging from outside of the incubator portholes would have made capturing images of the whole of the infant back a challenge. Thus, imaging from above the infant enabled thermograms of the infant back to be captured. Further, open resuscitaires, similar to open cots, are enclosed by opaque plastic walls, which in the exploration of infant BAT heat production, are advantages, since they prevent sudden changes in airflow which can affect skin temperature recordings.

However, the reflective heat from the overhead heater questions the significance of initial findings from phase 1. Thus, the imaging protocol was improved in phase 2, so images were captured from full-term infants in an open cot. This method was advantageous in obtaining clear, non-distorted thermograms, which were not affected by overhead radiant heat or humidity and which demonstrated greater skin temperatures over the interscapular region, compared to a reference site over the lower back. However, in both phases of the study, infants demonstrated restless behavior, with a number of newborns excluded from the study due to distress,

which could be due to the length of study. It was not known whether infants would tolerate the hour-long protocol, since previous thermal imaging protocols in neonates have monitored infant skin temperatures for up to 30 minutes (Abbas et al, 2011; Abbas et al, 2014; Rice et al, 2010). Perhaps this would be a preferential length of study for exploring BAT heat generation in newborns.

5.4.4 Future considerations

The measurement of newborn superficial skin temperature is challenging and significant work remains to be conducted to standardise and refine the protocol here from phase 2.

In clinically stable infants, the appropriate imaging platforms were chosen, with refinements in phase 2, to a babytherm cot, improved the quality of thermograms, without comprising neonatal core temperature; a concern raised by the ethics committee. However, overcoming the issue of neonatal movement which affects lens focus of the camera and the quality of analysable thermograms, during imaging protocols, is difficult. Future development of imaging protocols for neonatal BAT heat detection, should consider the use of alternative thermal imaging means, such as that used by Abbas et al (2011). Preterm infants were imaged using IRT video recording which was capable of tracking selected ROIs over the neonate's skin to guarantee effective temperature detection over a period of time. Although infant movement still occurred, the ability to capture sequential images without the need to manually refocus the camera lens prior to capturing each image, results in an imaging method which can track movement variation and is easier to use.

Future studies may also consider the development of a custom made camera hole in the top of a full incubator, similar to that devised by Owen and colleagues (Owen & Ramlakhan, 2017). Healthy newborn infants could be positioned in the incubator, without the need for an overhead radiant heater. Fixing the camera onto the incubator directly above the infant,

could enable the capture of thermograms without disrupting the infant environment. However, since the camera would be positioned closer to the infant, skin temperature assessments of a specific region of the infant could only be made due to the smaller field of view.
Studies should also consider short imaging protocols in infants whilst asleep, opening up the potential to image the back of the infant, whilst being held in a flat prone position. This will flatten the skin of the neck and back to reduce skin-compression (notable in the current study). This is an important factor to consider when using IRT in healthy newborns, since the percentage of body fat in any given anatomical area is inversely correlated with skin temperature in that area and sub-scapular skinfold thickness, specifically, is negatively associated with lower local skin temperature (Neves et al, 2015). Thus, in clinically stable infants with a greater amount of subcutaneous fat around the upper neck and back regions, compression of the skin could affect the attenuation of heat signal. In preterm infants, however, this may not be an issue, considering fat deposition is mostly laid down in the final trimester of pregnancy and therefore, these infants possess thinner skin, with very little subcutaneous fat (WHO, 1993).

This pilot study has provided a good basis for investigative research, which assesses the potential for IRT to measure neonatal skin temperatures over regions of brown fat in clinically stable full-term infants. It is possible that the detection of early changes in skin temperature over BAT may allow for investigations in preterm infants whom present with poor vasomotor response to cold stress (Knobel et al, 2009; Lyon et al, 1997) and are prone to decreased core temperature (Jost et al, 2017), highlighting the potential for BAT dysfunction. Further, very low birth weight infants require a heated environment until they are thermally stable and if removed from the incubator too early, energy expenditure has been shown to increase due to presumed BAT activation to maintain core temperature (Dollberg, Mimouni & Weintraub, 2004). The ability of the infant

to increase energy expenditure may influence growth and potentially survival. Future studies of BAT thermoregulation in newborn infants will need to investigate the utility of IRT in such high risk infants.

Future work should also consider the use or IRT video recording and a short study protocols to overcome some of the observed limitations when assessing BAT activity in preterm and healthy infants. Indeed, the development of a non-contact imaging protocol, which could be used to assess early life BAT function, would be advantageous, especially considering that in preterm infants born IUGR are at an increased risk for the development of intra-abdominal body fat and reduction in insulin sensitivity in both children and adults (Modi et al, 2006; Modi et al, 2009; Ong et al, 2000; Regan et al, 2006; Rolfe et al, 2010; Uthaya et al, 2005). IRT may therefore propose a useful tool and biomarker for the assessment of BAT heat generative capacity and later metabolic health risk.

5.5 Conclusions

The use of infrared thermography in a range of fields in paediatric medicine has not been widely explored (Lahiri et al, 2012), with only a handful of investigations in to its use to assess preterm thermoregulation. The practical and ethical freedoms of IRT compared to PET-CT scanning, ensure the suitability of this method in newborn infants and children (Symonds et al, 2012). Despite the limited number of measurements, these preliminary results provide a good basis for further investigation of neonatal thermogenic activity over the inter-scapular BAT region. Figure 5.21 demonstrates a summary diagram of findings from both phases in the study. More studies performed under standardized clinical conditions are required, so that the method could be applied to assess BAT thermogenic function in preterm as well as clinically stable full-term infants. Thus, the developed protocol is a promising step towards establishing effective use of thermal imaging in the assessment of BAT function in early life.

(A)

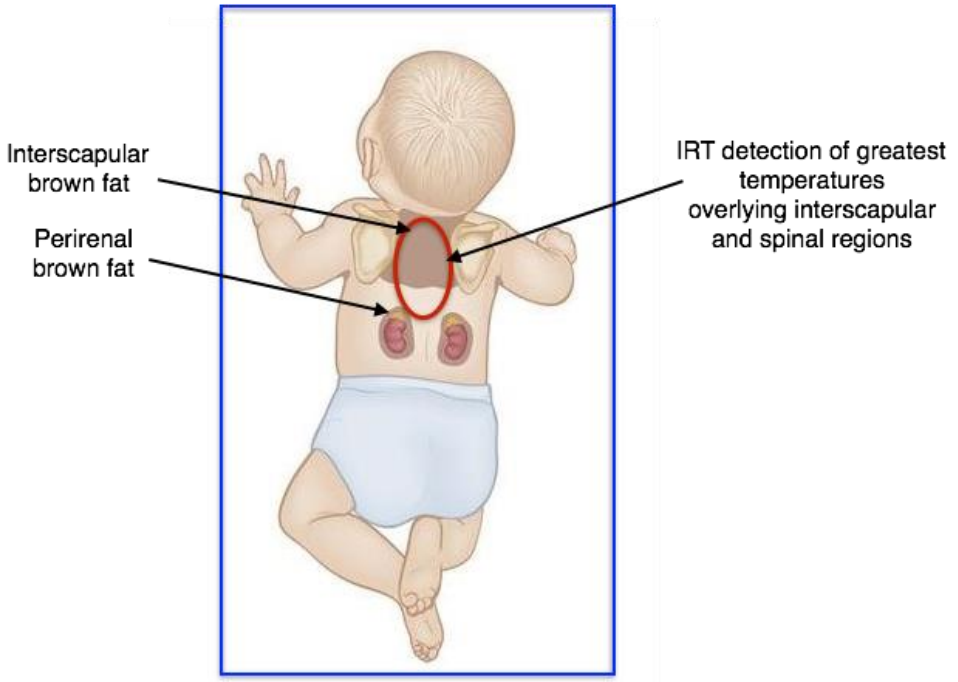

(B)

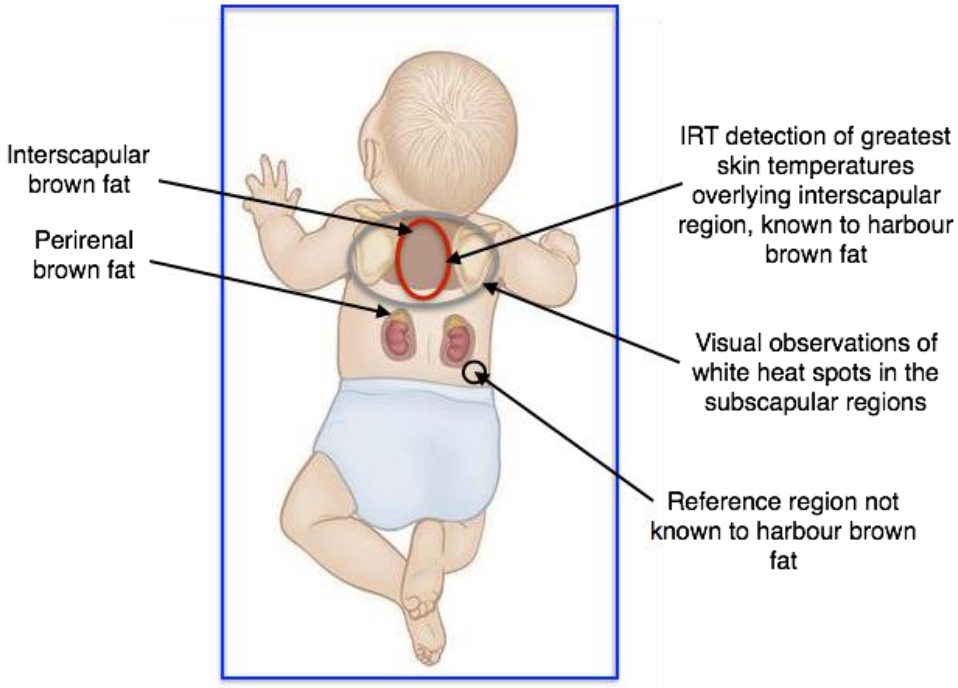

Figure 5.21. Summary of the assessment of skin temperatures performed over the back region of full-term infants in phase 1 (n=6) (A) and phase 2 (n=6) (B)

Chapter 6

A pilot study to assess how acute early postnatal stress will impact on selected BAT genes and markers of brain damage in the subsequent 24 hours

6.1 Introduction

In humans and large mammals, cortisol plays a vital stimulatory role alongside a range of endocrine factors, to drive fetal BAT growth and deposition in the final few weeks of gestation (Symonds et al, 2012), which parallel the increases in UCP1 gene expression (Mostyn et al, 2002). Collectively, these endocrine changes ensure that the newborn can effectively adapt to the extra-uterine environment at birth. However, as introduced in Chapter 4, prematurity consequential of intrauterine stress, can raise the susceptibility for programming postnatal metabolic consequences, such as increased intra-abdominal fat and insulin resistance in infancy (Modi et al, 2009; Ravelli et al, 1998; Regan et al, 2006). In humans, such metabolic adaptations have been attributed to the dysregulation of HPA axis at varying levels, whether at the level of the hypothalamus, where the PVN secretes corticotrophin releasing hormone (CRH); the pituitary, where CRH stimulates adrenocorticotropin (ACTH) release; the adrenal glands which secrete GCs or; GC's negative feedback loop on the upper levels of the HPA axis (Rask et al, 2002). These impairments result in alterations in the production and release of the stress hormone, cortisol (Ward et al, 2004). In adults, chronic hypercortisolism is the pathophysiologic underpinning of Cushing's syndrome (Abraham, Rubino and Nieman, 2013; Chrousos, 2000) and may play a role in the development and maintenance of obesity and the metabolic syndrome (Chanson and Salenave, 2010; Min, 2016).

A further important regulator of cortisol activity is exerted in peripheral tissues by tissue-specific pre-receptor metabolism, determining the access of cortisol to corticosteroid receptors (Lee et al, 2008). The key enzyme in adipose tissue is 11-Beta-dehydrocorticosterone (11β-HSD), in which its

type 1 isoform (11β-HSD1), determines intracellular tissue GC availability by the conversion of inactive corticosterone to active cortisol (corticosterone in rodents) (Doig et al, 2017). Elevated 11β-HSD1 mRNA expression in adults, has been demonstrated to correlate positively with BMI and adipocyte size (Engeli et al, 2004; Kannisto et al, 2004; Lee et al, 2008; Rask et al, 2002), indicating that stress induced increases in this enzyme may contribute to the characteristics of the metabolic syndrome (Masuzaki et al, 2001). The type 2 isoform (11β-HSD2) rapidly inactivates GCs (Shams et al, 1998) and plays an imperative role prenatally in the placenta, to protect the developing fetal brain from excess GCs.

Early life stress refers to the responses to severe stressors experienced during both pre- and postnatal development and before puberty (Loman et al. 2010 (van Bodegom et al, 2017). Excessive exposure to GCs in the postnatal period in rodents, is minimised by a stress hyporesponsive period (HRP); a period in the first 4 – 14 days, characterised by low circulating corticosterone concentrations and a blunted release of corticosterone to mild stressors (Avishai-Eliner et al, 1995; Cirulli et al, 1994; Levine, 2002; Schmidt et al, 2002; Walker et al, 1991). Adequate maternal contact during the HRP assists in ensuring a healthy maturation of the HPA axis (van Bodegom et al, 2017). Whilst not identical to rodents, preterm infants, particularly those who have experienced IUGR or who are born extremely premature, also exhibit very low cortisol levels in the first few days of life (Gunnar & Donzella, 2002; van Bodegom et al, 2017). Whether this is a protective strategy against the effects of excess GCs or a resulting consequence of excess GC exposure is largely unknown, given that healthy infants exhibit a period of dampened HPA axis responsiveness between 6-12 months of age (van Bodegom et al, 2017).

As the direct examination of early life stress in a newborn is not ethically viable, the development of animal models can permit the exploration of the effects of postnatal stress on the development of adipose tissue characteristics over short and long-term periods. Rodent offspring are born rela-

tively immature, with maximal growth phase initiated early in the postnatal period (Nedergaard & Cannon, 2017). The maturation of BAT involves multiple transcription factors to promote adipocyte differentiation, such as PRDM16, PPARγ and PGC-1α; the master regulator of mitochondrial biogenesis, to induce the expression of brown fats' unique UCP1 and the β3-AR through which it acts (Harms et al, 2014). Collectively, the maturation of BAT and the HPA axis primarily occur within the HRP (Cannon et al, 1988), in accordance with maximal thermoregulation, as pups gain the ability to thermoregulate independently (Kleitman and Satinoff, 1982; Mcdonald et al, 1989). Early postnatal life across species is thus a critical period for neurobiological and metabolic development and any severe, adverse physical or psychological experience during the first few weeks of life, can permanently alter HPA axis function (Ivy et al, 2008; Sapolsky & Meaney, 1986), brain development (Roceri et al, 2004) and metabolic profile (Miki et al, 2013) during adulthood.

Several paradigms of early life stress have been modelled to induce heightened levels of corticosterone. Interventions have included those which alter the level of maternal care such as maternal separation (Schmidt et al, 2003); which involves isolation of pups from their dam, intermittently, for 3 hours per day for up to 2 weeks, beginning at postnatal day (PND) 4, is a well-described intervention (Hofer, 1973; Levine et al, 1991; Liu et al, 2000; Meaney & Aitken, 1985; Schmidt et al, 2003), as well as corticosterone administration (Feve et al, 1992). Indeed, pups exposed to early life stress during the HRP by these interventions, have demonstrated large elevations in corticosterone response at PND 21, observed to be superior in females, in accordance with HPA hypersensitivity (Moussaoui et al, 2016); a reduction in body weight (Nilsson et al, 2002) and; reduction in the expression of brown fat genes, including UCP1 and β3-AR, vital for adequate maximal thermogenesis (Feve et al, 1992; Miki et al, 2013; Soumano et al, 2000; Viengchareun et al, 2001).

Stress induced by whole body vibration (WBV) has commonly been used when investigating the effects of heightened corticosterone on the development of brain injury in adult rodents (Craig et al, 2003; Dobbing, 1970; Yan et al, 2015). Its use to assess changes in metabolic profile has so far only been demonstrated in obese adults to increase energy expenditure (Sun et al, 2015). Chronic WBV for 30 minutes per day/ 6 days a week, for 8 weeks, has been shown to reduce body weight, alongside a reduction in the size of white adipocytes in the retroperitoneal WAT depot (Maddalozzo et al, 2008). Further, increases in BAT characteristics, such as UCP1 and PGC1α, were observed in WAT depot at of obese rats at 8 weeks of age (Sun et al, 2015). Thus, chronic WBV during adulthood may be capable of altering lipid metabolism in rats, to promote brown fat-like change in WAT. However, the effects of WBV on BAT characteristics during early maturation, has not previously been explored.

Changes to neurobiological development when stressed during the HRP period have also been reported in juvenile and adult rats and include; reductions in glucocorticoid receptor (GR) mRNA expression in the hippocampus (Barbazanges et al, 1996; Meaney, 2001) and upregulation of CRH mRNA expression in the hypothalamus (Avishai-Eliner et al, 2002; Brunson et al, 2001; Hatalski, Guirguis, & Baram, 1998). Indeed, these observations of poor stress regulation in adult rats exposed to early life stress, are consistent with the large body of human data which indicates in preterm IUGR infants the set point of HPA axis can be permanently altered. This can result in hypersensitivity of HPA activity and cortisol levels ultimately predisposing the infant to cardiovascular disease and metabolic syndromes (Andrews et al, 2002; Rosmond & Bjorntorp, 2000; Welberg & Seckl, 2001).

Collectively, although interventions of early life stress are capable of mounting a corticosterone response, variations in the length and type of stress employed, together with the factor of age, appear to result in a variation of metabolic effects at structural level, as well as inducing neurobiological effects, which may have implications for HPA axis function and GC

handling in later life. It remains unclear whether stress-related alterations in the HPA axis and adipose tissue characteristics are detectable at an earlier developmental stage, that is, in infancy.

6.1.1 Aims

We created a rodent model of early life stress to investigate the short-term consequences of postnatal stress employed through WBV on parameters of; HPA axis activation, including plasma levels of corticosterone and; biological characteristics of BAT in female pups, including the mRNA expression of UCP1, β3-AR (ADRB3), PRDM16, PPARγ, FGF21 and 11β-HSD-1 at PND 7 and PND 21.

6.2 Materials and Methods

Animals

Six adult, pregnant Sprague Dawley dams arrived at the University of Nottingham Biomedical Sciences Unit in 3 groups (dam 1/dam 2-4/dam 5-6) within the time frame of 1 month. Cages were inspected for the presence of pups at a 12 hour intervals and the date of birth was labelled as day 0. On PND 1, between 9:00 and 10:00am pups were sexed and female pups were designated into cohorts; PND 7, 14 or 21 and further, randomised to receive either an acute bout of vibrational stress (WBV) or control intervention (no vibrational stress) (Control). It must be acknowledged that both groups were taken from their dams to conduct the intervention in a separate room and thus, all pups were maternally separated for the duration of study.

Cohorts were designed to split the pups evenly. One pup per dam, per cohort and treatment, was taken from PND 7 (during the HRP) and PND 21 (post HRP) and entered into this study (Figure 6.1). Pups were housed with their mothers with free access to food and water. Pups remained with

their dam until their designated cohort day. The environmental temperature was kept constant at 21°C and a 12:12 light: dark schedule (lights on at 0800 hours) was maintained.

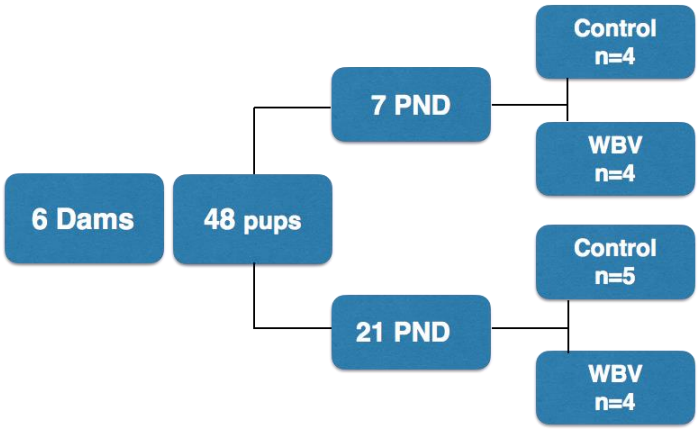

Figure 6.1. Experimental design of Chapter 6
Forty-eight female pups were born to 6 dams. Upon randomisation in to cohorts (7 or 21 PND), one pup per dam per treatment was taken and entered into the study. PND, postnatal day.

Experimental postnatal conditions

Brief maternal separation procedure

Brief maternal separation was experienced in all pups receiving vibration or no vibration. Pups were taken from their housing conditions to a separated temperature controlled room. Control pups with no vibration were placed in a small box positioned in the corner of the same room where the vibration took place. All pups were exposed to the same length of maternal separation.

Whole body vibration

WBV of pups at varying developmental ages was conducted. Pups were separated from their dams and were placed, not anaesthetised, into a segmented box fixed to a vibration platform (Multi-function 3D rotator PS-M3D, Grant-bio) (Figure 6.2). Vibration compartments and control holding

boxes contained a small amount of bedding material. Pups were exposed to 90-minutes of WBV and subsequently returned to their cage.

Experimental Design

The study experimentation was conducted by Dr Ian Bloor, Dr Lara Shipley and myself in the Biomedical Science Unit of the Medical School at the University of Nottingham. All experimental procedures were conducted in accordance with the guidelines set by the UK Animals Act of 1986 (Project licence: PPL 40/3560).

On the designated cohort day, pups were removed from their mothers to a separate room and were either exposed to a 90-minute vibration period, or no WBV exposure. The 90-minute vibration program represents a period of early life stress in neonates, based on a comparable experience during an average ambulance transfer in the UK, as determined by (Blaxter et al, 2016). The program was set at an average intensity of $2m/s^2$ and included short breaks mimicking brief stopping by the ambulance and jolts to mimic defects in the road (i.e. speed bumps). Control pups remained in a box in the same room as the vibrated pups without vibration exposure. Upon cessation of the vibration, both experimental and controls were marked under their ear to make clear which intervention they had received and for further identification. Rat pups were then returned to their original cage with their mothers for the subsequent 24 hours, before sacrifice. This period was chosen based on adult rodents studies demonstrating a 24-hour peak time frame for alterations in corticosterone levels (Altholtz, Fowler, Badura, & Kovacs, 2006) and pro-inflammatory cytokines, which saturate the HPA axis during a stress response (Himmerich et al, 2006). The subsequent day, the vibrated and control rats were humanely euthanized by Dr Ian Bloor and Dr Lara Shipley, by the procedure of cervical dislocation and death was confirmed by decapitation, carried out according to Schedule 1 of the Animal (Scientific Procedures) Act 1986. BAT samples were dissected as described in Chapter 2, alongside

plasma serum, which was removed directly from the heart following confirmation of death and subsequently stored at -80°C prior to use for RNA extraction. Serum samples were brought up to room temperature and then centrifuged at 2000 rpm for 10 minutes. The supernatant was removed and subsequently frozen at -80°C for further analysis.

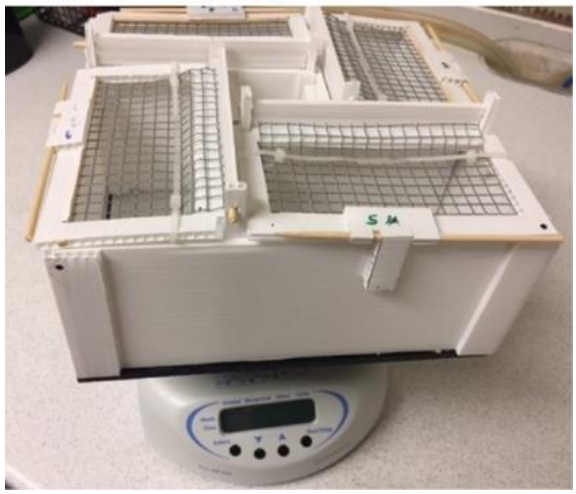

Figure 6.2. Vibration platform used to induce acute stress
A personalised vibration box was developed and comprised of four individual compartments, each could hold a single rat pup. All compartments contained a small amount of nesting material taken from the varying dams cages.

Laboratory procedures

Total RNA was prepared from female BAT samples as described in Chapter 2.3.4.3, in order to assess BAT biomolecular markers such as UCP1, ARβ3, PRDM16, PPARγ and FGF21 and a marker of whole body stress, 11β-HSD1, using RT-PCR (Chapter 2.3.4.4). Plasma corticosterone concentrations were assessed by myself according to the procedures described in Chapter 2.3.10.

Development and optimisation of the mRNA primers was performed by Dr I. Bloor, Mr M. Pope and myself. Normalisation and expression values for the mRNA gene results were calculated with GeNormTM software against

two reference genes. Where appropriate, any sample or analytical omissions are explained in the relevant results section.

Statistical Analysis

Statistical comparisons were performed using two-way ANOVAs adjusted for multiple comparisons, alongside Tukey *post hoc* tests, to assess the effects of treatment (control vs. WBV) and age (PND 7 and PND 21). The difference between values obtained from the different treatment groups was carried out using Mann-Whitney U tests. Statistical significance was set at $P < 0.05$.

6.3 Results

6.3.1 Expression stability of Reference Genes

As described in the Materials and Methods chapter of this thesis (Chapter 2.3.10), the cycle threshold (C_t) value of each reference gene was obtained from RT-PCR analysis. The mean C_t value of the reference genes ranged from 12 to 25 cycles, with *r18S* having the highest (11.71 ± 2.45) and *TBP* having the lowest (25.48 ± 0.74) transcript levels. Inter-group variation in the mRNA expression of *r18s*, YWHAZ and RPLPO in BAT was observed, whereas, the mRNA expression of TBP and B2m remained stable between control and vibration groups at 7 and 21 days (Figure 6.3).

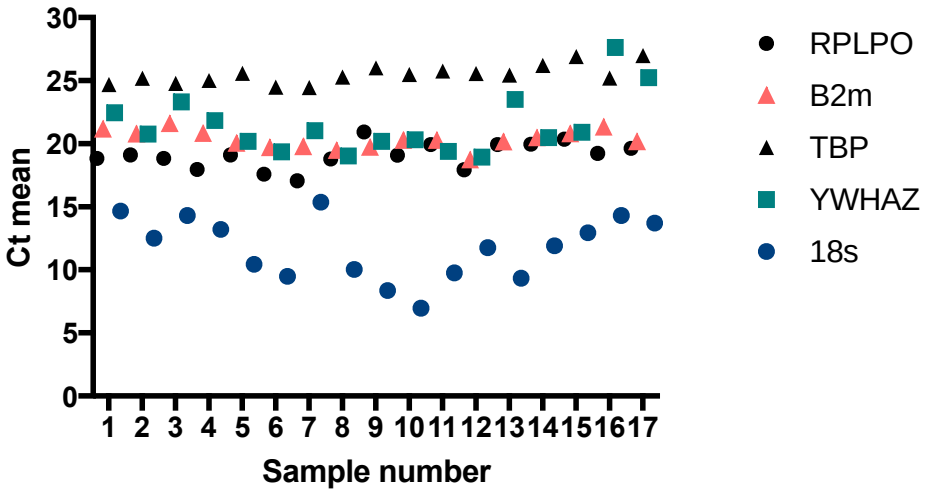

Figure 6.3. Expression stability of reference genes
The cycle threshold (C_t) values of TBP and B2m remained stable across samples.

The geNorm analysis demonstrated that the combination of two pairs of reference genes had an M value of below 0.5, which is the maximum value for acceptable gene expression stability as defined by Vandesompele et al (2002). The reference gene pair with the lowest M value has the most stable expression. As shown in Table 6.1, the ranking of M value combinations in BAT with the combination of TBP:B2m (M = 0.25) the most stable pairing of reference genes, whilst r18S:B2m was the least stable pairing of reference genes. QPCR analysis was performed on BAT was normalised using the two most stable reference genes.

Table 6.1. Expression stability of reference gene pairings
The most stable pairing of reference genes was TBP:B2m (M = 0.25).

Gene 1	Gene 2	Paired M value
TBP	B2m	**0.25**
RPLPO	TBP	**0.32**
RPLPO	B2m	**0.58**
RPLPO	YWHAZ	**0.59**
TBP	YWHAZ	**0.92**
YWHAZ	B2m	**1.18**
YWHAZ	18s	**1.99**
RPLPO	18s	**2.59**
TBP	18s	**2.91**
B2m	18s	**3.17**

6.3.2 Body weight and BAT weights

Expectedly, there was a significant increase in body weight with age (P = 0.001). WBV did not affect weight at 24 hours post exposure (Figure 6.4a) (P = 0.650). In line with the maturation of BAT, interscapular BAT weight significantly increased from PND 7 to PND 21 (P = 0.001). Acute WBV did not affect BAT weight (P = 0.735) (Figure 6.4b).

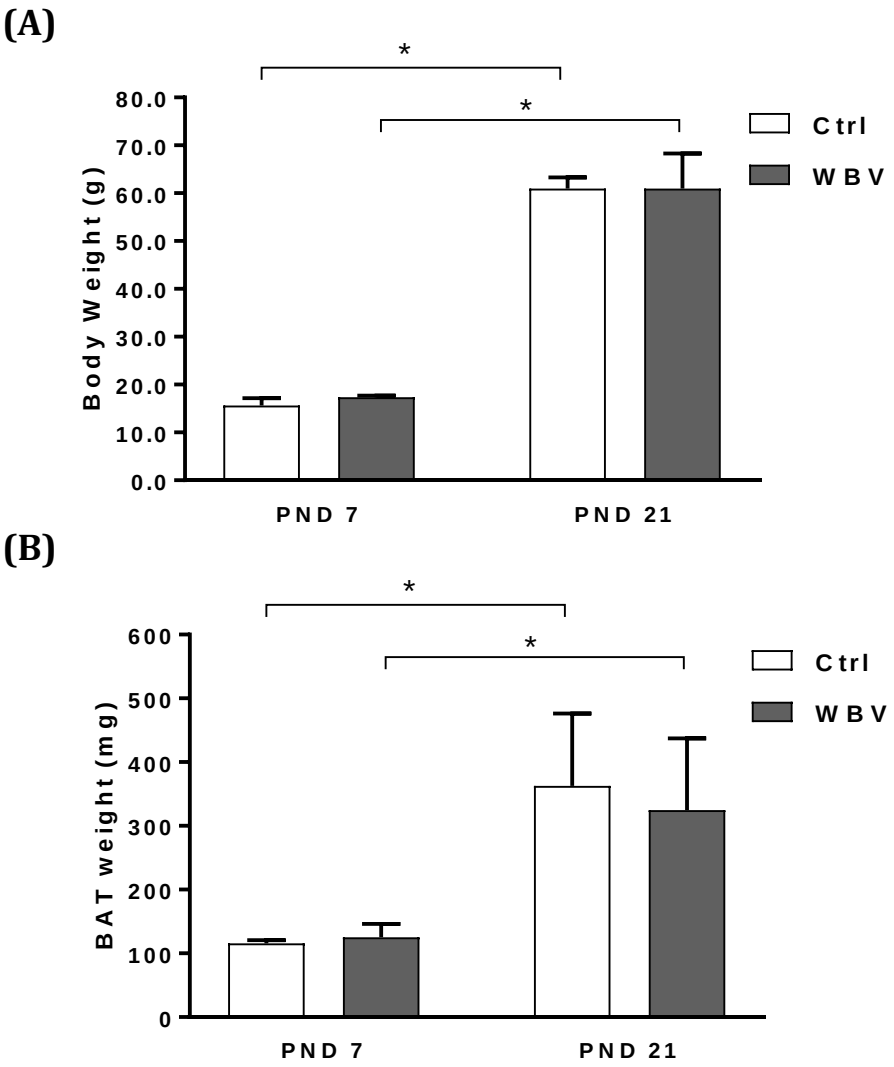

Figure 6.4. Influence of WBV on body weight (BW) and Interscapular BAT weight (Interscap BAT) at PND 7 and 21

Age increased body weight (A) and BAT weight (B). There was a strong correlation between interscap BAT weight and BW (C). Values are mean ± SD, **P* <0.05. Ctrl, control; WBV, whole body vibration. PND 7; ctrl n=4, wbv n=4; PND 21; ctrl n=5, wbv n=4. Data are shown as mean ± standard deviation. **p* < 0.05 vs. control.

6.3.3 Early life stress induced alterations in the stress response

As expected, circulating concentrations of corticosterone increased with age under both control (P = 0.004) and vibrated (P = 0.001) conditions (Figure 6.5), in line with maturation of the HPA axis. WBV increased corticosterone responses in pups after the HRP, at PND 21 only (PND 21, P = 0.001; PND 7, P =0.993).

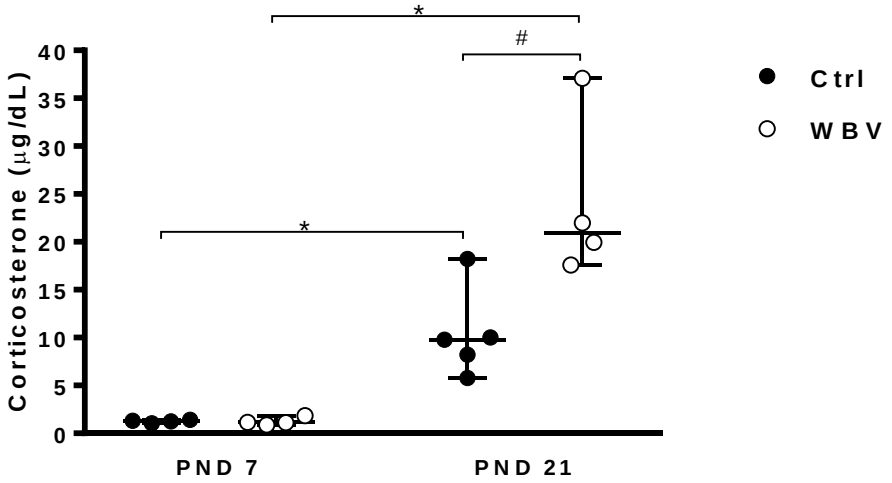

Figure 6.5. Corticosterone plasma levels in control and WBV groups at PND 7 and PND 21

Trunk blood was collected after decapitation between 9:00 and 11:00 am. Data are mean ± 95% confidence interval. (4–5 pups per group). (*) denotes a significant difference with age (P <0.05). (#) denotes a significant difference compared to control group (P <0.05). Ctrl, Control; WBV, whole-body vibration.

6.3.4 The effects whole body vibration on the mRNA expression of selected BAT genes at 7 and 21 days of life

Two-way analysis of variance corrected for multiple comparisons, demonstrate a marked effect of age on UCP1 mRNA concentration ($F(1, 20) = 6.94$, $P = 0.015$) (Figure 6.6a). There was no effect of age on the relative mRNA expression of the following BAT responsive genes; β3-AR ($F(1, 20) = 0.042$, $P = 0.838$), 11β-HSD1 ($F(1, 20) = 0.017$, $P = 0.896$), PRDM16 ($F(1, 20) = 7.33$, $P = 0.061$), PPARγ ($F(1, 20) = 3.43$, $P = 0.078$), and FGF21 ($F(1, 20) = 0.01$, $P = 0.910$) under control conditions (Figure 6.6b-f).

WBV treatment was not seen to affect the mRNA expression of UCP1 (treatment, $F(1, 20) = 4.20$, $P = 0.051$; interaction, $F(1, 20) = 1.43$, $P = 0.244$), β3-AR (treatment, $F(1, 20) = 2.48$, $P = 0.130$; interaction, $F(1, 20) = 0.10$, $P = 0.746$), or FGF21 (treatment, $F(1, 20) = 2.95$, $P = 0.101$; interaction, $F(1, 20) = 2.25$, $P = 0.148$) (Figure 6.6a-f).

However, at PND 21, in accordance with the stress-induced elevation in corticosterone concentrations, WBV induced a significant elevation in relative mRNA concentrations of the enzyme, 11β-HSD1, compared to control treatment ($P = 0.023$, Figure 6.6c) (main treatment effect, $F(1, 20) = 7.33$, $P = 0.013$; interaction, $F(1, 20) = 1.101$, $P = 0.306$). At PND 21, WBV also resulted in reductions in the mRNA concentrations of PRDM16 ($P = 0.021$) (main treatment effect, $F(1, 20) = 12.36$, $P = 0.002$; interaction, $F(1, 20) = 0.08$, $P = 0.769$) and PPARγ ($P = 0.031$) (main treatment effect, $F(1, 20) = 10.9$, $P = 0.003$; interaction, $F(1, 20) = 2.34$, $P = 0.141$).

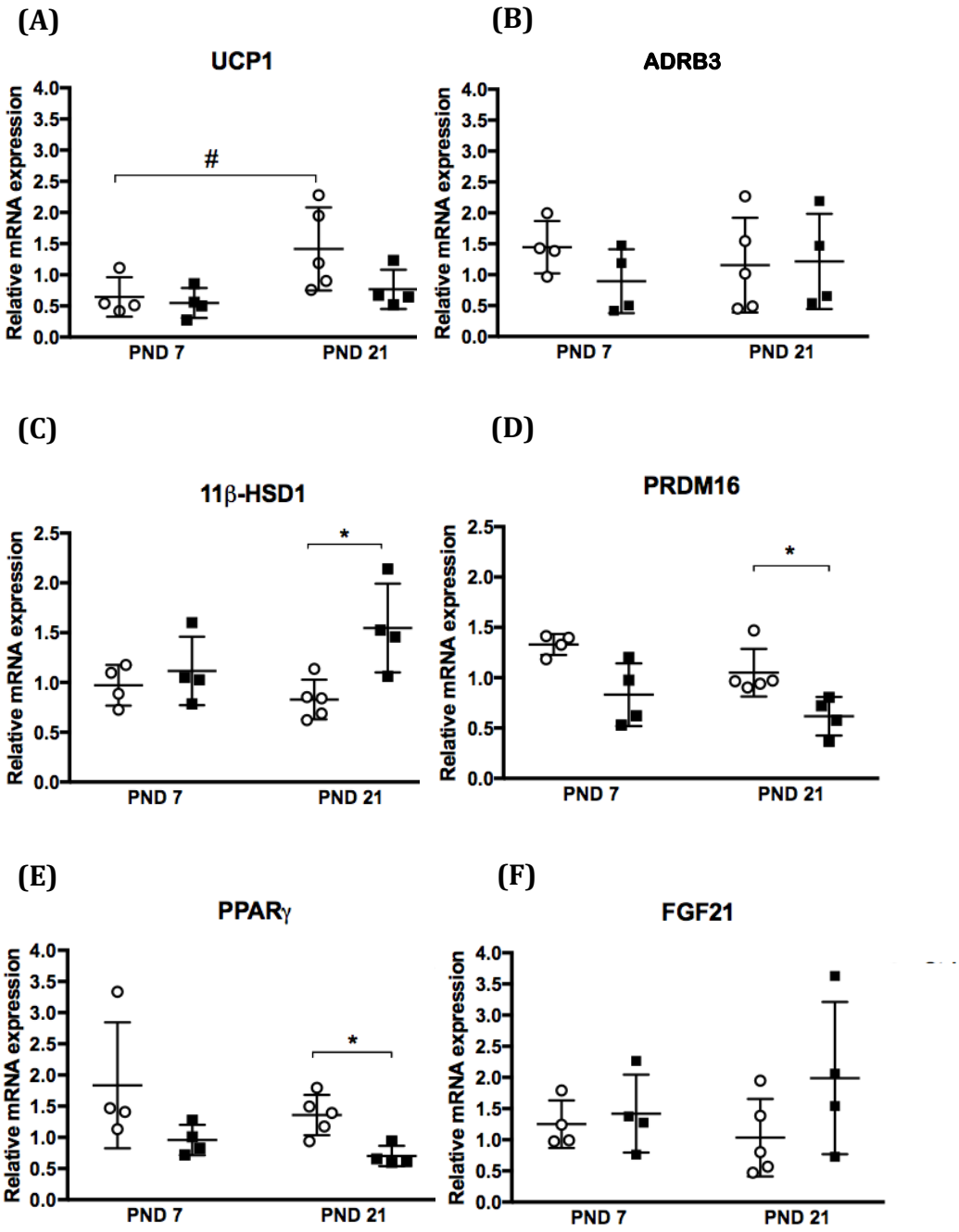

Figure 6.6. Effect of whole body vibration (WBV, black squares) on the mRNA expression of selected BAT adipogenic and molecular genes at postnatal days 7 and 21, compared to control (Ctrl, white circles)

Values are mean ± standard deviation. Significance set at $P < 0.05$. (#) denotes a significant difference with age; (*) denotes a significant difference in response to WBV. postnatal day; UCP1, uncoupling protein 1; PRDM16, PR domain containing 16; ADRB3**,** beta-3 (β3)-adrenoreceptor; FGF21, fibroblast growth factor 21; PPARγ, peroxisome proliferator-activated receptor gamma**;** 11β-HSD1, 11-Beta-dehydrocorticosterone 1.

6.4 Discussion

Major challenges remain in defining the mechanisms through which early adverse experiences may facilitate immediate changes to the adipose tissue profile and later risk for metabolic disorders. These include difficulties in determining the most sensitive periods during which exposure to stress has its greatest impact on adipose tissue development and the length and severity of early life stress exposure to elicit changes in BAT characteristics. The present study assessed the effects of an acute early life stress intervention at defined developmental stages during the HRP and thereafter, on HPA axis responsiveness and the mRNA expression of selected BAT genes. Significant increases in corticosterone were observed with age and levels at PND 21, were elevated to a greater extent upon WBV. The elevation in corticosterone with WBV at PND 21, was associated with an increased expression of 11β-HSD1 mRNA and downregulation of genes involved in the transcriptional control of BAT; PRDM16, PPARγ. The mRNA expression of UCP1, β3-AR and FGF21 remained unchanged with WBV exposure.

6.4.1 Early postnatal changes in mRNA expression of genes regulating BAT transcriptional control and development

Adequate prenatal adipose tissue development and deposition is essential for postnatal thermogenesis in the defence against hypothermia in both large mammals and rodents (Symonds, 2013). Numerous transcription factors and co-regulators have been identified as promotors of embryonic development and acquisition of the BAT-specific gene expression profile, including UCP1, prior to birth. Amongst them, PRDM16, a zinc-finger containing transcription factor, specifically determines brown fat cell identity from *Mf15*$^{+}$ adipocyte linage (Kajimura et al, 2009). In fact, PRDM16 acts primarily through co-regulating peroxisome proliferator activated receptor-γ (PPARγ) and CCAA T/enhancer binding proteins (C/EBPs) required for adipogenesis and PGC-1; the master regulator of mitochondrial biogen-

esis, to induce the expression of brown fats' unique UCP1 and the β3 adrenoreceptor through which it acts (β3-AR) (Harms et al, 2014; Hondares et al, 2011; Kajimura et al, 2009; Seale et al, 2008; Seale et al., 2007). As BAT in rodents primarily matures postnatally, the differentiation of adipocytes requires the presence of the above highlighted transcription factors (Harms et al, 2014). The current study revealed an elevated mRNA expression of PRDM16 and PPARγ in the interscapular BAT depot of control pups at PND 7, which did not significantly change at PND 21, in line with the commitment of brown fat lineage from myoblast progenitors during embryonic development (Schulz & Tseng, 2013). Indeed, Harms and colleagues (2014) found that PRDM16 is required postnatally (assessed from 6 weeks to 9 months of age) to repress the transcription of many WAT genes (Retn, Agt), enabling the interscapular BAT depot to retain its classic brown characteristics (Harms et al, 2014).

As expected, there was an increase in body weight and BAT weight with age. These results are in accordance with increasing lipid deposition during BAT maturation in the first 2 weeks of life (Schulz & Tseng, 2013; Zhao et al, 2014). Further, the expansion in catecholaminergic innervation of BAT parenchyma (Kajimura et al, 2009) sympathetically stimulates BAT mitochondrial biogenesis and the expression of thermogenic genes (Puigserver et al, 1998). Indeed, the observed increases in UCP1 mRNA expression in control pups from PND 7 to 21, suggests the maturation of the BAT depot as committed progenitor cells transition into classic brown adipocytes during BAT differentiation (Kajimura et al, 2009; Schulz & Tseng, 2013). This critical developmental phase enables the transition from huddling to independent thermoregulation during weaning (Farrell et al, 2007; Kleitman and Satinoff, 1982). However, no significant changes in the mRNA expression of β3-AR were observed with age, presumably due to the already elevated expression at PND 7. This is in support of sympathetically mediated BAT recruitment with a subsequent marked amplification of the capability of BAT to produce heat during weaning (Cannon & Nedergaard, 2004).

6.4.2 Effects of early life stress on alterations in the mRNA expression of BAT genes regulating transcriptional control and development

Adequate postnatal maturation of the HPA axis is essential for the normal functioning of stress-response during adulthood (Schmidt et al, 2003). However, severe early life stress experienced during the HRP including; maternal separation (Hofer, 1973; Levine et al, 1991; Liu et al, 2000; Meaney & Aitken, 1985; Miki et al, 2013; Schmidt et al, 2003) and limited nesting stress (Ivy et al, 2008; Molet et al, 2014), can alter HPA axis function (Ivy et al, 2008; Sapolsky & Meaney, 1986), which can subsequently promote weight gain and food intake in rats during adulthood (Jahng, 2011; Kalinichev et al, 2002). However, the effects of early life stress on immediate AT development are less well known.

In the current study, WBV was utilized to induce early life stress and a heightened concentration of corticosterone, in order to assess its consequential effects of BAT characteristics. I report that corticosterone concentrations of both control and WBV groups at PND 7, were extremely low, in accordance with the protective effects of the hyporesponsive period on the developing brain (Schmidt et al, 2003). The low values of plasma corticosterone at PND 7 in both groups, were similar to those reported in rat pups between PND 2 or 10 (Moussaoui et al, 2016; Smotherman, 1983) and control corticosterone levels at PND 7 were greater than the basal corticosterone levels of control pups at PND 5-7 (Enthoven et al, 2010), These effects are due to the variations in the experimental protocols between studies in rodents, during the HRP. In the current study, control pups were exposed to a short period of maternal separation at PND 7, whereas control pups from other studies have remained with their dam 7 (Enthoven et al, 2010).

In the current study, age contributed to a 9-fold increase in plasma corticosterone levels in the control from PND 7 to PND 21, in accordance with maturation of the HPA axis. At this age, WBV pups displayed a 53% increase in plasma corticosterone levels compared to control pups. The plasma corticosterone levels in WBV group at PND 21, are greater than

that observed in female rat pups of the same age when limited nesting stress was conducted at PND 2-10, followed by 11 days of normal housing (Moussaoui et al, 2016). The mean concentration of corticosterone in the control group at PND 21 in the current study was also greater than that reported in female pups at PND 21 upon brief separation stress; 15 minutes of maternal separation from PND 2-9 (Moussaoui et al, 2016). Indeed, Moussaoui and colleagues also reported corticosterone responses to limited nesting stress at PND 21 in female pups were 80% superior to those in male pups of the same age (P <0.001). Their findings point to a sex difference in developmental hyper-responsiveness to early life stress and its sustained effects on HPA axis dysregulation.

Collectively this study observed corticosterone responses that are consistent with the age-related maturation of the HPA axis (Henning, 1978; Moussaoui et al, 2014), and the experimental early life stress induced a significant elevation in plasma corticosterone compared to control at PND 21. The increases in corticosterone at PND 21 with vibrational stress may have longer term implications for HPA axis function, since other studies have demonstrated that as adults, pups exposed to chronic maternal separation during the HRP exhibit permanent alterations in hypothalamic gene expression of corticotropin releasing factor (CRF) (Ivy et al, 2008), alongside its end-product, cortisol (Barreau et al, 2007; Rosenfeld et al, 1991; Schoenfeld, Leathem & Rabii, 1980; Walker et al, 1991).

Whilst not entirely identical to rodents, healthy full-term infants are responsive to stress in the first months of life, followed by a similar HRP period to rodents, between 6 and 12 months of age (Gunnar & Donzella, 2002; van Bodegom et al, 2017). However, in newborn infants, particularly extreme preterm infants who spend length periods of time on the neonatal intensive care unit (NICU), are exposed to many stressful events which creates a period of long-standing stress (Smith et al, 2011). Chronic stress experienced on NICU has been suggested to play a role in modifying brain development (Rangon et al, 2007) and authors have suggested that prematurity alters HPA regulation (Tu et al, 2007), since pre-term infants have

been demonstrated to exhibit HPA axis hyper-responsiveness between 8 and 18 months (corrected age for prematurity), with levels of cortisol in the tiniest preterm infants, greater than that of healthy full-term infants (Gunnar & Donzella, 2002). Thus, it may be hypothesised that chronic early life stress through prematurity, could exhibit greater deleterious effects on brain development, with subsequent impact on metabolic disease risk later in life (Modi et al, 2006).

Considering BAT is an essential feature for early postnatal thermoregulation, it is surprising that few studies have investigated the consequences of early life stress on its characteristics during maturation at critical developmental stages prior to adulthood.

The excess production of GCs by the subcutaneous administration of corticosterone (Strack et al, 1995) has been demonstrated to suppress of an array of transcriptional genes which regulate non-shivering thermogenesis particularly in adulthood, including UCP1 and β3-AR (Feve et al, 1992; Garrel, 1997; Soumano et al, 2000; Viengchareun et al, 2001) by mechanisms involving the interference with sympathetic adrenergic signalling (Kozak et al, 1994). Further, Miki et al (2013) demonstrated that maternal separation of female rats for 3 hours per day, during PND 10-15, resulted in a significant reduction in β3-AR mRNA expression, whilst UCP1 mRNA remained unchanged relative to control at 10 weeks of age (Miki et al, 2013). The functional effects of β3-AR depend on the recruitment of UCP1 (Inokuma et al, 2006) and thus, in the current study, the unchanged β3-AR and UCP1 mRNA levels observed in response to WBV at PND 21, indicate attenuated UCP1 activity, since the activity of UCP-1 is initially recruited by β3-AR mediated signalling (Inokuma et al, 2006). Further, FGF21 is known to regulate energy metabolism by promoting UCP1 gene expression in both BAT and WAT under conditions of cold-stimulation (Fisher et al, 2012; Lin, Liu & Hu, 2017). The promotion of brown like characteristics in WAT, demonstrates FGF21 to be an important regulator of thermogenesis. Although the effects of early life stress on FGF21 regulation are unknown, it is not surprising that this gene remained unchanged, since WBV failed to induce changes to UCP1 mRNA.

It remains surprising that the increased 11β-HSD1 mRNA expression at PND 21, was not associated with alterations in UCP1, considering 11β-HSD1 knockout in mice subjected to excess GCs through, supplementing drinking water with corticosterone,
has been demonstrated to elevate UCP1 mRNA (Doig et al, 2017; Liu et al, 2000) associated with increases in core body temperature (Morton et al, 2001; Morton et al, 2004) and BAT thermogenesis (Liu et al, 2000). Whereas in controls with no 11β-HSD1 knockout, a diminished expression of such genes has been observed (Liu et al, 2013). Further, elevated adipose tissue derived 11β-HSD1 mRNA expression, has been demonstrated to correlate positively with BMI and adipocyte size (Engeli et al, 2004; Kannisto et al, 2004; Lee et al, 2008; Rask et al, 2002; Tomlinson et al, 2002), highlighting the potential for BAT dysfunction in the presence of the 11β-HSD1 enzyme. The failure of early life stress to induce alterations in UCP1 in the current study, could be a functionality of the low number of pups per group or alternatively, the singular episode of early life stress and animal sacrifice during the early developmental period, given that chronic stress induced in early life, can mediate alterations in BAT genes during adulthood.

Given that UCP1 mRNA cannot functionally produce heat (Nedergaard & Cannon, 2013), the tendency to only focus on the alterations in UCP1 mRNA may cloud the interpretations of the thermogenic capacity of BAT. The measurement of total amount of UCP1 protein from the interscapular depot should also be conducted, which will quantify a biochemically thermogenic parameter from in-vitro data. Nedergaard and Cannon (2013) reported that UCP1 mRNA levels observed after cold acclimation were increased by 50%, whereas UCP1 protein content from the same BAT depot, increased by 10-fold (Nedergaard and Cannon, 2013). Thus, it would be easy to underestimate the true physiological significance of UCP1. Further, UCP1 protein levels have a half-life of up to 6 days (Clarke et al, 2012; Puigserver, 1992), thus it would've been interesting to have left a period of

a week between intervention and sacrifice, to assess alterations in UCP1 over a longer time frame.

The extent of GC mediated effects depends on the balance between the two isoforms of the 11β-HSD enzyme. Increased GC levels have been proposed to inhibit 11β-HSD2 activity (Quinkler et al, 1999), which catalyses the reverse conversion of active GCs (corticosterone in rats, cortisol in humans) to their inactive 11-keto derivatives (11*β*-dehydrocorticosterone in rats, cortisone in humans) (Fernando et al, 2013). Placental 11β-HSD2 plays a vital role during gestation, to minimise the effects of excess GC exposure to the fetal brain. However, the influx of excessive levels of maternal or exogenous antenatal corticosteroids (Edwards et al, 1993), required for fetal development and organ maturation, particularly in infants at risk of preterm birth (Lunghi et al, 2010), can result in decreased activity of 11β-HSD2. Subsequent consequences involve the negative interference with fetal growth and maturation, leading to prematurity and low birth weight (Edwards et al, 1993; Nyirenda et al, 1998; Rondo et al, 2003). Thus, future studies should also consider the potential for 11β-HSD2 as a mechanism providing a negative-feedback loop, which could prevent excessive formation of GCs over time and for which could influence *in utero* AT deposition.

In search for further mechanisms which may underpin the previously demonstrated alterations in UCP1 expression and reduced BAT thermogenesis after early life stress, Yoshitomi et al (1999) demonstrated that the c-Jun N-Terminal Kinase (JNK), which is a key player in adipose tissue inflammation and provides a link between nutrient excess, inflammation, and impaired insulin signalling (Zhang et al, 2011), reduces both basal and PKA-induced transcription of UCP1 in differentiated brown adipocytes (Yoshitomi et al, 1998). Thus, it may be plausible to suggest that glucocorticoid excess mediates increased activity of the glucocorticoid receptor (GR), and initiates the interaction between glucocorticoid response element (GRe) and JNK, which binds to the proximal cAMP response element (-139/-122) located on the UCP1 gene promotor region (Kozak et al, 1994), which may inhibit UCP1 expression and thus, BAT function

(Viengchareun et al, 2001). In addition, Ramage et al (2016) demonstrated the activation of a number of glucocorticoid-dependent genes, such as Adipose Triglyceride Lipase (ATGL) and Hormone Sensitive Lipase (HSL), is thought to trigger the GR signalling pathway in both murine and human adipocytes upon synthetic glucocorticoid administration. However, GR binding in BAT has not been examined to date, so it is unclear if GR binds directly to the UCP1 promotor region altering its transcription (Ramage et al, 2016).

Early life stress has also been shown to alter adipose tissue characteristics in later life, with Miki and colleagues (2013) demonstrating an elevated WAT prohibitin (a proliferative protein) mRNA expression in mice at 10 weeks of age after early life stress experienced between PND 10-15 (Miki et al, 2013). These findings are consistent with associated alterations in body weight after early life stress. Lee et al (2007) demonstrated that chronic maternal separation in the first 2 weeks of life, increased body weight during adulthood, compared to age-matched control animals (Lee et al, 2007). These effects are widely accepted consequences of early life chronic stress in adult rodents (Lee et al, 2007; Ryu et al, 2009) and are in part, due to the effects of increased food intake (Penke et al, 2002). In the present study, acute WBV stress did not induce any differences in BAT weight or body weight at PND 7 or PND 21. It is possible that the differences observed across studies are due to the variations in experimental protocol. The current study initiated a single bout of early life stress either during the HRP pre-weaning period and animal sacrifice was conducted some 24-hours later. Whereas previous models of early life stress, have elicited chronic bouts of stress during the HRP, followed by either isolated rearing (Lee et al, 2007) or return to their mothers before sacrifice during adulthood (Miki et al, 2017). Thus, repeated stress may be required in order to mediate changes in BAT thermogenic gene expression, considering chronic stress exposure during infancy, downregulates BAT thermogenic program in adulthood (Feve et al, 1992; Garrel, 1997; Soumano et al, 2000; Viengchareun et al, 2001).

To date, WBV has only been utilised to assess the effects on metabolic profile in obese individuals or rodents (Maddalozzo et al, 2008). This in part due to the beneficial effects of WBV exercise interventions to reduce body weight through increasing energy expenditure (Maddalozzo et al, 2008), together with demonstrations of increases in the expression of key functional genes of BAT; PGC1α and UCP1 in WAT of obese, adult rats compared to healthy age-matched controls (Sun et al, 2015). These data infer that chronic WBV may be a useful strategy to promote brown-like-characteristics in WAT to induce long term weight loss, at least in obese adults (Sun et al, 2015). Indeed, in healthy adults, 30 minutes of WBV increased blood flow and muscle and skin temperature 24 hours after vibration, compared to no vibration in the same individuals (Hazell & Lemon, 2012). Future WBV studies should therefore consider the use of IRT in the assessment of early life stress on BAT function, considering thermal energy is a specific end product of UCP1- mediated metabolism in BAT and its detection is an ideal surrogate of BAT activity (Ca et al, 2015; Crane et al, 2014). In support, IRT imaging has successfully been used to detect UCP1 mediated increases in thermogenesis in stimulated rodents acclimated to 23℃ or 30℃ (Akesson et al, 2007; Crane et al, 2014; Jackson et al, 2001), albeit predominantly in anesthetised or restrained animals. It would have been of interest to have used IRT imaging in the current study to provide insight into the thermoregulatory aspects of WBV. However, since pups were not anesthetized, imaging pups at PND 7 would be easier, since they demonstrated no signs of restless behaviours. Pups at PND 21 demonstrated tendencies to climb and holding onto the cage ceiling of their individual boxes and thus, IRT at this age would be challenging unless pups could be restrained.

Evidently there are variations in the effects of early life stress on postnatal BAT functional genes may be due to the following factors; differences in the type of stress experienced by the pups, when early-postnatal stress was experienced, the period of stress and the time frame over which stress could mediate changes to in BAT gene expression. It could be hypothesised

that repeated severe stress in the early postnatal period, as oppose to a single acute bout may be required in order to elicit changes in BAT mRNA expression. Indeed, the current study only assessed the relative change in mRNA expression of a handful of BAT responsive genes and thus the mechanisms which may underpin the alterations in BAT characteristics in response to early life stress, can only be postulated since the biological relevance of the current data is limited without further protein analysis (Cannon and Nedergaard, 2007). Thus, the detailed molecular mechanisms underpinning the stress-induced changes to adipose tissue-associated markers are yet to be fully understood and require exploration.

6.4.3 Early life stress induces dysregulation of the HPA axis; broader implications for the development of brain injury and metabolic disturbance

The driving force behind structural abnormalities of the brain and metabolic disturbances upon early life stress, may be the functionality of the HPA axis resulting in the release of GCs (Avishai-Eliner et al, 2002; Maniam et al, 2014; McEwen, 2000; van Bodegom et al, 2017). GCs play avital role in the hippocampus to promote adaptation and recovery from stress (De Kloet & Derijk, 2004; van Bodegom et al, 2017). Adequate functioning of this HPA axis negative feedback loop is critical for handling of acute stress, especially in early life and the avoidance of the deleterious effects of prolonged exposure to high levels of GCs, which can impair growth and maturation and alter metabolic disease susceptibility in later life (Bhutta & Anand, 2002; Sanchez, Ladd & Plotsky, 2001; Welberg & Seckl, 2001).

Research understanding the early life stress induced changes in neurobiology have focused on alterations in neuronal activation, cell proliferation and cell death predominantly in hypothalamic, hippocampus and frontal cortex regions of the brain. Prenatal stress has been demonstrated to increases apoptosis in the fetal rodent hypothalamus (Tobe et al, 2005). Repeated restraint stress (for 30 min daily for 5 days from gestational days

17–21) reduced Fos mRNA expression, a marker of neuronal activation (Chowdhury, Fujioka & Nakamura, 2000), due to the significant increase in the number of apoptotic cells in the PVN. Early life stress has also demonstrated increases in neuronal density post the HRP, alongside reduced levels of apoptosis-stimulating proteins and enzymes, whilst cell survival-stimulating protein levels were increased (Irles et al, 2014).

In an adjacent study, short WBV exposure induced significant increases in apoptosis of the frontal cortex in female pups during the HRP, at PND 7 and thereafter, at PND 21 (data not shown). The frontal cortex is critical in repressing the HPA axis upon stress, restoring a state of homeostasis through its inhibitory connections to the PVN, where it inhibits CRH release (Radley, Arias & Sawchenko, 2006). Both prenatal stress, through forced swim tests (Sowa et al, 2015) and early life stress through maternal separation (Gondré-Lewis et al, 2016) and WBV (Oliveira et al, 2015) have been demonstrated to impair frontal cortex functioning, suggesting a role for GCs which mediate changes to HPA axis function through this regulatory pathway. Further, maternal separation for 24 hours in rat pups at PND 3 has been demonstrated to result in a volumetric reduction of the prefrontal cortex (Sarabdjitsingh et al, 2017).

No observable differences in brain weight upon WBV compared to control (data not shown) were observed, indicative of an unchanged brain volume, due to the short 24-hour period between WBV and sacrifice. Although analysis of specific regions of the frontal cortex which have previously shown reduce in response to early life stress; ventromedial and orbitofrontal cortex (Sarabdjitsingh et al, 2017), have yet to be analysed from the current study. Collectively, current data indicate that stress experienced at this developmental time, may influence the structural reorganization of the PVN and frontal cortex in the very early developmental stages, which may thereby alter homeostatic and HPA-axis regulation.

HPA axis dysregulation could also be caused by the disruption of the blood brain barrier (which is essential for enabling GC-mediated effects at their receptors in the hippocampus and hypothalamus); potentially reducing

the HPA negative feedback loop and lead to the influx of inflammatory cells resulting in potential damage to several areas of the brain (Avishai-Eliner et al, 2002). An enhanced inflammatory response can mediate impairments to GR function in the hippocampus (Webster et al, 2001). Similarly, in rat pups of low versus high-care dams and GR expression is reduced (Weaver, Meaney & Szyf, 2006). Barbazanges and colleagues also reported that in rats born from dams prenatally exposed to stress, during adulthood, the responsiveness to GCs is reduced, alongside a reduction in MR and GR in the hippocampus, impairing the HPA axis negative feedback loop (Barbazanges et al, 1996). The upregulation of CRH mRNA expression in the hypothalamus has also been reported in associated with increased inflammatory markers (Avishai-Eliner et al, 2002; Brunson et al, 2001; Hatalski et al, 1998), suggesting early life stress exerts its influence across multiple brain regions. Thus, the development of brain injury in early life, may have implications for HPA axis function and GC handling. This is important, since in many preterm infants, brain injury may be a component of metabolic disturbance (Blüml et al, 2014). The analysis of the effects of early life stress on pro-inflammatory markers during early development, has yet to be conducted in the current study, thus, disruption of the BBB via enhanced inflammatory response can only be speculated at this time.

6.4.4 Study limitations

The experimental design of the study was primarily set up to assess the effects of WBV on the development of brain injury (neuronal damage in the cortex), with secondary aims to evaluate additional organ dysfunction. The development of this rodent model is the first to use WBV to explore the genetic profile of BAT. Previous rodent studies of early life stress have predominantly employed maternal separation, since maternal care; licking and grooming and delivery of milk to the gut (Suchecki et al, 1993), is an essential part of HPA axis development during the HRP. However, WBV is not an uncommon approach and has been used as a popular intervention to explore the development of brain injury in Sprague Dawley rats (Yan et

al, 2015). Thus, I was opportunistic in utilising this model to test further hypotheses, in order to maximise the amount of information obtained per animal. The study therefore considered the three ethical principles of animal welfare (The three Rs) (Russell, Burch, & Universities Federation for Animal, 1992) by using Reduction alternatives to avoid the subsequent additional use of animals; Refinement alternatives, by initially only obtaining 1 pregnant dam to the biomedical sciences unit to ensure that the WBV intervention did not result in harm to the pups and; Replacement alternatives, using rodents instead of newborn infants to assess of early life stress on aspects of neurobiological and BAT characteristics.

The addition of a maternal control group for PND 7 and PND 21 would have benefited this study, had the early life stress model been developed to assess BAT characteristics. The controls would have remained with their dams, without handling, until the relevant day of sacrifice. This is important since brief maternal separation for 15 minutes during the HRP has been shown to influence corticosterone concentrations during development and in adulthood (Moussaoui et al, 2016). The study would therefore reduce any confounding effect of additional stress on the response of to selected genes. However, both groups in the current study, experienced maternal separation for equal periods of time.

Further, on PND 1, pups from the 6 dams were sexed and then randomised into separate cohorts. Cohorts were designed to split the pups evenly, though some cohorts were uneven in pup numbers in control and WBV groups. To correct for the effects of genetic variation when comparing control and WBV groups, samples from 1 pup per dam per treatment group were analysed. However, not all dams had pups in control and WBV at PND 7 and PND 21 developmental time points. Thus, ANOVAs corrected for multiple comparisons, were conducted to take into account the influence of genetic similarity. Ideally, randomization would result in 6 samples per dam (PND 7, Control with dam [n=1], maternally separated control [n=1], WBV [n=1]; PND 21, Control with dam [n=1], maternally separated control [n = 1], WBV [n=1]).

With regards to the data analysed in the current study, it was limited to analysis of mRNA expression of a handful of BAT responsive genes, in part due to the difficulties in obtaining a stable reference gene pair.

Literature regarding qPCR analysis of human and rodent BAT utilising samples from perirenal and interscapular depots, has identified robust reference genes, including; TATA binding protein (TBP) (Cypess et al, 2013; Svensson et al, 2014; Taube et al, 2015); cyclophiliactin (ACTB) (Lee et al, 2011; Lidell et al, 2013; Sun et al, 2015); glyceraldehyde-3-phosphate dehydrogenase (GAPDH) (Chechi et al, 2013) and; large ribosomal protein P0 (RPLP0) (Svensson et al, 2014; Svensson et al, 2011; Yam et al, 2017). However, BAT is heterogeneous, reflected in the variable M values (Cypess et al, 2013; Svensson et al, 2014). Variability within the reference genes may also increase the total variability of the results. In the current study, a large amount of variation within three of the reference genes was identified, potentially due to the nature of the intervention in young pups. Yam and colleagues (2017) demonstrated the use of TBP and RPLPO as stable housekeeping genes in a study of stress on rodent BAT, in pups at PND 9 (Yam et al, 2017). Whereas, WBV studies to assess BAT in adult rats, have utilised ACTB and B2m as most stable reference genes (Sun et al, 2015). This issue affected the amount of time which subsequently could be allocated to analysing further BAT genes of interest, including GR and PGC1α. A stronger consensus of which housekeeping genes to use in the analysis of human and rodent BAT is required and would increase comparability of different gene expression studies as well as the fidelity of the results.

As mentioned previously, the current study assessed changes in mRNA expression in a handful of BAT genes. Whilst changes in mRNA expression indicate the tissue responsiveness to a stimulus, used alone, such changes are not valid parameters for estimating BAT physiological function. Whether mRNA changes would be translated into protein upon 24 hours after stress are unknown, since there is a delay between the increased mRNA levels and increased UCP1 protein levels particularly with UCP1 (Nedergaard and Cannon, 2007), thus, this is a clear limitation to body

temperature measures and UCP1 itself. Further studies therefore require additional protein analysis to understand the biological relevance of early life stress on BAT phenotype (Golozoubova, Cannon and Nedergaard, 2006; Nedergaard and Cannon, 2007). Additionally, the effect of stress on the turnover of mRNA in BAT responsive and proliferative genes such as UCP1, β3-AR, FGF21, PPARγ is rapid. The half-life of specifically UCP1 mRNA, is in the order of some hours, depending on physiological conditions i.e. housing temperatures (Jacobsson, Cannon and Nedergaard, 1987; Pico et al, 1994). The standard laboratory housing temperature for rodents is ≈21-22 °C (Cui et al, 2016), however suggestions that this temperature imposes a metabolic stress on the rodent, have stemmed from observations that mice have three times greater metabolic rates than their resting metabolic rate when housed at this temperature (Fischer, Cannon & Nedergaard, 2018). Whereas, in rodents housed within their thermoneutral zone encompassing some degrees around 30 °C, energy expenditure to maintain body temperature is minimal (Lichtenbelt et al, 2014) and mice displayed a decrease in the expression of thermogenic program in both brown and white fat depots with larger adipocytes (Cui et al, 2016). Thus, animal housing conditions may have a significant impact on the outcomes of metabolic studies (Cannon & Nedergaard, 2011; Feldmann et al, 2009). In addition to housing temperatures, large diurnal variations in UCP1 mRNA levels have been observed, with day/ night conditions halving or doubling UCP1 mRNA levels (Cannon and Nedergaard, 2007). These data infer that mRNA of BAT thermogenic genes is extremely sensitive to acute events, which must be taken into consideration when designing a rodent model of early life stress.

Considering the multitude of effects of stress on adipose tissue characteristics and HPA axis development observed from the plethora of early life studies, a larger scaled study would be required to include components of the HPA axis; CRH, ATCH, corticosterone production and pro-inflammatory markers, together with further BAT characteristics such as GR. Incorporation of such components, would provide a well-rounded insight into

the effects of early life stress during developmental time points and into adulthood.

6.5 Conclusion

To my knowledge, there are no previous studies of single, acute early life stress which focus on the alterations in HPA axis responsiveness and its consequential alterations in BAT characteristics solely during early development. Clearly, stress experienced during the first few weeks of life can induce a heightened corticosterone response during adulthood, which may blunt the negative feedback loop of the HPA axis, thereby mediating changes to HPA function and BAT (Figure 6.7). Although WBV was capable of mounting a corticosterone response associated with elevations in its activating enzyme, 11β-HSD1, in pups at 21 days of age, its failure to elicit significant changes in many of the BAT genes analysed, including UCP1, maybe a functional limitation of assessments during a short-time frame of early life development and of a single bout of stress during early life, considering previous chronic studies have demonstrated reductions in BAT characteristics in adulthood. The functional significance of this data is limited without future protein analysis and future work is required to assess UCP1 protein content as well as mRNA in a chronic model of WBV induced in the early development period, which may induce marked effects on brain structure, function and AT characteristics during the pre-pubertal period and in later life.

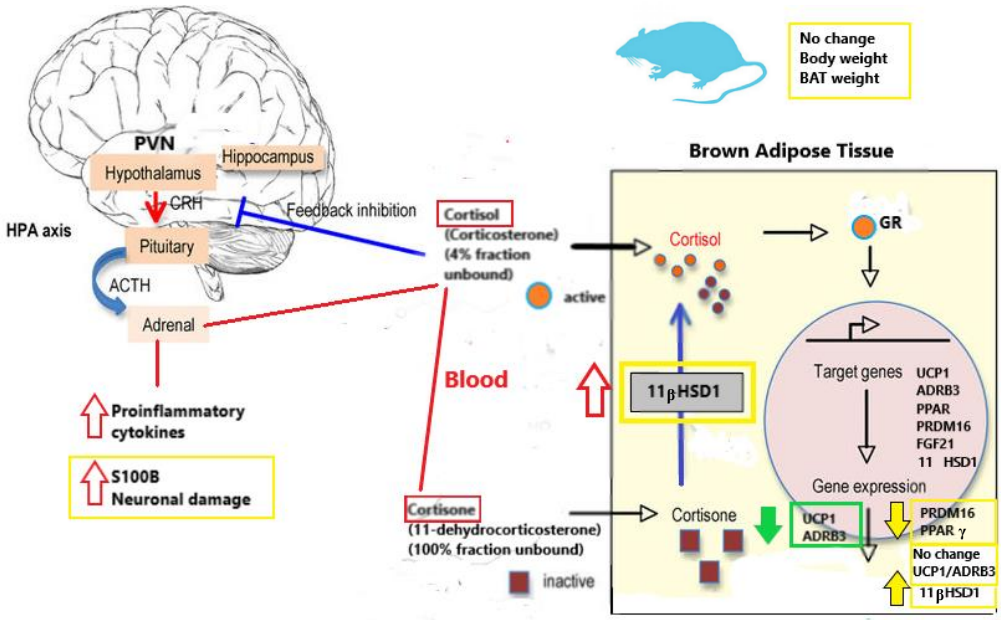

Figure 6.7. Early life stress-induced effects on HPA axis regulation and BAT characteristics in rodents

Early life stress induced by WBV at PND 7 was not shown to increase the stress-hormone corticosterone, or mediate alterations in BAT genes, due to the protective effects of the stress-hyporesponsive period in the first two weeks of life. At PND 21, WBV increased corticosterone concentrations, which was associated with elevations in mRNA expression of its activating enzyme; 11β-HSD1, in BAT. WBV induced at this age, also demonstrated to reduce mRNA expression of transcription factors PRDM16 and PPARγ, with no effects on UCP1 or the β3-AR through with its acts. Mechanisms driving the reductions in BAT genes have been directed towards dysfunction of the HPA axis resulting in the elevation of the 11β-HSD1 enzyme. Although further studies are required to investigate the effects of WBV stress in early life on HPA axis functionality; concentrations of CRH and ATCH, as well as the subsequent downstream effects on 11β-HSD1 and BAT genes. Observations demonstrated from the current study are in yellow boxes. Observations from published studies of early life stress effects in adult rodents, are in green boxes. Figure modified from (Yau & Seckl, 2012).

Chapter 7

Conclusion

Overall aims

The re-discovery and definitive identification of functional BAT in adult humans, demonstrates the importance of this tissue beyond that of thermoregulation at birth (Avishai-Eliner et al, 2002; Cypess et al, 2009; Saito et al, 2009; Virtanen et al, 2009). My thesis aimed to explore the potential for standardised and reproducible non-invasive methodologies to assess BAT activation in humans and in particular, those methodologies that may be more suitable for children and babies.

This thesis supports the use of IRT in the measurement of BAT activation in healthy adults during pharmacological and cold-stimulated means. The complementary use of NIRS in addition to IRT, revealed BAT heat production is accompanied by increased blood flow at the surface of the skin overlying the SCR region. Both of these technologies allow for the real-time assessment of BAT function in adult humans. This thesis also aimed to develop an imaging protocol to utilise IRT to investigate BAT function in newborn infants. This study demonstrated the challenging nature of performing IRT in this population and methodologies will require future development. However, there is great potential for this technique to successfully analyse BAT heat production in newborn infants.

This thesis also aimed to explore the role of GCs and stress on BAT, given that excess GCs may alter lipid characteristics (Chanson and Salenave, 2010; Min, 2016). However, studies investigating the effects of excess GCs on BAT function are limited. This thesis demonstrates that the pharmacological induction of hypercortisolaemia results in an increase in BAT activity in healthy adults, presumably through enhanced UCP1 activity. Furthermore, BAT plays a vital thermoregulatory role at birth (in humans) and during early life in rodents, for which alterations in the HPA axis regulation and its end-point cortisol (corticosterone in rodents) due to stress

experienced prenatally, or during the critical early-postnatal developmental period, can modify BAT function (Feve et al, 1992; Miki et al, 2013) and influence subsequent disease risk in later life. Thus, my study also aimed to develop a rodent model to explore the effects of stress in the early postnatal period on key genes in rodent BAT during critical developmental time. Whilst stress induced at PND 21 elevated corticosterone levels, there were no effects acute period of stress on important BAT thermoregulatory genes at this age. Future studies should continue to investigate the effects of stress induced in early life on the long-term regulation of BAT function.

Summary of Findings

GCs modulate effects on BAT function

Thermogenesis in mammals is tightly controlled and orchestrated by the brain (Cannon & Nedergaard, 2004). Stress-induced activation of the HPA axis not only induces catecholamine release by the PVN and the subsequent binding to β3-AR in brown adipocytes, but also elevates GC release from the adrenals; the end-product of HPA axis. The increase in GC in response to acute stress promotes adaptation and recovery through a negative feedback loop. Cortisol also plays a major stimulatory role at birth, initiating thermogenic function, for adaption to the extra uterine environment. However, HPA axis dysfunction and excess GC exposure is associated with obesity and the metabolic syndrome during adulthood (Macfarlane et al, 2008). In adults, chronic hypercortisolism is the pathophysiologic underpinning of Cushing's syndrome (Abraham, Rubino and Nieman, 2013; Chrousos, 2000) and excess GCs may play a role in the development of obesity and alterations in lipid characteristics (Chanson and Salenave, 2010; Min, 2016). However, studies investigating the effects of excess GCs on BAT function are limited. This thesis demonstrates that the pharmacological induction of hypercortisolaemia results in an increase in

BAT activity in healthy adults, presumably through enhanced UCP1 activity. The mechanisms underpinning enhanced BAT activity during elevated cortisol concentrations requires further investigation, however, Ramage and colleagues (2016) have suggested that variations in the regulation of UCP1 between species, could play a major role (Ramage et al, 2016).
In rodents, stress experienced in the early postnatal development period during hypo-responsiveness of low-circulating cortisol, is known to result in the hyper-activation of the HPA axis (Moussaoui et al, 2016; Schmidt et al, 2003) and it's associated with increases in body weight and reductions in the expression of BAT genes including UCP1 and β3-AR, during adulthood (Miki et al, 2013; Nilsson et al, 2002). This thesis demonstrates a single, short period of stress was associated with large increases in corticosterone, compared to age matched controls at PND 21, but not at PND 7. Acute stress was found to reduce the expression of important genes not directly involved in thermogenesis, namely, PRMD16 and PPARγ at PND21 and did not alter genes vital for BAT thermogenic function, namely, UCP1 and β3-AR at this age. The importance of these findings require further work to establish if these have any long-term and functional implications.

BAT assessment using non-radioactive technologies

Use of IRT in human population

The use of PET-CT with $^{[18]}$F-FDG has been instrumental in the identification of BAT in humans. Due to the risk of radiation with the use of this method, focus has been directed towards alternative measures of BAT activation. This thesis successfully demonstrates the use of IRT in the measurement of BAT activation in healthy adults during pharmacological and cold-stimulated means. This work contributes to the plethora of studies over the past 7 years which have collectively established IRT as a valid tool for the assessment of BAT function in humans as well as rodents (Ang et al, 2017; El Hadi et al, 2016; Gatidis et al, 2016; Jang et al, 2014; Law et al, 2017; Lee et al, 2011; Peterson et al, 2016; Robinson et al, 2016; Salem et al, 2016; Symonds et al, 2012) This thesis also reveals the challenges

surrounding the use of IRT for the assessment of BAT in newborn infants. Further studies are required to develop the imaging protocol devised here, however, there is great potential for this methodology to successfully assess surface skin temperature over known BAT regions in infants.

NIRS

A common reported criticism of IRT is that the increase in heat deposition over the SCR region has been suggested to be due to increased blood flow, rather than due to purely BAT activation (Ang et al, 2017; Law et al, 2018). While it can be acknowledged that an increase in surface skin blood flow can account for the increase in heat energy output detected by IRT, this thesis supports the increased IR heat power over the SCR is related to BAT activation. This thesis revealed that BAT activation (surface skin temperature) is accompanied by an increase in tissue blood flow potentially due to the increased demands of oxygen and nutrients required for thermogenesis. This thesis supports an association between increased BAT thermogenesis and increased perfusion. However, it is clear that during cold-exposure, the expected physiological thermoregulatory response is to conserve body heat by vasoconstriction, which reduced heat loss through shunting blood away from the skin, as demonstrated by the reduction in oxygenation in the cooled forearm.

Study limitations

The use of continuous wave NIRS system

Whilst this study demonstrated the capability of continuous wave NIRS in sampling tissue oxygenation of healthy adults, this device can only provide relative values of tissue oxygenation. continuous wave NIRS devices cannot assess the path of NIR light through biological tissues (Hamaoka et al, 2011). More detailed inferences about tissue oxygen use over supply are possible, but with the use of more complex NIRS systems, which require a greater depth of understanding and come at a cost. Time-resolved NIRS

can non-invasively quantify optical properties of tissue such as the light path length, absorption coefficient (μ_a), reduced scattering coefficient (μ_s'), tissue oxygenation [oxy-Hb], deoxygenation [deoxy-Hb], and total hemoglobin [total-Hb] concentrations (Hamaoka et al, 2007). Given that BAT has abundant capillaries and mitochondria compared to WAT, BAT density has been assessed using quantitative indicators of total-Hb; an index of blood volume or tissue vasculature and reduced scattering coefficient (μ_s'); an index of mitochondrial concentration, demonstrating these parameters to correlate with $^{[18]}$F-FDG uptake (Nirengi et al, 2015). Future work should aim to develop understandings of the metabolic capabilities of BAT in adults and in children utilising time-resolved NIRS, with focus on how skin thickness may alter light scattering properties, since this will be an important factor in the future use of this device in obese individuals at any age.

IRT imaging in newborns

The protocol devised in this study was based on previous exploratory protocols from the assessment of limb skin temperatures in preterm infants (Abbas et al, 2011). Whilst these studies were focused on premature infants, my study focused on the measurement of surface skin temperatures over the back in healthy term infants, and thus, the imaging platform was amended to suit the physiological development of these infants. Challenges in imaging the infants arose in both phases of the study. Many thermograms capture during phase 1 were excluded due to reflective heat from the overhead heater. In phase 2, thermograms were captured from full-term infants laid in an open cot. Whilst, this approach enabled the acquisition of clearer, non-distorted thermograms, the length of study time opened up the possibility for infants to become distressed. Thus, numerous infants were excluded from the study due to demonstrating restless behaviours, which in turn resulted in movement artefacts.

Future developments in imaging protocols for neonatal BAT heat detection, should consider the use of alternative IRT means, such as IRT video

to ease the disruption to the neonatal environment and alteration of the imaging platform to include a custom made camera hole in the top of a full incubator (Owen & Ramlakhan, 2017). Certainly the development of a non-contact imaging protocol in these infants, would be beneficial for the assessment of BAT function and its influence on metabolic health.

Challenges of modelling early life stress in rodents

Due to the fundamental differences in brain maturation between humans and rodents, careful consideration must be taken during study design and when translating findings to a clinical context. Original observations attempted to compare the developmental stages of rodent and human brains based on the single variables of brain growth (Dobbing & Sands, 1979) and brain weight (Clancy et al, 2007). However, since brain regions develop at varying rates (Clancy, Darlington & Finlay, 2001), using anatomical brain weight alone does not consider its functional maturation (Romijn, Hofman & Gramsbergen, 1991). Thus, studies modelling human development in rodents should consider a developmental time point where a variable of the brain in a rodent coincides with the development of the same outcome variable in the infant (Craig et al, 2003). Based on the views of Craig et al (2003), in the current study, WBV stress was conducted at postnatal days 7 and 21, which corresponded to a 32 gestational week human infant and a full term infant respectively (Craig et al, 2003).

An abundance of data on the maturation of the brain in various species show the complexities of developmental timing (Clancy et al, 2001; Craig et al, 2003; Romijn et al, 1991). Thus, attention must be taken to the study design and outcome of interest, when using rodent models of early developmental neonatal life.

Selecting an intervention of early-life stress

Various paradigms of postnatal early life stress in rodents and humans have explored the effects of environmental insults on metabolic function.

Mother-offspring interactions such as licking and feeding providing critical input for normal neurobiological development and HPA axis function (Suchecki et al,1993; van Oers et al, 1998). Alterations in maternal care have been demonstrated to impact on the development of adipose tissue and the transcription of BAT genes (Ivy et al, 2008; Miki et al, 2013), which may favour the proliferation of WAT in later life (Miki et al, 2013).

A small number of rodent studies have explored the effects of WBV on neurovascular injury and muscle metabolism (Hubbard et al., 2015; Yan et al, 2015). have used this model for the first time to study BAT gene expression. Although WBV did not significantly alter the expression of BAT specific thermoregulatory genes, WBV did elevate corticosterone concentrations at PND 21, by 5.5 fold greater than that which has previously been reported upon 8 hours of maternal deprivation at this age (Schmidt et al, 2001). Thus, WBV was considered as an effective acute early life stress intervention.

Future work and perspectives

GCs modulate adipose tissue function

GCs are powerful regulators of energy metabolism. Abnormalities in the responsiveness of the HPA axis or excess cortisol secretion, has been associated with obesity (Marin et al, 1992), type 2 diabetes and dyslipidaemia (Macfarlane, Forbes and Walker, 2008). These observations are supported by findings which have demonstrated adrenalectomy reduces body fat mass and increase BAT activity (Ashizawa et al, 2007). In rodents, the use of the GR antagonist, RU38486 can increase BAT thermogenesis and UCP1 levels (Beukel et al, 2014; Strack et al, 1995). Similarly, the pharmacological inhibition of 11β-HSD1 or knockout, enhances BAT activation in murine brown adipocytes (Liu et al, 2013). Such effects are suggested to be mediated through the GC-induced hypothalamic influences on BAT activity and potentially by the enzyme, 11β-HSD1 (Berthiaume et al, 2004;

Stimson et al, 2009). Future studies should therefore continue to investigate the effects of steroids on metabolism and adipose tissue regulation to gain greater insights into the mechanistic underpinning of acute and chronic effects of GC on disease development. Particularly since it is unknown whether the disturbances in cortisol secretion and 11β-HSD1 enzyme activity, are a cause or a consequence of obesity.

Greater work to decipher the abnormalities in energy storage associated with excess GCs especially in early in life, is required since excess GC exposure pre- and perinatally, has been demonstrated to result in increased body weight and abdominal fatness (Modi et al, 2006) and influence mortality risk. Despite the surge in interest in examining early life programming of later disease risk in both humans and rodents, progress in this field will require a greater level of consistency.

Inconsistency in the observed alterations in BAT gene expression across studies, could be due to marked differences in study design. A broad variation in protocols fall under the term 'early life stress', including MS and LNS. Thus, the duration, age at time of study, room temperature, whether pups are isolated from littermates, and whether pups return to their dams or continued to be isolated after intervention, have all been shown to influence brain function and adipose tissue development, differently.

Rodent models using MS as an intervention of stress in early life, must therefore consider the influence of maternal care on long-term outcomes, particularly since preterm infants have a reduced maternal contact in early life. The use of rodent models permits the exploration of the mechanisms regulating adipose tissue development and components of HPA axis, under conditions of stress in early postnatal life.

Animal models should also reflect the human conditions upon which they are based, conveying the need for adequate and valid controls. Further, the combined utilisation of non-invasive techniques such as IRT for measuring skin temperature in rodents and humans, NIRS for the assessment of BAT oxygenation, doubly labelled water for measuring energy expenditure and the measurement of cortisol concentration in saliva, collectively will aid to

shed more light on this important field of research in endocrinology and nutrition.

Surrogate assessments of BAT activity and function

In the last decade, the increased development of multiple techniques to more accurately assess substrate metabolism and heat production by BAT, have enabled a greater insight into BAT's potential role in energy metabolism (Cypess & Kahn, 2010; van Marken Lichtenbelt et al, 2002; van Marken Lichtenbelt et al, 2009). This thesis provides supporting evidence for the use of recently developed methods of quantitative IRT and NIRS for studying BAT function in healthy humans, which can be used in a serial fashion to assess BAT activation over multiple time points in individual subjects. These techniques have the advantages of being cost efficient and free of radiation. However, before these measurements can be fully evaluated and widely utilised for the assessment of BAT metabolism, the optimisation and standardisation of cold-exposure protocol along with imaging protocols must be implemented regardless of the modality (Law et al, 2017).

Significant challenges also remain to ensure the reproducibility in imaging acquisition and analysis to enable the comparison of results. IRT protocols to assess BAT heat production of the SCR region in adults, suggest that the subject should be seated in a chair with the IRT camera positioned at 1m away from the face (Law et al, 2017; Symonds et al, 2012), while thermograms are acquired at predefined intervals of between 15 seconds and 5 minutes (Law et al, 2017; Lee et al, 2011; Ramage et al, 2016; Robinson et al, 2014; Salem et al, 2016; Symonds et al, 2012). Certainly in infants, where the major BAT depot it located in the interscapular region (Gilsanz, Hu and Kajimura, 2013), such recommendations have to be amended and the infant environment (imaging platform) and imaging distance, need to be carefully considered in accordance with the physiology of the infant (i.e. pre-term infants with thin skin and very little/no subcutaneous fat vs.

full-term infants with a layer of subcutaneous fat; Knobel et al, 2017). Future studies using IRT to assess BAT heat production in newborn infants, should attempt to capture images from specially-designed incubators such as a cut-out in the roof, to minimise any disruption to the newborn.

Future work utilising IRT will ultimately involve further development and optimisation of thermogram processing tools for BAT quantification. Thermograms are analysed using vendor provided software (FLIR R&D) (El Hadi et al, 2016; Jang et al, 2014; Ramage et al, 2016; Robinson et al, 2016; Symonds et al, 2012) programming platforms, with specifically designed algorithms (MatLab) (Law et al, 2017; Peterson et al, 2016) and commercially available software (Gatidis et al, 2016; Salem et al, 2016). Once the image has been opened within the desired software, the region of interest (ROI) needs to be identified and further, analysed. However, ROIs defining the skin overlying both the SCR and control regions have not been consistent amongst studies (Knobel et al, 2017; Law et al, 2017; Robinson et al, 2017). The SCR region has been defined by using circular, squared or triangular ROIs and manual approximations of the contour of the shoulder between the clavicle and sternocleidomastoid muscle (Law et al, 2017). Unfortunately, these processes rely on variable degrees of subjective placement and/or poor approximation to the contour of the neck (El Hadi et al, 2016) and may result in apparent inclusion of the background region (Peterson et al, 2016). Ang and colleagues have proposed the seeded approach which has the benefit of identifying a discrete single hotspot of the highest temperature (i.e. the 'seed') and expanding it to include voxels, which share a set of defined characteristics (Ang et al, 2017).

The proposed use of NIRS as a surrogate BAT assessment tool, has generated interest, since this non-invasive technique is sensitive to hemodynamic changes and is capable of assessing fluctuations in blood flow, volume, and oxygenation over a region of interest (Niwayama, Murata and Shinohara, 2006). Indeed, this thesis demonstrates its potential use in the assessment of BAT activity, alongside other studies which have reported a strong positive correlation between BAT density (i.e. basal vascularity and mitochondrial density) and $^{[18]}$F-FDG uptake in BAT, suggesting that NIRS

may be capable of detecting BAT presence independent of cold exposure (Nirengi et al, 2015). However, as demonstrated in the study by Hartwig and colleagues, optic imaging NIRS can suffer from photon absorption and scatter, which worsens with depth and tissue density (Hartwig et al, 2017). Thus, NIRS could be highly influenced by the thickness of subcutaneous adipose tissue and is limited to measuring to the depth of 4cm, with potential susceptibility to noise created by the cross-talk of nearby tissues (i.e. blood flow of large upper thorax and neck vessels).
Future work within the functional assessment of BAT using such tools, will therefore pose a greater level of complexity and require greater computational processing tools and algorithms (Law et al, 2017). However, the continuous development of sensitive, safe, portable, low cost tools for assessing BAT activity in humans and rodents, is an attractive proposition and will help to drive the field forward in gaining an understanding of BAT morphology and function.

Research is still delignating the differences in BAT physiology, morphology and regulation in early-life and adulthood. The findings in this thesis shed light on the regulation of BAT activity and specific genes required for its function, during situations of heightened cortisol concentrations during early life and adulthood. This thesis also demonstrates the development of non-invasive tools to assess BAT activity in real-time in humans with particular relevance to children as the tools are non-invasive and radiation free. The importance of future developments of tools to measure BAT function should not be ignored, since the dysregulation of BAT may hold implications for metabolic disease risk.

References

Abbas, A. K., Heimann, K., Jergus, K., Orlikowsky, T., & Leonhardt, S. (2011). Neonatal non-contact respiratory monitoring based on real-time infrared thermography. *BioMedical Engineering OnLine, 10*(1), 93.

Abbas, A. K., & Leonhardt, S. (2014). Intelligent neonatal monitoring based on a virtual thermal sensor. *BMC Medical Imaging, 14*, 9-9.

Adelman, R., D., Restaino, I, R., Alon, U, S., Blowey, D, L. (2001). Proteinuria and focal segmental glomerulosclerosis in severely obese adolescents. *Journal of Pediatrics, 138*, 481-485.

Aherne, W., & Hull, D. (1966). Brown adipose tissue and heat production in the newborn infant. *The Journal of pathology and bacteriology, 91*(1), 223-234.

Ahmad, Q. I., Ahmad, C. B., & Ahmad, S. M. (2010). Childhood Obesity. *Indian J Endocrinol Metab, 14*(1), 19-25.

Akesson, L., Hawkins, T., Jensen, R., Fuller, J. M., Breslow, N. E., & Lernmark, A. (2007). Decreased core temperature and increased beta(3)-adrenergic sensitivity in diabetes-prone BB rats. *Diabetes Technol Ther, 9*(4), 354-362.

Alberto, M. (2000). *Principles of cardiovascular neural regulation in health and disease*. Boston, Mass. ; London : Kluwer Academic, c2000: Boston, Mass. ; London : Kluwer Academic, c2000.

Alexander, G., & Bell, W. (1975). Quantity and calculated oxygen consumption during summit metabolism of brown adipose tissue in newborn lambs. *Neonatology, 26*(3-4), 214-220.

Altholtz, L. Y., Fowler, K. A., Badura, L. L., & Kovacs, M. S. (2006). Comparison of the Stress Response in Rats to Repeated Isoflurane or CO2:O2 Anesthesia Used for Restraint During Serial Blood Collection via the Jugular Vein. *Journal of the American Association for Laboratory Animal Science, 45*(3), 17-22.

American Heart Association. (1997). Heart and Stroke Statistics. Retrieved from http://www.heart.org/en/about-us/heart-and-stroke-association-statistics

Andersen, S., Kleinschmidt, K., Hvingel, B., & Laurberg, P. (2012). Thyroid hyperactivity with high thyroglobulin in serum despite sufficient

iodine intake in chronic cold adaptation in an Arctic Inuit hunter population. *Eur J Endocrinol, 166*(3), 433-440.

Ando, H., & Noguchi, R. (2003). Dependence of palmar sweating response and central nervous system activity on the frequency of whole-body vibration. *Scandinavian Journal of Work, Environment & Health, 29*(3), 216-219.

Andrews, E. T., Ashton, J. J., Pearson, F., Beattie, R. M., & Johnson, M. J. (2018). Early postnatal growth failure in preterm infants is not inevitable. *Archives of Disease in Childhood - Fetal and Neonatal Edition*.

Andrews, J. A., & Neises, K. D. (2012). Cells, biomarkers, and post-traumatic stress disorder: evidence for peripheral involvement in a central disease. *J Neurochem, 120*(1), 26-36.

Andrews, R. C., Herlihy, O., Livingstone, D. E., Andrew, R., & Walker, B. R. (2002). Abnormal cortisol metabolism and tissue sensitivity to cortisol in patients with glucose intolerance. *J Clin Endocrinol Metab, 87*(12), 5587-5593.

Ang, Q. Y., Goh, H. J., Cao, Y., Li, Y., Chan, S. P., Swain, J. L., Henry, C. J., Leow, M. K. (2017). A new method of infrared thermography for quantification of brown adipose tissue activation in healthy adults (TACTICAL): a randomized trial. *J Physiol Sci, 67*(3), 395-406.

Arch, J. R. S. (2011). Challenges in β(3)-Adrenoceptor Agonist Drug Development. *Therapeutic Advances in Endocrinology and Metabolism, 2*(2), 59-64.

Arita, Y., Kihara, S., Ouchi, N., Takahashi, M., Maeda, K., Miyagawa, J-I., Hotta, K., Shimomura, I., Nakamura, T., Miyaoka, K. (1999). Paradoxical decrease of an adipose-specific protein, adiponectin, in obesity. *Biochemical and biophysical research communications, 257*(1), 79-83.

Arya, M., Shergill, I. S., Williamson, M., Gommersall, L., Arya, N., & Patel, H. R. (2005). Basic principles of real-time quantitative PCR. *Expert Rev Mol Diagn, 5*(2), 209-219.

Ashizawa, N., Takagi, M., Seto, S., Suzuki, S., & Yano, K. (2007). Serum adiponectin and leptin in a patient with Cushing's syndrome before and after adrenalectomy. *Intern Med, 46*(7), 383-385.

Arbor Assays. (2018). *Arbour Assays Builds Detection and Immunoassay Products.* [online] Arbor Assays. Available at: https://www.arborassays.com/.

Astrup, A., Bulow, J., & Madsen, J. (1984). Interscapular brown adipose tissue blood flow in the rat. Determination with 133xenon clearance compared to the microsphere method. *Pflugers Arch, 401*(4), 414-417.

Astrup, A., Bulow, J., Madsen, J., & Christensen, N. J. (1985). Contribution of BAT and skeletal muscle to thermogenesis induced by ephedrine in man. *Am J Physiol, 248*(5 Pt 1), E507-515.

Au-Yong, I. T., Thorn, N., Ganatra, R., Perkins, A. C., & Symonds, M. E. (2009). Brown adipose tissue and seasonal variation in humans. *Diabetes, 58*(11), 2583-2587.

Avishai-Eliner, S., Brunson, K. L., Sandman, C. A., & Baram, T. Z. (2002). Stressed-out, or in (utero)? *Trends in Neurosciences, 25*(10), 518-524.

Avishai-Eliner, S., Yi, S. J., Newth, C. J., & Baram, T. Z. (1995). Effects of maternal and sibling deprivation on basal and stress induced hypothalamic-pituitary-adrenal components in the infant rat. *Neurosci Lett, 192*(1), 49-52.

Babcock, L., Byczkowski, T., Wade, S. L., Ho, M., & Bazarian, J. J. (2013). Inability of S100B to Predict Post-Concussion Syndrome in Children who Present to the Emergency Department with Mild Traumatic Brain Injury: A Brief Report. *Pediatric emergency care, 29*(4), 458-461.

Bachman, E. S., Dhillon, H., Zhang, C.-Y., Cinti, S., Bianco, A. C., Kobilka, B. K., & Lowell, B. B. (2002). βAR signaling required for diet-induced thermogenesis and obesity resistance. *Science, 297*(5582), 843-845.

Bakker, L. E., Boon, M. R., van der Linden, R. A., Arias-Bouda, L. P., van Klinken, J. B., Smit, F., Verberne, H. J., Jukema, J. W., Tamsma, J. T., & Havekes, L. M. (2014). Brown adipose tissue volume in healthy lean south Asian adults compared with white Caucasians: a prospective, case-controlled observational study. *The Lancet Diabetes & Endocrinology, 2*(3), 210-217.

Banet, M., & Hensel, H. (1976). Nonshivering thermogenesis induced by repetitive hypothalamic cooling in the rat. *American Journal of Physiology--Legacy Content, 230*(2), 522-526.

Barbazanges, A., Piazza, P. V., Le Moal, M., & Maccari, S. (1996). Maternal glucocorticoid secretion mediates long-term effects of prenatal stress. *J Neurosci, 16*(12), 3943-3949.

Barclay, J. L., Agada, H., Jang, C., Ward, M., Wetzig, N., & Ho, K. K. (2015). Effects of glucocorticoids on human brown adipocytes. *Journal of Endocrinology, 224*(2), 139-147.

Barker, D. J. (1992). Fetal growth and adult disease. *Br J Obstet Gynaecol, 99*(4), 275-276.

Barker, D. J. (1997). The long-term outcome of retarded fetal growth. *Clin Obstet Gynecol, 40*(4), 853-863.

Barlow, S. E., & Dietz, W. H. (1998). Obesity evaluation and treatment: expert committee recommendation. *Paediatrics, 102*, e29.

Barreau, F., Ferrier, L., Fioramonti, J., & Bueno, L. (2007). New insights in the etiology and pathophysiology of irritable bowel syndrome: contribution of neonatal stress models. *Pediatr Res, 62*(3), 240-245.

Bauwens, M., Wierts, R., van Royen, B., Bucerius, J., Backes, W., Mottaghy, F., & Brans, B. (2014). Molecular imaging of brown adipose tissue in health and disease. *Eur J Nucl Med Mol Imaging, 41*(4), 776-791.

Beauvoit, B., & Chance, B. (1998). Time-resolved spectroscopy of mitochondria, cells and tissues under normal and pathological conditions. In *Bioenergetics of the Cell: Quantitative Aspects* (pp. 445-455): Springer.

Bedrosian, T. A., & Nelson, R. J. (2017). Timing of light exposure affects mood and brain circuits. *Translational Psychiatry, 7*, e1017.

Bernardini, R., Iurato, M. P., Chiarenza, A., Lempereur, L., Calogero, A. E., & Sternberg, E. M. (1996). Adenylate-Cyclase-Dependent Pituitary Adrenocorticotropin Secretion Is Defective in the Inflammatory-Disease-Susceptible Lewis Rat. *Neuroendocrinology, 63*(5), 468-474.

Berry, D., & Daniel, H. (1970). Sympathetic nerve development in the brown adipose tissue of the rat. *Canadian journal of physiology and pharmacology, 48*(3), 160-168.

Berry, D. C., Stenesen, D., Zeve, D., & Graff, J. M. (2013). The developmental origins of adipose tissue. *Development, 140*(19), 3939-3949.

Berthiaume, M., Sell, H., Lalonde, J., Gelinas, Y., Tchernof, A., Richard, D., & Deshaies, Y. (2004). Actions of PPARgamma agonism on adipose tissue remodeling, insulin sensitivity, and lipemia in absence of glucocorticoids. *Am J Physiol Regul Integr Comp Physiol, 287*(5), R1116-1123.

Beukel, J. C. v. d., Grefhorst, A., Quarta, C., Steenbergen, J., Mastroberardino, P. G., Lombès, M., Delhanty, P. J., Mazza, R., Pagotto, U., Lely, A. J., & Themmen, A. P. N. (2014). Direct activating effects of adrenocorticotropic hormone (ACTH) on brown adipose tissue are attenuated by corticosterone. *The FASEB Journal, 28*(11), 4857-4867.

Bhutta, A. T., & Anand, K. J. (2002). Vulnerability of the developing brain. Neuronal mechanisms. *Clin Perinatol, 29*(3), 357-372.

Bianco, A. C., Salvatore, D., Gereben, B., Berry, M. J., & Larsen, P. R. (2002). Biochemistry, cellular and molecular biology, and physiological roles of the iodothyronine selenodeiodinases. *Endocrine reviews, 23*(1), 38-89.

Biddie, S. C., Conway-Campbell, B. L., & Lightman, S. L. (2012). Dynamic regulation of glucocorticoid signalling in health and disease. *Rheumatology (Oxford), 51*(3), 403-412.

Bispham, J., Budge, H., Mostyn, A., Dandrea, J., Clarke, L., Keisler, D. H., Symonds. M. E., & Stephenson, T. (2002). Ambient temperature, maternal dexamethasone, and postnatal ontogeny of leptin in the neonatal lamb. *Pediatric Research, 52*(1), 85-90.

Bjorntorp, P., & Rosmond, R. (2000). Obesity and cortisol. *Nutrition, 16*(10), 924-936.

Blaxter, L., Yeo, M., McNally, D., Crowe, J., Henry, C., Hill, S., Mansfield, N., Leslie, A. and Sharkey, D., 2017. Neonatal head and torso vibration exposure during inter-hospital transfer. *Proceedings of the Institution of Mechanical Engineers, Part H: Journal of Engineering in Medicine*, *231*(2), pp.99-113.

Blondin, D. P., Frisch, F., Phoenix, S., Guerin, B., Turcotte, E. E., Haman, F., Richard, D., & Carpentier, A. C. (2017). Inhibition of Intracellular Triglyceride Lipolysis Suppresses Cold-Induced Brown Adipose Tissue Metabolism and Increases Shivering in Humans. *Cell Metab, 25*(2), 438-447.

Blondin, D. P., Labbé, S. M., Turcotte, E. E., Haman, F., Richard, D., & Carpentier, A. C. (2015). A critical appraisal of brown adipose tissue metabolism in humans. *Clinical Lipidology, 10*(3), 259-280.

Blüml, S., Wisnowski, J. L., Nelson, M. D., Jr., Paquette, L., & Panigrahy, A. (2014). Metabolic Maturation of White Matter Is Altered in Preterm Infants. *PLoS One, 9*(1), e85829.

Bonet, M. L., Oliver, P., & Palou, A. (2013). Pharmacological and nutritional agents promoting browning of white adipose tissue. *Biochim Biophys Acta, 1831*(5), 969-985.

Boon, M. R., Bakker, L. E. H., van der Linden, R. A. D., Pereira Arias-Bouda, L., Smit, F., Verberne, H. J., van Marken Lichenbelt, W. D., Jazet, I. M., & Rensen, P. C. N. (2014). Supraclavicular Skin Temperature as a Measure of 18F-FDG Uptake by BAT in Human Subjects. *PLoS One, 9*(6), e98822.

Boss, O., Samec, S., Kühne, F., Bijlenga, P., Assimacopoulos-Jeannet, F., Seydoux, J., Giacobino, J-P., & Muzzin, P. (1998). Uncoupling Protein-3 Expression in Rodent Skeletal Muscle Is Modulated by Food Intake but Not by Changes in Environmental Temperature. *Journal of Biological Chemistry, 273*(1), 5-8.

Boss, O., Samec, S., Paoloni-Giacobino, A., Rossier, C., Dulloo, A., Seydoux, J., Muzzin, P., & Giacobino, J. P. (1997). Uncoupling protein-3: a new member of the mitochondrial carrier family with tissue-specific expression. *FEBS Lett, 408*(1), 39-42.

Bozkurt, A., Rosen, A., Rosen, H., & Onaral, B. (2005). A portable near infrared spectroscopy system for bedside monitoring of newborn brain. *Biomed Eng Online, 4*, 29.

Brent, G. A. (1994). The molecular basis of thyroid hormone action. *New England Journal of Medicine, 331*(13), 847-853.

Broeders, E., Bouvy, N. D., & van Marken Lichtenbelt, W. D. (2015). Endogenous ways to stimulate brown adipose tissue in humans. *Ann Med, 47*(2), 123-132.

Broeders, E. P., Vijgen, G. H., Havekes, B., Bouvy, N. D., Mottaghy, F. M., Kars, M., Schaper, N. C., Schrauwen, P., Brans, B., & van Marken Lichtenbelt, W. D. (2016). Thyroid Hormone Activates Brown Adipose Tissue and Increases Non-Shivering Thermogenesis-A Cohort Study in a Group of Thyroid Carcinoma Patients. *PLoS One, 11*(1), e0145049.

Brunson, K. L., Eghbal-Ahmadi, M., Bender, R., Chen, Y., & Baram, T. Z. (2001). Long-term, progressive hippocampal cell loss and dysfunction induced by early-life administration of corticotropin-releasing hormone reproduce the effects of early-life stress. *Proc Natl Acad Sci U S A, 98*(15), 8856-8861.

Budge, H., & Symonds, M. (2006). Fetal and neonatal nutrition—lipid and carbohydrate requirements and adaptations to altered supply at birth. *Textbook of Perinatal Medicine*, 1007-1016.

Bustin, S. A., Benes, V., Garson, J. A., Hellemans, J., Huggett, J., Kubista, M., Mueller, R., Nolan, T., Pfaffl, M. W., Shipley, G. L., Vandesompele, J., & Wittwer, C. T. (2009). The MIQE guidelines: minimum information

for publication of quantitative real-time PCR experiments. *Clin Chem, 55*(4), 611-622.

Całkosiński, I.,Dobrzyński, M., Rosińczuk, J., Dudek, K., Chrószcz, A.,Fita, K., & Dymarek, R. (2015). The Use of Infrared Thermography as a Rapid, Quantitative, and Noninvasive Method for Evaluation of Inflammation Response in Different Anatomical Regions of Rats. *BioMed research international, 2015*, 9.

Calogero, A. E., Sternberg, E. M., Bagdy, G., Smith, C., Bernardini, R., Aksentijevich, S., Wilder, R. L., Gold, P. W., & Chrousos, G. P. (1992). Neurotransmitter-induced hypothalamic-pituitary-adrenal axis responsiveness is defective in inflammatory disease-susceptible Lewis rats: in vivo and in vitro studies suggesting globally defective hypothalamic secretion of corticotropin-releasing hormone. *Neuroendocrinology, 55*(5), 600-608.

Cannon, B., & Nedergaard, J. (2004). Brown Adipose Tissue: Function and Physiological Significance. *Physiological Reviews, 84*(1), 277-359.

Cannon, B., & Nedergaard, J. (2011). Nonshivering thermogenesis and its adequate measurement in metabolic studies. *J Exp Biol, 214*(Pt 2), 242-253.

Cao, W., Medvedev, A. V., Daniel, K. W., & Collins, S. (2001). β-adrenergic activation of p38 MAP kinase in adipocytes cAMP induction of the uncoupling protein 1 (UCP1) gene requires p38 map kinase. *Journal of Biological Chemistry, 276*(29), 27077-27082.

Carey, A. L., Formosa, M. F., Van Every, B., Bertovic, D., Eikelis, N., Lambert, G. W., Kalff, V., Duffy, S., Cherk, M. H., & Kingwell, B. A. (2013). Ephedrine activates brown adipose tissue in lean but not obese humans. *Diabetologia, 56*(1), 147-155.

Carmen Wong, K. Y., Wong, V., Ho, J. T., Torpy, D. J., McLean, M., & Cheung, N. W. (2010). High cortisol levels in hyperglycaemic myocardial infarct patients signify stress hyperglycaemia and predict subsequent normalization of glucose tolerance. *Clin Endocrinol (Oxf), 72*(2), 189-195.

Carpentier, A. C., Blondin, D. P., Virtanen, K. A., Richard, D., Haman, F., & Turcotte, É. E. (2018). Brown Adipose Tissue Energy Metabolism in Humans. *Frontiers in Endocrinology, 9*(447).

Carter, E. A., Bonab, A. A., Paul, K., Yerxa, J., Tompkins, R. G., & Fischman, A. J. (2011). Association of Heat Production with 18F-FDG Accumulation in Murine Brown Adipose Tissue After Stress. *Journal of Nuclear Medicine, 52*(10), 1616-1620.

Casteilla, L., Forest, C., Robelin, J., Ricquier, D., Lombet, A., & Ailhaud, G. (1987). Characterization of mitochondrial-uncoupling protein in bovine fetus and newborn calf. *American Journal of Physiology - Endocrinology and Metabolism, 252*(5), E627-E636.

Cawthorne, M. A., Sennitt, M. V., Arch, J. R., & Smith, S. A. (1992). BRL 35135, a potent and selective atypical beta-adrenoceptor agonist. *Am J Clin Nutr, 55*(1 Suppl), 252s-257s.

Celi, F. S., Le, T. N., & Ni, B. (2015). Physiology and relevance of human adaptive thermogenesis response. *Trends in Endocrinology & Metabolism, 26*(5), 238-247.

Cerri, M., & Morrison, S. (2005). Activation of lateral hypothalamic neurons stimulates brown adipose tissue thermogenesis. *Neuroscience, 135*(2), 627-638.

Chance, B., Dait, M. T., Zhang, C., Hamaoka, T., & Hagerman, F. (1992). Recovery from exercise-induced desaturation in the quadriceps muscles of elite competitive rowers. *American Journal of Physiology-Cell Physiology, 262*(3), C766-C775.

Charmandari, E., Tsigos, C., & Chrousos, G. (2005). Endocrinology of the stress response. *Annu Rev Physiol, 67*, 259-284.

Chechi, K., Blanchard, P. G., Mathieu, P., Deshaies, Y., & Richard, D. (2013). Brown fat like gene expression in the epicardial fat depot correlates with circulating HDL-cholesterol and triglycerides in patients with coronary artery disease. *Int J Cardiol, 167*(5), 2264-2270.

Chechi, K., Nedergaard, J., & Richard, D. (2014). Brown adipose tissue as an anti-obesity tissue in humans. *Obes Rev, 15*(2), 92-106.

Chen, C., Zhao, X. L., Li, Z. H., Zhu, Z. G., Qian, S. H., & Flewitt, A. J. (2017). Current and Emerging Technology for Continuous Glucose Monitoring. *Sensors (Basel), 17*(1).

Chen, K. Y., Cypess, A. M., Laughlin, M. R., Haft, C. R., Hu, H. H., Bredella, M. A., Enerback, S., Kinahan, P.E., Litchenbelt, W., Lin, F. L., Sunderland, J. J., Virtanen, K. A., & Wahl, R. L. (2016). Brown Adipose Reporting Criteria in Imaging Studies (BARCIST 1.0): Recommendations for Standardized FDG-PET/CT Experiments in Humans. *Cell Metab, 24*(2), 210-222.

Chen, Y., Cypess, A. M., Sass, C. A., Brownell, A. L., Jokivarsi, K. T., Kahn, C. R., & Kwong, K. K. (2012). Anatomical and functional assessment of brown adipose tissue by magnetic resonance imaging. *Obesity, 20*(7), 1519-1526.

Chowdhury, G. M., Fujioka, T., & Nakamura, S. (2000). Induction and adaptation of Fos expression in the rat brain by two types of acute restraint stress. *Brain Res Bull, 52*(3), 171-182.

Ci, X., Frisch, F., Lavoie, F., Germain, P., Lecomte, R., van Lier, J. E., Benard, F., & Carpentier, A. C. (2006). The effect of insulin on the intracellular distribution of 14(R,S)-[18F]Fluoro-6-thia-heptadecanoic acid in rats. *Mol Imaging Biol, 8*(4), 237-244.

Cinti, S. (2006). The role of brown adipose tissue in human obesity. *Nutrition, Metabolism and Cardiovascular Diseases, 16*(8), 569-574.

Cirulli, F., Santucci, D., Laviola, G., Alleva, E., & Levine, S. (1994). Behavioral and hormonal responses to stress in the newborn mouse: Effects of maternal deprivation and chlordiazepoxide. *Developmental Psychobiology, 27*(5), 301-316.

Clancy, B., Finlay, B. L., Darlington, R. B., & Anand, K. J. (2007). Extrapolating brain development from experimental species to humans. *Neurotoxicology, 28*(5), 931-937.

Clarke, I., Heasman, L., & Symonds, M. (1998). Influence of maternal dexamethasone administration on thermoregulation in lambs delivered by caesarean section. *Journal of Endocrinology, 156*(2), 307-314.

Clarke, K. J., Adams, A. E., Manzke, L. H., Pearson, T. W., Borchers, C. H., & Porter, R. K. (2012). A role for ubiquitinylation and the cytosolic proteasome in turnover of mitochondrial uncoupling protein 1 (UCP1). *Biochim Biophys Acta, 1817*(10), 1759-1767.

Clarke, L., Buss, D. S., Juniper, D. T., Lomax, M. A., & Symonds, M. E. (1997). Adipose tissue development during early postnatal life in ewe-reared lambs. *Experimental physiology, 82*(6), 1015-1027.

Clarke, L., Heasman, L., Firth, K., & Symonds, M. E. (1997). Influence of route of delivery and ambient temperature on thermoregulation in newborn lambs. *Am J Physiol, 272*(6 Pt 2), R1931-1939.

Cole, A. L., Herman, R. A., Jr., Heimlich, J. B., Ahsan, S., Freedman, B. A., & Shuler, M. S. (2012). Ability of near infrared spectroscopy to measure oxygenation in isolated upper extremity muscle compartments. *J Hand Surg Am, 37*(2), 297-302.

Collins, S., & Surwit, R. S. (2001). The beta-adrenergic receptors and the control of adipose tissue metabolism and thermogenesis. *Recent Prog Horm Res, 56*, 309-328.

Considine, R. V., Sinha, M. K., Heiman, M. L., Kriauciunas, A., Stephens, T. W., Nyce, M. R., Ohannesian, J. P., Marco, C. C., McKee, L. J., & Bauer,

T. L. (1996). Serum immunoreactive-leptin concentrations in normal-weight and obese humans. *New England Journal of Medicine, 334*(5), 292-295.

Cox, R. A., & Arnstein, H. R. V. (1963). The isolation, characterization and acid–base properties of ribonucleic acid from rabbit-reticulocyte ribosomes. *Biochemical Journal, 89*(3), 574-585.

Craig, A., Luo, N. L., Beardsley, D. J., Wingate-Pearse, N., Walker, D. W., Hohimer, A. R., & Back, S. A. (2003). Quantitative analysis of perinatal rodent oligodendrocyte lineage progression and its correlation with human. *Experimental neurology, 181*(2), 231-240.

Crane, J. D., Mottillo, E. P., Farncombe, T. H., Morrison, K. M., & Steinberg, G. R. (2014). A standardized infrared imaging technique that specifically detects UCP1-mediated thermogenesis in vivo. *Mol Metab, 3*(4), 490-494.

Crookes, B. A., Cohn, S. M., Bloch, S., Amortegui, J., Manning, R., Li, P., Proctor, M. S., Hallal, A., Blackbourne, L. H., & Benjamin, R. (2005). Can near-infrared spectroscopy identify the severity of shock in trauma patients? *Journal of Trauma and Acute Care Surgery, 58*(4), 806-816.

Cui, X., Nguyen, N. L. T., Zarebidaki, E., Cao, Q., Li, F., Zha, L., Bartness, T., Shi, H., & Xue, B. (2016). Thermoneutrality decreases thermogenic program and promotes adiposity in high-fat diet-fed mice. *Physiological Reports, 4*(10), e12799.

Cunningham, S., Leslie, P., Hopwood, D., Illingworth, P., Jung, R., Nicholls, D., Peden, N., Rafael, J., & Rial, E. (1985). The characterization and energetic potential of brown adipose tissue in man. *Clinical science (London, England: 1979), 69*(3), 343-348.

Cypess, A. M., Chen, Y. C., Sze, C., Wang, K., English, J., Chan, O., Holman, A. R., Tal, I., Palmer, M. R., Kolodny, G. M., & Kahn, C. R. (2012). Cold but not sympathomimetics activates human brown adipose tissue in vivo. *Proc Natl Acad Sci U S A, 109*(25), 10001-10005.

Cypess, A. M., & Kahn, C. R. (2010). The role and importance of brown adipose tissue in energy homeostasis. *Curr Opin Pediatr, 22*(4), 478-484.

Cypess, A. M., Lehman, S., Williams, G., Tal, I., Rodman, D., Goldfine, A. B., Kuo, F. C., Palmer, E. L., Tseng, Y-H., Doria, A., Kolodny, G. M., & Kahn, C. R. (2009). Identification and Importance of Brown Adipose Tissue in Adult Humans. *New England Journal of Medicine, 360*(15), 1509-1517.

Cypess, A. M., Weiner, L. S., Roberts-Toler, C., Elía, E. F., Kessler, S. H., Kahn, P. A., English, J., Chatman, K., Trauger, S. A., & Doria, A. (2015). Activation of human brown adipose tissue by a β3-adrenergic receptor agonist. *Cell metabolism, 21*(1), 33-38.

Cypess, A. M., White, A. P., Vernochet, C., Schulz, T. J., Xue, R., Sass, C. A., Huang, T. L., Roberts-Toler, C., Weiner, L. S., Sze, C., Chacko, A. T., Deschamps, L. N., Herder, L, M., Truchan, N., Glasgow, A.L., Holman, A. R., Gavrila, A., Hasselgren, P-O., Mori, M. A., Molla, M., & Tseng, Y.-H. (2013). Anatomical localization, gene expression profiling and functional characterization of adult human neck brown fat. *Nat Med, 19*(5), 635-639.

Davie, S. N., & Grocott, H. P. (2012). Impact of extracranial contamination on regional cerebral oxygen saturation: a comparison of three cerebral oximetry technologies. *Anesthesiology, 116*(4), 834-840.

De Kloet, E. R., & Derijk, R. (2004). Signaling pathways in brain involved in predisposition and pathogenesis of stress-related disease: genetic and kinetic factors affecting the MR/GR balance. *Ann N Y Acad Sci, 1032*, 14-34.

De Onis, M., Blössner, M., & Borghi, E. (2010). Global prevalence and trends of overweight and obesity among preschool children. *The American journal of clinical nutrition, 92*(5), 1257-1264.

Deng, Z.-S., & Liu, J. (2004). Mathematical modeling of temperature mapping over skin surface and its implementation in thermal disease diagnostics. *Computers in biology and medicine, 34*(6), 495-521.

Desjardins, P., & Conklin, D. (2010). NanoDrop Microvolume Quantitation of Nucleic Acids. *Journal of Visualized Experiments: JoVE*(45), 2565.

Dewal, R. S., & Stanford, K. I. (2018). Effects of exercise on brown and beige adipocytes. *Biochimica et Biophysica Acta (BBA) - Molecular and Cell Biology of Lipids*.

Dieffenbach, C. W., Lowe, T. M., & Dveksler, G. S. (1993). General concepts for PCR primer design. *PCR Methods Appl, 3*(3), S30-37.

Diehl, L. A., Silveira, P. P., Leite, M. C., Crema, L. M., Portella, A. K., Billodre, M. N., Nunes, E., Henriques, T. P., Fidelix-da-Silva, L. B., Heis, M. D., Goncalves, C. A., Quillfeldt, J. A., & Dalmaz, C. (2007). Long lasting sex-specific effects upon behavior and S100b levels after maternal separation and exposure to a model of post-traumatic stress disorder in rats. *Brain Res, 1144*, 107-116.

Dipietro, L., Katz, L, D., Nadel, E, R. (1999). Excess abdominal adiposity re mains correlated with altered lipid concentrations in healthy older

women. *International Journal of Obesity Related Metabolic Disor ders, 23:* 432–436.

Divakaruni, A. S., & Brand, M. D. (2011). The regulation and physiology of mitochondrial proton leak. *Physiology (Bethesda), 26*(3), 192-205.

Dobbing, J. (1970). Undernutrition and the developing brain: the relevance of animal models to the human problem. *American Journal of Diseases of Children, 120*(5), 411-415.

Dobbing, J., & Sands, J. (1979). Comparative aspects of the brain growth spurt. *Early human development, 3*(1), 79-83.

Doig, C. L., Fletcher, R. S., Morgan, S. A., McCabe, E. L., Larner, D. P., Tomlinson, J. W., Stewartm P. M., Philip, A., & Lavery, G. G. (2017). 11β-HSD1 Modulates the Set Point of Brown Adipose Tissue Response to Glucocorticoids in Male Mice. *Endocrinology, 158*(6), 1964-1976.

Dollberg, S., Mimouni, F. B., & Weintraub, V. (2004). Energy expenditure in infants weaned from a convective incubator. *American journal of perinatology, 21*(05), 253-256.

Domouzoglou, E. M., & Maratos-Flier, E. (2011). Fibroblast growth factor 21 is a metabolic regulator that plays a role in the adaptation to ketosis. *The American journal of clinical nutrition, 93*(4), 901S-905S.

Dorak, T. (2006). *Real-time PCR*. 2 Park Square, Milton Park, Abingdon, OX14 4RN: Taylor & Francis Group.

Drubach, L. A., Palmer, E. L., Connolly, L. P., Baker, A., Zurakowski, D., & Cypess, A. M. (2011). Pediatric brown adipose tissue: detection, epidemiology, and differences from adults. *The Journal of pediatrics, 159*(6), 939-944.

Ebbeling, C., B., Pawlak, D, B., & Ludwig, D, S. (2002). Childhood Obesity: Public-health crisis, common sense cure. *Lancet, 360*, 473-482.

Edwards, C. R., Benediktsson, R., Lindsay, R. S., & Seckl, J. R. (1993). Dysfunction of placental glucocorticoid barrier: link between fetal environment and adult hypertension? *Lancet, 341*(8841), 355-357.

El Hadi, H., Frascati, A., Granzotto, M., Silvestrin, V., Ferlini, E., Vettor, R., & Rossato, M. (2016). Infrared thermography for indirect assessment of activation of brown adipose tissue in lean and obese male subjects. *Physiol Meas, 37*(12), N118-n128.

Enerbäck, S. (2010). Human brown adipose tissue. *Cell metabolism, 11*(4), 248-252.

Enerback, S., Jacobsson, A., Simpson, E. M., & Guerra, C. (1997). Mice lacking mitochondrial uncoupling protein are cold-sensitive but not obese. *Nature, 387*(6628), 90.

Engeli, S., Böhnke, J., Feldpausch, M., Gorzelniak, K., Heintze, U., Janke, J., Luft, F. C., Sharma, A. M. (2004). Regulation of 11β-HSD Genes in Human Adipose Tissue: Influence of Central Obesity and Weight Loss. *Obes Res, 12*(1), 9-17.

Enthoven, L., Schmidt, M. V., Cheung, Y. H., van der Mark, M. H., de Kloet, E. R., & Oitzl, M. S. (2010). Ontogeny of the HPA axis of the CD1 mouse following 24 h maternal deprivation at pnd 3. *Int J Dev Neurosci, 28*(2), 217-224.

Epstein, C. D., & Haghenbeck, K. T. (2014). Bedside assessment of tissue oxygen saturation monitoring in critically ill adults: an integrative review of the literature. *Crit Care Res Pract, 2014*, 709683.

Farrell, W. J., & Alberts, J. R. (2007). Rat behavioral thermoregulation integrates with nonshivering thermogenesis during postnatal development. *Behavioral neuroscience, 121*(6), 1333.

Feldman, D. (1978). Evidence that brown adipose tissue is a glucocorticoid target organ. *Endocrinology, 103*(6), 2091-2097. doi:10.1210/endo-103-6-2091

Feldmann, H. M., Golozoubova, V., Cannon, B., & Nedergaard, J. (2009). UCP1 Ablation Induces Obesity and Abolishes Diet-Induced Thermogenesis in Mice Exempt from Thermal Stress by Living at Thermoneutrality. *Cell metabolism, 9*(2), 203-209.

Fernando, H. A., Chin, H.-F., Ton, S. H., & Abdul Kadir, K. (2013). Stress and Its Effects on Glucose Metabolism and 11β-HSD Activities in Rats Fed on a Combination of High-Fat and High-Sucrose Diet with Glycyrrhizic Acid. *Journal of Diabetes Research, 2013*, 190395.

Ferguson, M., A., Gutin, B., Owens, S., Litaker, M., Tracy, R, P., Allison, J. (1998). Fat distribution and hemostatic measures in obese children. . *American Journal of Clinical Nutrition, 67*, 1136–1140.

Ferrari, M., Mottola, L., & Quaresima, V. (2004). Principles, techniques, and limitations of near infrared spectroscopy. *Can J Appl Physiol, 29*(4), 463-487.

Feve, B., Baude, B., Krief, S., Strosberg, A. D., Pairault, J., & Emorine, L. J. (1992). Inhibition by dexamethasone of beta 3-adrenergic receptor responsiveness in 3T3-F442A adipocytes. Evidence for a transcriptional mechanism. *J Biol Chem, 267*(22), 15909-15915.

Fischer, A. W., Cannon, B., & Nedergaard, J. (2018). Optimal housing temperatures for mice to mimic the thermal environment of humans: An experimental study. *Molecular metabolism, 7*, 161-170.

Fisher, F. M., Kleiner, S., Douris, N., Fox, E. C., Mepani, R. J., Verdeguer, F., Wu, J., Kharitonenkov, A., Flier, J. S., Maratos-Flier, E., Spiegelman, B. M. (2012). FGF21 regulates PGC-1alpha and browning of white adipose tissues in adaptive thermogenesis. *Genes Dev, 26*(3), 271-281.

Fleury, C., Neverova, M., Collins, S., Raimbault, S., Champigny, O., Levi-Meyrueis, C., Bouillaud, F., Seldin, M. F., Surwit, R. S., Ricquier, D., & Warden, C. H. (1997). Uncoupling protein-2: a novel gene linked to obesity and hyperinsulinemia. *Nat Genet, 15*(3), 269-272.

Fonken, L. K., & Nelson, R. J. (2014). The Effects of Light at Night on Circadian Clocks and Metabolism. *Endocrine reviews, 35*(4), 648-670. doi:10.1210/er.2013-1051.

Ford, E., S., Galuska, D, A., Gillespie, C., Will, J, C., Giles, W, H., Dietz, W, H. (2001). C-reactive protein and body mass index in children: findings from the Third National Health and Nutrition Examination Survey, 1988–1994. *Paediatrics, 138*, 486–492.

Formenti, D., Ludwig, N., Gargano, M., Gondola, M., Dellerma, N., Caumo, A., & Alberti, G. (2013). Thermal imaging of exercise-associated skin temperature changes in trained and untrained female subjects. *Annals of biomedical engineering, 41*(4), 863-871.

Foster, D. O., & Frydman, M. L. (1979). Tissue distribution of cold-induced thermogenesis in conscious warm- or cold-acclimated rats reevaluated from changes in tissue blood flow: The dominant role of brown adipose tissue in the replacement of shivering by nonshivering thermogenesis. *Canadian journal of physiology and pharmacology, 57*(3), 257-270.

Franceschini, M. A., Boas, D. A., Zourabian, A., Diamond, S. G., Nadgir, S., Lin, D. W., Moore, J. B., & Fantini, S. (2002). Near-infrared spiroximetry: noninvasive measurements of venous saturation in piglets and human subjects. *J Appl Physiol (1985), 92*(1), 372-384.

Frayn, K. N. (2010). *Metabolic Regulation: A Human Perspective* (3rd Edition ed.): Wiley.

Fredriksson, I., Fors, C., & Johansson, J. (2007). Laser doppler flowmetry-a theoretical framework. *Department of Biomedical Engineering, Linköping University*, 6-7.

Freedman, D., S., Dietz, W, H., Srinivasan, S, R., Berenson, G, S. (1999). The relation of overweight to cardiovascular risk factors among children and adolescents: the Bogalusa Heart Study. *Paediatrics, 103*, 1175–1182.

Frontini, A., & Cinti, S. (2010). Distribution and Development of Brown Adipocytes in the Murine and Human Adipose Organ. *Cell metabolism, 11*(4), 253-256.

Fruebis, J., Tsao, T.-S., Javorschi, S., Ebbets-Reed, D., Erickson, M. R. S., Yen, F. T., Bihain, B. E., & Lodish, H. F. (2001). Proteolytic cleavage product of 30-kDa adipocyte complement-related protein increases fatty acid oxidation in muscle and causes weight loss in mice. *Proceedings of the National Academy of Sciences, 98*(4), 2005-2010.

Garrel, D. R. (1997). Glucocorticoids and energy expenditure: relevance to the regulation of energy balance in man. *Nutrition, 13*(5), 482-483.

Gatidis, S., Schmidt, H., Pfannenberg, C. A., Nikolaou, K., Schick, F., & Schwenzer, N. F. (2016). Is It Possible to Detect Activated Brown Adipose Tissue in Humans Using Single-Time-Point Infrared Thermography under Thermoneutral Conditions? Impact of BMI and Subcutaneous Adipose Tissue Thickness. *PLoS One, 11*(3), e0151152.

Germon, T., Evans, P., Barnett, N., Wall, P., Manara, A., & Nelson, R. (1999). Cerebral near infrared spectroscopy: emitter-detector separation must be increased. *British journal of anaesthesia, 82*(6), 831-837.

Gessner, K. (1551). Conradi Gesneri Medici Tigurine Historiae Animalium Lib. I De Quadripedibus Uiuiparis. *842*.

Gilbert, C., McCafferty, D. J., Giroud, S., Ancel, A., & Blanc, S. (2012). Private heat for public warmth: how huddling shapes individual thermogenic responses of rabbit pups. *PLoS One, 7*(3), e33553.

Gilles, E. E., Schultz, L., & Baram, T. Z. (1996). Abnormal corticosterone regulation in an immature rat model of continuous chronic stress. *Pediatr Neurol, 15*(2), 114-119.

Gillman, M. W. (2008). The first months of life: a critical period for development of obesity. *The American journal of clinical nutrition, 87*(6), 1587-1589.

Gilsanz, V., Hu, H. H., & Kajimura, S. (2013). Relevance of brown adipose tissue in infancy and adolescence. *Pediatr Res, 73*(1), 3-9. doi:10.1038/pr.2012.141.

Giordano, A., Frontini, A., & Cinti, S. (2016). Convertible visceral fat as a therapeutic target to curb obesity. *Nature Reviews Drug Discovery, 15*(6), 405-424.

Giralt, M., Martin, I., Iglesias, R., Vinas, O., Villarroya, F., & Mampel, T. (1990). Ontogeny and perinatal modulation of gene expression in rat brown adipose tissue. *European journal of biochemistry, 193*(1), 297-302.

Glick, Z., & Raum, W. J. (1986). Norepinephrine turnover in brown adipose tissue is stimulated by a single meal. *American Journal of Physiology-Regulatory, Integrative and Comparative Physiology, 251*(1), R13-R17.

Glick, Z., Teague, R. J., & Bray, G. A. (1981). Brown adipose tissue: thermic response increased by a single low protein, high carbohydrate meal. *Science, 213*(4512), 1125-1127.

Glick, Z., Wu, S. Y., Lupien, J., Reggio, R., Bray, G. A., & Fisher, D. A. (1985). Meal-induced brown fat thermogenesis and thyroid hormone metabolism in rats. *American Journal of Physiology - Endocrinology and Metabolism, 249*(5), E519-E524.

Gnanalingham, M. G., Mostyn, A., Symonds, M. E., & Stephenson, T. (2005). Ontogeny and nutritional programming of adiposity in sheep: potential role of glucocorticoid action and uncoupling protein-2. *American Journal of Physiology-Regulatory, Integrative and Comparative Physiology, 289*(5), R1407-R1415.

Going, S., Thompson, J., Cano, S., Stewart, D., Stone, E., Harnack, L., Hastings, C., Norman, J., & Corbin, C. (2003). The effects of the Pathways Obesity Prevention Program on physical activity in American Indian children. *Preventive Medicine, 37, Supplement 1*, S62-S69.

Goland, R. S., Jozak, S., Warren, W. B., Conwell, I. M., Stark, R. I., & Tropper, P. J. (1993). Elevated levels of umbilical cord plasma corticotropin-releasing hormone in growth-retarded fetuses. *J Clin Endocrinol Metab, 77*(5), 1174-1179.

Golozoubova, V., Hohtola, E., Matthias, A., Jacobsson, A., Cannon, B., & Nedergaard, J. (2001). Only UCP1 can mediate adaptive nonshivering thermogenesis in the cold. *The FASEB Journal, 15*(11), 2048-2050.

Gondré-Lewis, M. C., Warnock, K. T., Wang, H., June, H. L., Bell, K. A., Rabe, H., Phani Babu Tiruveedhula, V. V. N., & June, H. L. (2016). Early Life Stress is a Risk Factor for Excessive Alcohol Drinking and Impulsivity in Adults, mediated via a CRF/GABA(A) Mechanism. *Stress (Amsterdam, Netherlands), 19*(2), 235-247.

Gortmaker, S. L., Peterson, K., Wiecha, J., Sobol, A. M., Dixit, S., Fox, M. K., & Laird, N. (1999). Reducing obesity via a school-based interdisciplinary intervention among youth: Planet health. *Archives of Pediatrics & Adolescent Medicine, 153*(4), 409-418.

Goubern, M., Yazbeck, J., Senault, C., & Portet, R. (1990). Non-shivering thermogenesis and brown adipose tissue activity in essential fatty acid deficient rats. *Archives internationales de physiologie et de biochimie, 98*(2), 193-199.

Grausz, J. (1970). Interscapular skin temperatures in the newborn infant. *The Journal of pediatrics, 76*(5), 752-756.

Greenberg, A. S., & Obin, M. S. (2006). Obesity and the role of adipose tissue in inflammation and metabolism. *The American journal of clinical nutrition, 83*(2), 461S-465S.

Greisen, G., Andresen, B., Plomgaard, A. M., & Hyttel-Sørensen, S. (2016). Cerebral oximetry in preterm infants: an agenda for research with a clear clinical goal. *Neurophotonics, 3*(3), 031407.

Griggio, M. A. (1982). The participation of shivering and nonshivering thermogenesis in warm and cold-acclimated rats. *Comparative Biochemistry and Physiology Part A: Physiology, 73*(3), 481-484.

Grimpo, K., Völker, M. N., Heppe, E. N., Braun, S., Heverhagen, J. T., & Heldmaier, G. (2014). Brown adipose tissue dynamics in wild-type and UCP1-knockout mice: in vivo insights with magnetic resonance. *Journal of lipid research, 55*(3), 398-409.

Güngör, N. K. (2014). Overweight and obesity in children and adolescents. *J Clin Res Pediatr Endocrinol, 6*(3), 129-143.

Gunnar, M. R., & Donzella, B. (2002). Social regulation of the cortisol levels in early human development. *Psychoneuroendocrinology, 27*(1-2), 199-220.

Gunnell, D., J., Frankel, S, J., Nanchahal, K., Peters, T, J., Smith, G, D. (1998). Childhood obesity and adult cardiovascular mortality: a 57-year follow-up study based on the Boyd Orr cohort. *American Journal of Clinical Nutrition, 67*, 1111-1118.

Hadi, M., Chen, C. C., Whatley, M., Pacak, K., & Carrasquillo, J. A. (2007). Brown fat imaging with 18F-6-fluorodopamine PET/CT, 18F-FDG PET/CT, and 123I-MIBG SPECT: a study of patients being evaluated for pheochromocytoma. *Journal of Nuclear Medicine, 48*(7), 1077-1083.

Halaas, J. L., Gajiwala, K. S., Maffei, M., & Cohen, S. L. (1995). Weight-reducing effects of the plasma protein encoded by the obese gene. *Science, 269*(5223), 543.

Halpern, B., Mancini, M. C., & Halpern, A. (2014). Brown adipose tissue: what have we learned since its recent identification in human adults. *Arq Bras Endocrinol Metabol, 58*(9), 889-899.

Hamann, A., Flier, J. S., & Lowell, B. B. (1996). Decreased brown fat markedly enhances susceptibility to diet-induced obesity, diabetes, and hyperlipidemia. *Endocrinology, 137*(1), 21-29.

Hamann, A., & Matthaei, S. (1996). Regulation of energy balance by leptin. *Experimental and Clinical Endocrinology & Diabetes, 104*(04), 293-300.

Hamaoka, T., McCully, K. K., Niwayama, M., & Chance, B. (2011). The use of muscle near-infrared spectroscopy in sport, health and medical sciences: recent developments. *Phil. Trans. R. Soc. A, 369*(1955), 4591-4604.

Hamaoka, T., McCully, K. K., Quaresima, V., Yamamoto, K., & Chance, B. (2007). Near-infrared spectroscopy/imaging for monitoring muscle oxygenation and oxidative metabolism in healthy and diseased humans. *Journal of biomedical optics, 12*(6), 062105-062105-062116.

Hammarlund, K., Strömberg, B., & Sedin, G. (1986). Heat loss from the skin of preterm and fullterm newborn infants during the first weeks after birth. *Neonatology, 50*(1), 1-10.

Haq, T., Crane, J. D., Kanji, S., Gunn, E., Tarnopolsky, M. A., Gerstein, H. C., . . . Morrison, K. M. (2017). Optimizing the methodology for measuring supraclavicular skin temperature using infrared thermography; implications for measuring brown adipose tissue activity in humans. *Scientific Reports, 7*, 11934.

Hara, K., Boutin, P., Mori, Y., Tobe, K., Dina, C., Yasuda, K., .Yamauchi, T., Otabe, S., Okada, T., & Eto, K. (2002). Genetic variation in the gene encoding adiponectin is associated with an increased risk of type 2 diabetes in the Japanese population. *Diabetes, 51*(2), 536-540.

Harms, M. J., Ishibashi, J., Wang, W., Lim, H. W., Goyama, S., Sato, T., Kurokawa, M., Won, K. J., & Seale, P. (2014). Prdm16 is required for the maintenance of brown adipocyte identity and function in adult mice. *Cell Metab, 19*(4), 593-604.

Hatai, S. (1902). On the presence in human embryos of an interscapular gland corresponding to the so-called hibernating gland of lower mammals. *Anat Anz, 21*, 369-373.

Hatalski, C. G., Guirguis, C., & Baram, T. Z. (1998). Corticotropin Releasing Factor mRNA Expression in the Hypothalamic Paraventricular Nucleus and the Central Nucleus of the Amygdala is Modulated by Repeated Acute Stress in the Immature Rat. *J Neuroendocrinol, 10*(9), 663-669.

Hayano, J., Sakakibara, Y., Yamada, M., Kamiya, T., Fujinami, T., Yokoyama, K., Watanabe, Y., & Takata, K. (1990). Diurnal variations in vagal and sympathetic cardiac control. *Am J Physiol, 258*(3 Pt 2), H642-646.

Hayes, M., Chustek, M., Heshka, S., Wang, Z., Pietrobelli, A., & Heymsfield, S. B. (2004). Low physical activity levels of modern Homo sapiens among free-ranging mammals. *Int J Obes Relat Metab Disord, 29*(1), 151-156.

Hazell, T. J., & Lemon, P. W. R. (2012). Synchronous whole-body vibration increases VO2 during and following acute exercise. *European Journal of Applied Physiology, 112*(2), 413-420.

Health and Social Care Information Centre, HSCIC. (2015). Statistics on Obesity, Physical Activity and Diet; England. http://content.digital.nhs.uk/catalogue/PUB16988/obes-phys-acti-diet-eng-2015.pdf

Heasman, L., Clarke, L., & Symonds, M. E. (2000). Influence of thyrotropin-releasing hormone administration at birth on thermoregulation in lambs delivered by cesarean. *American journal of obstetrics and gynecology, 183*(5), 1257-1262.

Heaton, J.M., 1972. The distribution of brown adipose tissue in the human. *Journal of anatomy*, *112*(Pt 1), p.35.

Heim, C., Newport, D. J., Mletzko, T., Miller, A. H., & Nemeroff, C. B. (2008). The link between childhood trauma and depression: insights from HPA axis studies in humans. *Psychoneuroendocrinology, 33*(6), 693-710.

Heimann, K., Jergus, K., Abbas Abbas, K., Heussen, N., Leonhardt, S., & Orlikowsky, T. (2013). Infrared thermography for detailed registration of thermoregulation in premature infants. In *Journal of Perinatal Medicine* (Vol. 41, pp. 613).

Henning, S. J. (1978). Plasma concentrations of total and free corticosterone during development in the rat. *American Journal of Physiology-Endocrinology and Metabolism, 235*(5), E451.

Herschorn, S., Barkin, J., Castro-Diaz, D., Frankel, J. M., Espuna-Pons, M., Gousse, A. E., Stolzel, M., Martin, N., Gunther, A., & Van Kerrebroeck, P. (2013). A phase III, randomized, double-blind, parallel-group,

placebo-controlled, multicentre study to assess the efficacy and safety of the beta(3) adrenoceptor agonist, mirabegron, in patients with symptoms of overactive bladder. *Urology, 82*(2), 313-320.

Hibi, M., Oishi, S., Matsushita, M., Yoneshiro, T., Yamaguchi, T., Usui, C., Yasunaga, K., Katsuragi, Y., Kubota., Tanaka, S., & Saito, M. (2016). Brown adipose tissue is involved in diet-induced thermogenesis and whole-body fat utilization in healthy humans. *Int J Obes (Lond), 40*(11), 1655-1661.

Higuchi, R., Fockler, C., Dollinger, G., & Watson, R. (1993). Kinetic PCR analysis: real-time monitoring of DNA amplification reactions. *Biotechnology (N Y), 11*(9), 1026-1030.

Hill, A., J., & Silver, E, K. (1995). Fat, friendless and unhealthy: 9-year old children's perception of body shape stereotypes. *Journal of the International Association for the Study of Obesity, 19*(6), 423-430.

Himes, J. H., Ring, K., Gittelsohn, J., Cunningham-Sabo, L., Weber, J., Thompson, J., Harnack, L., & Suchindran, C. (2003). Impact of the Pathways intervention on dietary intakes of American Indian school children. *Preventive Medicine, 37, Supplement 1*, S55-S61.

Himmerich, H., Fischer, J., Bauer, K., Kirkby, K. C., Sack, U., & Krugel, U. (2013). Stress-induced cytokine changes in rats. *Eur Cytokine Netw, 24*(2), 97-103.

Himms-Hagen, J. (1984). Thermogenesis in brown adipose tissue as an energy buffer. Implications for obesity. *N Engl J Med, 311*(24), 1549-1558.

Hofer, M. A. (1973). Maternal separation affects infant rats' behavior. *Behavioral Biology, 9*(5), 629-633.

Hoffmans, M., Kromhout, D., & de Lezenne Coulander, C. (1988). The impact of body mass index of 78,612 18-year old Dutch men on 32-year mortality from all causes. *Journal of clinical epidemiology, 41*(8), 749-756.

Holstila, M., Virtanen, K. A., Grönroos, T. J., Laine, J., Lepomäki, V., Saunavaara, J., Lisinen, I., Kormu, M., Hannukainen, J. C., & Nuutila, P. (2013). Measurement of brown adipose tissue mass using a novel dual-echo magnetic resonance imaging approach: a validation study. *Metabolism, 62*(8), 1189-1198.

Hondares, E., Rosell, M., Díaz-Delfín, J., Olmos, Y., Monsalve, M., Iglesias, R., Villarroya, F., & Giralt, M. (2011). Peroxisome Proliferator-activated Receptor α (PPARα) Induces PPARγ Coactivator 1α (PGC-1α) Gene Expression and Contributes to Thermogenic Activation of Brown

Fat: Involvement of PRDM16. *The Journal of Biological Chemistry, 286*(50), 43112-43122.

Hondares, E., Rosell, M., Gonzalez, F. J., Giralt, M., Iglesias, R., & Villarroya, F. (2010). Hepatic FGF21 expression is induced at birth via PPARα in response to milk intake and contributes to thermogenic activation of neonatal brown fat. *Cell metabolism, 11*(3), 206-212.

Hotamisligil, G., S. (2006). Inflammation and metabolic disorders. *Nature, 444*, 860-867.

Hotta, K., Funahashi, T., Arita, Y., Takahashi, M., Matsuda, M., Okamoto, Y., Iwahashi, H., Kurriyama, H., Ouchi, N., & Maeda, K. (2000). Plasma concentrations of a novel, adipose-specific protein, adiponectin, in type 2 diabetic patients. *Arteriosclerosis, thrombosis, and vascular biology, 20*(6), 1595-1599.

Hu, H. H., Perkins, T. G., Chia, J. M., & Gilsanz, V. (2013). Characterization of human brown adipose tissue by chemical-shift water-fat MRI. *American Journal of Roentgenology, 200*(1), 177-183.

Hu, H. H., Tovar, J. P., Pavlova, Z., Smith, M. L., & Gilsanz, V. (2012). Unequivocal identification of brown adipose tissue in a human infant. *Journal of Magnetic Resonance Imaging, 35*(4), 938-942.

Hubbard, R. J. (2015). Muscle Dynamics as the Result of Whole Body Vibration and Plyometrics. Loma Linda University Electronic Theses, Dissertations & Projects. 284. http://scholarsrepository.llu.edu/etd/284

Hull, D., & Segall, M. (1965). Heat production in the new-born rabbit and the fat content of the brown adipose tissue. *The Journal of physiology, 181*(3), 468.

Hull, D., & Vinter, J. (1984). The development of cold-induced thermogenesis and the structure of brown adipocyte mitochondria in genetically-obese (ob/ob) mice. *British journal of nutrition, 52*(1), 33-39.

Huttunen, P., Hirvonen, J., & Kinnula, V. (1981). The occurrence of brown adipose tissue in outdoor workers. *European journal of applied physiology and occupational physiology, 46*(4), 339-345.

Huysman, M. W., Hokken-Koelega, A. C., De Ridder, M. A., & Sauer, P. J. (2000). Adrenal function in sick very preterm infants. *Pediatr Res, 48*(5), 629-633.

Hwang, J. J., Yeckel, C. W., Gallezot, J. D., Aguiar, R. B., Ersahin, D., Gao, H., Ding, Y. S. (2015). Imaging human brown adipose tissue under room temperature conditions with (11)C-MRB, a selective norepinephrine transporter PET ligand. *Metabolism, 64*(6), 747-755.

Inokuma, K., Okamatsu-Ogura, Y., Omachi, A., Matsushita, Y., Kimura, K., Yamashita, H., & Saito, M. (2006). Indispensable role of mitochondrial UCP1 for antiobesity effect of beta3-adrenergic stimulation. *Am J Physiol Endocrinol Metab, 290*(5), E1014-1021.

Irles, C., Nava-Kopp, A. T., Morán, J., & Zhang, L. (2014). Neonatal maternal separation up-regulates protein signalling for cell survival in rat hypothalamus. *Stress, 17*(3), 275-284.

Israel, A. C., Guile, C. A., Baker, J. E., & Silverman, W. K. (1994). An evaluation of enhanced self-regulation training in the treatment of childhood obesity. *Journal of Pediatric Psychology, 19*(6), 737-749.

Ito, T., Tanuma, Y., Yamada, M., & Yamamoto, M. (1991). Morphological studies on brown adipose tissue in the bat and in humans of various ages. *Arch Histol Cytol, 54*(1), 1-39.

Ivy, A. S., Brunson, K. L., Sandman, C., & Baram, T. Z. (2008). Dysfunctional nurturing behavior in rat dams with limited access to nesting material: a clinically relevant model for early-life stress. *Neuroscience, 154*(3), 1132-1142.

Jackson, D., Hambly, C., Trayhurn, P., & Speakman, J. (2001). Can non-shivering thermogenesis in brown adipose tissue following NA injection be quantified by changes in overlying surface temperatures using infrared thermography? *Journal of thermal biology, 26*(2), 85-93.

Jacobsson, A., Muhleisen, M., Cannon, B., & Nedergaard, J. (1994). The uncoupling protein thermogenin during acclimation: indications for pretranslational control. *American Journal of Physiology-Regulatory, Integrative and Comparative Physiology, 267*(4), R999-R1007.

Jadvar, H., & Parker J, A. (2005). *Clinical PET and PET/CT*: Springer, London.

Jahng, J. W. (2011). An animal model of eating disorders associated with stressful experience in early life. *Hormones and Behavior, 59*(2), 213-220.

Jang, C., Jalapu, S., Thuzar, M., Law, P. W., Jeavons, S., Barclay, J. L., & Ho, K. K. Y. (2014). Infrared thermography in the detection of brown adipose tissue in humans. *Physiological Reports, 2*(11), e12167.

Jebb, S., A., Prentice A, M., Goldberg, G, R., Murgatroyd., Black, A, E., Coward, A, W. (1996). Changes in macronutrient balance during over- and underfeeding assessed by 12-d continuous whole-body calorimetry. *The American journal of clinical nutrition, 64*, 259-266.

Jespersen, Naja Z., Larsen, Therese J., Peijs, L., Daugaard, S., Homøe, P., Loft, A., de Jong, J., Mathur, N., Cannon, B., Nedergaard, J., Perdersen, B. K., Moller, K., & Scheele, C. (2013). A Classical Brown Adipose Tissue mRNA Signature Partly Overlaps with Brite in the Supraclavicular Region of Adult Humans. *Cell metabolism, 17*(5), 798-805.

Jobsis, F. F. (1977). Noninvasive, infrared monitoring of cerebral and myocardial oxygen sufficiency and circulatory parameters. *Science, 198*(4323), 1264-1267.

Johnson, F., Mavrogianni, A., Ucci, M., Vidal-Puig, A., & Wardle, J. (2011). Could increased time spent in a thermal comfort zone contribute to population increases in obesity? *Obes Rev, 12*(7), 543-551.

Jost, K., Pramana, I., Delgado-Eckert, E., Kumar, N., Datta, A. N., Frey, U., & Schulzke, S. M. (2017). Dynamics and complexity of body temperature in preterm infants nursed in incubators. *PLoS One, 12*(4), e0176670.

Jun, H.-J., Gettys, T. W., & Chang, J. S. (2012). Transcriptional Activity of PGC-1 and NT-PGC-1 Is Differentially Regulated by Twist-1 in Brown Fat Metabolism. *PPAR Research, 2012*, 7.

Kajimura, S., Seale, P., Kubota, K., Lunsford, E., Frangioni, J. V., Gygi, S. P., & Spiegelman, B. M. (2009). Initiation of myoblast to brown fat switch by a PRDM16-C/EBP-beta transcriptional complex. *Nature, 460*(7259), 1154-1158.

Kalinichev, M., Easterling, K. W., Plotsky, P. M., & Holtzman, S. G. (2002). Long-lasting changes in stress-induced corticosterone response and anxiety-like behaviors as a consequence of neonatal maternal separation in Long-Evans rats. *Pharmacol Biochem Behav, 73*(1), 131-140.

Kannisto, K., Pietilainen, K. H., Ehrenborg, E., Rissanen, A., Kaprio, J., Hamsten, A., & Yki-Jarvinen, H. (2004). Overexpression of 11beta-hydroxysteroid dehydrogenase-1 in adipose tissue is associated with acquired obesity and features of insulin resistance: studies in young adult monozygotic twins. *J Clin Endocrinol Metab, 89*(9), 4414-4421.

Kaul, S., Rothney, M. P., Peters, D. M., Wacker, W. K., Davis, C. E., Shapiro, M. D., & Ergun, D. L. (2012). Dual-energy X-ray absorptiometry for quantification of visceral fat. *Obesity (Silver Spring), 20*(6), 1313-1318.

Kearney, M. T., Cowley, A. J., & Macdonald, I. A. (1995). The cardiovascular responses to feeding in man. *Experimental physiology, 80*(5), 683-700.

Kelbaek, H., Munck, O., Christensen, N. J., & Godtfredsen, J. (1989). Central haemodynamic changes after a meal. *British Heart Journal, 61*(6), 506-509.

Keytel, L. R., Goedecke, J. H., Noakes, T. D., Hiiloskorpi, H., Laukkanen, R., van der Merwe, L., & Lambert, E. V. (2005). Prediction of energy expenditure from heart rate monitoring during submaximal exercise. *J Sports Sci, 23*(3), 289-297.

Khashan, A. S., McNamee, R., Abel, K. M., Pedersen, M. G., Webb, R. T., Kenny, L. C., Mortensen, P. B., & Baker, P. N. (2008). Reduced infant birthweight consequent upon maternal exposure to severe life events. *Psychosom Med, 70*(6), 688-694.

Kiskinis, E., Chatzeli, L., Curry, E., Kaforou, M., Frontini, A., Cinti, S., . . . Christian, M. (2014). RIP140 Represses the "Brown-in-White" Adipocyte Program Including a Futile Cycle of Triacyclglycerol Breakdown and Synthesis. *Molecular Endocrinology, 28*(3), 344-356.

Kissebah, A. H., Sonnenberg, G. E., Myklebust, J., Goldstein, M., Broman, K., James, R. G., Marks, J. A., Krakower, G. R., Jacob, H. J., & Weber, J. (2000). Quantitative trait loci on chromosomes 3 and 17 influence phenotypes of the metabolic syndrome. *Proceedings of the National Academy of Sciences, 97*(26), 14478-14483.

Klieverik, L. P., Coomans, C. P., Endert, E., Sauerwein, H. P., Havekes, L. M., Voshol, P. J., Rensen, P. C., Romijn, L. A., Kalsbeek, A., & Fliers, E. (2009). Thyroid hormone effects on whole-body energy homeostasis and tissue-specific fatty acid uptake in vivo. *Endocrinology, 150*(12), 5639-5648.

Kleitman, N., & Satinoff, E. (1982). Thermoregulatory behavior in rat pups from birth to weaning. *Physiol Behav, 29*(3), 537-541.

Klingenspor, M., & Fromme, T. (2014). Brown Adipose Tissue. *Molecular Nutritional Medicine*, 1-45.

Knobel, R. B., Holditch-Davis, D., Schwartz, T. A., & Wimmer, J. E., Jr. (2009). Extremely low birth weight preterm infants lack vasomotor response in relationship to cold body temperatures at birth. *J Perinatol, 29*(12), 814-821.

Knobel-Dail, R. B., Holditch-Davis, D., Sloane, R., Guenther, B. D., & Katz, L. M. (2017). Body temperature in premature infants during the first

week of life: Exploration using infrared thermal imaging. *Journal of thermal biology, 69*, 118-123.

Kondo, H., Shimomura, I., Matsukawa, Y., Kumada, M., Takahashi, M., Matsuda, M., Ouchi, N., Kihara, S., Kawamoto, T., & Sumitsuji, S. (2002). Association of adiponectin mutation with type 2 diabetes. *Diabetes, 51*(7), 2325-2328.

Konishi, M., Mikami, T., Yamasaki, M., Miyake, A., & Itoh, N. (2000). Fibroblast Growth Factor-16 Is a Growth Factor for Embryonic Brown Adipocytes. *Journal of Biological Chemistry, 275*(16), 12119-12122.

Koskensalo, K., Raiko, J., Saari, T., Saunavaara, V., Eskola, O., Nuutila, P., Saunavaara, J., Parkkola, R. & Virtanen, K. A. (2017). Human Brown Adipose Tissue Temperature and Fat Fraction Are Related to Its Metabolic Activity. *J Clin Endocrinol Metab, 102*(4), 1200-1207.

Kozak, L. P. (2010). Brown Fat and the Myth of Diet-Induced Thermogenesis. *Cell metabolism, 11*(4), 263-267.

Kozak, U. C., Kopecky, J., Teisinger, J., Enerbäck, S., Boyer, B., & Kozak, L. P. (1994). An upstream enhancer regulating brown-fat-specific expression of the mitochondrial uncoupling protein gene. *Molecular and cellular biology, 14*(1), 59-67.

Kreeger, R. N., Ramamoorthy, C., Nicolson, S. C., Ames, W. A., Hirsch, R., Peng, L. F., Glatz, A. C., Hill, K. D., Hoffman, J., Tomasson, J., & Tomasson, J. (2012). Evaluation of pediatric near-infrared cerebral oximeter for cardiac disease. *The Annals of thoracic surgery, 94*(5), 1527-1533.

Kumar, P., & Clarke, M. L. (2012). *Clinical Medicine*: Saunders Ltd.; 8 edition (20 July 2012).

Labbe, S. M., Caron, A., Bakan, I., Laplante, M., Carpentier, A. C., Lecomte, R., & Richard, D. (2015). In vivo measurement of energy substrate contribution to cold-induced brown adipose tissue thermogenesis. *Faseb j, 29*(5), 2046-2058.

Lahesmaa, M., Orava, J., Schalin-Jäntti, C., Soinio, M., Hannukainen, J. C., Noponen, T., Kirjavainen, A., Iida, H., Kudomi, N., & Enerbäck, S. (2013). Hyperthyroidism increases brown fat metabolism in humans. *The Journal of Clinical Endocrinology & Metabolism, 99*(1), E28-E35.

Lahiri, B., Bagavathiappan, S., Jayakumar, T., & Philip, J. (2012). Medical applications of infrared thermography: a review. *Infrared Physics & Technology, 55*(4), 221-235.

Lai, M.-C., Holmes, G. L., Lee, K.-H., Yang, S.-N., Wang, C.-A., Wu, C.-L., Tiao, M-M., Hsieh, C-S., Lee, C-H., & Huang, L.-T. (2006). Effect of neonatal isolation on outcome following neonatal seizures in rats--the role of corticosterone. *Epilepsy research, 68*(2), 123-136.

Larsen, T. M., Toubro, S., van Baak, M. A., Gottesdiener, K. M., Larson, P., Saris, W. H., & Astrup, A. (2002). Effect of a 28-d treatment with L-796568, a novel beta(3)-adrenergic receptor agonist, on energy expenditure and body composition in obese men. *Am J Clin Nutr, 76*(4), 780-788.

Law, J., Bloor, I., Budge, H. and Symonds, M.E. (2014). The influence of sex steroids on adipose tissue growth and function. *Hormone molecular biology and clinical investigation*, *19*(1), pp.13-24.

Law, J., Chalmers, J., Morris, D. E., Robinson, L., Budge, H., & Symonds, M. E. (2018). The use of infrared thermography in the measurement and characterization of brown adipose tissue activation. *Temperature, 5*(2), 147-161.

Law, J., Morris, D. E., Izzi-Engbeaya, C., Salem, V., Coello, C., Robinson, L., Jayasinghe, M., Scott, R., Gunn, R., Rabiner, E., Tan, T., Dhillo, W. S., Bloom, S., Budge, H., & Symonds, M. E. (2017). Thermal Imaging Is a Noninvasive Alternative to PET/CT for Measurement of Brown Adipose Tissue Activity in Humans. *J Nucl Med, 59*(3), 516-522.

Lean, M., James, W., Jennings, G., & Trayhurn, P. (1986). Brown adipose tissue uncoupling protein content in human infants, children and adults. *Clinical science (London, England: 1979), 71*(3), 291-297.

Lee, J. H., Kim, H. J., Kim, J. G., Ryu, V., Kim, B. T., Kang, D. W., & Jahng, J. W. (2007). Depressive behaviors and decreased expression of serotonin reuptake transporter in rats that experienced neonatal maternal separation. *Neurosci Res, 58*(1), 32-39.

Lee, M. J., Fried, S. K., Mundt, S. S., Wang, Y., Sullivan, S., Stefanni, A., Daugherty, B. L., & Hermanowski-Vosatka, A. (2008). Depot-specific regulation of the conversion of cortisone to cortisol in human adipose tissue. *Obesity (Silver Spring), 16*(6), 1178-1185.

Lee, M. J., Pramyothin, P., Karastergiou, K., & Fried, S. K. (2014). Deconstructing the roles of glucocorticoids in adipose tissue biology and the development of central obesity. *Biochim Biophys Acta, 1842*(3), 473-481.

Lee, P., Greenfield, J. R., Ho, K. K., & Fulham, M. J. (2010). A critical appraisal of prevalence and metabolic significance of brown adipose tissue in adult humans. *American Journal of Physiology-Endocrinology and Metabolism*.

Lee, P., Ho, K., & Greenfield, J. (2011). Hot fat in a cool man: infrared thermography and brown adipose tissue. *Diabetes, Obesity and Metabolism, 13*(1), 92-93.

Lee, P., Swarbrick, M. M., & Ho, K. K. (2013). Brown adipose tissue in adult humans: a metabolic renaissance. *Endocr Rev, 34*(3), 413-438.

Lee, P., Zhao, J. T., Swarbrick, M. M., Gracie, G., Bova, R., Greenfield, J. R., Freund, J., & Ho, K. K. (2011). High prevalence of brown adipose tissue in adult humans. *The Journal of Clinical Endocrinology & Metabolism, 96*(8), 2450-2455.

Lee, Y.-A., Yamaguchi, Y., & Goto, Y. (2015). Neurodevelopmental Plasticity in Pre- and Postnatal Environmental Interactions: Implications for Psychiatric Disorders from an Evolutionary Perspective. *Neural Plasticity, 2015*, 9.

Levine, S. (1994). The ontogeny of the hypothalamic-pituitary-adrenal axis. The influence of maternal factors. *Ann N Y Acad Sci, 746*, 275-288; discussion 289-293.

Levine, S. (2002). Regulation of the hypothalamic-pituitary-adrenal axis in the neonatal rat: the role of maternal behavior. *Neurotox Res, 4*(5-6), 557-564.

Levine, S., Huchton, D. M., Wiener, S. G., & Rosenfeld, P. (1991). Time course of the effect of maternal deprivation on the hypothalamic-pituitary-adrenal axis in the infant rat. *Developmental Psychobiology, 24*(8), 547-558.

Li, H. t., Zhou, Y. b., & Liu, J. m. (2013). The impact of cesarean section on offspring overweight and obesity: a systematic review and meta-analysis. *Int J Obes, 37*(7), 893-899.

Li, X., Wilder-Smith, C. H., Kan, M. E., Lu, J., Cao, Y., & Wong, R. K. (2014). Combat-training stress in soldiers increases S100B, a marker of increased blood-brain-barrier permeability, and induces immune activation. *Neuro Endocrinol Lett, 35*(1), 58-63.

Lichtenbelt, W., Kingma, B., van der Lans, A., & Schellen, L. (2014). Cold exposure--an approach to increasing energy expenditure in humans. *Trends Endocrinol Metab, 25*(4), 165-167.

Lidell M.E. (2018) Brown Adipose Tissue in Human Infants. In: . Handbook of Experimental Pharmacology. Springer, Berlin, Heidelberg. p1-17.

Lidell, M. E., Betz, M. J., Leinhard, O. D., Heglind, M., Elander, L., Slawik, M., Mussack, T., Nilsson, D., Romu, T., Nuutila, P., Virtanen, K. A. Beuschlein, F., Persson, A., Borga, M., & Enerbäck, S. (2013). Evidence for two types of brown adipose tissue in humans. *Nature medicine, 19*, 631.

Limjeerajarus, C. (2014). Laser Doppler flowmetry: basic principle, current clinical and research applications in dentistry. *Chulalongkorn University Dental Journal, 37*(1), 123-136.

Lin, C., & Klingenberg, M. (1980). Isolation of the uncoupling protein from brown adipose tissue mitochondria. *FEBS letters, 113*(2), 299-303.

Lin, X., Liu, Y. B., & Hu, H. (2017). Metabolic role of fibroblast growth factor 21 in liver, adipose and nervous system tissues. *Biomed Rep, 6*(5), 495-502.

Liu, D., Caldji, C., Sharma, S., Plotsky, P. M., & Meaney, M. J. (2000). Influence of neonatal rearing conditions on stress-induced adrenocorticotropin responses and norepinepherine release in the hypothalamic paraventricular nucleus. *Journal of neuroendocrinology*, *12*(1), 5-12.

Liu, J., Kong, X., Wang, L., Qi, H., Di, W., Zhang, X., Wu, L., Chen, X., Yu, J., Zha, J., Lv, S., Zhang, A., Cheng, P., Hu, M., Li, Y., Bi, L., Li, Y., Hu, F., Zhong, Y., Xu, Y., & Ding, G. (2013). Essential roles of 11beta-HSD1 in regulating brown adipocyte function. *J Mol Endocrinol, 50*(1), 103-113.

Livak, K. J., & Schmittgen, T. D. (2001). Analysis of relative gene expression data using real-time quantitative PCR and the 2(-Delta Delta C(T)) Method. *Methods, 25*(4), 402-408.

Loman, M. M., & Gunnar, M. R. (2010). Early experience and the development of stress reactivity and regulation in children. *Neurosci Biobehav Rev, 34*(6), 867-876.

Lomax, M. A., Sadiq, F., Karamanlidis, G., Karamitri, A., Trayhurn, P., & Hazlerigg, D. G. (2007). Ontogenic loss of brown adipose tissue sensitivity to β-adrenergic stimulation in the ovine. *Endocrinology, 148*(1), 461-468.

Louzada, R. A., Santos, M. C., Cavalcanti-de-Albuquerque, J. P. A., Rangel, I. F., Ferreira, A. C., Galina, A., Werneck-de-Castro, J. P. S., & Carvalho, D. P. (2014). Type 2 iodothyronine deiodinase is upregulated in rat slow-and fast-twitch skeletal muscle during cold exposure. *American Journal of Physiology-Endocrinology and Metabolism, 307*(11), E1020-E1029.

Lowell, B. B., S-Susulic, V., Hamann, A., Lawitts, J. A., Himms-Hagen, J., Boyer, B. B., Kozak, L. P., & Flier, J. S. (1993). Development of obesity in transgenic mice after genetic ablation of brown adipose tissue. *Nature, 366*(6457), 740-742.

Ludwig, D. S., & Ebbeling, C. B. (2001). Type 2 diabetes mellitus in children: Primary care and public health considerations. *JAMA, 286*(12), 1427-1430.

Lunghi, L., Pavan, B., Biondi, C., Paolillo, R., Valerio, A., Vesce, F., & Patella, A. (2010). Use of glucocorticoids in pregnancy. *Curr Pharm Des, 16*(32), 3616-3637.

Lupien, J. R., Glick, Z., Saito, M., & Bray, G. A. (1985). Guanosine diphosphate binding to brown adipose tissue mitochondria is increased after single meal. *American Journal of Physiology-Regulatory, Integrative and Comparative Physiology, 249*(6), R694-R698.

Lyon, A. J., Pikaar, M. E., Badger, P., & McIntosh, N. (1997). Temperature control in very low birthweight infants during first five days of life. *Arch Dis Child Fetal Neonatal Ed, 76*(1), F47-50.

Macfarlane, D. P., Forbes, S., & Walker, B. R. (2008). Glucocorticoids and fatty acid metabolism in humans: fuelling fat redistribution in the metabolic syndrome. *Journal of Endocrinology, 197*(2), 189-204.

MacLeod, D., & Ikeda, K. (2009). NONIN Equanox 8004CA advance cerebral oximeter sensor provides valid assessment of true tissue oxygen saturation. *DUKE University medical centre, Durham, NC, USA*.

MacLeod, D. B., Ikeda, K., Vacchiano, C., Lobbestael, A., Wahr, J. A., & Shaw, A. D. (2012). Development and validation of a cerebral oximeter capable of absolute accuracy. *J Cardiothorac Vasc Anesth, 26*(6), 1007-1014.

Maddalozzo, G. F., Iwaniec, U. T., Turner, R. T., Rosen, C. J., & Widrick, J. J. (2008). Whole-body vibration slows the acquisition of fat in mature female rats. *International journal of obesity*, *32*(9), 1348.

Maffei, M., Halaas, J., Ravussin, E., Pratley, R., Lee, G., Zhang, Y., Fei, H., Kim, S., Lallone, R., & Ranganathan, S. (1995). Leptin levels in human and rodent: measurement of plasma leptin and ob RNA in obese and weight-reduced subjects. *Nature medicine, 1*(11), 1155-1161.

Malik, M., van Gelderen, E. M., Lee, J. H., Kowalski, D. L., Yen, M., Goldwater, R., Mujais, S. K., Schaddelee, M. P., de Koning. P., Kaibara, A., Moy, S.S., & Keirns, J. J. (2012). Proarrhythmic safety of repeat doses of

mirabegron in healthy subjects: a randomized, double-blind, placebo-, and active-controlled thorough QT study. *Clin Pharmacol Ther, 92*(6), 696-706.

Mancini, D. M., Bolinger, L., Li, H., Kendrick, K., Chance, B., & Wilson, J. R. (1994). Validation of near-infrared spectroscopy in humans. *Journal of Applied Physiology, 77*(6), 2740-2747.

Maniam, J., Antoniadis, C., & Morris, M. J. (2014). Early-Life Stress, HPA Axis Adaptation, and Mechanisms Contributing to Later Health Outcomes. *Front Endocrinol (Lausanne), 5*, 73.

Manolopoulos, K. N., Karpe, F., & Frayn, K. N. (2012). Marked resistance of femoral adipose tissue blood flow and lipolysis to adrenaline in vivo. *Diabetologia, 55*(11), 3029-3037.

Marchi, N., Granata, T., Freri, E., Ciusani, E., Ragona, F., Puvenna, V., Teng, Q., Alexopolous, A., & Janigro, D. (2011). Efficacy of anti-inflammatory therapy in a model of acute seizures and in a population of pediatric drug resistant epileptics. *PLoS One, 6*(3), e18200.

Marchi, N., Rasmussen, P., Kapural, M., Fazio, V., Kight, K., Mayberg, M. R., Kanner, A., Ayumar, B., Albensi, B., Cavaglia, M., & Janigro, D. (2003). Peripheral markers of brain damage and blood-brain barrier dysfunction. *Restorative neurology and neuroscience, 21*(0), 109-121.

Marin, P., Darin, N., Amemiya, T., Andersson, B., Jern, S., & Bjorntorp, P. (1992). Cortisol secretion in relation to body fat distribution in obese premenopausal women. *Metabolism, 41*(8), 882-886.

Markelic, M., Velickovic, K., Golic, I., Otasevic, V., Stancic, A., Jankovic, A., Vucetic, M., Buzadzic, B., Korac, B., & Korac, A. (2011). Endothelial cell apoptosis in brown adipose tissue of rats induced by hyperinsulinaemia: the possible role of TNF-α. *Eur J Histochem, 55*(4).

Marks, A., Vianna, D. M., & Carrive, P. (2009). Nonshivering thermogenesis without interscapular brown adipose tissue involvement during conditioned fear in the rat. *Am J Physiol Regul Integr Comp Physiol, 296*(4), R1239-1247.

Marlatt, K. L., Chen, K. Y., & Ravussin, E. (2018). Is activation of human brown adipose tissue a viable target for weight management? *American Journal of Physiology-Regulatory, Integrative and Comparative Physiology, 315*(3), R479-R483.

Martin, R., Hausman, G., & Hausman, D. (1998). Regulation of adipose cell development in utero. *Proceedings of the Society for Experimental Biology and Medicine, 219*(3), 200-210.

Martinez-deMena, R., Calvo, R. M., Garcia, L., & Obregon, M. J. (2016). Effect of glucocorticoids on the activity, expression and proximal promoter of type II deiodinase in rat brown adipocytes. *Mol Cell Endocrinol, 428*, 58-67.

Martinsson, A., Lindvall, K., Melcher, A., & Hjemdahl, P. (1989). Beta-adrenergic receptor responsiveness to isoprenaline in humans: concentration-effect, as compared with dose-effect evaluation and influence of autonomic reflexes. *British Journal of Clinical Pharmacology, 28*(1), 83-94.

Mastorakos, G., & Ilias, I. (2003). Maternal and fetal hypothalamic-pituitary-adrenal axes during pregnancy and postpartum. *Annals of the New York Academy of Sciences, 997*(1), 136-149.

Masuzaki, H., Paterson, J., Shinyama, H., Morton, N. M., Mullins, J. J., Seckl, J. R., & Flier, J. S. (2001). A Transgenic Model of Visceral Obesity and the Metabolic Syndrome. *Science, 294*(5549), 2166-2170.

Matthias, A., Ohlson, K. B. E., Fredriksson, J. M., Jacobsson, A., Nedergaard, J., & Cannon, B. (2000). Thermogenic Responses in Brown Fat Cells Are Fully UCP1-dependent: UCP2 or UCP3 do not substitute for UCP1 in adrenergically or fatty acod-induced thermogenesis. *Journal of Biological Chemistry, 275*(33), 25073-25081.

Maxwell, G. M., Nobbs, S., Fourie, F., & Bates, D. J. (1988). Thermogenesis and the effect of injected catecholamines on the oxygen consumption of cafeteria-fed rats. *Clin Exp Pharmacol Physiol, 15*(5), 391-400.

McCafferty, D. J. (2007). The value of infrared thermography for research on mammals: previous applications and future directions. *Mammal Review, 37*(3), 207-223.

McCormick, C. M., Kehoe, P., & Kovacs, S. (1998). Corticosterone release in response to repeated, short episodes of neonatal isolation: evidence of sensitization. *Int J Dev Neurosci, 16*(3-4), 175-185.

McEwen, B. S. (1992). Steroid hormones: effect on brain development and function. *Horm Res, 37 Suppl 3*, 1-10.

McEwen, B. S. (2000). Effects of adverse experiences for brain structure and function. *Biol Psychiatry, 48*(8), 721-731.

McGill, H., C., McMahan, A., Henderick, E, E., Gray, M, T., Richard, T, E., Strong, J, P. (2000). Origin of Atherosclerosis in childhood and adolescence. *American Journal of Clinical Nutrition, 72*, 1307S–1315S.

Meaney, M. J. (2001). Maternal care, gene expression, and the transmission of individual differences in stress reactivity across generations. *Annu Rev Neurosci, 24*, 1161-1192.

Meaney, M. J., & Aitken, D. H. (1985). The effects of early postnatal handling on hippocampal glucocorticoid receptor concentrations: temporal parameters. *Brain Res, 354*(2), 301-304.

Medicine, A. o. I. (1993). Methods for voluntary weight loss and control: NIH technology assessment conference panel. In (Vol. 119, pp. 764–770.

Mesquida, J., Gruartmoner, G., & Espinal, C. (2013). Skeletal muscle oxygen saturation (StO2) measured by near-infrared spectroscopy in the critically ill patients. *BioMed research international, 2013*.

Mi, J., Law, C., Zhang, K. L., Osmond, C., Stein, C., & Barker, D. (2000). Effects of infant birthweight and maternal body mass index in pregnancy on components of the insulin resistance syndrome in China. *Ann Intern Med, 132*(4), 253-260.

Miki, T., Liu, J.-Q., Ohta, K.-i., Suzuki, S., Kusaka, T., Warita, K., Yokoyama, T., Jamal, M., Ueki, M., Yakura, T., Tamai, M., Sumitani, K., Hosomi, N., & Takeuchi, Y. (2013). Early postnatal maternal separation causes alterations in the expression of β3-adrenergic receptor in rat adipose tissue suggesting long-term influence on obesity. *Biochemical and biophysical research communications, 442*(1-2), 68-71.

Miller-Keane, & O'Toole, M. T. (2005). Miller-Keane Encyclopedia & Dictionary of Medicine, Nursing & Allied Health -- Revised Reprint, 7th Edition. In (7th Edition ed.): Rutgers University, College of Nursing, Coordinator of the Camden Nursing Program, Camden, New Jersey.

Mitchell, P. (1961). Coupling of phosphorylation to electron and hydrogen transfer by a chemi-osmotic type of mechanism. *Nature, 191*(4784), 144-148.

Miura, H., Ozaki, N., Sawada, M., Isobe, K., Ohta, T., & Nagatsu, T. (2008). A link between stress and depression: shifts in the balance between the kynurenine and serotonin pathways of tryptophan metabolism and the etiology and pathophysiology of depression. *Stress, 11*(3), 198-209.

Modi, N., Thomas, E. L., Harrington, T. A., Uthaya, S., Dore, C. J., & Bell, J. D. (2006). Determinants of adiposity during preweaning postnatal growth in appropriately grown and growth-restricted term infants. *Pediatr Res, 60*(3), 345-348.

Modi, N., Thomas, E. L., Uthaya, S. N., Umranikar, S., Bell, J. D., & Yajnik, C. (2009). Whole body magnetic resonance imaging of healthy newborn infants demonstrates increased central adiposity in Asian Indians. *Pediatr Res, 65*(5), 584-587.

Molet, J., Maras, P. M., Avishai-Eliner, S., & Baram, T. Z. (2014). Naturalistic rodent models of chronic early-life stress. *Dev Psychobiol, 56*(8), 1675-1688.

Moores, B., & Regulla, D. (2011). A review of the scientific basis for radiation protection of the patient. *Radiation protection dosimetry, 147*(1-2), 22-29.

Moragas, A., & Torán, N. (1983). Prenatal development of brown adipose tissue in man. *Neonatology, 43*(1-2), 80-85.

Moreira, D. G., Costello, J. T., Brito, C. J., Adamczyk, J. G., Ammer, K., Bach, A. J., Costa, C. M. A., Eglin, C., Fernandes, A. A., & Fernández-Cuevas, I. (2017). Thermographic imaging in sports and exercise medicine: a Delphi study and consensus statement on the measurement of human skin temperature. *Journal of thermal biology, 69*, 155-162.

Morgan, S. A., Hassan-Smith, Z. K., & Lavery, G. G. (2016). Mechanisms in Endocrinology: Tissue-specific activation of cortisol in Cushing's syndrome. *Eur J Endocrinol, 175*(2), R83-89.

Morrison, S. F., Nakamura, K., & Madden, C. J. (2008). Central control of thermogenesis in mammals. *Experimental physiology, 93*(7), 773-797.

Mostyn, A., Bispham, J., Pearce, S., Evens, Y., Raver, N., Keisler, D.H., Webb, R., Stephenson, T. and Symonds, M.E. (2002). Differential effects of leptin on thermoregulation and uncoupling protein abundance in the neonatal lamb. *The FASEB Journal*, *16*(11), pp.1438-1440.

Mostyn, A., Pearce, S., Budge, H., Elmes, M., Forhead, A., Fowden, A., Stephensen, T., & Symonds, M. (2003). Influence of cortisol on adipose tissue development in the fetal sheep during late gestation. *Journal of Endocrinology, 176*(1), 23-30.

Mostyn, A., Pearce, S., Stephenson, T., & Symonds, M. E. (2004). Hormonal and Nutritional Regulation of Adipose Tissue Mitochondrial Development and Function in the Newborn. *Exp Clin Endocrinol Diabetes, 112*(01), 2-9.

Moussaoui, N., Braniste, V., Ait-Belgnaoui, A., Gabanou, M., Sekkal, S., Olier, M., Theodorou, V., Martin, P. G. P., & Houdeau, E. (2014). Changes in Intestinal Glucocorticoid Sensitivity in Early Life Shape the Risk of

Epithelial Barrier Defect in Maternal-Deprived Rats. *PLoS One, 9*(2), e88382.

Moussaoui, N., Larauche, M., Biraud, M., Molet, J., Million, M., Mayer, E., & Taché, Y. (2016). Limited Nesting Stress Alters Maternal Behavior and In Vivo Intestinal Permeability in Male Wistar Pup Rats. *PLoS One, 11*(5), e0155037.

Mullis, K. B. (1990). The unusual origin of the polymerase chain reaction. *Sci Am, 262*(4), 56-61, 64-55.

Münzberg, H., Flier, J. S., & Bjørbæk, C. (2004). Region-specific leptin resistance within the hypothalamus of diet-induced obese mice. *Endocrinology, 145*(11), 4880-4889.

Murkin, J., & Arango, M. (2009). Near-infrared spectroscopy as an index of brain and tissue oxygenation. *British journal of anaesthesia, 103*(suppl 1), i3-i13.

Muzi, M., O'Sullivan, F., Mankoff, D. A., Doot, R. K., Pierce, L. A., Kurland, B. F., Linden, H. M., & Kinahan, P. E. (2012). Quantitative assessment of dynamic PET imaging data in cancer imaging. *Magn Reson Imaging, 30*(9), 1203-1215.

Muzik, O., Mangner, T. J., Leonard, W. R., Kumar, A., Janisse, J., & Granneman, J. G. (2013). 15O PET measurement of blood flow and oxygen consumption in cold-activated human brown fat. *J Nucl Med, 54*(4), 523-531.

Nader, N., Chrousos, G. P., & Kino, T. (2010). Interactions of the circadian CLOCK system and the HPA axis. *Trends Endocrinol Metab, 21*(5), 277-286.

Nagai, N., Sakane, N., Ueno, L. M., Hamada, T., & Moritani, T. (2003). The–3826 A→ G variant of the uncoupling protein-1 gene diminishes postprandial thermogenesis after a high fat meal in healthy boys. *The Journal of Clinical Endocrinology & Metabolism, 88*(12), 5661-5667.

Nagase, I., Yoshida, T., & Saito, M. (2001). Up-regulation of uncoupling proteins by β-adrenergic stimulation in L6 myotubes. *FEBS letters, 494*(3), 175-180.

Nagashima, T., Ohinata, H., & Kuroshima, A. (1994). Involvement of nitric oxide in noradrenaline-induced increase in blood flow through brown adipose tissue. *Life Sci, 54*(1), 17-25.

Nakamura, K., & Morrison, S. F. (2008). A thermosensory pathway that controls body temperature. *Nature neuroscience, 11*(1), 62-71.

Nakayama, A., Bianco, A. C., Zhang, C. Y., Lowell, B. B., & Frangioni, J. V. (2003). Quantitation of brown adipose tissue perfusion in transgenic mice using near-infrared fluorescence imaging. *Mol Imaging, 2*(1), 37-49.

Nedergaard, J., Bengtsson, T., & Cannon, B. (2007). Unexpected evidence for active brown adipose tissue in adult humans. *American Journal of Physiology - Endocrinology and Metabolism, 293*(2), E444-E452.

Nedergaard, J., & Cannon, B. (2010). The changed metabolic world with human brown adipose tissue: therapeutic visions. *Cell metabolism, 11*(4), 268-272.

Nedergaard, J., & Cannon, B. (2013). UCP1 mRNA does not produce heat. *Biochimica et Biophysica Acta (BBA) - Molecular and Cell Biology of Lipids, 1831*(5), 943-949.

Nedergaard, J., & Cannon, B. (2017). 35 - Brown Adipose Tissue: Development and Function. In R. A. Polin, S. H. Abman, D. H. Rowitch, W. E. Benitz, & W. W. Fox (Eds.), *Fetal and Neonatal Physiology (Fifth Edition)* (pp. 354-363.e354): Elsevier.

Nicholls, D. G., Bernson, V. S., & Heaton, G., M. (1978). The identification of the component in the inner membrane of brown adipose tissue mitochondria responsible for regulating energy dissipation. *Experimentia Supplementum, 32*, 89-93.

Nieman, L. K., & Chanco Turner, M. L. (2006). Addison's disease. *Clinics in Dermatology, 24*(4), 276-280.

Nilsson, C., Jennische, E., Ho, H. P., Eriksson, E., Bjorntorp, P., & Holmang, A. (2002). Increased insulin sensitivity and decreased body weight in female rats after postnatal corticosterone exposure. *Eur J Endocrinol, 146*(6), 847-854.

Nilsson, G., Salerud, G., Strömberg, T., Wårdell, K., & Larsson, M. (2003). Laser Doppler perfusion monitoring and imaging.

Nirengi, S., Yoneshiro, T., Sugie, H., Saito, M., & Hamaoka, T. (2015). Human brown adipose tissue assessed by simple, noninvasive near-Infrared time-resolved spectroscopy. *Obesity, 23*(5), 973-980.

Niwayama, M., Murata, H., & Shinohara, S. (2006). Noncontact tissue oxygenation measurement using near-infrared spectroscopy. *Review of Scientific Instruments, 77*(7), 073102.

Nonin Medical. Inc. (2014). Retrieved from https://www.nonin.com/documents/SenSmart/SenSmartPediatricCoreSalesAid.pdf

Novais, A., Monteiro, S., Roque, S., Correia-Neves, M., & Sousa, N. (2017). How age, sex and genotype shape the stress response. *Neurobiology of Stress, 6*, 44-56.

Nyirenda, M. J., Lindsay, R. S., Kenyon, C. J., Burchell, A., & Seckl, J. R. (1998). Glucocorticoid exposure in late gestation permanently programs rat hepatic phosphoenolpyruvate carboxykinase and glucocorticoid receptor expression and causes glucose intolerance in adult offspring. *J Clin Invest, 101*(10), 2174-2181.

Oda, M., Yamashita, Y., Nakano, T., Suzuki, A., Shimizu, K., Hirano, I., Shimomura, F., Ohmae, E., Suzuchi, T., & Tsuchiya, Y. (2000). *Near-infrared time-resolved spectroscopy system for tissue oxygenation monitor*.

Ojha S., B. H. a. S. M. E. (2014). *Adipocytes in Normal Tissue Biology* (R. N. M. Linda M. McManus Ed.): Elsevier.

Oliveira, T. G., Chan, R. B., Bravo, F. V., Miranda, A., Silva, R. R., Zhou, B., Marques, F., Pinto, V., Cerqueira, J. J., Di Paolo, G., & Sousa, N. (2015). The impact of chronic stress on the rat brain lipidome. *Molecular Psychiatry, 21*, 80.

Orava, J., Nuutila, P., Lidell, M. E., Oikonen, V., Noponen, T., Viljanen, T., Scheinin, M., Taittonen, M., Niemi, T., Enerback, S., & Virtanen, K. A. (2011). Different metabolic responses of human brown adipose tissue to activation by cold and insulin. *Cell Metab, 14*(2), 272-279.

Ouchi, N., Kihara, S., Arita, Y., Nishida, M., Matsuyama, A., Okamoto, Y., Ishigami, M., Kuriyama, H., Kishida, K., & Nishizawa, H. (2001). Adipocyte-derived plasma protein, adiponectin, suppresses lipid accumulation and class A scavenger receptor expression in human monocyte-derived macrophages. *Circulation, 103*(8), 1057-1063.

Ouellet, V., Labbé, S. M., Blondin, D. P., Phoenix, S., Guérin, B., Haman, F., Tucotte, E., Richard, D., & Carpentier, A. C. (2012). Brown adipose tissue oxidative metabolism contributes to energy expenditure during acute cold exposure in humans. *The Journal of clinical investigation, 122*(2), 545-552.

Ouellet, V., Routhier-Labadie, A., Bellemare, W., Lakhal-Chaieb, L., Turcotte, E., Carpentier, A. C., & Richard, D. (2011). Outdoor temperature, age, sex, body mass index, and diabetic status determine the prevalence, mass, and glucose-uptake activity of 18F-FDG-detected BAT in humans. *The Journal of Clinical Endocrinology & Metabolism, 96*(1), 192-199.

Owen, R., & Ramlakhan, S. (2017). Infrared thermography in paediatrics: a narrative review of clinical use. *BMJ paediatrics open*, *1*(1).

Owen-Reece, H., Smith, M., Elwell, C. E., & Goldstone, J. C. (1999). Near infrared spectroscopy. *Br J Anaesth, 82*(3), 418-426.

Payal, V., Jora, R., Sharma, P., Gupta, P. K., & Gupta, M. (2016). Premature birth and insulin resistance in infancy: A prospective cohort study. *Indian J Endocrinol Metab, 20*(4), 497-505.

Pearce, S., Budge, H., Mostyn, A., Genever, E., Webb, R., Ingleton, P., Walker, A. M., Symonds, M. E., & Stephenson, T. (2005). Prolactin, the prolactin receptor and uncoupling protein abundance and function in adipose tissue during development in young sheep. *Journal of Endocrinology, 184*(2), 351-359.

Peirce, V., Carobbio, S., & Vidal-Puig, A. (2014). The different shades of fat. *Nature, 510*(7503), 76-83.

Penke, Z., Fernette, B., Nyakas, C., Max, J. P., & Burlet, A. (2002). Neonatal maternal deprivation modifies feeding in response to pharmacological and behavioural factors in adult rats. *Neuropharmacology, 42*(3), 421-427.

Peterson, C. M., Lecoultre, V., Frost, E. A., Simmons, J., Redman, L. M., & Ravussin, E. (2016). The thermogenic responses to overfeeding and cold are differentially regulated. *Obesity, 24*(1), 96-101.

Pi-Sunyer, F, X. (2000). Obesity: criteria and classification. *Proceedings of the Nutrition Society, 59*: 505–509.

Podbegar, M., & Možina, M. (2015). Near infrared spectroscopy for evaluation of skeletal muscle tissue oxygenation in different types of shock. *Signa Vitae, 10*(1), 10-24.

Poirier, P., Giles, T. D., Bray, G. A., Hong, Y., Stern, J. S., Pi-Sunyer, F. X., & Eckel, R. H. (2006). Obesity and cardiovascular disease: pathophysiology, evaluation, and effect of weight loss: an update of the 1997 American Heart Association Scientific Statement on Obesity and Heart Disease from the Obesity Committee of the Council on Nutrition, Physical Activity, and Metabolism. *Circulation, 113*(6), 898-918.

Poissonnet, C. M., Burdi, A. R., & Garn, S. M. (1984). The chronology of adipose tissue appearance and distribution in the human fetus. *Early human development, 10*(1-2), 1-11.

Pope, M., Budge, H., & Symonds, M. (2014). The developmental transition of ovine adipose tissue through early life. *Acta Physiologica, 210*(1), 20-30.

Powell, S. M., Ferguson, S. H., Bowman, J. P., & Snape, I. (2006). Using Real-Time PCR to Assess Changes in the Hydrocarbon-Degrading Microbial Community in Antarctic Soil During Bioremediation. *Microbial Ecology, 52*(3), 523-532.

Preitner, F., Muzzin, P., Revelli, J. P., Seydoux, J., Galitzky, J., Berlan, M., Lafontan, M., & Giacobino, J. P. (1998). Metabolic response to various β-adrenoceptor agonists in β3-adrenoceptor knockout mice: Evidence for a new β-adrenergic receptor in brown adipose tissue. *British journal of pharmacology, 124*(8), 1684-1688.

Pruessner, J. C., Dedovic, K., Pruessner, M., Lord, C., Buss, C., Collins, L., Dagher, A., & Lupien, S. J. (2010). Stress regulation in the central nervous system: evidence from structural and functional neuroimaging studies in human populations - 2008 Curt Richter Award Winner. *Psychoneuroendocrinology, 35*(1), 179-191.

Public Health England. (2016). Child Obesity; UK prevalence. Retrieved from https://www.gov.uk/government/publications/childhood-obesity-a-plan-for-action.

Puchalski, W., Bockler, H., Heldmaier, G., & Langefeld, M. (1987). Organ blood flow and brown adipose tissue oxygen consumption during noradrenaline-induced nonshivering thermogenesis in the Djungarian hamster. *J Exp Zool, 242*(3), 263-271.

Puigserver, P., Herron, D., Gianotti, M., Palou, A., Cannon, B., & Nedergaard, J. (1992). Induction and degradation of the uncoupling protein thermogenin in brown adipocytes in vitro and in vivo. Evidence for a rapidly degradable pool. *Biochemical Journal, 284*(Pt 2), 393-398.

Puigserver, P., Wu, Z., Park, C. W., Graves, R., Wright, M., & Spiegelman, B. M. (1998). A cold-inducible coactivator of nuclear receptors linked to adaptive thermogenesis. *Cell, 92*(6), 829-839.

Quaresima, V., Komiyama, T., & Ferrari, M. (2002). Differences in oxygen re-saturation of thigh and calf muscles after two treadmill stress tests. *Comp Biochem Physiol A Mol Integr Physiol, 132*(1), 67-73.

Quinkler, M., Johanssen, S., Großmann, C., Bähr, V., Müller, M., Oelkers, W., & Diederich, S. (1999). Progesterone metabolism in the human kidney and inhibition of 11β-hydroxysteroid dehydrogenase type 2 by progesterone and its metabolites. *The Journal of Clinical Endocrinology & Metabolism, 84*(11), 4165-4171.

Raabe, F. J., & Spengler, D. (2013). Epigenetic risk factors in PTSD and depression. *Frontiers in psychiatry*, *4*, 80. p1-17.

Radley, J. J., Arias, C. M., & Sawchenko, P. E. (2006). Regional differentiation of the medial prefrontal cortex in regulating adaptive responses to acute emotional stress. *J Neurosci, 26*(50), 12967-12976.

Ramage, L. E., Akyol, M., Fletcher, A. M., Forsythe, J., Nixon, M., Carter, R. N., van Beek, E. J. R., Morton, N. M ., Walker, B. R., & Stimson, R. H. (2016). Glucocorticoids acutely increase brown adipose tissue activity in humans, revealing species-specific differences in UCP-1 regulation. *Cell metabolism, 24*(1), 130-141.

Ramanathan, N. (1964). A new weighting system for mean surface temperature of the human body. *Journal of Applied Physiology, 19*(3), 531-533.

Rangon, C.-M., Fortes, S., Lelièvre, V., Leroux, P., Plaisant, F., Joubert, C., Lanfumey, L., Cohen-Salmon, C., & Gressens, P. (2007). Chronic Mild Stress during Gestation Worsens Neonatal Brain Lesions in Mice. *The Journal of Neuroscience, 27*(28), 7532.

Rask, E., Walker, B. R., Soderberg, S., Livingstone, D. E., Eliasson, M., Johnson, O., Andrew, R., & Olsson, T. (2002). Tissue-specific changes in peripheral cortisol metabolism in obese women: increased adipose 11beta-hydroxysteroid dehydrogenase type 1 activity. *J Clin Endocrinol Metab, 87*(7), 3330-3336.

Rasmussen, J. M., Entringer, S., Nguyen, A., van Erp, T. G. M., Guijarro, A., Oveisi, F., Swanson, J. M., Piomelli, D., Wadhwa, P. D., Buss, C., & Potkin, S. G. (2013). Brown Adipose Tissue Quantification in Human Neonates Using Water-Fat Separated MRI. *PLoS One, 8*(10), e77907.

Ravelli, A. C., van der Meulen, J. H., Michels, R. P., Osmond, C., Barker, D. J., Hales, C. N., & Bleker, O. P. (1998). Glucose tolerance in adults after prenatal exposure to famine. *Lancet, 351*(9097), 173-177.

Razzoli, M., Frontini, A., Gurney, A., Mondini, E., Cubuk, C., Katz, L. S., Cero, C., Bolan, P. J., Dopazo, J., & Vidal-Puig, A. (2016). Stress-induced activation of brown adipose tissue prevents obesity in conditions of low adaptive thermogenesis. *Molecular metabolism, 5*(1), 19-33.

Reaven, G., M. . (1988). Banting Lecture: The role of insulin resistance in human disease. *Diabetes, 37*, 1595-1607.

Reddy, N. L., Jones, T. A., Wayte, S. C., Adesanya, O., Sankar, S., Yeo, Y. C., Tripathi, G., McTernan, P. G., Randeva, H. S., & Kumar, S. (2014). Identification of brown adipose tissue using MR imaging in a hu-

man adult with histological and immunohistochemical confirmation. *The Journal of Clinical Endocrinology & Metabolism, 99*(1), E117-E121.

Redman, L. M., de Jonge, L., Fang, X., Gamlin, B., Recker, D., Greenway, F. L., Smith, S. R., & Ravussin, E. (2007). Lack of an effect of a novel beta3-adrenoceptor agonist, TAK-677, on energy metabolism in obese individuals: a double-blind, placebo-controlled randomized study. *J Clin Endocrinol Metab, 92*(2), 527-531.

Reed, N., & Fain, J. N. (1968). Potassium-dependent Stimulation of Respiration in Brown Fat Cells by Fatty Acids and Lipolytic Agents. *Journal of Biological Chemistry, 243*(23), 6077-6083.

Regan, F. M., Cutfield, W. S., Jefferies, C., Robinson, E., & Hofman, P. L. (2006). The Impact of Early Nutrition in Premature Infants on Later Childhood Insulin Sensitivity and Growth. *Pediatrics, 118*(5), 1943.

Rehnmark, S., Nechad, M., Herron, D., Cannon, B., & Nedergaard, J. (1990). Alpha-and beta-adrenergic induction of the expression of the uncoupling protein thermogenin in brown adipocytes differentiated in culture. *Journal of Biological Chemistry, 265*(27), 16464-16471.

Reijne, A. C., Ciapaite, J., van Dijk, T. H., Havinga, R., van der Zee, E. A., Groen, A. K., Reijngoud, D-J., Bakker, B. M., & van Dijk, G. (2016). Whole-Body Vibration Partially Reverses Aging-Induced Increases in Visceral Adiposity and Hepatic Lipid Storage in Mice. *PLoS One, 11*(2), e0149419.

Revelli, J-P., Preitner, F., Samec, S., Muniesa, P., Kuehne, F., Boss, O., Vassalli, J-D., Dulloo, A., Seydoux, J., & Giacobino, J.-P. (1997). Targeted gene disruption reveals a leptin-independent role for the mouse beta3-adrenoceptor in the regulation of body composition. *Journal of Clinical Investigation, 100*(5), p1098-1016.

Ribeiro, M. O., Carvalho, S. D., Schultz, J. J., Chiellini, G., Scanlan, T. S., Bianco, A. C., & Brent, G. A. (2001). Thyroid hormone–sympathetic interaction and adaptive thermogenesis are thyroid hormone receptor isoform–specific. *The Journal of clinical investigation, 108*(1), 97-105.

Rice, H. E., Hollingsworth, C. L., Bradsher, E., Danko, M. E., Crosby, S. M., Goldberg, R. N., . . . Knobel, R. B. (2010). Infrared thermal imaging (thermography) of the abdomen in extremely low birthweight infants. *J Surg Radiol, 1*(2), 61-122.

Riva, C., Ross, B., & Benedek, G. B. (1972). Laser Doppler measurements of blood flow in capillary tubes and retinal arteries. *Investigative Ophthalmology & Visual Science, 11*(11), 936-944.

Robidoux, J., Kumar, N., Daniel, K. W., Moukdar, F., Cyr, M., Medvedev, A. V., & Collins, S. (2006). Maximal β3-adrenergic regulation of lipolysis involves Src and epidermal growth factor receptor-dependent ERK1/2 activation. *Journal of Biological Chemistry, 281*(49), 37794-37802.

Robinson, L. J., Law, J. M., Symonds, M. E., & Budge, H. (2016). Brown adipose tissue activation as measured by infrared thermography by mild anticipatory psychological stress in lean healthy females. *Experimental physiology, 101*(4), 549-557.

Roceri, M., Cirulli, F., Pessina, C., Peretto, P., Racagni, G., & Riva, M. A. (2004). Postnatal repeated maternal deprivation produces age-dependent changes of brain-derived neurotrophic factor expression in selected rat brain regions. *Biol Psychiatry, 55*(7), 708-714.

Rodgers, R. J., Tschöp, M. H., & Wilding, J. P. (2012). Anti-obesity drugs: past, present and future. *Disease models & mechanisms, 5*(5), 621-626.

De Lucia Rolfe, E., Loos, R. J., Druet, C., Stolk, R. P., Ekelund, U., Griffin, S.J., Forouhi, N.G., Wareham, N.J. and Ong, K.K. (2010). Association between birth weight and visceral fat in adults. *The American journal of clinical nutrition*, *92*(2), 347-352.

Romijn, H. J., Hofman, M. A., & Gramsbergen, A. (1991). At what age is the developing cerebral cortex of the rat comparable to that of the full-term newborn human baby? *Early human development, 26*(1), 61-67.

Rondo, P. H., Ferreira, R. F., Nogueira, F., Ribeiro, M. C., Lobert, H., & Artes, R. (2003). Maternal psychological stress and distress as predictors of low birth weight, prematurity and intrauterine growth retardation. *Eur J Clin Nutr, 57*(2), 266-272.

Rosen, E. D. (2015). Two paths to fat. *Nat Cell Biol, 17*(4), 360-361.

Rosenfeld, P., Gutierrez, Y. A., Martin, A. M., Mallett, H. A., Alleva, E., & Levine, S. (1991). Maternal regulation of the adrenocortical response in preweanling rats. *Physiol Behav, 50*(4), 661-671.

Rosmond, R., & Bjorntorp, P. (2000). The hypothalamic-pituitary-adrenal axis activity as a predictor of cardiovascular disease, type 2 diabetes and stroke. *J Intern Med, 247*(2), 188-197.

Rothwell, N. J., & Stock, M. J. (1979). A role for brown adipose tissue in diet-induced thermogenesis. *Nature, 281*(5726), 31-35.

Rothwell, N. J., & Stock, M. J. (1997). A role for brown adipose tissue in diet-induced thermogenesis. *Obes Res, 5*(6), 650-656.

Rousseau, C., Bourbouloux, E., Campion, L., Fleury, N., Bridji, B., Chatal, J., Resche, I., & Campone, M. (2006). Brown fat in breast cancer patients: analysis of serial 18F-FDG PET/CT scans. *European journal of nuclear medicine and molecular imaging, 33*(7), 785-791.

Rozansky, D. J., Wu, H., Tang, K., Parmer, R. J., & O'Connor, D. T. (1994). Glucocorticoid activation of chromogranin A gene expression. Identification and characterization of a novel glucocorticoid response element. *J Clin Invest, 94*(6), 2357-2368.

Russell, W. M. S., Burch, R. L., & Universities Federation for Animal, W. (1992). *The Principles of humane experimental technique*. Wheathampstead: Universities Federation for Animal Welfare.

Rylander, E., Pribylova, H., & Lind, J. (1972). A thermographic study of infants exposed to cold. *Acta Pædiatrica, 61*(1), 42-48.

Ryu, V., Yoo, S. B., Kang, D.-W., Lee, J.-H., & Jahng, J. W. (2009). Post-weaning isolation promotes food intake and body weight gain in rats that experienced neonatal maternal separation. *Brain Res, 1295*, 127-134.

Saito, M., Okamatsu-Ogura, Y., Matsushita, M., Watanabe, K., Yoneshiro, T., Nio-Kobayashi, J., Iwanaga, T., Miyagawa, M., Kameya, T., Nakada, K., Kawai, Y., & Tsujisaki, M. (2009). High Incidence of Metabolically Active Brown Adipose Tissue in Healthy Adult Humans: Effects of Cold Exposure and Adiposity. *Diabetes, 58*(7), 1526-1531.

Salem, V., Izzi-Engbeaya, C., Coello, C., Thomas, D. B., Chambers, E. S., Comninos, A. N., Buckley, A., Win, Z., Al-Nahhas, A., Rabiner, E. A., Gunn, R. N., Budge, H., Symonds, M. E., Bloom, S. R. Tan T. M., & Dhillo, W. S. (2016). Glucagon increases energy expenditure independently of brown adipose tissue activation in humans. *Diabetes, Obesity & Metabolism, 18*(1), 72-81.

Sanchez, M. M., Ladd, C. O., & Plotsky, P. M. (2001). Early adverse experience as a developmental risk factor for later psychopathology: evidence from rodent and primate models. *Dev Psychopathol, 13*(3), 419-449.

Sapolsky, R. M., & Meaney, M. J. (1986). Maturation of the adrenocortical stress response: neuroendocrine control mechanisms and the stress hyporesponsive period. *Brain Res, 396*(1), 64-76.

Sarabdjitsingh, R. A., Loi, M., Joëls, M., Dijkhuizen, R. M., & van der Toorn, A. (2017). Early life stress-induced alterations in rat brain structures measured with high resolution MRI. *PLoS One, 12*(9), e0185061.

Sarr, O., Yang, K., & Regnault, T. R. H. (2012). In Utero Programming of Later Adiposity: The Role of Fetal Growth Restriction. *Journal of Pregnancy, 2012*, 10.

Schawlow, A. L., & Townes, C. H. (1958). Infrared and optical masers. *Physical Review, 112*(6), 1940.

Scheele, C., & Nielsen, S. (2017). Metabolic regulation and the anti-obesity perspectives of human brown fat. *Redox Biol, 12*, 770-775.

Schlogl, M., Piaggi, P., Thiyyagura, P., Reiman, E. M., Chen, K., Lutrin, C., Krakoff, J., & Thearle, M. S. (2013). Overfeeding over 24 hours does not activate brown adipose tissue in humans. *J Clin Endocrinol Metab, 98*(12), E1956-1960.

Schmidt, F. E. W., Fry, M. E., Hillman, E. M. C., Hebden, J. C., & Delpy, D. T. (2000). A 32-channel time-resolved instrument for medical optical tomography. *Review of Scientific Instruments, 71*(1), 256-265.

Schmidt, M. V., Enthoven, L., van der Mark, M., Levine, S., de Kloet, E. R., & Oitzl, M. S. (2003). The postnatal development of the hypothalamic-pituitary-adrenal axis in the mouse. *Int J Dev Neurosci, 21*(3), 125-132.

Schmidt, M. V., Oitzl, M. S., Levine, S., & de Kloet, E. R. (2002). The HPA system during the postnatal development of CD1 mice and the effects of maternal deprivation. *Brain Res Dev Brain Res, 139*(1), 39-49.

Schoenfeld, N. M., Leathem, J. H., & Rabii, J. (1980). Maturation of adrenal stress responsiveness in the rat. *Neuroendocrinology, 31*(2), 101-105.

Schulz, T. J., & Tseng, Y. H. (2013). Brown adipose tissue: development, metabolism and beyond. *Biochem J, 453*(2), 167-178.

Scotney, H., Symonds, M. E., Law, J., Budge, H., Sharkey, D., & Manolopoulos, K. N. (2017). Glucocorticoids modulate human brown adipose tissue thermogenesis in vivo. *Metabolism, 70*, 125-132.

Seale, P., Bjork, B., Yang, W., Kajimura, S., Chin, S., Kuang, S., Scieme, A., Devarakonda, S., Conroe, H. M., Erdjument-Bromage, H., Tempst, P., Rudnicki, M. A., Beier, D. R., & Spiegelman, B. M. (2008). PRDM16 controls a brown fat/skeletal muscle switch. *Nature, 454*, 961.

Seale, P., Kajimura, S., Yang, W., Chin, S., Rohas, L. M., Uldry, M., Tavernier, G., Langin, D., & Spiegelman, B. M. (2007). Transcriptional control of brown fat determination by PRDM16. *Cell Metab, 6*(1), 38-54.

Seckl, J. R. (1997). Glucocorticoids, feto-placental 11β-hydroxysteroid dehydrogenase type 2, and the early life origins of adult disease. *Steroids, 62*(1), 89-94.

Seckl, J. R. (2004). Prenatal glucocorticoids and long-term programming. *Eur J Endocrinol, 151 Suppl 3*, U49-62.

Seckl, J. R., & Holmes, M. C. (2007). Mechanisms of disease: glucocorticoids, their placental metabolism and fetal 'programming' of adult pathophysiology. *Nat Clin Pract Endocrinol Metab, 3*(6), 479-488.

Segal, S. S. (2005). Regulation of blood flow in the microcirculation. *Microcirculation, 12*(1), 33-45.

Seidell, J., Han, T., Feskens, E., Lean, M. (1997). Narrow hips and broad waist circumference independently contribute to increased risk of non-insulin dependent diabetes mellitus. *Journal of International Medicine, 242*: 401–406.

Seron-Ferre, M., Reynolds, H., Mendez, N. A., Mondaca, M., Valenzuela, F., Ebensperger, R., Valenzuela, F., Ebensperger, G. J., Herrera, E. A., Llanos, A. J., & Torres-Farfan, C. (2014). Impact of Maternal Melatonin Suppression on Amount and Functionality of Brown Adipose Tissue (BAT) in the Newborn Sheep. *Frontiers in Endocrinology, 5*, 232.

Serpero, L. D., Pluchinotta, F., & Gazzolo, D. (2015). The clinical and diagnostic utility of S100B in preterm newborns. *Clinica chimica acta; international journal of clinical chemistry, 444*, 193-198.

Shalev, H., Serlin, Y., & Friedman, A. (2009). Breaching the Blood-Brain Barrier as a Gate to Psychiatric Disorder. *Cardiovascular Psychiatry and Neurology, 2009*, 7.

Shams, M., Kilby, M. D., Somerset, D. A., Howie, A. J., Gupta, A., Wood, P. J., Afnan, M., & Stewart, P. M. (1998). 11Beta-hydroxysteroid dehydrogenase type 2 in human pregnancy and reduced expression in intrauterine growth restriction. *Hum Reprod, 13*(4), 799-804.

Shimizu, Y., Kielar, D., Minokoshi, Y., & Shimazu, T. (1996). Noradrenaline increases glucose transport into brown adipocytes in culture by a mechanism different from that of insulin. *Biochem J, 314 (Pt 2)*, 485-490.

Shimizu, Y., Nikami, H., Tsukazaki, K., Machado, U. F., Yano, H., Seino, Y., & Saito, M. (1993). Increased expression of glucose transporter GLUT-4 in brown adipose tissue of fasted rats after cold exposure. *Am J Physiol, 264*(6 Pt 1), E890-895.

Sidery, M. B., & Macdonald, I. A. (1994). The effect of meal size on the cardiovascular responses to food ingestion. *Br J Nutr, 71*(6), 835-848.

Silverman, M. N., & Sternberg, E. M. (2012). Glucocorticoid regulation of inflammation and its behavioral and metabolic correlates: from HPA axis to glucocorticoid receptor dysfunction. *Annals of the New York Academy of Sciences, 1261*, 55-63.

Simonson, S. G., & Piantadosi, C. A. (1996). Near-Infrared Spectroscopy. *Critical Care Clinics, 12*(4), 1019-1029.

Skala, J. P. (1984). Mechanisms of hormonal regulations in brown adipose tissue of developing rats. *Canadian journal of biochemistry and cell biology, 62*(7), 637-647.

Slater, A. (2002). Visual perception in the newborn infant: issues and debates. *Intellectica, 34*, 57-76.

Smith, G. C., Gutovich, J., Smyser, C., Pineda, R., Newnham, C., Tjoeng, T. H., Vavasseur, C., Wallendorf, M., Neil, J., & Inder, T. (2011). Neonatal intensive care unit stress is associated with brain development in preterm infants. *Annals of Neurology, 70*(4), 541-549.

Smith, M. A., Kim, S. Y., van Oers, H. J., & Levine, S. (1997). Maternal deprivation and stress induce immediate early genes in the infant rat brain. *Endocrinology, 138*(11), 4622-4628.

Smith, R. E. (1961). Thermogenic activity of the hibernating gland in the cold-acclimatized rat. *Physiologist, 4*, 113.

Smotherman, W. P. (1983). Mother-infant interaction and the modulation of pituitary-adrenal activity in rat pups after early stimulation. *Developmental Psychobiology, 16*(3), 169-176.

Sorrells, S. F., Caso, J. R., Munhoz, C. D., & Sapolsky, R. M. (2009). The stressed CNS: when glucocorticoids aggravate inflammation. *Neuron, 64*(1), 33-39.

Soumano, K., Desbiens, S., Rabelo, R., Bakopanos, E., Camirand, A., & Silva, J. E. (2000). Glucocorticoids inhibit the transcriptional response of the uncoupling protein-1 gene to adrenergic stimulation in a brown adipose cell line. *Mol Cell Endocrinol, 165*(1-2), 7-15.

Sowa, J., Bobula, B., Glombik, K., Slusarczyk, J., Basta-Kaim, A., & Hess, G. (2015). Prenatal stress enhances excitatory synaptic transmission and impairs long-term potentiation in the frontal cortex of adult offspring rats. *PLoS One, 10*(3), e0119407.

Srinivasan, S., R., Myers, L., Berenson, G, S. (2002). Predictability of childhood adiposity and insulin for developing insulin resistance syndrome (syndrome X) in young adulthood: the Bogalusa Heart Study. *Diabetes, 52*, 204–209.

Stanford, K. I., & Goodyear, L. J. (2016). Exercise regulation of adipose tissue. *Adipocyte, 5*(2), 153-162.

Steketee, J. (1973). Spectral emissivity of skin and pericardium. *Phys Med Biol, 18*(5), 686-694.

Stern, M. (1975). In vivo evaluation of microcirculation by coherent light scattering.

Sternberg, E. M., Hill, J. M., Chrousos, G. P., Kamilaris, T., Listwak, S. J., Gold, P. W., & Wilder, R. L. (1989). Inflammatory mediator-induced hypothalamic-pituitary-adrenal axis activation is defective in streptococcal cell wall arthritis-susceptible Lewis rats. *Proc Natl Acad Sci U S A, 86*(7), 2374-2378.

Stevens, J., Cai, J., Pamuk, E, R., Williamson, D, F., Thun, M, J., Wood, J, L. (1998). The effect of age on the association between body mass in dex and mortality. *New England Journal of Medicine, 338:* 1–7.

Stimson, R. H., Andersson, J., Andrew, R., Redhead, D. N., Karpe, F., Hayes, P. C., Olsson, T., & Walker, B. R. (2009). Cortisol release from adipose tissue by 11β-hydroxysteroid dehydrogenase type 1 in humans. *Diabetes, 58*(1), 46-53.

Strack, A. M., Sebastian, R. J., Schwartz, M. W., & Dallman, M. F. (1995). Glucocorticoids and insulin: reciprocal signals for energy balance. *Am J Physiol, 268*(1 Pt 2), R142-149.

Strauss, R., S. (2000). Childhood obesity and self-esteem. *Paediatrics, 105*(1), 1-5.

Stuart, J. A., Harper, J. A., Brindle, K.M., Jekabsons, M. B., & Brand, M. D. (2001). A mitochondrial uncoupling artifact can be caused by expression of uncoupling protein 1 in yeast. *Biochemical Journal, 356*(3), 779-789.

Suchecki, D., Rosenfeld, P., & Levine, S. (1993). Maternal regulation of the hypothalamic-pituitary-adrenal axis in the infant rat: the roles of feeding and stroking. *Brain Res Dev Brain Res, 75*(2), 185-192.

Suhaimi, F. M., Chase, J. G., Pretty, C. G., Elliott, R., & Shaw, G. M. (2013). Pulse oximeter concept for vascular occlusion test. *International Journal of Medical, Pharmaceutical Science and Engineering, 7*(11), 29-33.

Sun, C., Zeng, R., Cao, G., Song, Z., Zhang, Y., & Liu, C. (2015). Vibration Training Triggers Brown Adipocyte Relative Protein Expression in Rat White Adipose Tissue. *BioMed research international, 2015*, 919401. doi:10.1155/2015/919401

Susulic, V. S., Frederich, R. C., Lawitts, J., Tozzo, E., Kahn, B. B., Harper, M.-E., Himms-Hagen, J., Flier, J. S., & Lowell, B. B. (1995). Targeted disruption of the β3-adrenergic receptor gene. *Journal of Biological Chemistry, 270*(49), 29483-29492.

Svensson, P. A., Jernas, M., Sjoholm, K., Hoffmann, J. M., Nilsson, B. E., Hansson, M., & Carlsson, L. M. (2011). Gene expression in human brown adipose tissue. *Int J Mol Med, 27*(2), 227-232.

Svensson, P.-A., Lindberg, K., Hoffmann, J. M., Taube, M., Pereira, M. J., Mohsen-Kanson, T., Hafner, A-L., Rizell, M., Palming, J., Dani, C., & Svensson, M. K. (2014). Characterization of brown adipose tissue in the human perirenal depot. *Obesity, 22*(8), 1830-1837.

Swinburn, B. A., Sacks, G., Hall, K. D., McPherson, K., Finegood, D. T., Moodie, M. L., & Gortmaker, S. L. (2011). The global obesity pandemic: shaped by global drivers and local environments. *The Lancet, 378*(9793), 804-814.

Symonds, M., Andrews, D., & Johnson, P. (1989). The control of thermoregulation in the developing lamb during slow wave sleep. *Journal of developmental physiology, 11*(5), 289-298.

Symonds, M., Bird, J., Sullivan, C., Wilson, V., Clarke, L., & Stephenson, T. (2000). Effect of delivery temperature on endocrine stimulation of thermoregulation in lambs born by cesarean section. *Journal of Applied Physiology, 88*(1), 47-53.

Symonds, M., Mostyn, A., Pearce, S., Budge, H., & Stephenson, T. (2003). Endocrine and nutritional regulation of fetal adipose tissue development. *Journal of Endocrinology, 179*(3), 293-299.

Symonds, M., Mostyn, A., & Stephenson, T. (2001). Cytokines and cytokine receptors in fetal growth and development. In: Portland Press Limited.

Symonds, M., Pope, M., Sharkey, D., & Budge, H. (2012). Adipose tissue and fetal programming. *Diabetologia, 55*(6), 1597-1606.

Symonds, M. E. (1995). The Nutrition Society 1994 Silver Medal Lecture. *Proceedings of the Nutrition Society, 54*, 329-343.

Symonds, M. E. (2013). Brown adipose tissue growth and development. *Scientifica, 2013*. p1-14.

Symonds, M. E., Bird, J. A., Clarke, L., Gate, J. J., & Lomax, M. A. (1995). Nutrition, temperature and homeostasis during perinatal development. *Experimental physiology, 80*(6), 907-940.

Symonds, M. E., Budge, H., Perkins, A. C., & Lomax, M. A. (2011). Adipose tissue development–impact of the early life environment. *Progress in biophysics and molecular biology, 106*(1), 300-306.

Symonds, M. E., Henderson, K., Elvidge, L., Bosman, C., Sharkey, D., Perkins, A. C., & Budge, H. (2012). Thermal imaging to assess age-related changes of skin temperature within the supraclavicular region co-locating with brown adipose tissue in healthy children. *The Journal of pediatrics, 161*(5), 892-898.

Symonds, M. E., & Lomax, M. A. (1992). Maternal and environmental influences on thermoregulation in the neonate. *Proceedings of the Nutrition Society, 51*(02), 165-172.

Symonds, M. E., Mostyn, A., Pearce, S., Budge, H., & Stephenson, T. (2003). Endocrine and nutritional regulation of fetal adipose tissue development. *Journal of Endocrinology, 179*(3), 293-299.

Symonds, M. E., Sebert, S., & Budge, H. (2011). The obesity epidemic: from the environment to epigenetics–not simply a response to dietary manipulation in a thermoneutral environment. *Frontiers in genetics, 2*, 24.

Symonds, M. E., Sebert, S. P., & Budge, H. (2010). Nutritional regulation of fetal growth and implications for productive life in ruminants. *animal, 4*(Special Issue 07), 1075-1083.

Taga, H., Chilliard, Y., Meunier, B., Chambon, C., Picard, B., Zingaretti, M. C., Cinti, S., & Bonnet, M. (2012). Cellular and molecular large-scale features of fetal adipose tissue: Is bovine perirenal adipose tissue Brown1685. *Journal of Cellular Physiology, 227*(4), 1688-1700.

Takahashi, M., Arita, Y., Yamagata, K., Matsukawa, Y., Okutomi, K., Horie, M., Shimomura, I., Hotta, Kuriyama, H., & Kihara, S. (2000). Genomic structure and mutations in adipose-specific gene, adiponectin. *International journal of obesity, 24*(7), p861-868.

Tanuma, Y., Tamamoto, M., Ito, T., & Yokochi, C. (1975). The occurrence of brown adipose tissue in perirenal fat in Japanese. *Arch Histol Jpn, 38*(1), 43-70.

Taube, M., Andersson-Assarsson, J. C., Lindberg, K., Pereira, M. J., Gäbel, M., Svensson, M. K., Eriksson, J. W., & Svensson, P.-A. (2015). Evaluation of reference genes for gene expression studies in human brown adipose tissue. *Adipocyte, 4*(4), 280-285.

Thornhill, J., & Halvorson, I. (1993). Intrascapular brown adipose tissue (IBAT) temperature and blood flow responses following ventromedial hypothalamic stimulation to sham and IBAT-denervated rats. *Brain Res, 615*(2), 289-294.

Tobe, I., Ishida, Y., Tanaka, M., Endoh, H., Fujioka, T., & Nakamura, S. (2005). Effects of repeated maternal stress on FOS expression in the hypothalamic paraventricular nucleus of fetal rats. *Neuroscience, 134*(2), 387-395.

Tosh, W., & Patteril, M. (2016). Cerebral oximetry. *BJA Education, 16*(12), 417-421.

Tounian, P., Aggoun, Y., Dubern, B., Varille, V., Guy-Grand, B., Sidi, D., Girardet, J,P., Bonnet, D. (2001). Presence of increased stiffness of the common carotid artery and endothelial dysfunction in severely obese children: a prospective study. *Lancet, 358*, 1400–1404.

Tseng, Y.-H., Cypess, A. M., & Kahn, C. R. (2010). Cellular bioenergetics as a target for obesity therapy. *Nature Reviews Drug Discovery, 9*(6), 465-482.

Tu, M. T., Grunau, R. E., Petrie-Thomas, J., Haley, D. W., Weinberg, J., & Whitfield, M. F. (2007). Maternal stress and behavior modulate relationships between neonatal stress, attention, and basal cortisol at 8 months in preterm infants. *Dev Psychobiol, 49*(2), 150-164.

Ueta, C. B., Fernandes, G. W., Capelo, L. P., Fonseca, T. L., Maculan, F. D. A., Gouveia, C. H., Brum, P. C., Christoffolete, M. A., Aoki, M. S., & Lancellotti, C. L. (2012). β1 Adrenergic receptor is key to cold-and diet-induced thermogenesis in mice. *Journal of Endocrinology, 214*(3), 359-365.

Ursino, M. G., Vasina, V., Raschi, E., Crema, F., & De Ponti, F. (2009). The beta3-adrenoceptor as a therapeutic target: current perspectives. *Pharmacol Res, 59*(4), 221-234.

Uthaya, S., Thomas, E. L., Hamilton, G., Doré, C. J., Bell, J., & Modi, N. (2005). Altered adiposity after extremely preterm birth. *Pediatric Research, 57*(2), 211.

van Baak, M. A. (2008). Meal-induced activation of the sympathetic nervous system and its cardiovascular and thermogenic effects in man. *Physiol Behav, 94*(2), 178-186.

Van Beekvelt, M. C., Colier, W. N., Wevers, R. A., & Van Engelen, B. G. (2001). Performance of near-infrared spectroscopy in measuring local O(2) consumption and blood flow in skeletal muscle. *J Appl Physiol (1985), 90*(2), 511-519.

van Bodegom, M., Homberg, J. R., & Henckens, M. J. A. G. (2017). Modulation of the Hypothalamic-Pituitary-Adrenal Axis by Early Life Stress Exposure. *Front Cell Neurosci, 11*(87).

van der Lans, A. A., Vosselman, M. J., Hanssen, M. J., Brans, B., & van Marken Lichtenbelt, W. D. (2016). Supraclavicular skin temperature and BAT activity in lean healthy adults. *J Physiol Sci, 66*(1), 77-83.

van der Lans, A. A., Wierts, R., Vosselman, M. J., Schrauwen, P., Brans, B., & van Marken Lichtenbelt, W. D. (2014). Cold-activated brown adipose tissue in human adults: methodological issues. *Am J Physiol Regul Integr Comp Physiol, 307*(2), R103-113.

van der Lans, A. A. J. J., Hoeks, J., Brans, B., Vijgen, G. H. E. J., Visser, M., IIL, G. W., Vosselman, M. J., Hansen, J., Jorgensen, J. A., Wu, J., Mottaghy, F. M., Schrauwen, P., & van Marken Lichtenbelt, W. D. (2013). Cold acclimation recruits human brown fat and increases nonshivering thermogenesis. *The Journal of clinical investigation, 123*(8), 3395-3403.

van Marken Lichtenbelt, W. D., Schrauwen, P., van de Kerckhove, S., & Westerterp-Plantenga, M. S. (2002). Individual variation in body temperature and energy expenditure in response to mild cold. *American Journal of Physiology-Endocrinology and Metabolism, 282*(5), E1077-E1083.

van Marken Lichtenbelt, W. D., Vanhommerig, J. W., Smulders, N. M., Drossaerts, J. M. A. F. L., Kemerink, G. J., Bouvy, N. D., Schrauwen, P., & Teule, G. J. J. (2009). Cold-Activated Brown Adipose Tissue in Healthy Men. *New England Journal of Medicine, 360*(15), 1500-1508.

Vander Tuig, J. G., Ohshima, K., Yoshida, T., Romsos, D. R., & Bray, G. A. (1984). Adrenalectomy increases norepinephrine turnover in brown adipose tissue of obese (ob/ob) mice. *Life Sci, 34*(15), 1423-1432.

Vandesompele, J., De Preter, K., Pattyn, F., Poppe, B., Van Roy, N., De Paepe, A., & Speleman, F. (2002). Accurate normalization of real-time quantitative RT-PCR data by geometric averaging of multiple internal control genes. *Genome Biol, 3*(7), Research0034.

van Oers, H. J., de Kloet, E. R., & Levine, S. (1998). Early vs. late maternal deprivation differentially alters the endocrine and hypothalamic responses to stress. *Developmental Brain Research, 111*(2), 245-252.

Veldhuis, J. D., Roemmich, J. N., Richmond, E. J., & Bowers, C. Y. (2006). Somatotropic and gonadotropic axes linkages in infancy, childhood, and the puberty-adult transition. *Endocrine reviews, 27*(2), 101-140.

Vicennati, V., Pasqui, F., Cavazza, C., Pagotto, U., & Pasquali, R. (2009). Stress-related development of obesity and cortisol in women. *Obesity (Silver Spring), 17*(9), 1678-1683. doi:10.1038/oby.2009.76

Vidal-Puig, A., Solanes, G., Grujic, D., Flier, J. S., & Lowell, B. B. (1997). UCP3: An Uncoupling Protein Homologue Expressed Preferentially and Abundantly in Skeletal Muscle and Brown Adipose Tissue. *Biochemical and biophysical research communications, 235*(1), 79-82.

Viengchareun, S., Penfornis, P., Zennaro, M.-C., & Lombès, M. (2001). Mineralocorticoid and glucocorticoid receptors inhibit UCP expression and function in brown adipocytes. *American Journal of Physiology-Endocrinology and Metabolism, 280*(4), E640-E649.

Viengchareun, S., Servel, N., Fève, B., Freemark, M., Lombès, M., & Binart, N. (2008). Prolactin receptor signaling is essential for perinatal brown adipocyte function: a role for insulin-like growth factor-2. *PLoS One, 3*(2), e1535.

Vijgen, G., Bouvy, N., Teule, G., Brans, B., Hoeks, J., Schrauwen, P., & van Marken Lichtenbelt, W. (2012). Increase in brown adipose tissue activity after weight loss in morbidly obese subjects. *The Journal of Clinical Endocrinology & Metabolism, 97*(7), E1229-E1233.

Vinter, J., Hull, D., & Elphick, M. (1982). Onset of thermogenesis in response to cold in newborn mice. *Neonatology, 42*(3-4), 145-151.

Virtanen, K. A., Lidell, M. E., Orava, J., Heglind, M., Westergren, R., Niemi, T., Tattonen, M., Laine, J., Savisto, N-J., Enerback, S., & Nuutila, P. (2009). Functional Brown Adipose Tissue in Healthy Adults. *New England Journal of Medicine, 360*(15), 1518-1525.

Vosselman, M. J., Brans, B., van der Lans, A. A., Wierts, R., van Baak, M. A., Mottaghy, F. M., Schrauwen, P., & van Marken Lichtenbelt, W. D.

(2013). Brown adipose tissue activity after a high-calorie meal in humans. *The American journal of clinical nutrition, 98*(1), 57-64.

Vosselman, M. J., van der Lans, A. A., Brans, B., Wierts, R., van Baak, M. A., Schrauwen, P., & van Marken Lichtenbelt, W. D. (2012). Systemic beta-adrenergic stimulation of thermogenesis is not accompanied by brown adipose tissue activity in humans. *Diabetes, 61*(12), 3106-3113.

Vrieze, A., Schopman, J. E., Admiraal, W. M., Soeters, M. R., Nieuwdorp, M., Verberne, H. J., & Holleman, F. (2012). Fasting and postprandial activity of brown adipose tissue in healthy men. *Journal of Nuclear Medicine, 53*(9), 1407-1410.

Walker, C. D., Sapolsky, R. M., Meaney, M. J., Vale, W. W., & Rivier, C. L. (1986). Increased pituitary sensitivity to glucocorticoid feedback during the stress nonresponsive period in the neonatal rat. *Endocrinology, 119*(4), 1816-1821.

Walker, C. D., Scribner, K. A., Cascio, C. S., & Dallman, M. F. (1991). The pituitary-adrenocortical system of neonatal rats is responsive to stress throughout development in a time-dependent and stressor-specific fashion. *Endocrinology, 128*(3), 1385-1395.

Walker, C.-D., Kudreikis, K., Sherrard, A., & Johnston, C. C. (2003). Repeated neonatal pain influences maternal behavior, but not stress responsiveness in rat offspring. *Developmental Brain Research, 140*(2), 253-261.

Wahr, J. A., Tremper, K. K., Samra, S., & Delpy, D. T. (1996). Near-infrared spectroscopy: theory and applications. *J Cardiothorac Vasc Anesth, 10*(3), 406-418.

Ward, A. M. V., Syddall, H. E., Wood, P. J., Chrousos, G. P., & Phillips, D. I. W. (2004). Fetal Programming of the Hypothalamic-Pituitary-Adrenal (HPA) Axis: Low Birth Weight and Central HPA Regulation. *The Journal of Clinical Endocrinology & Metabolism, 89*(3), 1227-1233.

Warner, A., Rahman, A., Solsjo, P., Gottschling, K., Davis, B., Vennstrom, B., Arner, A., & Mittag, J. (2013). Inappropriate heat dissipation ignites brown fat thermogenesis in mice with a mutant thyroid hormone receptor alpha1. *Proc Natl Acad Sci U S A, 110*(40), 16241-16246.

Watterberg, K. L., Gerdes, J. S., & Cook, K. L. (2001). Impaired glucocorticoid synthesis in premature infants developing chronic lung disease. *Pediatr Res, 50*(2), 190-195.

Weaver, I. C., Meaney, M. J., & Szyf, M. (2006). Maternal care effects on the hippocampal transcriptome and anxiety-mediated behaviors in the

offspring that are reversible in adulthood. *Proc Natl Acad Sci U S A, 103*(9), 3480-3485.

Webster, J. C., Oakley, R. H., Jewell, C. M., & Cidlowski, J. A. (2001). Proinflammatory cytokines regulate human glucocorticoid receptor gene expression and lead to the accumulation of the dominant negative beta isoform: a mechanism for the generation of glucocorticoid resistance. *Proc Natl Acad Sci U S A, 98*(12), 6865-6870.

Wei, M., Gaskill, S, P., Haffner, S, M., Stern, M, P. (1997). Waist circumference as the best predictor of non-insulin dependent diabetes mellitus compared to BMI, WHR over other anthropometric measure ments in Mexican Americans: a 7-year prospective study. *Obesity Research Journal, 5*: 16–23.

Welberg, L. A., & Seckl, J. R. (2001). Prenatal stress, glucocorticoids and the programming of the brain. *J Neuroendocrinol, 13*(2), 113-128.

WelchAllyn (2015), https://www.welchallyn.com/content/dam/welchallyn/documents/upload-docs/Product-Literature/Specification-Sheet/SM4122RevB_BraunPRO6000_SpecSheet_MC11859.pdf.

Weyer, C., Tataranni, P. A., Snitker, S., Danforth, E., Jr., & Ravussin, E. (1998). Increase in insulin action and fat oxidation after treatment with CL 316,243, a highly selective beta3-adrenoceptor agonist in humans. *Diabetes, 47*(10), 1555-1561.

WHO. (2016). Fact Sheet number 311: obesity and overweight. Retrieved from http://www.who.int/mediacentre/factsheets/fs311/en/

Wijers, S. L., Saris, W. H., & Lichtenbelt, W. D. (2010). Cold-induced adaptive thermogenesis in lean and obese. *Obesity, 18*(6), 1092-1099.

Winking, H., Gerdes, J., & Traut, W. (2004). Expression of the proliferation marker Ki-67 during early mouse development. *Cytogenet Genome Res, 105*(2-4), 251-256.

Woerle, H. J., Meyer, C., Dostou, J. M., Gosmanov, N. R., Islam, N., Popa, E., Wittlin, S. D., Welle, S. L., & Gerich, J. E. (2003). Pathways for glucose disposal after meal ingestion in humans. *Am J Physiol Endocrinol Metab, 284*(4), E716-725.

World Health Organization. (1993). *Thermal control of the newborn: a practical guide*. Retrieved from http://apps.who.int/iris/bitstream/handle/10665/60042/WHO_FHE_MSM_93.2.pdf?sequence=1.

Wyatt, J. S., Cope, M., Delpy, D. T., Wray, S., & Reynolds, E. O. (1986). Quantification of cerebral oxygenation and haemodynamics in sick newborn infants by near infrared spectrophotometry. *Lancet, 2*(8515), 1063-1066.

Xiao, X. Q., Williams, S. M., Grayson, B. E., Glavas, M. M., Cowley, M. A., Smith, M. S., & Grove, K. L. (2007). Excess weight gain during the early postnatal period is associated with permanent reprogramming of brown adipose tissue adaptive thermogenesis. *Endocrinology, 148*(9), 4150-4159.

Yam, K. Y., Naninck, E. F. G., Abbink, M. R., la Fleur, S. E., Schipper, L., van den Beukel, J. C., Grefhorst, A., Oosting, A., van der Beek, E. M., Lucassen, P. J., & Korosi, A. (2017). Exposure to chronic early-life stress lastingly alters the adipose tissue, the leptin system and changes the vulnerability to western-style diet later in life in mice. *Psychoneuroendocrinology, 77*, 186-195.

Yamaguchi, O., Marui, E., Kakizaki, H., Homma, Y., Igawa, Y., Takeda, M., . . . Ohkawa, S. (2014). Phase III, randomised, double-blind, placebo-controlled study of the beta3-adrenoceptor agonist mirabegron, 50 mg once daily, in Japanese patients with overactive bladder. *BJU Int, 113*(6), 951-960.

Yamauchi, T., Kamon, J., Waki, H., Terauchi, Y., Kubota, N., Hara, K., . . . Tsuboyama-Kasaoka, N. (2001). The fat-derived hormone adiponectin reverses insulin resistance associated with both lipoatrophy and obesity. *Nature medicine, 7*(8), 941-946.

Yan, J.-G., Zhang, L.-l., Agresti, M., LoGiudice, J., Sanger, J. R., Matloub, H. S., & Havlik, R. (2015). Neural systemic impairment from whole-body vibration. *Journal of Neuroscience Research, 93*(5), 736-744.

Yau, J., & Seckl, J. (2012). Local amplification of glucocorticoids in the aging brain and impaired spatial memory. *Frontiers in Aging Neuroscience, 4*(24).

Yeung, H. W., Grewal, R. K., Gonen, M., Schoder, H., & Larson, S. M. (2003). Patterns of (18)F-FDG uptake in adipose tissue and muscle: a potential source of false-positives for PET. *J Nucl Med, 44*(11), 1789-1796.

Yoneshiro, T., Aita, S., Kawai, Y., Iwanaga, T., & Saito, M. (2012). Nonpungent capsaicin analogs (capsinoids) increase energy expenditure through the activation of brown adipose tissue in humans. *Am J Clin Nutr, 95*(4), 845-850.

Yoneshiro, T., Aita, S., Matsushita, M., Kayahara, T., Kameya, T., Kawai, Y., Iwanaga, T., & Saito, M. (2013). Recruited brown adipose tissue as an antiobesity agent in humans. *J Clin Invest, 123*(8), 3404-3408.

Yoneshiro, T., Matsushita, M., Hibi, M., Tone, H., Takeshita, M., Yasunaga, K., Katsuragi, Y., Kameya, T., Sugie, H., & Saito, M. (2017). Tea catechin and caffeine activate brown adipose tissue and increase cold-induced thermogenic capacity in humans. *Am J Clin Nutr, 105*(4), 873-881.

Yoneshiro, T., Ogawa, T., Okamoto, N., Matsushita, M., Aita, S., Kameya, T., Kawai, Y., Iwanaga, T., & Saito, M. (2013). Impact of UCP1 and β3AR gene polymorphisms on age-related changes in brown adipose tissue and adiposity in humans. *International journal of obesity, 37*(7), 993-998.

Yoshitomi, H., Yamazaki, K., Abe, S., & Tanaka, I. (1998). Differential Regulation of Mouse Uncoupling Proteins among Brown Adipose Tissue, White Adipose Tissue, and Skeletal Muscle in Chronic β3Adrenergic Receptor Agonist Treatment. *Biochemical and biophysical research communications, 253*(1), 85-91.

Young-Hyman, D., Schlundt, D, G., Herman, L., De Luca, F., Counts, D. (2001). Evaluation of the insulin resistance syndrome in 5-to 10 year-old overweight/obese aftrican-american children. *Diabetes Care, 24*(8), 1359-1364.

Yubero, P., Hondares, E., Carmona, M. C., Rossell, M., Gonzalez, F. J., Iglesias, R., Giralt, M., & Villarroya, F. (2004). The developmental regulation of peroxisome proliferator-activated receptor-γ coactivator-1α expression in the liver is partially dissociated from the control of gluconeogenesis and lipid catabolism. *Endocrinology, 145*(9), 4268-4277.

Zelazowski, P., Patchev, V. K., Zelazowska, E. B., Chrousos, G. P., Gold, P. W., & Sternberg, E. M. (1993). Release of hypothalamic corticotropin-releasing hormone and arginine-vasopressin by interleukin 1 beta and alpha MSH: studies in rats with different susceptibility to inflammatory disease. *Brain Res, 631*(1), 22-26.

Zhang, W.-X., Fan, J., Ma, J., Rao, Y.-S., Zhang, L., & Yan, Y.-E. (2016). Selection of Suitable Reference Genes for Quantitative Real-Time PCR Normalization in Three Types of Rat Adipose Tissue. *International Journal of Molecular Sciences, 17*(6), 968.

Zhao, L., Zou, X., Feng, Z., Luo, C., Liu, J., Li, H., Chang, L., Wang., H., Li, Y., Long, Y., Gao, J., & Liu, J. (2014). Evidence for association of mitochondrial metabolism alteration with lipid accumulation in aging rats. *Experimental Gerontology, 56*, 3-12.

Appendices

Appendix A - Published Paper

METABOLISM CLINICAL AND EXPERIMENTAL 70 (2017) 125–132

Available online at www.sciencedirect.com

Metabolism

www.metabolismjournal.com



Glucocorticoids modulate human brown adipose tissue thermogenesis in vivo

Hannah Scotney [a], Michael E. Symonds [a,b,*], James Law [a], Helen Budge [a], Don Sharkey [a], Konstantinos N. Manolopoulos [c,d,**]

[a] Division of Child Health, Obstetrics & Gynaecology, School of Medicine, University of Nottingham, Nottingham, NG7 2UH, UK
[b] Nottingham Digestive Diseases Biomedical Research Unit, Queens Medical Centre Campus, Nottingham, NG7 2UH
[c] Institute of Metabolism and Systems Research, University of Birmingham, Birmingham, B15 2TT, UK
[d] Centre for Endocrinology, Diabetes and Metabolism, Birmingham Health Partners, Birmingham, B15 2TT, UK

ARTICLE INFO

Article history:
Received 3 October 2016
Accepted 14 January 2017

Keywords:
Brown adipose tissue
Glucocorticoids
Humans
Infrared thermography
Beta adrenoceptor

ABSTRACT

Introduction. Brown adipose tissue (BAT) is a thermogenic organ with substantial metabolic capacity and has important roles in the maintenance of body weight and metabolism. Regulation of BAT is primarily mediated through the β-adrenoceptor (β-AR) pathway. The *in vivo* endocrine regulation of this pathway in humans is unknown. The objective of our study was to assess the *in vivo* BAT temperature responses to acute glucocorticoid administration.

Methods. We studied 8 healthy male volunteers, not pre-selected for BAT presence or activity and without prior BAT cold-activation, on two occasions, following an infusion with hydrocortisone (0.2 $mg.kg^{-1}.min^{-1}$ for 14 h) and saline, respectively. Infusions were given in a randomized double-blind order. They underwent assessment of supraclavicular BAT temperature using infrared thermography following a mixed meal, and during β-AR stimulation with isoprenaline (25 $ng.kg\ fat\text{-}free\ mass^{-1}.min^{-1}$ for 60 min) in the fasting state.

Results. During hydrocortisone infusion, BAT temperature increased both under fasting basal conditions and during β-AR stimulation. We observed a BAT temperature threshold, which was not exceeded despite maximal β-AR activation. We conclude that BAT thermogenesis is present in humans under near-normal conditions. Glucocorticoids modulate BAT function, representing important physiological endocrine regulation of body temperature at times of acute stress.

© 2017 The Authors. Published by Elsevier Inc. This is an open access article under the CC BY license (http://creativecommons.org/licenses/by/4.0/).

Abbreviations: ^{18}FDG-PET/CT, 18F-fluorodeoxyglucose-positron emission tomography/computed tomography; ATP, adenosine triphosphate; AUC, area under the curve; BAT, brown adipose tissue; CRF, clinical research facility; DXA, dual energy x-ray absorptiometry; HC, hydrocortisone; HOMA, homeostatic model assessment; ISO, isoprenaline; IT, infrared thermography; NEFA, non-esterified fatty acids; NIHR, National Institute for Health Research; NRES, National Research Ethics Service; REC, research ethics committee; tAUC, time-averaged area under the curve; T_{REF}, reference point temperature; T_{SCR}, supraclavicular temperature; UCP1, uncoupling protein 1; β-AR, beta adrenoceptor.

* *Correspondence to:* M.E. Symonds, Division of Child Health, Obstetrics & Gynaecology, School of Medicine, University of Nottingham, Nottingham, NG7 2UH, UK. Tel.: +44 115 823 0625.
** *Correspondence to:* K.N. Manolopoulos, Institute of Metabolism and Systems Research, University of Birmingham, IBR Tower Level 2, Room 228, Birmingham, B15 2TT, UK. Tel.: +44 121 414 7525.
E-mail address: k.manolopoulos@bham.ac.uk (K.N. Manolopoulos).

http://dx.doi.org/10.1016/j.metabol.2017.01.024
0026-0495/© 2017 The Authors. Published by Elsevier Inc. This is an open access article under the CC BY license (http://creativecommons.org/licenses/by/4.0/).

1. Introduction

There is increasing evidence that brown adipose tissue (BAT) has important physiological roles beyond thermoregulation in newborn infants and rodents [1]. Adult humans have significant amounts of BAT [2] and, as a highly metabolic tissue with the capacity to oxidize both glucose and lipid, attention has turned to its involvement in the pathogenesis of obesity and the metabolic syndrome [3]. BAT is characterized by the presence of uncoupling protein (UCP) 1 which uncouples adenosine triphosphate (ATP) production by the mitochrondrial respiratory chain, allowing the dissipation of excess chemical energy as heat [4]. The principal factors regulating BAT function in healthy adults have yet to be fully established due, in part, to the technical limitations of assessing BAT function *in vivo*. The majority of studies in humans have used 18F-fluorodeoxyglucose-positron emission tomography/computed tomography (^{18}FDG-PET/CT) as the gold standard to assess BAT activity, but this is constrained by exposure to ionizing radiation, the scanning protocols involved [5] and its unsuitability for live tracking of BAT activation especially after feeding. Systemic β-adrenoceptor (β-AR) activation promotes BAT activity in humans [6], but the role of other endocrine factors remains largerly unknown. The pre-partum elevation of cortisol is pivotal in the initiation of nonshivering BAT thermogenesis at birth [7], and glucocorticoids have recently been proposed as regulators of BAT activity in healthy adult females [8] and in individuals pre-selected for the presence of active BAT [9]. BAT has also been considered to contribute to dietary-induced thermogenesis [10,11], although this concept remains controversial [12]. We, therefore, studied whether BAT is activated by feeding, or by an acute increase in cortisol under basal and β-AR stimulated conditions.

2. Materials and Methods

2.1. Subjects

Eight healthy male volunteers participated in this randomized, double-blind, placebo controlled study, conducted between January and March 2015. Individuals were recruited using print and electronic advertising and none was selected or screened on the basis of presence of any active BAT. All subjects underwent a medical evaluation during a screening visit to ensure they were healthy. No subject had any significant past medical history, smoked tobacco or took any regular medications that could affect the study's outcome measures.

2.2. Study Approval

The study was approved by the Edgbaston NRES Committee, UK (REC reference 14/WM/1085). All participants provided written informed consent.

2.3. Study Design

2.3.1. Clinical Research Facility

All parts of this study were conducted in a temperature controlled room at the National Institute for Health Research (NIHR)/Wellcome Trust Clinical Research Facility (CRF) of the University of Birmingham at the Queen Elizabeth Hospital Birmingham, UK. Room temperature was held constant at 23-26 °C and was monitored using an ambient temperature probe.

2.3.2. Anthropometric Measurements

Measurements were taken during the screening visit. Waist circumference was measured midway between the lower margin of the last palpable rib and the top of the iliac crest, and hip circumference at the level of the greater trochanters. Total and regional fat masses were measured by dual-energy x-ray absorptiometry (DXA). Visceral fat mass was estimated by DXA using a proprietary algorithm provided by the manufacturer [13]. Core temperature was measured with a tympanic thermometer.

2.3.3. Study Visits

Study visits were identical, except for the nature of overnight infusion, and were at least 2 weeks apart (Fig. 1A). Subjects were admitted to the CRF in the afternoon, and a cannula for infusion purposes was inserted into a right antecubital fossa vein. At 1800 h, they were served a standardized calorie-controlled meal (vegetable lasagne; total energy 2634 kJ; typical nutritional values per 100 g of product: 1.9 g fat, 12.2 g carbohydrates, 3.3 g protein, 1.5 g fiber), and then fasted until study completion the next day. BAT thermogenesis assessment was performed immediately before and after the meal, which was ingested within 20 min and was accompanied by tap water at room temperature. At 1900 h, a constant infusion of either hydrocortisone (HC, 0.2 mg.kg^{-1}.h^{-1}) or normal saline (control study visit) was started and given until study completion the following day. Infusions were administered in a double-blind, randomized fashion. At 2200 h, lights were switched off for night rest. In the morning, cannulations for blood sampling purposes were performed and, at 0900 h, the isoprenaline infusion protocol commenced. After baseline measurements for 45 min, a one-step infusion of isoprenaline (ISO, 2.5 ng.kg fat-free mass^{-1}.min^{-1}) was given for 60 min. BAT thermogenic activity was measured at baseline and throughout the infusion.

2.4. BAT Thermogenesis Assessment

An infrared thermography (IT) camera (FLIR E60 2.3 Megapixel Infrared Camera; FLIR Systems, Danderyd, Sweden) was used to acquire images of the anterior neck and upper chest region, which were sequentially analyzed and processed by an automated analysis program, as described previously [14]. Areas of interest for temperature analysis were the supraclavicular region (T_{SCR}) representing BAT, and a non-adipose tissue reference point (T_{REF}) on the chest, close to the xiphoid. In addition, during the periods of IT, two skin contact temperature sensors (Britton DS1922L, Maxim Integrated, Winnersh, UK) recording skin temperature every minute were taped within the supraclavicular fossa (main BAT site) and lateral to the umbilicus (white adipose tissue). For skin contact temperature measurements, data were collected every minute, and analysis was performed using 5-min averages. For meal measurements, the mean of both study days was calculated. Fasting and pre-ISO baseline were defined as the average of time points −15 to 0 min. Postprandial and peak post-ISO infusion periods were defined as time points 0 to 15 min and 40 to 50 min, respectively. For the duration of the study,

Accepted Manuscript

participants were wearing a hospital gown, with their torso exposed for the duration of all measurements.

2.5. Analytical Methods

Blood samples were drawn into heparinized syringes, and plasma was prepared rapidly at 4 °C and immediately frozen at −80 °C before analysis. Plasma glucose and NEFA concentrations were measured enzymatically using commercially available kits on an ILAB600 or ILAB650 clinical analyzer (Instrumentation Laboratory UK, Warrington, UK). Insulin and C-peptide were measured by ELISA (Invitron, Monmouth, UK) at a reference laboratory (Diabetes Research Unit Cymru, Swansea University, UK). Cortisol was measured by a colorimetric assay (R&D Systems, Abingdon, UK).

2.6. Calculations and Statistics

Indexes of β-cell function and insulin resistance were calculated according to the homeostatic model assessment (HOMA) method, whereby the mean of three consecutive plasma glucose and insulin postabsorptive measurements was used. Energy expenditure was calculated based on heart rate, age and weight as previously described [15]. Area under the curve (AUC) was calculated using the trapezoid rule and is presented as a time-averaged value (tAUC; AUC divided by the relevant time period). Comparisons between groups were analyzed using t test or non-parametric tests for data that were not normally distributed. A $p < 0.05$ was considered statistically significant. Based on previous studies using a similar integrative physiology design [16], the sample size was designed to have 85% power to detect a difference of 0.75 standard deviations at the 5% significance level for metabolic parameters. Data were analyzed using IBM Statistics for Windows v21 and GraphPad Prism for Windows v6.05. All data are presented as mean ± SEM, unless otherwise stated.

Table 1 – Baseline anthropometric and metabolic characteristics of participants, n = 8.

Characteristic	
Age (years)	20 (18-34)
Weight (kg)	75.0 (61.5–81.7)
BMI (kg/m^2)	23.0 (20.6–24.2)
WHR	0.84 (0.78–0.9)
Trunk fat (kg)	7.7 (5.1–9.2)
Leg fat (kg)	5.5 (4.3–7.5)
Visceral fat (kg)	0.2 (0.1–0.4)
Systolic BP (mmHg)	124 (105–146)
Diastolic BP (mmHg)	72 (59-79)
Heart rate (bpm)	58 (53-62)
Fasting glucose (mg/dl)	113 (89–122)
Fasting insulin (pmol/L)	30.6 (14.4–68.5)
Fasting NEFA (μmol/L)	707 (450–873)
TSH (mIU/L)	1.30 (0.93–4.83)
FT4 (pmol/L)	17.7 (15.0–18.8)

Median and range shown. BMI, body mass index; WHR, waist-to-hip ratio; BP, blood pressure; TSH, thyroid stimulating hormone; FT4, free thyroxine.

3.2. Acute Hypercortisolemia Induces Peripheral Insulin Resistance and Increases Basal BAT Thermogenic Activity

Overnight HC infusion resulted in significantly increased plasma cortisol concentrations (Fig. 2A). From a metabolic perspective, basal plasma non-esterified fatty acids (NEFAs) were high due to fasting (Fig. 2B). HC increased basal NEFA and glucose (Fig. 2C), as well as insulin (basal insulin 30.4 ± 6.0 pmol/L vs. 55.2 ± 7.4 pmol/L, $p = 0.025$ control compared to hypercortisolemia) and C-peptide concentrations (basal C-peptide 0.25 ± 0.03 pmol/mL vs. 0.38 ± 0.04 pmol/mL, $p = 0.001$ control compared to hypercortisolemia). In line with this, HOMA indices of peripheral insulin resistance increased (HOMA IR index control 0.62 ± 0.11 vs. hypercortisolemia 1.11 ± 0.16, $p = 0.016$) (Table 2).

Acute hypercortisolemia increased T_{SCR} in the basal state (Fig. 2D). This was accompanied by an increase in basal core temperature (Fig. 2E), but we did not observe any effect on blood pressure or heart rate (Fig. 2F).

3. Results

3.1. Meal Ingestion Leads to Increased BAT Thermogenic Activity

Baseline anthropometric and metabolic characteristics of participants are shown in Table 1 and environmental temperature data for each individual study day are shown in Supplemental Table 1. There was no difference in outside or room temperature between study days. Following the mixed meal, postprandial T_{SCR} increased, whereas T_{ASF} remained stable (Fig. 1B). All participants responded with an increase in BAT thermogenic activity (Fig. 1C), while core temperature did not change (Fig. 1D). Skin contact measurements showed a similar postprandial temperature increase of 0.39 ± 0.10 °C over supraclavicular BAT ($p < 0.05$ compared to fasting), whereas skin temperature over white adipose tissue remained the same.

3.3. Acute β-AR Stimulation Increases BAT Thermogenic Activity During Control and Hypercortisolemia Conditions

From a metabolic perspective, ISO infusion significantly increased systemic NEFA concentrations, both under control and hypercortisolemia conditions (Fig. 2B). Despite the augmentation of basal systemic lipolysis by HC, the β-AR dependent rise in plasma NEFA was of similar magnitude compared to control conditions (Δ AUC 953 ± 155 vs 979 ± 175 μmol/L; $p = 0.926$ compared to control). Following the initial peak, there was a sharp decline in NEFA concentrations despite continuing ISO infusion. Control plasma glucose concentrations were unaffected by ISO, while the observed increase in concentrations during HC infusion is due to glucocorticoid-induced peripheral tissue insulin resistance (Fig. 2C). This is supported by the concomitant changes in insulin, C-peptide and

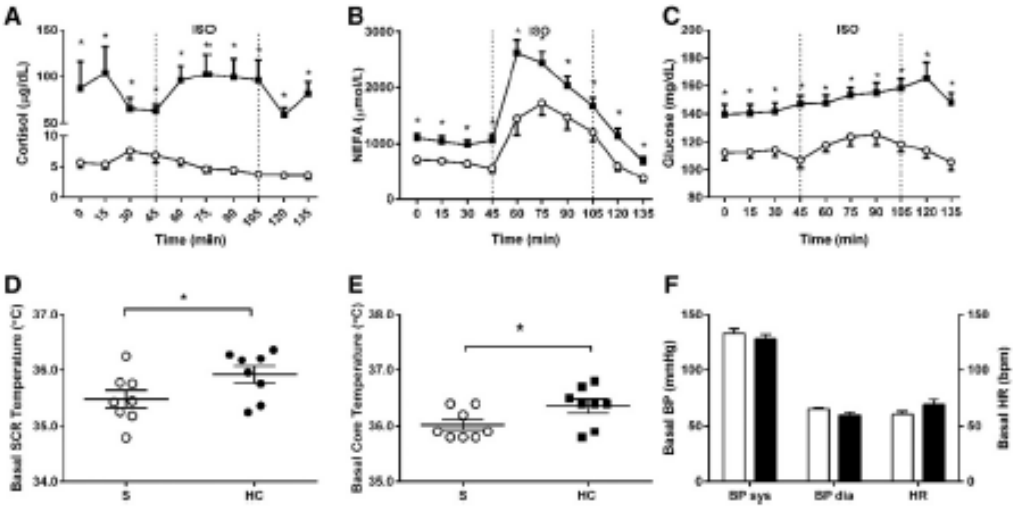

Fig. 2 – Metabolic and cardiovascular responses following saline infusion (S) or hydrocortisone infusion (HC) at baseline and during an isoprenaline infusion (ISO, dotted lines indicate infusion period). Plasma cortisol concentrations (saline, open circles; hydrocortisone, black squares) (A), non-esterified fatty acids (NEFA) (saline, open circles; hydrocortisone, black squares) (B), glucose (saline, open circles; hydrocortisone, black squares) (C), supraclavicular temperature (T_{SCR}) (saline, open circles; hydrocortisone, black circles) (D) and core temperature at baseline (saline, open squares; hydrocortisone, black squares) (E). Systolic (sys) and diastolic (dia) blood pressure (BP) and heart rate (HR) at baseline (saline, open bars; hydrocortisone, black bars) (F). *$p < 0.05$ vs. control, $n = 8$.

Table 2 – Comparison of insulin and C-peptide AUC, and homeostatic model assessment (HOMA) indexes during basal and isoprenaline-stimulated conditions, n = 8.

	Control		Cortisol		P value control vs cortisol		P value basal vs isoprenaline	
	Basal	ISO	Basal	ISO	Basal	ISO	Control	Cortisol
Insulin (pmol/L)	30.4 ± 6.0	100.4 ± 15.7	55.2 ± 7.4	206.7 ± 30.5	0.025	0.012	0.012	0.012
C-peptide (pmol/mL)	0.25 ± 0.03	0.47 ± 0.05	0.38 ± 0.04	0.90 ± 0.09	0.001	0.001	<0.0001	<0.0001

	Control	Cortisol	P value
Δ insulin basal to ISO (pmol/L)	70.0 ± 10.1	151.5 ± 28.9	0.012
ΔC-peptide basal to ISO (pmol/mL)	0.22 ± 0.03	0.52 ± 0.07	0.012
HOMA %B	42.2 ± 5.9	40.5 ± 4.5	0.731
HOMA %S	192.2 ± 29.5	105.9 ± 19.2	0.004
HOMA IR	0.62 ± 0.11	1.11 ± 0.16	0.016

Mean and SEM shown.

HOMA indexes showing a decrease in glucose sensitivity despite a significant increase in insulin and C-peptide concentrations during ISO infusion (Table 1). Expectedly, non-selective β-AR stimulation with ISO increased heart rate and systolic blood pressure, responses not significantly affected by HC (Fig. 2F and Supplemental Fig. 1). Basal and ISO-induced BAT thermogenic activity measures did not show any significant correlation with BMI or measures of adipose tissue distribution (data not shown).

HOMA indexes showing a decrease in glucose sensitivity despite a significant increase in insulin and C-peptide concentrations during ISO infusion (Table 1). Expectedly, non-selective β-AR stimulation with ISO increased heart rate and systolic blood pressure, responses not significantly affected by HC (Fig. 2F and Supplemental Fig. 1). Basal and ISO-induced BAT thermogenic activity measures did not show any significant correlation with BMI or measures of adipose tissue distribution (data not shown).

Adrenergic stimulation resulted in a highly localized increase in temperature within the supraclavicular region, representative of BAT thermogenic activity, both under control and hypercortisolemic conditions (Fig. 3). All study participants responded to ISO with an increase in BAT temperature (Supplemental Fig. 2). Under control conditions, ISO increased T_{SCR} by 0.7 °C, plateaued and then returned to baseline after the infusion, implying cessation of β-adrenergic-mediated BAT

Adrenergic stimulation resulted in a highly localized increase in temperature within the supraclavicular region, representative of BAT thermogenic activity, both under control and hypercortisolemic conditions (Fig. 3). All study participants responded to ISO with an increase in BAT temperature (Supplemental Fig. 2). Under control conditions, ISO increased T_{SCR} by 0.7 °C, plateaued and then returned to baseline after the infusion, implying cessation of β-adrenergic-mediated BAT

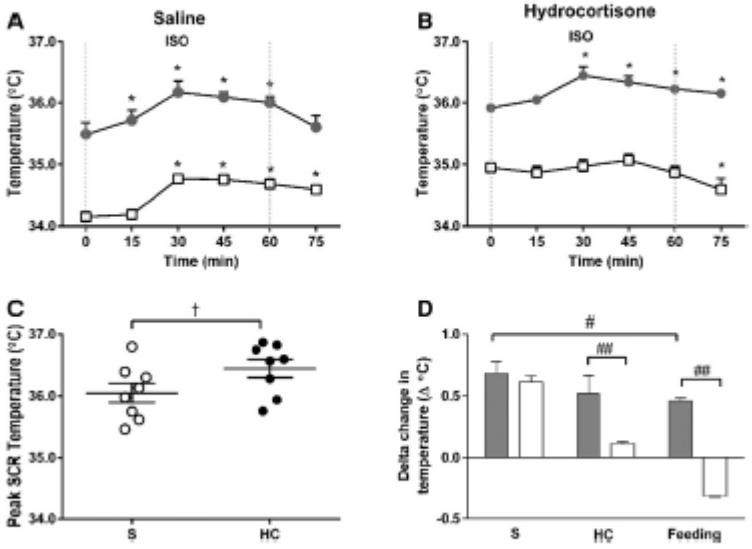

Fig. 3 – BAT thermogenic responses. Supraclavicular temperature (T_{SCR}) and non-adipose tissue reference point (T_{REF}) following saline (S) infusion (T_{SCR}, gray circles; T_{REF} open squares) (A) or hydrocortisone (HC) infusion (T_{SCR}, gray circles; T_{REF} open squares) (B) during and after isoprenaline stimulation (ISO, dotted lines indicate infusion period). Individual peak BAT temperatures during ISO (S, open circles; HC, black circles) (C). Change in temperature during ISO or following a standardized meal (T_{SCR}, gray bars; T_{REF} open bars) (D). *p < 0.001 vs. basal, †p < 0.05 vs. saline, #p < 0.001 vs. saline, ##p < 0.001 vs. T_{REF}, n = 8.

Activate Window

thermogenesis (Fig. 3A). These responses to ISO were similar during hypercortisolemia (Fig. 3B), whereby peak T_{SCR} was slightly higher (Fig. 3C). The ISO-induced T_{SCR} increase was greater than the physiological stimulus of diet-induced thermogenesis (Fig. 3D). Skin temperature showed similar results (Supplemental Fig. 3). Energy expenditure increased significantly during ISO (Supplemental Fig. 4). During hypercortisolemia, ISO-induced energy expenditure was closely correlated with basal T_{SCR} during control conditions (Pearson $r = 0.742$, $p = 0.035$) and peak T_{SCR} during HC ($r = 0.870$, $p = 0.005$). In response to ISO, peak core temperature was similar between control and hypercortisolemia conditions (Supplemental Fig. 5).

4. Discussion

Human supraclavicular BAT is characterized by the presence of thermogenically functional UCP1, with a respiratory capacity that substantially exceeds that of white fat [17]. Understanding the endocrine factors regulating BAT function is an important prerequisite before being able to utilize the metabolic capabilities of this tissue. In this study we sought to study BAT *in vivo* following exposure to a combination of physiological stimuli in order to determine the relative importance of diet and edocrine mediated effects.

BAT glucose uptake has been reported to be increased following a single carbohydrate-rich meal [18], although overfeeding for 24 h did not have any effect [19]. This has led to some controversy regarding the contribution of BAT to dietary-induced thermogenesis in humans. We sought to investigate this using a single standardized mixed meal, serving as a physiological stimulus. While we did not measure whole body energy expenditure, we observed selective temperature changes over the supraclavidular region only, immediately after the meal, suggesting direct BAT activation and not a thermic effect of food. Interestingly, from a mechanistic perspective, postprandial BAT activation would be characterized by both systemic cortisol secretion [20] and sympathetic β-AR stimulation [21], suggesting an acute maximal response following feeding.

Cortisol promotes important physiological maturation effects around the time of birth, including raised UCP1 abundance in adipose tissue [7,22]. However, in adult rodents, glucocorticoids inhibit BAT [23] by interfering with adrenergic signaling [24,25]. Human data are scarce with one study reporting dexamethasone-induced inhibition of UCP1 expression and metabolic rate in human brown adipocytes *in vitro* [26], and another reporting BAT activation following administration of the synthetic glucocorticoid prednisolone *in vivo* [9]. In our study, we chose hydrocortisone to model a physiological acute surge of cortisol, as seen during the perinatal period and at times of acute stress. We observed an increase of basal T_{SCR} during hypercortisolemia, supporting a physiological role for cortisol in BAT activation, as we did not observe any additive effects on blood pressure or heart rate. The duration of the infusion was chosen to allow for glucocorticoid-mediated genomic effects to take place [27]. While the achieved plasma cortisol concentrations were in excess of those typical for acute stress [28], it is important to note that tissue-responsiveness can be determined by tissue-specific glucocorticoid metabolism rather than absolute plasma concentrations [29]. Taken together our data indicate the positive relationship between cortisol and BAT temperature as previously indicated from a small study on healthy adult females [8].

β-AR stimulation induces BAT thermogenesis in humans [6,30], although findings are inconsistent depending on the β-AR employed [31,32]. We found a localized increase in supraclavicular temperature during ISO infusion both under control and hypercortisolemia conditions. This temperature change was temporally limited for the duration of the infusion, suggesting underlying BAT activation. T_{SCR} responses for all subjects increased within the first 5 min which is in accordance with acute cold exposure on BAT [14]. The observed T_{SCR} plateau is suggestive of a limit to BAT thermogenesis *in vivo*. The concomitant sharp decline in NEFA concentrations during the later stages of the infusion is consistent with β-AR desensitization due to maximal receptor stimulation [16]. The finding of a slightly higher peak T_{SCR} during hypercortisolemia suggests a minor synergistic effect between cortisol and β-AR stimulation. Interestingly, the two pathways are intrinsically connected as catecholamine synthesis is under glucocorticoid control [33].

Previous studies have shown that active BAT decreases with age and obesity, and its activation varies between sexes [14,34]. We studied BAT activity in healthy males using IT to assess temperature changes in the supraclavicular region and a non-adipose tissue reference point. Supraclavicular skin temperature increases upon BAT activation [35,36] and IT has been shown to measure changes in skin temperature overlying the main BAT depot in humans [14]. It has been confirmed as a reliable alternative for *in vivo* BAT activity assessment, correlating with ^{18}FDG-PET/CT [9,37], with the additional benefit of enabling real-time tracking of temperature changes. IT-derived BAT temperature measurements might be influenced by subcutaneous adipose tissue thickness [38], however, in our study participants were lean and we monitored dynamic temperature changes over time, as opposed to a single, static measurement. Adrenoceptor-induced vasodilation, both as a result of HC and ISO infusions, could increase skin blood flow and interfere with IT measurements. However, compared to T_{SCR}, there were clear temporal differences in the change in T_{AXS} which showed a later initial increase and a sustained increase post-infusion. Overall, we demonstrate a BAT-specific thermogenic and vasodilation response to both HC and ISO, clearly differentiated from non-BAT reference areas, confirming that the temperature responses we measured are confined to BAT.

Our findings support previous studies showing β-AR stimulation as a means of activating BAT in humans [6,30], confirming IT as a sensitive, non-invasive method for the *in vivo* assessment of BAT function in humans under near-normal conditions [9,14,37]. This is particularly important when comparing our results with those studies using glucose tracer uptake as an index of BAT activity. Similar ISO doses did not show any significant BAT glucose tracer uptake, likely due to competition between the tracer and fatty acids from ISO-induced lipolysis combined with increased insulin

resistance [32]. Given that BAT primarily utilizes fatty acids for heat generation [1], it is possible that ^{18}FDG-PET/CT underestimates the amount of active BAT in humans. This limitation has led to the development of alternative BAT assessment methods, in addition to IT, either using different PET/CT tracers [39], or based on magnetic resonance imaging techniques [40]. We demonstrate that temperature changes in the supraclavicular area upon β-AR stimulation are indicative of localized BAT activity in a cohort of unselected young individuals, maintained at room temperature. This supports the prospect of harnessing BAT activity and the associated increase in energy expenditure as a potential treatment for metabolic diseases. We provide further evidence that in humans, in contrast to rodents, acute hypercortisolemia does not inhibit BAT function, but results in BAT activation [9]. Despite this, there is a threshold of activity that cannot be overcome even during maximal short-term β-AR stimulation.

Our study has some limitations by design, including the small size of our sample, although it is standard for a healthy volunteer study of this type. The acute infusion of hydrocortisone limits the conclusions we can draw in relation to states of chronic glucocorticoid excess that are associated with profound metabolic changes, i.e. Cushing's Syndrome. In addition, the concomitant induction of relative insulin resistance during hydrocortisone infusion might have obscured glucocorticoid-specific effects on BAT function, especially since there is a complex relationship between insulin-mediated glucose uptake and BAT perfusion and activity in *vivo* [41]. The strenghts of our study are the randomized double-blind design of the infusion protocol and that all measurements were carried out within a short period of time, reducing the confounding effect of variations seasonal temperature, and thus endogenous BAT activity. In addition, by using IT for the assessment of BAT thermogenic activity, we were able to perform live tracking of BAT function in response to experimental stimuli.

In conclusion, glucocorticoids modulate BAT thermogenesis and may represent an important physiological mechanism for maintaining human body temperature at times of acute stress. Our study suggests that transient stress could act to promote BAT function. This suggests that depending on the type and magnitude of stress BAT could be utilized to improve body weight regulation and metabolic homeostasis.

Authors' contributions

KNM and MES designed the study; HS and KNM conducted the experiments and analyzed the data with JL, HS, MES, JL, HB, DS and KNM wrote the manuscript.

Funding

The study was funded by a Starter Grant for Clinical Lecturers of the Academy of Medical Sciences awarded to KNM; HS is supported by a Medical Research Council Doctoral Training Award.

Acknowledgments

We thank the research nursing staff at the NIHR/Wellcome Trust Clinical Research Facility at the Queen Elizabeth Hospital Birmingham for excellent study support, and the volunteers for participating.

Conflict of interest

No conflicts of interest, financial or otherwise, are declared by the authors.

Appendix A. Supplementary data

Supplementary data to this article can be found online at http://dx.doi.org/10.1016/j.metabol.2017.01.024.

REFERENCES

[1] Ouellet V, Labbe SM, Blondin DP, Phoenix S, Guerin B, Haman F, et al. Brown adipose tissue oxidative metabolism contributes to energy expenditure during acute cold exposure in humans. J Clin Invest 2012;122:545–52.

[2] van Marken Lichtenbelt WD, Vanhommerig JW, Smulders NM, Drossaerts JM, Kemerink GJ, Bouvy ND, et al. Cold-activated brown adipose tissue in healthy men. N Engl J Med 2009;360:1500–8.

[3] Nedergaard J, Cannon B. The changed metabolic world with human brown adipose tissue: therapeutic visions. Cell Metab 2010;11:268–72.

[4] Cannon B, Nedergaard J. Brown adipose tissue: function and physiological significance. Physiol Rev 2004;84:277–359.

[5] Cypess AM, Haft CR, Laughlin MR, Hu HH. Brown fat in humans: consensus points and experimental guidelines. Cell Metab 2014;20:408–15.

[6] Cypess AM, Weiner LS, Roberts-Toler C, Franquet Elia E, Kessler SH, Kahn PA, et al. Activation of human brown adipose tissue by a beta3-adrenergic receptor agonist. Cell Metab 2015;21:33–8.

[7] Mostyn A, Pearce S, Budge H, Elmes M, Forhead AJ, Fowden AL, et al. Influence of cortisol on adipose tissue development in the fetal sheep during late gestation. J Endocrinol 2003;176:23–30.

[8] Robinson LJ, Law JM, Symonds ME, Budge H. Brown adipose tissue activation as measured by infrared thermography by mild anticipatory psychological stress in lean healthy females. Exp Physiol 2016;101:549–57.

[9] Ramage LE, Akyol M, Fletcher AM, Forsythe J, Nixon M, Carter RN, et al. Glucocorticoids acutely increase brown adipose tissue activity in humans, revealing species-specific differences in UCP-1 regulation. Cell Metab 2016;24:130–41.

[10] Symonds ME, Pope M, Budge H. The ontogeny of brown adipose tissue. Annu Rev Nutr 2015;35:295–320.

[11] Hibi M, Oishi S, Matsushita M, Yoneshiro T, Yamaguchi T, Usui C, et al. Brown adipose tissue is involved in diet-induced thermogenesis and whole-body fat utilization in healthy humans. Int J Obes 2016.

[12] Kozak LP. Brown fat and the myth of diet-induced thermogenesis. Cell Metab 2010;11:263–7.

Activate Windows

[13] Kaul S, Rothney MP, Peters DM, Wacker WK, Davis CE, Shapiro MD, et al. Dual-energy x-ray absorptiometry for quantification of visceral fat. Obesity (Silver Spring) 2012;20:1313-8.
[14] Symonds ME, Henderson K, Elvidge L, Bosman C, Sharkey D, Perkins AC, et al. Thermal imaging to assess age-related changes of skin temperature within the supraclavicular region co-locating with brown adipose tissue in healthy children. J Pediatr 2012;161:892-8.
[15] Keytel LR, Goedecke JH, Noakes TD, Hiiloskorpi H, Laukkanen R, van der Merwe L, et al. Prediction of energy expenditure from heart rate monitoring during submaximal exercise. J Sports Sci 2005;23:289-97.
[16] Manolopoulos KN, Karpe F, Frayn KN. Marked resistance of femoral adipose tissue blood flow and lipolysis to adrenaline in vivo. Diabetologia 2012;55:3029-37.
[17] Porter C, Herndon DN, Chondronikola M, Chao T, Annamalai P, Bhattarai N, et al. Human and mouse brown adipose tissue mitochondria have comparable UCP1 function. Cell Metab 2016;24:246-55.
[18] Vosselman MJ, Brans B, van der Lans AA, Wierts R, van Baak MA, Mottaghy FM, et al. Brown adipose tissue activity after a high-calorie meal in humans. Am J Clin Nutr 2013;98:57-64.
[19] Schlogl M, Piaggi P, Thiyyagura P, Reiman EM, Chen K, Lutrin C, et al. Overfeeding over 24 hours does not activate brown adipose tissue in humans. J Clin Endocrinol Metab 2013;98:E1956-60.
[20] Korbonits M, Trainer PJ, Nelson ML, Howse I, Kopelman PG, Besser GM, et al. Differential stimulation of cortisol and dehydroepiandrosterone levels by food in obese and normal subjects: relation to body fat distribution. Clin Endocrinol 1996;45:699-706.
[21] van Baak MA. Meal-induced activation of the sympathetic nervous system and its cardiovascular and thermogenic effects in man. Physiol Behav 2008;94:178-86.
[22] Symonds ME, Pope M, Budge H. Adipose tissue development during early life: novel insights into energy balance from small and large mammals. Proc Nutr Soc 2012;71:363-70.
[23] van den Beukel JC, Grefhorst A, Quarta C, Steenbergen J, Mastroberardino PG, Lombes M, et al. Direct activating effects of adrenocorticotropic hormone (ACTH) on brown adipose tissue are attenuated by corticosterone. FASEB J 2014;28:4857-67.
[24] Soumano K, Desbiens S, Rabelo R, Bakopanos E, Camirand A, Silva JE. Glucocorticoids inhibit the transcriptional response of the uncoupling protein-1 gene to adrenergic stimulation in a brown adipose cell line. Mol Cell Endocrinol 2000;165:7-15.
[25] Martinez-deMena R, Calvo RM, Garcia L, Obregon MJ. Effect of glucocorticoids on the activity, expression and proximal promoter of type II deiodinase in rat brown adipocytes. Mol Cell Endocrinol 2016;428:58-67.
[26] Barclay JL, Agada H, Jang C, Ward M, Wetzig N, Ho KK. Effects of glucocorticoids on human brown adipocytes. J Endocrinol 2015;224:139-47.
[27] Biddie SC, Conway-Campbell BL, Lightman SL. Dynamic regulation of glucocorticoid signalling in health and disease. Rheumatology (Oxford) 2012;51:403-12.
[28] Carmen Wong KY, Wong V, Ho JT, Torpy DJ, McLean M, Cheung NW. High cortisol levels in hyperglycaemic myocardial infarct patients signify stress hyperglycaemia and predict subsequent normalization of glucose tolerance. Clin Endocrinol 2010;72:189-95.
[29] Morgan SA, Hassan-Smith ZK, Lavery GG. Mechanisms in endocrinology: tissue-specific activation of cortisol in Cushing's syndrome. Eur J Endocrinol 2016;175:R83-9.
[30] Carey AL, Formosa MF, Van Every B, Bertovic D, Eikelis N, Lambert GW, et al. Ephedrine activates brown adipose tissue in lean but not obese humans. Diabetologia 2013;56:147-55.
[31] Cypess AM, Chen YC, Sze C, Wang K, English J, Chan O, et al. Cold but not sympathomimetics activates human brown adipose tissue in vivo. Proc Natl Acad Sci U S A 2012;109:10001-5.
[32] Vosselman MJ, van der Lans AA, Brans B, Wierts R, van Baak MA, Schrauwen P, et al. Systemic beta-adrenergic stimulation of thermogenesis is not accompanied by brown adipose tissue activity in humans. Diabetes 2012;61:3106-13.
[33] Rozansky DJ, Wu H, Tang K, Parmer RJ, O'Connor DT. Glucocorticoid activation of chromogranin a gene expression. Identification and characterization of a novel glucocorticoid response element. J Clin Invest 1994;94:2357-68.
[34] Yoneshiro T, Aita S, Matsushita M, Okamatsu-Ogura Y, Kameya T, Kawai Y, et al. Age-related decrease in cold-activated brown adipose tissue and accumulation of body fat in healthy humans. Obesity (Silver Spring) 2011;19:1755-60.
[35] Boon MR, Bakker LE, van der Linden RA, Pereira Arias-Bouda L, Smit F, Verberne HJ, et al. Supraclavicular skin temperature as a measure of 18F-FDG uptake by BAT in human subjects. PLoS One 2014;9:e98822.
[36] van der Lans AA, Vosselman MJ, Hanssen MJ, Brans B, van Marken Lichtenbelt WD. Supraclavicular skin temperature and BAT activity in lean healthy adults. J Physiol Sci 2016;66:77-83.
[37] Salem V, Izzi-Engbeaya C, Coello C, Thomas DB, Chambers ES, Comninos AN, et al. Glucagon increases energy expenditure independently of brown adipose tissue activation in humans. Diabetes Obes Metab 2016;18:72-81.
[38] Gatidis S, Schmidt H, Pfannenberg CA, Nikolaou K, Schick F, Schwenzer NF. Is it possible to detect activated brown adipose tissue in humans using single-time-point infrared thermography under thermoneutral conditions? Impact of BMI and subcutaneous adipose tissue thickness. PLoS One 2016;11:e0151152.
[39] Hwang JJ, Yeckel CW, Gallezot J-D, Aguilar RB-D, Ersahin D, Gao H, et al. Imaging human brown adipose tissue under room temperature conditions with 11C-MRB, a selective norepinephrine transporter PET ligand. Metab Clin Exp 2015;64:747-55.
[40] Holstila M, Virtanen KA, Gronroos TJ, Laine J, Lepomaki V, Saunavaara J, et al. Measurement of brown adipose tissue mass using a novel dual-echo magnetic resonance imaging approach: a validation study. Metab Clin Exp 2013;62:1189-98.
[41] Orava J, Nuutila P, Lidell Martin E, Oikonen V, Noponen T, Viljanen T, et al. Different metabolic responses of human brown adipose tissue to activation by cold and insulin. Cell Metab 2011;14:272-9.

European Pharmaceutical Review
Activa

Appendix B - Conference abstracts

Non-selective Beta-Adrenergic Agonist Infusion Acutely Stimulates the Temperature of Brown Adipose Tissue in Adult Males

H Scotney[1], M Symonds[1], J Law[1], H Budge[1], D Sharkey[1] and K Manolopoulos[2]

1 Academic Child Health, School of Medicine, University of Nottingham, UK
2 Institute of Metabolism and Systems Research, University of Birmingham, UK

Poster communication by Hannah Scotney – Society for Endocrinology (SfE BES), 2-4th November 2015, Edinburgh International Conference Centre, Edinburgh, United Kingdom

Although brown adipose tissue (BAT) is present in small quantities in human adults (~100g) it can have a significant influence on metabolism. This effect is mediated by rapid activation of the BAT specific uncoupling protein (UCP)1, following stimulation of βadrenergic receptor (AR) by the sympathetic nervous system. AR agonists stimulate rodent BAT, but have so far provided inconsistent findings in humans when administered orally. Rapid activation of UCP1 at birth is mediated in part by the pre-partum surge in cortisol, but whether this has any influence on BAT function in adults remains to be fully established. Our study therefore aimed to determine whether the non-selective AR agonist Isoprenaline (ISO) increased the temperature of the main region of BAT in adult humans i.e. the supraclavicular region, and whether this could be modulated by chronic infusion of hydrocortisone (HC). Eight healthy young males (18-30 years) of normal body weight [body mass index: 18-24.9 kg/m^2] were recruited and underwent an overnight infusion of either HC or saline (S) [0.2 $mg.kg^{-1}.h^{-1}$] which continued for ~19 hours. The following morning, a 1h systemic infusion of ISO (25ng.kg fat-free $mass^{-1}.min^{-1}$) was performed, when BAT activity was continuously measured by thermal imaging, together with heart rate. The temperature of the room remained constant at 22-23°c. ISO resulted in a significant increase in temperature of the supraclavicular region (0.40±0.06°C) and heart rate (46±5 bpm), where peak responses occurred between 20 and 40 minutes, a response that was unaffected by HC ($P<.05$).
Infusion of a β-agonist stimulates the temperature of the main site of BAT in humans. This response appears to be unaffected by chronic infusion of HC, suggesting raised cortisol has limited influence on BAT activity in young adult males.

Glucocorticoids modulate *in vivo* brown adipose tissue thermogenesis in humans

H Scotney[1], M Symonds[1], J Law[1], H Budge[1], D Sharkey[1] and K Manolopoulos[2]

1 Academic Child Health, School of Medicine, University of Nottingham, UK
2 Institute of Metabolism and Systems Research, University of Birmingham, UK

Poster communication by Hannah Scotney – The Physiological Society, 29th - 31st July 2016, The Convention Centre, Dublin, Ireland

Introduction: There is increasing evidence that brown adipose tissue (BAT) has an important physiological role beyond that of thermoregulation in newborn infants and rodents. Adult humans thus have significant amounts of BAT and as a highly metabolic tissue with the capacity to oxidise both glucose and lipid, attention has turned to its involvement in the pathogenesis of obesity. Central regulation of BAT is through the adrenoreceptor activated cAMP pathway and the liberation of free-fatty acids (FFA), which are acute metabolic substrates for the BAT specific uncoupling protein (UCP1). Rapid activation of UCP1 at birth is mediated in part by the pre-partum surge in cortisol, but whether excess cortisol administration may potentiate sympathetic nervous system (SNS) induced BAT thermogenesis is unknown. This was the first in vivo study to examine the effects of acute hypercortisolemia on BAT function in healthy human subjects, assessed by thermal imaging. Methods: Eight healthy male volunteers (age 20y, weight 75 kg, BMI 23.0 kg/m^2) participated in this randomised, double-blind, placebo controlled study. Thermal imaging of the supraclavicular neck region (SCR) was conducted prior to and post a standardised calorie-controlled meal, proceeded by a 14hr constant infusion of hydrocortisone (HC; 0.2 mg.kg^{-1}.h^{-1}) or saline (S). The following morning, Isoprenaline (ISO; 25 ng.kg fat-free mass^{-1}.min^{-1}) was infused for 1hr. BAT thermogenic activity was measured at baseline and throughout the infusion. Blood samples were drawn throughout and analysed for cortisol, glucose, triglycerides, and FFA. Results: HC significantly increased plasma cortisol concentrations (AUC 143±16 vs 2358±290nmol/L, p<0.001) and basal NEFA (AUC 1073±98 μmol/L; p=0.027 compared to control). At thermoneutrality, acute hypercortisolaemia increased basal SCR (35.92 vs 35.49°C, p=0.004). ISO increased NEFA both under control conditions (AUC 1549±173 μmol/L; p=0.001 compared to basal) and during HC (AUC 2039±194 μmol/L; p=0.001). HC did not have any effect on the magnitude of plasma NEFA increase in response to ISO (Δ AUC 953±155 vs 979±175 μmol/L). Plasma glucose concentrations did not change during ISO infusion. β-adrenergic stimulation resulted in a highly localized increase in SCR temperature (0.68±0.18°C, p=0.001) representative of BAT thermogenic activity, both under control and hypercortisolaemia conditions

(0.52±0.14°C, p=0.001). Conclusions: GCs can modulate human BAT activation by the induction of ß-AR-induced lipolysis and provide a novel insight into the potential role of BAT in targeting obesity and cushing's syndrome disorders.

Real-time quantification of brown adipose tissue thermogenesis in humans

H Scotney[1], M E Symonds[1], D Sharkey[1]

1 Division of Child Health, Obstetrics & Gynaecology, School of Medicine, University of Nottingham, Nottingham, NG7 2UH, UK

Poster communication by Hannah Scotney – Keystone Symposia-Obesity and Adipose Tissue Biology (J4), 22nd-26th January 2017, Keystone Resort, Keystone, Colorado, USA

Brown Adipose Tissue (BAT) thermogenesis may be assessed by Thermal Imaging (IRT), but it could be argued it measures the superficial temperature over a BAT depot which may not result from BAT thermogenesis. Combining TI with other surrogate measures of BAT activation (i.e. increased metabolic activity), may allow safe, real-time quantitative assessment in young children and babies. The aim of the study was to perform a pilot validation study to quantify BAT activation by means of TI, Near Infrared Spectrophotometry (NIRS) and Laser Doppler Flowmetry (LDF).
Fifteen healthy adult volunteers were exposed to an acute 15-minute arm cooling challenge at 16℃. NIRS sensors were placed over the deltoid (reference) and left supraclavicular BAT (SBAT) depot. An LDF sensor was placed next to the SBAT NIRS sensor. These measures assessed BAT O_2 uptake/utilisation (NIRS) and dermal blood flow (LDF).
IRT of their right SBAT depot before, during and after the challenge were measured. Data are reported as mean ± SD.
Core temperature remained unchanged (*P*=.456). Cold exposure increased IRT SBAT temperature by 0.29±0.12℃ at 10 minutes (*P*=.000), in parallel with a maximal rise in BAT venous oxygen saturations of 7±4% (*P*=.000). A rise in dermal blood flow peaked 15 minutes (16±14AU; *P*=.001). The deltoid NIRS remained unchanged (*P*=.169).
IRT can be combined with NIRS to assess BAT activation in real-time in adults. These data suggest that heat is originating from within BAT and is then conducted towards the skins surface, supporting the hypothesis that TI measures heat produced from BAT, rather than that of the surrounding vasculature. Further work is required to establish if these modalities could be used to quantify BAT activation in children and babies.

Appendix B Details of suppliers

Abcam®, 330 Cambridge Science Park, Cambridge, CB4 0FL, UK; www.abcam.com

Abgene Ltd, Abgene House, Blenheim Road, Epsom, KT19 9AP, UK; www.abgene.com

Alpha Laboratories Ltd, 40 Parnham Drive, Eastleigh, Hampshire, SO50 4NU, UK; www.alphalabs.co.uk

Applied Biosystems, 5791 Van Allen Way, PO Box 6482, Carlsbad, California (CA), USA; www.appliedbiosystems.com

Arbor Assays®, 1514 Eisenhower Place, Ann Arbor, Michigan 48108, USA; www.ArborAssays.com

Bibby Scientific Ltd, Beacon Road, Stone, Staffordshire, ST15 0SA, UK; www.techne.com Biotek UK, 6 Bull Street, Potton, Befordshire, SG19 2NR, UK; www.biotek.com

Bio-Rad Laboratories Ltd, Bio-Rad House, Maxted Road, Hemel Hempstead, Hertfordshire, HP2 7DX, UK; www.bio-rad.com

Cell Biolabs Inc., 7758 Arjons Drive, San Diego, California (CA), 92126, USA; www.cellbiolabs.com

Diagnostic Products Corporation, Llanberis, Glyn Rhonwy, Caernarfon, Gwynedd, LL55 4EL, UK; www.pharmaceutical-int.com

Draeger Medical UK Ltd, The Willows, Mark Road, Hemel Hempstead, HP2 7BW, UK; www.draeger.com

Ecolabs®, 370 Wabasha St N, Saint Paul, Minnesota (MN), 55102, USA; www.ecolab.com

Fisher Scientific UK Ltd, Bishop Meadow Road, Loughborough, Leicestershire, LE11 5RG, UK; www.fisher.co.uk

Flir® Systems, Inc. 2 Kings Hill Ave, Kings Hill, West Malling, ME19 4AQ; www.flir.co.uk

Genetex Inc., 2456 Alton Parkway, Irvine, California (CA), 92606, USA; www.genetex.com GraphPad Software Inc., 2236, Avenida de la Playa, La Jolla, California (CA), 92037, USA; www.graphpad.com

Grenier Bio-One Ltd, Brunel Way, Stroudwater Business Park, Stonehouse, GL10 3SX, UK; www.greinerbioone.com

Hill-Rom Inc. Hill-Rom Clintron House, Ashby Park, Ashby de la Zouch, Leicestershire, LE65 1JG; www.hill-rom.com

Hoefer® Inc., 84 October Hill Road, Holliston, Massachusetts (MA), 01746, USA; www.hoeferinc.com

IBM UK Ltd, PO Box 41, North Harbour, Portsmouth, Hampshire, PO6 3AU, UK; www.spss.com

Invitrogen Ltd, 3 Fountain Drive, Inchinnan Business Park, Paisley, PA4 9RF, UK; www.invitrogen.com

Maxim Integrated Ltd, 160 Rio Robles, San Jose, CA 95134, USA; www.maximintegrated.com

Microsoft Corporation, One Microsoft Way, Redmond, Washington (WA), 98052, USA; www.microsoft.com

Minitab Ltd, Brandon Court, Unit E1-E2, Progess Way, Coventry, CV3 2TE, UK; www.minitab.com

Moor Instruments Ltd, Millwey, Axminster, Devon, EX13 5HU, UK; www.moor.co.uk

Nonin Medical Inc. 13700 1st Avenue, North Plymouth, Minnesota 55441-5443, USA; www.nonin.com

PerkinElmer, Saxon Way Bar Hill, Cambridge, Cambridgeshire, CB23 8SL, UK; www.perkinelmer.co.uk

Premier Biosoft International, 3786 Corina Way, Palo Alto, California (CA), 94303, USA; www.premierbiosoft.com

Primer Design Ltd, Millbrook Technology Campus, Second Avenue, South-ampton, Hampshire, SO15 0DJ, UK; www.primerdesign.co.uk

Qiagen UK Ltd, Qiagen House, Fleming Way, Crawley, West Sussex, RH10 9NQ, UK; www.qiagen.com

Roche Diagnostics Ltd, Applied Science, Charles Avenue, Burgess Hill, West Sussex, RH15 9RY, UK; www.rocheuk.com

Scientific Laboratory Supplies (SLS) Ltd, Orchard House, The Square, Hessle, East Riding of Yorkshire, HU13 0AE, UK; www.scientificlabs.co.uk

Severn Biotech Ltd, Unit 2, Park Lane, Kidderminster, Worcestershire, DY11 6TJ, UK; www.severnbiotech.com

Sigma-Aldrich Company Ltd, Fancy Road, Poole, Dorset, BH12 4QH, UK; www.sigmaaldrich.com Simport Ltd, 2588 Bernard-Pilon, Beloeil, Quebec (QC) J3G 4S5, Canada; www.simport.com

The MathWorks. Inc, 1 Apple Hill Drive, Natick, MA 01760-2098, https://uk.mathworks.com

Wolf Laboratories Ltd, Colenso House, 1 Deans Lane, Pocklington, York, YO42 2PX, UK; www.wolflabs.co.uk